

# **Liquid Absorption and Wiping Behaviour of Hydroentangled Baby Wipe Fabrics**

Alaa Memari

Submitted in accordance with the requirements for the degree of  
Doctor of Philosophy

The University of Leeds  
School of Design

October 2017

The candidate confirms that the work submitted is his own and that appropriate credit has been given where reference has been made to the work of others.

This copy has been supplied on the understanding that it is copyright material and that no quotation from the thesis may be published without proper acknowledgement.

The right of Alaa Memari to be identified as Author of this work has been asserted by him in accordance with the Copyright, Designs and Patents Act 1988.

© 2017 The University of Leeds and Alaa Memari

# Acknowledgements

There are many people I would like to thank for their help and support in my work and my life throughout the years of my PhD. Those of which I would like to name:

My supervisor Steve. You have been a great supervisor, manager and mentor. You never failed to give me that motivating push so that I ended up giving this project 120% of my efforts. Thank you for always being so positive and down to earth. Thanks for believing in me. I have learnt so much from you and I would not have reached the finish line without your help.

My supervisor in P&G, John. I can only imagine how difficult it is to maintain a strong connection and relevance between the long term project that is the PhD and the fast moving consumer goods industry. Yet you managed to do that over 4 years without breaking a sweat. Thank you for having faith in me and for all your efforts and support.

My sponsor, P&G. I have been very lucky to have my PhD project entirely funded by Procter & Gamble. Special thanks to Joerg for pushing the idea through to the attention of P&G's management. Also thanks to Patricia, Natascha, Wendy, Randy and everyone at P&G who supported me.

Many thanks to NIRI for their help getting things done and training me on the lab equipment. Thank you Vera, Andrew and Manoj. And thanks to Chris, Matt and Mike for their support when I was in need.

Thanks to my friends and colleagues who were my comfort zone when things got too rough and stormy. Thank you Sophie, Jihane and Alice. I am so lucky to have met and befriended you. Thank you Annie for being the best landlady I have ever had. And to you my best friend Ammar, there is not much I could say here to express my gratitude. I am so grateful.

And of course thank you my lovely parents and brothers for bearing with me all these years and for being so patient with my complaining. I owe everything to you. Thank you uncle Aboud again and again and thanks to my extended family for their kind supporting words with every chance they had.

# Abstract

The wipes industry is worth scores of billions with a lot of room for technological improvements. The requirements for an efficient baby wipe fabric have been asserted by the major industrial players and there has been a gap in the science that involves several aspects of the fabric design and how it influences its wiping efficiency. This research reviews the previous scientific efforts made in the subjects of wiping and substance removal from surfaces, the underlying wiping mechanisms and the methods previously dedicated to assess wiping efficiency. The composition of BM, found to be complex and variable, was substituted by an artificial analogue in the form of a slurry. The artificial BM had been proven to simulate the relevant properties of real BM which made it suitable for this study.

The experimental work presented in this project includes test method development, the making of fabric prototypes and the means to introduce design properties to the fabrics structure which were expected to improve their absorption and wiping behaviour. The absorption function of baby wipes fabrics was addressed and the influence of fabric structure on the absorption behaviour was investigated. Additionally the mechanical removal of BM was also investigated. Prototype fabrics were designed and made with certain structure which was expected to improve the wipes dynamic removal of BM from the skin.

The results of the absorption experimentation of BM slurry showed promising improvements with an industrially viable change of the fabrics structure. A change in the manufacturing parameters was proven to result in improved absorption behaviour within the boundary conditions of the manual wiping process. The results of the investigation of the influence of fabric structure on the dynamic removal of BM were positive and significant in some aspects. The surface features introduced to the fabric prototypes showed to have improved and it is possible to achieve such structures with minimum changes in the manufacturing process.

There are several advantages of the fabric structure changes discussed in this work. They do not require substantial change in the manufacturing process which makes them strongly adoptable by the industry. Secondly, these features, normally in the form of embossed or apertured patterns, are introduced for visual appearance reasons which leaves a lot of room for potential improvement in the wiping efficiency.

# Table of Contents

<b>Acknowledgements</b> .....	<b>iii</b>
<b>Abstract</b> .....	<b>iv</b>
<b>Table of Contents</b> .....	<b>v</b>
<b>List of Tables</b> .....	<b>x</b>
<b>List of Figures</b> .....	<b>xi</b>
<b>CHAPTER 1 Introduction</b> .....	<b>1</b>
<b>1.1 Aims and Objectives</b> .....	<b>3</b>
<b>CHAPTER 2 Literature Review</b> .....	<b>4</b>
<b>2.1 Nonwoven Materials</b> .....	<b>4</b>
2.1.1 Definitions.....	4
2.1.2 Manufacturing Processes .....	5
2.1.3 Raw Materials .....	5
<b>2.2 Nonwoven Substrates for Pre-Moistened Baby Wipes</b> .....	<b>6</b>
<b>2.3 Wiping Mechanisms</b> .....	<b>7</b>
2.3.1 Definitions.....	8
2.3.2 BM Removal .....	8
2.3.3 Shearing Elements .....	15
2.3.4 Design of the Fabric's Structural Features.....	19
2.3.5 Capture of BM by a Fabric.....	22
<b>2.4 Wiping Evaluation Methods</b> .....	<b>25</b>
2.4.1 Sled Methods.....	25
2.4.2 Rotary Dynamic Cleaning Method (DCM).....	26
<b>2.5 Artificial Bowel Movement Material</b> .....	<b>33</b>
2.5.1 Chemical Composition of BM.....	33
2.5.2 Mechanical and Rheological Properties of BM .....	34
2.5.3 Preparation of Artificial BM .....	37

<b>2.6 Skin Biology, Structure and Morphology.....</b>	<b>39</b>
2.6.1 Skin's Mechanical Properties.....	39
2.6.2 Surface Morphology.....	40
2.6.3 Surface Chemistry .....	41
<b>2.7 Summary.....</b>	<b>42</b>
<b>CHAPTER 3 Materials and Methodology.....</b>	<b>43</b>
<b>3.1 Manufacture of Nonwoven Fabric Samples.....</b>	<b>43</b>
3.1.1 Fibre Opening and Blending .....	43
3.1.2 Carding and Web Formation.....	44
3.1.3 Hydroentanglement and Pattern Application.....	46
3.1.4 Drying and Cutting: .....	48
<b>3.2 Fabric Porosity.....</b>	<b>49</b>
<b>3.3 Fabric Pre-Moistening .....</b>	<b>50</b>
3.3.1 Materials and Methods .....	50
3.3.2 Development of the Lotion Loading Procedure.....	50
<b>3.4 Measurement of BM Wiping Efficiency .....</b>	<b>53</b>
<b>3.5 Image Processing and Analysis .....</b>	<b>53</b>
<b>3.6 Experimental Design.....</b>	<b>55</b>
<b>CHAPTER 4 Artificial Bowel Movement (BM) Absorption by Wipes.....</b>	<b>57</b>
<b>4.1 Introduction.....</b>	<b>57</b>
<b>4.2 Influence of Global Porosity on BM Absorptive Capacity .....</b>	<b>57</b>
4.2.1 Introduction.....	57
4.2.2 Materials and Methodology.....	58
4.2.3 Results.....	59
<b>4.3 Influence of Global Porosity on the BM Absorption Rate .....</b>	<b>60</b>
4.3.1 Materials and Methodology.....	60
4.3.2 Results.....	66

4.3.3 Discussion .....	68
<b>4.4 Influence of Global Porosity on Slurry Absorption.....</b>	<b>71</b>
4.4.1 Absorption Behaviour using Tensiometry .....	71
4.4.2 Materials and Methodology.....	74
4.4.3 Results and Discussion .....	78
<b>4.5 Influence of Local Porosity on BM Slurry Absorption.....</b>	<b>84</b>
4.5.1 Introduction.....	84
4.5.2 Experimental Design.....	85
4.5.3 Testing BM Slurry Absorption .....	89
<b>4.6 Influence of Local Porosity Profiles in the Fabric Cross Direction on BM Slurry Absorption.....</b>	<b>99</b>
4.6.1 Introduction.....	99
4.6.2 Experimental Aim.....	101
4.6.3 BM Slurry Absorption Behaviour Using Tensiometry .....	102
4.6.4 Materials and Methodology.....	102
4.6.5 Results and Discussion .....	105
4.6.6 Summary and Conclusions.....	113
<b>4.7 Influence of Local Porosity Profiles in the Machine Direction on BM Slurry Absorption .....</b>	<b>114</b>
4.7.1 Introduction.....	114
4.7.2 Aims and Objectives .....	120
4.7.3 Materials and Methodology.....	120
4.7.4 Results and Discussion .....	122
4.7.5 Summary and Conclusions.....	127
<b>4.8 Influence of Local Porosity Profiles in the Z Direction on BM Slurry Absorption.....</b>	<b>129</b>
4.8.1 Background.....	129

4.8.2 Measurement of BM Slurry Absorption in the Z Direction .....	130
4.8.3 Transplanar BM Slurry Absorption with Local Porosity Variation in the Z Direction .....	136
4.8.4 Materials and Methodology.....	137
4.8.5 Results and Discussion .....	137
4.8.6 Summary and conclusions.....	145
<b>CHAPTER 5 Influence of Lotion on Absorption Behaviour .....</b>	<b>147</b>
<b>5.1 Introduction .....</b>	<b>147</b>
<b>5.2 Effect of Lotion Loading on BM Slurry Absorption in the Machine Direction (MD) .....</b>	<b>147</b>
5.2.1 Materials and Methodology.....	147
5.2.2 Results and Discussion .....	148
<b>5.3 Effect of Lotion on Transplanar BM Slurry Absorption .....</b>	<b>150</b>
5.3.1 Materials and Methodology.....	150
5.3.2 Results and Discussion .....	151
<b>5.4 Effect of Lotion Loading on Transplanar BM Slurry Absorption</b>	<b>157</b>
5.4.1 Materials and Methodology.....	158
5.4.2 Results and Discussion .....	158
<b>5.5 Summary.....</b>	<b>164</b>
<b>CHAPTER 6 Effect of Surface Features on BM Slurry Removal.....</b>	<b>166</b>
<b>6.1 Materials and Methodology .....</b>	<b>166</b>
6.1.1 Area and Shape of the BM Slurry Smudge.....	168
6.1.2 Formation of the BM Slurry Smudge for DCM Measurements...	168
6.1.3 BM Smudge Thickness for the Film Removal Scale .....	173
<b>6.2 Influence of Fabric Surface Texture on Dynamic Wiping Efficiency .....</b>	<b>177</b>
6.2.1 Fabric Manufacture .....	177

6.2.2 Assessment of Wiping Efficiency using the DCM .....	179
<b>6.3 Influence of Structural Geometric Surface Features on Wiping Efficiency.....</b>	<b>192</b>
6.3.1 Fabric Prototyping.....	192
6.3.2 Assessment of Wiping Efficiency .....	195
<b>CHAPTER 7 Conclusions .....</b>	<b>198</b>
7.1 Contributions .....	199
7.2 Limitations.....	200
7.3 Recommendations for Future Work .....	200
<b>CHAPTER 8 References.....</b>	<b>201</b>
<b>CHAPTER 9 Appendices.....</b>	<b>210</b>
9.1 Appendix 1.....	210
9.2 Appendix 2.....	211

# List of Tables

Table 1: Design specifications of the fabric's structural features .....	19
Table 2: Baby Bowel Movement (BM) Properties.....	36
Table 3: Summary of in vivo Young's moduli of human skin (Hendriks, 2005) .....	40
Table 4: Resulting area, weight and basis weight of the carded batts.....	45
Table 5: Variation of lotion loading results using the hand mangle method.	52
Table 6: Liquid absorptive capacity (LAC) for samples of high (95.6%) and low (90.2%) porosities .....	59
Table 7: Results of the linear fit model's slope of the 1 <sup>st</sup> and 2 <sup>nd</sup> seconds of the tensiometer BM slurry absorption curves for global porosity samples (high and low) and local porosity samples (patterns A and B).....	110
Table 8: Results of the linear fit model slopes for the 1 <sup>st</sup> and 2 <sup>nd</sup> seconds of the tensiometer BM slurry absorption curves for patterns (A, B, C and D).	126
Table 9: Basis weights of the experimental fabrics .....	178
Table 10: IDV results of the processing of the fluorescence images of the skin mimic specimens for the three fabric samples. The missing data in the table are due to a fault in the test such as the slip of wipe on the cylinder which produced no results or unrealistic results .....	184
Table 11: IDV results of the processing of the fluorescence images of the skin mimic specimens for the two fabric options, new structure and plain .....	196
Table 12: Lotion loading results using the pad mangle method .....	210
Table 13: Lotion loading results variation using the hand mangle method	211

# List of Figures

Figure 2.1: Examples of wiping fabrics with different structure patterns. A: Corrugation, B: Apertured, C: Embossing pattern, D: Fabric density pattern, E: Corrugation pattern, F: Fabric density pattern, G: Corrugation pattern, H: Corrugation pattern, I: Apertured and surface finished.....	7
Figure 2.2: Schematic of the three cases of BM removal: a: BM dissolution, b: BM rupture, c: BM washing .....	9
Figure 2.3: Multiscale Tools for Mechanical Cleaning .....	10
Figure 2.4: Schematic of an adhering particle showing the acting forces (Burdick et al., 2005) .....	12
Figure 2.5: Raised surfaces of the wipe designed to maximize the „shovel effect“ (Mason, Procter & Gamble Internal Communications) .....	15
Figure 2.6: a series of shearing elements on a metal cutting tool (broach)(Kalpakjian and Schmid, 2008) .....	17
Figure 2.7: Rake angle and relief angle (clearance angle) in metal cutting tools (Kalpakjian and Schmid, 2008) .....	17
Figure 2.8: Different arrangements of shearing elements, a) straight alignment, b) offset alignment, c) checkers alignment.....	18
Figure 2.9: Surface of diamond grinding wheels, Top: random arrangement, bottom: ordered micro-arrays (Butler-Smith et al., 2011) .....	19
Figure 2.10: 3D drawing of several designs of the shearing element. From left to right: initial design, shearing element design (single direction), shearing element design (double direction), shearing element design (quadriple direction) and shearing element design (all directions) .....	20
Figure 2.11: Top, side and front views of the shearing element. The clearance angle and rake angles are shown. They have a great importance on the performance and cutting efficiency regarding cutting forces and friction .....	21
Figure 2.12: 3D drawing of the single shearing element .....	21
Figure 2.13: An array of repeated shearing elements in checkers arrangement.....	22

Figure 2.14: Sled method apparatus (Chatterjee, 2002) .....	26
Figure 2.15: Areas of contact between the wipe and the skin. Matching numbers indicate which area of the skin is wiped by which area of the wipe .....	27
Figure 2.16: Wiping test apparatus using a rotating cylinder as the wipe holder .....	28
Figure 2.17: Dynamic Cleaning Method rig used to assess the wiping efficiency. 1: lid, 2: aluminium cylinder to hold the sample, 3: weights to control wiping pressure, 4: rails to guide the cylinder's horizontal motion, 5: servo-motor for linear motion, 6: servo-motor for rotational motion .....	30
Figure 2.18: DCM linear horizontal motion mechanism .....	31
Figure 2.19: Top view of the bridge with the double elbow shaft marked in red .....	31
Figure 2.20: DCM bridge disks and the ramps .....	32
Figure 2.21: Second servo motor attached to the bridge to provide the rotational movement to the cylinder .....	32
Figure 2.22: Distribution of BM consistencies by diet. Charts reproduced from P&G private communications (Roe et al., Procter & Gamble Internal Communications) .....	35
Figure 2.23: Comparison of shear storage modulus vs. shear stress curves for artificial BM and real BM obtained by Dynamic mechanical analysis (DMA). Red curve: artificial BM, Blue curves: real BM samples. (Qin, Procter & Gamble Internal Communications) .....	38
Figure 2.24: Schematic of the cross section of stratum corneum. The process of corneocyte renewal (Levi, 2009) .....	41
Figure 3.1: Manual mixing of the fibre types in preparation for the blending phase. The fibres were laid over each other to make four equal sandwiches of the three fibre types. They were then mixed manually in a vertical fashion .....	44
Figure 3.2: Diagram of the hydroentanglement process for the preparation of fabric prototypes. Carded batts are pre-wetted then passed under the waterjet	

to produce the hydroentangled fabrics. During this process, a patterned mesh could be placed under the batts to imprint the pattern onto the fabrics .....	46
Figure 3.3: Mesh used for the production of the apertured fabric. Manufacturer: GKD - Gebr. Kufferath AG, Dueren, Germany. Item ref. no. 40565800 .....	47
Figure 3.4: Screening wire mesh used to make deep corrugations in the fabric. Manufacturer: GKD - Gebr. Kufferath AG, Dueren, Germany. Item ref. no. 40560820 .....	48
Figure 3.5: Schematic of the fabric compression set up using a hydraulic press .....	49
Figure 3.6: Lotion loading as function of Nip Pressure using Xiamen Rapid Co. Ltd P-B0 .....	52
Figure 3.7: Example of the density data window in which the resulting IDVs of an image are displayed .....	55
Figure 3.8: Diagram showing the experimental structure of the work presented in chapters 4 to 6.....	55
Figure 4.1: Liquid absorptive capacity for the high porosity (95.6%) and low porosity (90.2%) samples.....	59
Figure 4.2: Test setup for the capture of BM slurry absorption. The camera is mounted vertically above the test table facing downwards. Incident lighting is provided from both sides left and right. ....	61
Figure 4.3: Droplet of slurry placed on top of the high porosity (95.6%) fabric sample.....	62
Figure 4.4: Pool of slurry on the polyethylene plate .....	62
Figure 4.5: High porosity (95.6%) fabric sample placed over the pool of slurry; duration: 2 min .....	62
Figure 4.6: Image processing of the video frames captured during method 1 experiment at $t = 120$ s. a: image of low porosity sample (90.2%). b: image of high porosity sample (95.6%). c: inverted image of low porosity sample (90.2%). d: inverted image of high porosity sample (95.6%) .....	64

Figure 4.7: Image processing of the video frames captured during method 2 experiment at $t = 120$ s. a: image of low porosity sample (90.2%). b: image of high porosity sample (95.6%). c: inverted image of low porosity sample (90.2%). d: inverted image of high porosity sample (95.6%) .....	65
Figure 4.8: IDV data for the low (90.2%) and high (95.6%) porosity fabrics; duration: 10 s .....	66
Figure 4.9: IDV data for the low (90.2%) and high (95.6%) porosity fabrics; duration: 120 s (2 min) .....	67
Figure 4.10: IDV data for the low (90.2%) and high (95.6%) porosity fabrics; duration: 10 s .....	67
Figure 4.11: IDV data for the low (90.2%) and high (95.6%) porosity fabrics; duration: 120 s (2 min) .....	68
Figure 4.12: Hypothetical graph of absorption behaviour curves of two fabric samples which differ in porosity but identical in other properties. Blue curve: high porosity sample, red curve: low porosity sample .....	69
Figure 4.13: Spread of BM slurry in 90.2% low porosity fabric (top) and 95.6% high porosity fabric (bottom) showing heterogeneous phase separation in the low porosity fabric.....	70
Figure 4.14: Kruss Force Tensiometer K100 (Kruss-GmbH).....	73
Figure 4.15: Schematic of the main parts of the tensiometer. Control of immersion is via the motorised table. ....	74
Figure 4.16: BM Slurry absorption using the tensiometer showing the final specimen position after the experiment and the end of the fabric wetted with BM slurry .....	76
Figure 4.17: Sample preparation. Specimens were cut in the dimensions 45 x 20 (mm) such that the MD was vertically aligned prior to immersion of 0.5 mm of the lower edge being immersed in the BM slurry for absorption measurement. ....	77
Figure 4.18: Summary of conditions used during tensiometry measurements. ....	78

Figure 4.19: BM slurry absorption curves for the high porosity (95.6%) sample in the MD determined by tensiometry.....	80
Figure 4.20: BM slurry absorption curves for the low porosity (90.2%) sample in the MD determined by tensiometry.....	81
Figure 4.21: BM slurry absorption curves for high (95.6%) and low (90.2%) porosity samples in the MD determined by tensiometry.....	81
Figure 4.22: A plot of the tensiometer absorption curves for high (95.6%) and low (90.2%) porosity samples during the first two seconds of contact with BM slurry. ....	82
Figure 4.23: BM slurry weight absorption gradient for the first two seconds in MD.....	83
Figure 4.24: Summary of experimental approaches used to modulate variations in local porosity and to determine resultant BM slurry absorption behaviour .....	85
Figure 4.25: Illustrator drawing of the mould design showing the different sizes of the local compression areas.....	87
Figure 4.26: Mould template. The square side lengths are from left to right: 50 mm, 20 mm, 10 mm, 5 mm, 3 mm and 1mm.....	88
Figure 4.27: Schematic of the fabric compression set up using the prototype mould to introduce areas of different local porosities to the sample.....	88
Figure 4.28: Nonwoven fabric after compression using the mould template for 20 min at a pressure of 0.745 MPa. ....	89
Figure 4.29: Slurry absorption in 1D as it occurs in parallel to the porosity borderline. Left: introduction of slurry to the edge of the fabric sample, right: magnified image of the sample after 2 min.....	91
Figure 4.30: 1: Enhanced image of 1D BM absorption sample after 2 min 2: corresponding flow front of the BM slurry in the high porosity area.....	92
Figure 4.31: Gravimetric data for each region in the 1D BM absorption experimentt .....	93

Figure 4.32: Image processing steps of the 1 mm pattern. This sample was taken from the part of the fabric to which local porosity areas of 1 mm<sup>2</sup> were introduced. The images were converted to greyscale then their colours were inverted. Both the clean image when t = 0 s (background) and the image taken at t = 120 s (2 min) underwent those two image processing steps. The final image is the result of subtracting the two images taken at t = 120 s and t = 0 s respectively. .... 96

Figure 4.33: Image processing steps of the 3 mm pattern. This sample was taken from the part of the fabric to which local porosity areas of 9 mm<sup>2</sup> (3-mm-sided squares) were introduced. The images were converted to greyscale then their colours were inverted. Both the clean image when t = 0 s (background) and the image taken at t = 120 s (2 min) underwent those two image processing steps. The final image is the result of subtracting the two images taken at t = 120 s and t = 0 s respectively. .... 97

Figure 4.34: Comparing the initial shape of the slurry drop with the shape of its spread within the patterned nonwoven fabric after 2 min. **A:** 1 mm patterned fabric (Figure 4.32) at t = 0 s. **B:** processed image of A. **C:** 3 mm patterned fabric (Figure 4.33) at t = 0 s. **D:** processed image of C..... 98

Figure 4.35: Local porosity hydroentangled nonwoven fabric samples. A: Pattern A contains two equal areas which differ in porosity and are separated by a vertical porosity borderline. B: Pattern B contains four equal areas alternating in porosity between high (95.6%) and low (90.2%), and are separated by three vertical porosity borderlines..... 105

Figure 4.36: Tensiometry BM slurry absorption curves for patterns A and B for a duration of 60 s ..... 106

Figure 4.37: A plot of the tensiometer BM slurry absorption curves for patterns A and B during the first two seconds of contact with the BM slurry surface. The first 2 seconds of contact are of high importance when fabrics are used as baby wipes. The difference in the slopes of the curves represent the difference in the weight of BM slurry absorbed per unit time. .... 107

Figure 4.38: BM slurry absorption rate of the samples low porosity, high porosity, pattern A and pattern B for the first 2 s. Only the difference between

the low porosity sample and pattern A proved to be statistically significant .....	107
Figure 4.39: Linear fit result from the first second of the tensiometer BM slurry absorption curve of pattern A sample in MD. The fit model shows a value of $R^2 = 0.99$ .....	108
Figure 4.40: Linear fit result from the second second of the tensiometer BM slurry absorption curve of pattern A sample in MD. The fit model shows a value of $R^2 = 0.99$ .....	108
Figure 4.41: Linear fit result from the first second of the tensiometer BM slurry absorption curve of pattern B sample in MD. The fit model shows a value of $R^2 = 0.99$ .....	109
Figure 4.42: Linear fit result from the second second of the tensiometer BM slurry absorption curve of the pattern B sample in the MD, where $R^2 = 0.99$ .....	109
Figure 4.43: Schematic illustrating the proposed influence of the two local porosity regions, separated by a porosity borderline (Pb) showing how the expected unequal spread of BM slurry in the local porosity areas can lead to an increase in the length of the effective porosity borderline (E) with time. 1: BM slurry spread at the 1 <sup>st</sup> second where ( $E_1$ ) is relatively small. 2: BM slurry spread at the 2 <sup>nd</sup> second where ( $E_2$ ) is relatively large.....	111
Figure 4.44: A schematic showing the two local porosity patterns A and B where local porosities are separated by porosity borderlines (Pb) showing how different distributions of local porosity for samples of identical global porosity can lead to different total lengths of porosity borderlines and subsequently different lengths of effective porosity borderlines (E). Pattern A has one porosity borderline (Pb) and subsequently one effective porosity borderline ( $E_A$ ). Pattern B has three porosity borderlines ( $3 \times Pb$ ) and subsequently three effective porosity borderlines with a total length of ( $E_B = 3 \times E_A$ ).....	112
Figure 4.45: Schematic of the porosity borderline (B) separating two areas of different porosities ( $P_1$ ) and ( $P_2$ ) and its representation into Cartesian components: ( $B_y$ ) parallel to the machine direction (MD) and the absorption	

direction (A), and (B <sub>x</sub> ) parallel to the cross direction (CD) and perpendicular to the absorption direction (A) .....	117
Figure 4.46: (a) uniform tube with height H and radius R, (b) heterogenous tube with two sections of heights h <sub>1</sub> and h <sub>2</sub> and two radii r <sub>1</sub> and r <sub>2</sub> (Shou et al., 2014b).....	118
Figure 4.47: (a) uniform porous medium with a cross-sectional area S, porosity E and height H, (b) heterogeneous double-layered porous medium with a cross-sectional area S, porosities ε <sub>1</sub> and ε <sub>2</sub> and heights h <sub>1</sub> and h <sub>2</sub> for the respective layers (Shou et al., 2014b).....	118
Figure 4.48: Normalised absorption time (t <sub>p</sub> ) in the heterogenous layered porous medium plotted against the layers' height ratio (n) at different global porosities (E) and local porosity ratios (m) (Shou et al., 2014b) a) Porosity ratio $m \geq 1$ : negative porosity gradient b) Porosity ratio $m \leq 1$ : positive porosity gradient.....	119
Figure 4.49: Local porosity nonwoven fabric samples C: Pattern C starts with a low porosity (90.2%) area from the leading edge with a height of 1mm, it then transitions to the high porosity area (95.6%) for the rest of the sample through a horizontal porosity borderline. D: Pattern D starts with a high porosity (95.6%) area from the leading edge with a height of 1 mm, it then transitions to the low (90.2%) porosity area for the rest of the sample through a horizontal porosity borderline .....	121
Figure 4.50: Tensiometry BM slurry absorption curves for samples C and D, with two different local porosity patterns for a duration of 60 s.....	122
Figure 4.51: A plot of the tensiometer BM slurry absorption curves for patterns C and D during the first two seconds of contact with the BM slurry surface. The first 2 seconds of contact are of high importance when fabrics are used as baby wipes. The difference in the slopes of the curves represent the difference in the weight of slurry absorbed per unit time. ....	123
Figure 4.52: BM slurry absorption rate of the samples with porosity patterns A, B, C and D for the first 2 s. Only the differences between patterns C and A and between patterns C and B are statistically significant.....	123

Figure 4.53: Linear fit result from the 1<sup>st</sup> second of the tensiometer BM slurry absorption curve of pattern C. The fit model shows a value of  $R^2 = 0.99$  . 124

Figure 4.54: Linear fit result from the 2<sup>nd</sup> second of the tensiometer BM slurry absorption curve of pattern C. The fit model shows a value of  $R^2 = 0.99$  . 124

Figure 4.55: Linear fit result from the 1<sup>st</sup> second of the tensiometer BM slurry absorption curve of pattern D. The fit model shows a value of  $R^2 = 0.99$  . 125

Figure 4.56: Linear fit result from the 2<sup>nd</sup> second of the tensiometer BM slurry absorption curve of pattern D. The fit model shows a value of  $R^2 = 0.99$  . 125

Figure 4.57: Schematic of the instrumental setup for Z-direction BM slurry absorption ..... 132

Figure 4.58: Test plate with BM slurry and fabric mounted on the platen prior to the Z-direction absorption measurement..... 133

Figure 4.59: An example of how the specimens appear after the z-direction BM slurry absorption experiment. Left: fabric specimen with a smudge of slurry picked up after contact. Right: plastic plate with residual slurry after contact. .... 135

Figure 4.60: Average BM slurry absorption force curves during the z-direction absorption experiments. Duration of 60 s. Side A: Conveyor side. Side B: Water jet side ..... 137

Figure 4.61: The three phases of the BM slurry absorption force curve during z-direction measurements. 1: The approach phase as the fabric sample is moved towards the BM slurry droplet. 2: Total time of travel for the upper grips holding the fabric sample, which includes contact between the fabric sample and BM slurry droplet. 3: BM slurry absorption time..... 138

Figure 4.62: BM slurry deformation at the end of the approach phase. Fabric specimen (white) applies pressure on the BM slurry (orange), which is deformed horizontally over the plastic plate (blue) ..... 139

Figure 4.63: Meniscus of the BM slurry formed between the plastic plate and the fabric surface during phase 3. .... 139

Figure 4.64: Average curves showing the force measurements at the point of contact for each of the fabric sides. Side A: Conveyor side. Side B: Water jet side.....	140
Figure 4.65: Comparison of mean peak force between the two samples. Sample A: Conveyor side. Sample B: Water jet side .....	141
Figure 4.66: Comparison of the mean of highest recorded force change rate of the two samples. Sample A: Conveyor side. Sample B: Water jet side.	142
Figure 4.67: Comparison of the mean forces measured at $t = 60$ s. Sample: Conveyor side. Sample B: Water jet side .....	143
Figure 4.68: Comparison of the mean weight of the slurry residues left by the two samples after separating the fabric from the slurry. Sample A: Conveyor side. Sample B: Water jet side .....	144
Figure 4.69: : Comparison of the mean weight of the slurry retained by the two samples after separation. Sample A: Conveyor side. Sample B: Water jet side .....	145
Figure 5.1: Sample preparation. Specimens were cut in the dimensions 45 x 20 (mm) such that the MD was vertical. The leading edge was immersed in BM slurry at a depth of 0.5 mm .....	148
Figure 5.2: Tensiometry slurry absorption curves for the dry and wet hydroentangled samples .....	149
Figure 5.3: Plot of the tensiometer BM slurry absorption curves for dry and wet hydroentangled samples during the first two seconds of contact with the BM slurry surface.....	149
Figure 5.4: Transplanar BM slurry absorption force curves showing the replicate results the dry fabric specimens measured over the duration of 60 s. The average curve is drawn as a continuous line. ....	151
Figure 5.5: Transplanar BM slurry absorption force curves showing the replicate results the wet, lotion-loaded fabric specimens measured over the duration of 60 s. The average curve is drawn as a continuous line.....	152
Figure 5.6: Comparison of the average transplanar BM slurry absorption force curves for the dry and wet samples for a duration of 60 s .....	152

Figure 5.7: Comparison of the mean slopes of the absorption curves of the dry and wet fabric samples at the point of contact after transplanar BM slurry absorption .....	153
Figure 5.8: Comparison between the mean peak force measurements of the dry and wet samples .....	154
Figure 5.9: Comparison between the mean force measurements of the dry and wet samples after 60 s .....	154
Figure 5.10: Schematic illustrating BM slurry deformation as the fabric specimen approaches the plastic plate after contact occurs with the BM slurry surface. ....	156
Figure 5.11: The hypothetical influence of lotion loading on the peak force. The continuous line represents the resistance to wetting and the dashed line represents the resistance to inlet. ....	158
Figure 5.12: Average BM slurry absorption force curves for each of the lotion loaded samples .....	159
Figure 5.13: Comparison of the mean slopes of the absorption curves of the dry and different lotion load samples at the point of contact. Shown are lotion loads 0%, 100%, 200% and 440% respectively .....	159
Figure 5.14: Tukey ANOVA for the slopes of the absorption force curves at the point of contact for samples with different lotion loadings. On the vertical axis, the pairs of samples are shown. 0 represents the dry sample, 1 represents the 100% lotion load, 2 for 200% and 4.4 for 440%. ....	160
Figure 5.15: Average peak force measurements for the samples with different lotion loading. On the horizontal axis, the samples are represented by numbers. 0 represents the dry sample, 1 represents the 100% lotion load, 2 for 200% and 4.4 for 440%. ....	161
Figure 5.16: Tukey ANOVA for the peak force measurements for the samples with different lotion loadings. On the vertical axis, the pairs of samples are shown. 0 represents the dry sample, 1 represents the 100% lotion load, 2 for 200% and 4.4 for 440%. ....	161

Figure 5.17: Average absorption force measurements at $t = 60 s$ for the samples with different lotion loadings. On the horizontal axis, the samples are represented by numbers. 0 represents the dry sample, 1 represents the 100% lotion load, 2 for 200% and 4.4 for 440%. .....	162
Figure 5.18: Tukey ANOVA for the force measurements at $t = 60 s$ for the samples with different lotion loadings. On the vertical axis, the pairs of samples are shown. 0 represents the dry sample, 1 represents the 100% lotion load, 2 for 200% and 4.4 for 440%. .....	162
Figure 5.19: The hypothetical influence of lotion load on the measured force at $t = 60 s$ . The continuous line represents the resistance due to slurry's viscosity and the dashed line represents the resistance to inlet.....	164
Figure 6.1: Classification of the scales of BM removal from the skin surface .....	167
Figure 6.2: K Control Coater device. Courtesy of RK PrintCoat Instruments Ltd. ....	169
Figure 6.3: BM smudge formation apparatus .....	170
Figure 6.4: BM application apparatus in action .....	170
Figure 6.5: Microscopic images of the BM smudge lower left corner for the nominal thicknesses of 123 $\mu m$ (left), 200 $\mu m$ (middle) and 450 $\mu m$ (right). (reflected light, bright field) .....	171
Figure 6.6: Macroscopic images of the BM smudge for the nominal thicknesses of 123 $\mu m$ (left), 200 $\mu m$ (middle) and 450 $\mu m$ (right) .....	171
Figure 6.7: Linear fit of data points for BM smudge nominal thickness versus mean BM slurry smudge weight .....	172
Figure 6.8: Macroscopic images of the contaminated dry wipe surface (left) and the contaminated wet wipe surface (lotion loading 440%) (right). .....	174
Figure 6.9: Macroscopic images of the dry-wiped skin mimic surface (left) and the wet-wiped skin mimic surfac (lotion loading 440%) (right).....	174
Figure 6.10: Microscopic images of the dry-wiped skin mimic sample (left) and wet-wiped skin mimic sample (lotion loading 440%) (right) (reflected light, bright field) .....	175

Figure 6.11: Microscopic images of the wiped skin mimic samples (left: dry, right: wet 440%) showing dimension measurements of contaminant particles (reflected light, bright field) .....	175
Figure 6.12: Plain prototype fabric (Control).....	177
Figure 6.13: Prototype fabric with apertures.....	178
Figure 6.14: Prototype fabric with corrugation.....	178
Figure 6.15: Example of a greyscale image of a skin mimic with BM residues obtained using fluorescence imaging. The blue frames represent the areas of interest for IDV readings (left frame: background, right frame: object) .....	180
Figure 6.16: Composite image layout of a skin mimic specimen using fluorescence imaging. 24 areas of interest and one background area .....	181
Figure 6.17: Composite image layout of a used wipe sample. 24 areas of interest and one separate background area.....	181
Figure 6.18: Composite image layout of a wipe specimen using white light. 24 areas of interest and one background area.....	182
Figure 6.19: Composite image layout of a wipe specimen using light microscopy. 24 areas of interest and one background area.....	183
Figure 6.20: A graph of the mean IDVs for each of the three tested options .....	185
Figure 6.21: Statistical means comparison of the average IDVs of the three options.....	185
Figure 6.22: Average cleaning profile curves for the skin mimic samples wiped by the three texture options (fluorescence imaging).....	186
Figure 6.23: Average cleaning profile curves for the wipes samples for the three texture options (fluorescence imaging) .....	186
Figure 6.24: Average cleaning profile curves for the three fabric samples produced from images of the wipes samples taken under white light .....	187
Figure 6.25: Average cleaning profile curves for the three fabric samples produced from coloured images of the wipes.....	187

Figure 6.26: Coloured images of the wipes' surface after the DCM wipe cycle. The images on the left are areas of the wipes which fall at distances from the leading edge where the BM slurry distribution is homogeneous. The images on the right are areas of the wipes near the trailing edge where smearing occurs. A: apertured sample, B: corrugated sample, C: plain sample .....	188
Figure 6.27: BM accumulation in the apertures on the wipe's surface .....	189
Figure 6.53: 3D rendered image of the female mould plate .....	192
Figure 6.54: Resulting fabric from compression at 12 tons for the duration of 30 min .....	193
Figure 6.55: Resulting fabric from compression at 5 tons for the duration of 30 min .....	194
Figure 6.56: Resulting fabric from compression at 50 kg/cm <sup>2</sup> for the duration of 30 min .....	194
Figure 6.32: A graph of the average IDVs for each of the tested options, the plain and the new structured fabric.....	196
Figure 6.33: On the left, BM residues on a skin mimic after 3 wipes with plain hydroentangled fabric. On the right, BM residues on a skin mimic after 3 wipes with the new structured hydroentangled fabric .....	196
Figure 6.34: On the left, first wipe of the plain plain hydroentangled fabric. On the right, first wipe of the new structured hydroentangled fabric .....	197
Figure 6.35: On the left, second wipe of the plain plain hydroentangled fabric. On the right, second wipe of the new structured hydroentangled fabric ....	197
Figure 6.36: On the left, third wipe of the plain plain hydroentangled fabric. On the right, third wipe of the new structured hydroentangled fabric .....	197

# CHAPTER 1

## Introduction

Over the past decade, an increasingly diverse range of disposable, single-use personal hygiene pre-moistened wipe products have become available. The growth of the markets for such products is evidence of their popularity with the public. The appeal of pre-moistened wipes in both consumer and health-care markets is primarily one of convenience and ease of use. Busy lifestyles created by the combinations of job pressures, increased activities for children and an overall faster pace of life, mean that many people find themselves pressed for time and wipes allow them to perform daily tasks in substantially less time (EDANA, 2013).

A baby wipe is a disposable product designed for skin care and hygiene. It is typically made of a nonwoven material which is pre-moistened with a lotion and packed in stacks before packaging. The main application of the product is to clean a baby's bottom during baby diaper changes. However, utilisation as to the use of pre-moistened wipes has expanded to other applications such as hand and face cleaning. Compared to single use baby diapers, disposable baby wipes are a relatively new product category in the baby care market. The first disposable diaper for the mass market was launched by Proctor and Gamble (P&G) under the Pampers® brand in the spring of 1961 for the United States (US) market and, twelve years later, in 1973, it was also launched in the German market. However, it was not until the early 1990's that single use baby wipes appeared in the market as a complement for baby diapering (Memari, 2011, Celen, Procter & Gamble Internal Communications).

The constant increases of work pressures and busy lifestyles kept pressing on the efficiency of products like the wet wipes, demanding innovative solutions to bring the products up to the task. Consumer studies on the currently available baby wipes showed complaints of smearing and the need to use multiple wipes to ensure the cleanliness of the babies' skins. This necessitated the development of a new baby wipes' product that perform with higher efficiency leading to the need to use a fewer number of wipes per diaper

change with the minimum amount of smearing per swipe. These consumer needs had to be translated into technical requirements before they can be addressed. There has been a lack of understanding of the wiping mechanisms and the factors influencing them.

Attempts to study and understand baby wipes' functionality and behaviour face several challenges. The presence of lotion on the nonwoven wipe substrate is a challenge because it creates a dynamic system in which four distinct elements need to be considered: the fibrous substrate, the lotion, the contaminant and the biological surface, which is skin. Scientific investigations of the functionality and efficiency of surface wiping have focused mainly on dry wipes and in such cases the main objective of a wipe normally relate to the absorption of liquids or the removal of particles. Whilst liquid interactions with nonwovens have been intensively studied, interactions with the bowel movement (BM) are much less well understood.

Lotion is added to baby wipes for several purposes, primarily to assist in the BM removal process, but also to contribute to skin care and odour management. Moreover, baby wipes not only remove BM but they also deposit lotion on the baby's skin surface. This further increases the complexity of the system being investigated because it may be necessary to minimise residual lotion deposition to avoid skin irritation. Thus, the wiping process in practice involves a complex set of interacting factors, relating to the nonwoven fibrous substrate itself, the aqueous lotion and the dynamics of this composite system over the skin surface.

There are few fundamental studies of baby diaper wiping behaviour and efficiency in the scientific literature as much of the published information is either proprietary or is confined to patent disclosures. This reflects the commercial importance of the sector. A number of research challenges exist in this field when attempting to pursue a systematic laboratory study. This includes adoption of a satisfactory substitute for BM due to the complex nature of the real bowel movement and its inherent variability. It is known, for example, that the chemical, mechanical and rheological properties depend on several factors, such as diet, age and health. The way in which baby wipes

are used by parents during diaper changes can also be expected to vary, but some simplification of the process is required to enable a systematic study of the underlying wiping mechanics in the laboratory. Simulating BM and wiping mechanics effectively in the laboratory is therefore necessary to permit laboratory assessment of cleaning efficiency by wipes.

## **1.1 Aims and Objectives**

In an effort to increase the cleaning efficiency of baby wipes, there is a need to develop a greater understanding of the mechanisms dominating the wiping process and the influencing factors, particularly in relation to nonwoven substrate parameters. The purpose of the research presented herein is therefore to address this challenge, specifically in relation to the removal of BM from a simulated skin surface. Accordingly, the aim is to understand how the structure of the nonwoven wiping substrate influences BM wiping efficiency.

The specific objectives are:

- To study the principal mechanisms of BM removal and retention in industrially-relevant nonwoven wiping substrates.
- To determine the influence of fabric microstructure and the geometric arrangement of fibres on the mechanisms of capture and retention of simulated biological material, specifically BM, from a skin substitute surface.
- To develop new techniques for characterising the dynamic wiping performance of nonwoven fabrics and their interaction with BM.
- To identify fabric parameters capable of improving wiping performance in nonwoven fabrics as compared to an existing industry benchmark.

# CHAPTER 2

## Literature Review

This chapter critically reviews current understanding of the basic mechanisms of material and particle removal from surfaces during wiping as well as existing test methodology relevant to the evaluation of wipe substrates and their performance. It also discusses typical nonwoven substrates, specifically in relation to pre-moistened baby wipes, the nature of BM and approaches to preparing artificial BM to facilitate laboratory studies.

### 2.1 Nonwoven Materials

#### 2.1.1 Definitions

The nonwovens industry has developed from the textiles, paper and polymer processing industries. The European Disposables And Nonwovens Association (EDANA) defines a nonwoven as “*a manufactured sheet, web or batt of directionally or randomly orientated fibres, bonded by friction and/or cohesion and/or adhesion*”. North America’s Association of the Nonwoven Fabrics Industry describes nonwoven fabrics as “*sheet or web structures bonded together by entangling fibres or filaments, by various mechanical, thermal and/or chemical processes. These are made directly from separate fibres or from molten plastic or plastic film*”. The main constituent in nonwovens is fibres or filaments which are laid to form a sheet or a bat and then consolidated either mechanically, chemically or thermally. Nonwovens are engineered to serve a specific task or have a certain function. While there are many applications for the nonwoven materials, hygiene is by far the largest of them accounting for over 33% of the European production (Russell, 2007).

There are two main differences between the paper materials and the nonwovens materials. The fibrous content ratio in nonwovens is typically higher than 50% by mass, and in some cases 30% when density is less than  $0.4 \text{ g.m}^{-3}$ . The other difference is related to the fibres length and aspect ratios. The fibres in nonwovens have an aspect ratio of at least 300 and are typically between 10 mm and 200 mm long (Russell, 2007, EDANA, 2013).

## **2.1.2 Manufacturing Processes**

The making of nonwovens involves two main stages, laying and bonding. Fibre laying processes varies depending on the industry from which the nonwoven materials were developed. Dry laying originates from the textiles industry, wet laying from the paper industry and polymer laying from the plastics industry.

Web formation is converting the fibre staples or filaments into a two-dimensional web or a three-dimensional bat, depending on the process. The orientation of the fibres in the web can be controlled during the laying and conversion processes. It has a significant effect of the isotropy of the nonwovens properties and most nonwovens are anisotropic. It is common to measure the machine direction/cross direction (MD/CD) of the web or fabric. Typically, measuring the tensile strength in MD and CD serves the purpose of measuring fibre orientation.

Web bonding has a great influence on many properties of the nonwoven fabrics. It has a major effect on the mechanical properties, particularly the strength, the porosity, flexibility, softness and density.

Mechanical web bonding include needlepunching, stitchbonding and hydroentangling. Chemical bonding involves either the application of a chemical binder such as latex or the softening or solvating of the fibre surfaces by using chemical solvents to bind the fibres over their crossing points. In thermal bonding, heat and often pressure are used to soften and fuse the surfaces of thermoplastic fibres to allow them to weld together.

## **2.1.3 Raw Materials**

The global use of fibres in the nonwovens industry is dominated by the man-made fibres with an increase of the use of viscose rayon due to its important properties and role in the making of spunlace (hydroentangled) wipes market. Man-made fibres make more than 90% of the fibres used in the nonwovens industry. They are mostly polypropylene (63%), polyester (23%), viscose rayon (8%) and acrylic (2%).

## 2.2 Nonwoven Substrates for Pre-Moistened Baby Wipes

The types of nonwovens used in baby wipes include carded and hydroentangled, spunbond, carded and thermobond, etc. Typical fibre compositions include wood pulp (natural cellulosic fibres of lengths ranging between 1-3 mm) and PET or viscose (regenerated cellulosic fibres of lengths typically ranging between 6-40 mm) and polyolefins. Wipe fabrics are usually made with the basis weights ranging between 40 g.m<sup>-2</sup> and 120 g.m<sup>-2</sup>. The wipes industry is worth tens of billions of dollars and the baby wipes is a multi-billion dollar industry.

In hydroentanglement, the fibre segments in the web are migrated by the water jets to entwine and consolidate, thereby increasing frictional resistance to slippage and fabric strength. Many factors affect the ease of fibre entanglement. The level of specific energy is a major parameter governing the properties of the fabric. Also, the process requires fibres to bend easily around small radii while possessing some degree of mobility. The important properties include those related to polymer composition and fibre properties, such as bending modulus, linear density, fibre length, fibre wettability, fibre cross-section shape and fibre-to-fibre friction.

When supported on a porous belt, fibres in the web may also be displaced to produce texture and pattern in the resulting fabric. Fibre segments bridging the top of cross-over points (knuckles) in a woven conveyor for example, are displaced in to the surrounding areas producing apertures, or three-dimensional patterns if the conveyor surface is profiled (Figure 2.1). Hydroentangled fabrics rely primarily on fibre-to-fibre friction to achieve physical integrity and are characterized by relatively high strength, softness, drape and conformability, making them attractive as personal care and baby wipes.

Pre-moistened wipes are prepared by adding an aqueous lotion to the nonwoven substrate, the majority of which contain mostly water. Loading levels are in the range 200-450% depending on the absorbent capacity of the

fabric. In addition to water the lotions contain perfumes and odour management ingredients, preservatives and skin care ingredients.

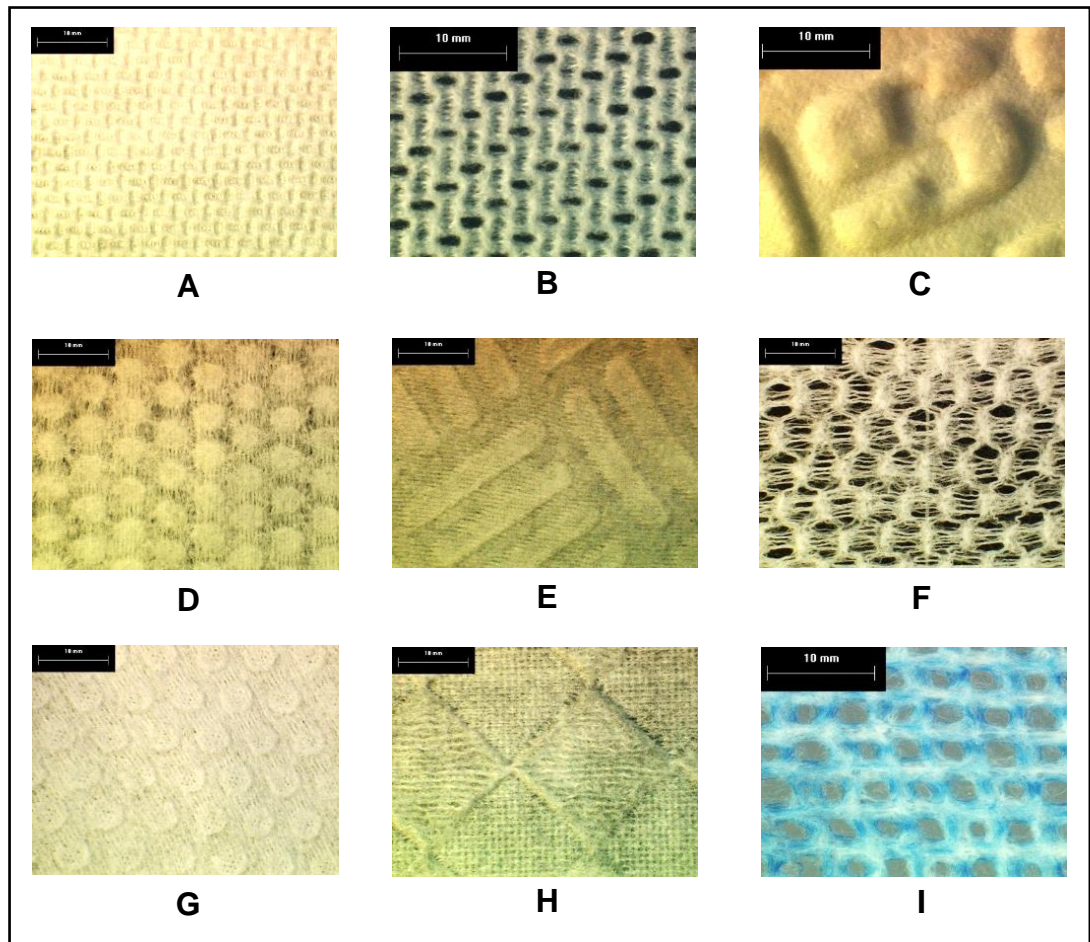


*Figure 2.1: Examples of wiping fabrics with different structure patterns. A: Corrugation, B: Apertured, C: Embossing pattern, D: Fabric density pattern, E: Corrugation pattern, F: Fabric density pattern, G: Corrugation pattern, H: Corrugation pattern, I: Apertured and surface finished*

## 2.3 Wiping Mechanisms

During wiping, the nonwoven fabric, which is compressible porous medium, is made to dynamically interact under pressure with a surface and transfer of dirt must take place. Wiping therefore involves the separation of a substance residing on the surface such that it is captured within the pore volume of the wipe or on its fibre surfaces. Fundamental to the process is understanding the basic removal and capture mechanisms.

### 2.3.1 Definitions

The removal of BM from the contaminated surface involves a number of considerations, and different definitions as outlined below.

### 2.3.2 BM Removal

BM removal is the separation of BM from the skin. The forces attaching BM to the skin are merely adhesion forces. For this separation to happen the adhesion forces must be overcome by the forces introduced during the wiping process. There are three situations in which separation is possible, Figure 2.2.

- a. **BM dissolution** in the lotion: The IUPAC compendium of chemical terminology defines dissolution as the mixing of two phases with the formulation of one new homogeneous phase i.e. the solution (McNaught and Wilkinson). This solution of BM and lotion will be referred to as a “slurry” throughout the experimental sections. The Dissolution rate depends on several factors and can be described by Equation 2.1.

$$\frac{dm}{dt} = A \frac{D}{d} (C_s - C_b) \quad 2.1$$

Where:

m, mass of dissolved material.

t, time.

A, surface area of the interface between the dissolving substance and the solvent.

D, diffusion coefficient.

d, thickness of the boundary layer of the solvent at the surface of the dissolving substance.

C<sub>s</sub>, mass concentration of the substance on the surface.

C<sub>b</sub>, mass concentration of the substance in the bulk of the solvent.

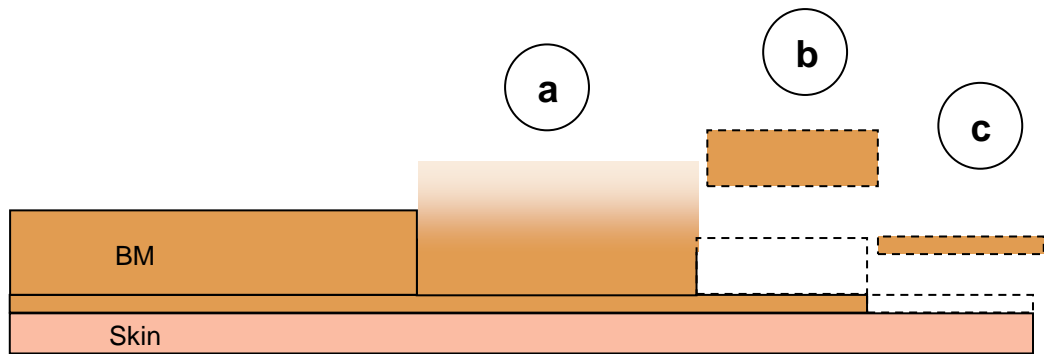


Figure 2.2: Schematic of the three cases of BM removal: a: BM dissolution, b: BM rupture, c: BM washing

- b. BM rupture:** This occurs when the BM cohesiveness is overcome. Hypothetically, shearing forces exerted by the fibres slicing through the BM affect the propensity for rupture. Adhesion forces between the BM and the fibres also have the potential to overcome the BM cohesiveness.
- c. BM washing:** This occurs when the lotion surface tension overcomes the adhesion forces between the BM and the skin and surrounds the BM with a layer of lotion.

Dirt removal happens when the forces attaching the dirt to the surface being wiped are overcome, therefore it is necessary to identify these forces. This attachment highly depends on the physical properties and chemical composition of the removed substance and the surface, thus, the characteristics of both need to be considered.

During wiping, the fibres interact with the BM slurry with the objective of separating it from the skin surface on which it resides. Generally, mechanisms of mechanical removal and capture of substances from surfaces can be achieved using a variety of tools. From a scale-of-magnitude point of view, it happens over a wide spectrum. Tools of mechanical removal vary in size according to the amount of material required to be removed, Figure 2.3. When examining these tools, and considering their dimensions and the mechanisms by which they operate, a basic pattern in their design emerges, which can be replicated at different size scales.



*Figure 2.3: Multiscale Tools for Mechanical Cleaning*

With reference to Figure 2.3, the first group relies on a single cleaning element whereas the other two groups utilise more. The logic behind this is that in the first group the material to be removed tends to be bulky and the objective during cleaning is to overcome substantial inertia and weight by employing sufficient lifting forces. By contrast, the substances to be removed by the second and third groups tend to be spread over the surface and are less bulky. Here, the objective is to achieve physical contact with as many particles as possible when in contact.

The structural geometry of nonwoven fabrics has neither the geometrical features of the cleaning elements in group 1 nor the systematic order of the elements in group 2. To introduce additional cleaning elements in to the structure of the fabric to improve mechanical removal of BM slurry, a systematic approach was followed to produce surface features that could potentially modulate improvements in BM slurry removal, inspired by the cleaning elements summarised in Figure 2.3.

When analysing the dirt removal mechanisms using pre-moistened wipes it is worth distinguishing between two cases. The first case is when the bulk properties of the BM are not significantly changed by the wipe. Here, BM removal is driven mainly by shear and attachment forces between the BM and the wipe. The second case is when the lotion in the wipe significantly changes the properties of the BM, by for example partially dissolving it, and subsequently the dissolved BM in the lotion can be more easily absorbed by the wipe. The two cases may well occur simultaneously during the wiping process.

The attachment of the solid part of baby BM should be analysed. Solids may take the form of particles of various sizes which can be nanometre-scale or as large as a few millimetres. In general, attachment between particles and surfaces can take different forms. These include chemical bonds, physical bonds such as van der Waals forces, capillary forces, electrostatic attraction or mechanical entrapment or interlocking. In the present study, chemical bonds can be excluded due to the chemical nature of BM and skin. It is also suggested that in the presence of a cleaning liquid only van der Waals forces among the various physical bonds need to be taken into consideration (Bardina, 1988).

Analyses of particle adhesion to surfaces have been performed in different disciplines where the process of removing particles from surfaces has been studied. For example, several methods of particle removal have been studied by the microelectronics industry, which are insightful in any investigation of wiping mechanics. Burdick et al. worked on developing and validating a model to predict particle removal from semi-conductor surfaces in which removal is modulated by the influence of a flowing liquid. In the force analysis shown in Figure 2.4 they present the forces acting on a micron scale adhering particle in the presence of an aqueous fluid under laminar flow (Burdick et al., 2005).

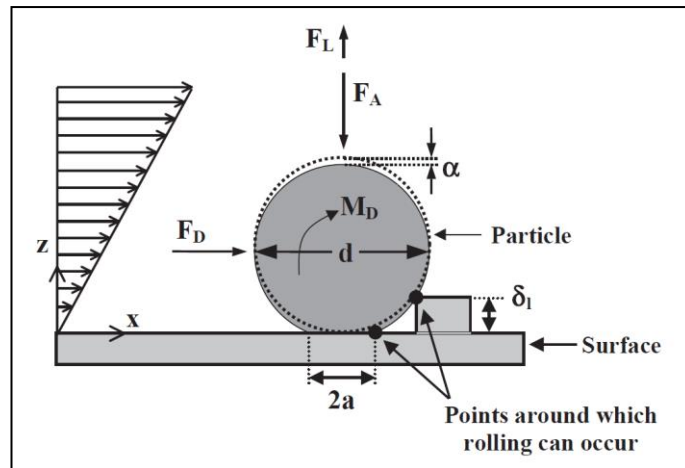


Figure 2.4: Schematic of an adhering particle showing the acting forces  
(Burdick et al., 2005)

The acting forces on this particle can be defined as adhesion ( $F_A$ ), drag ( $F_D$ ), and lift ( $F_L$ ), in addition to the moment of surface stresses ( $M_D$ ). The suggested removal mechanisms are therefore lifting, sliding and rolling. The removal criteria for a particle were defined by the balance of forces between the horizontal direction for sliding and in the vertical direction for lifting. For rolling, the removal criterion was the balance of moments around the rolling point. A theoretical model was built based on this, wherein the model expresses the removal criteria and calculates the particle removal percentage based on several aspects of the system such as geometry, morphology, deformation and fluid flow properties (Burdick et al., 2005).

Although assumptions were made to simplify the system, the model predictions fell within the range of values shown by experimental results. The geometrical and morphological aspects of this model can be well considered in the case of removing baby BM particles from the skin for the purpose of simplification. But when considering deformation and moduli, caution must be taken as the materials and their mechanical properties differ between the two cases. There is however, potential to consider the forces resulting from the fluid flow, i.e. drag force and lift force, as this is due to similarities in the presence of an aqueous fluid and the hydrodynamics of the two systems. This can relate to the aforementioned case of removal mechanism where there is no direct contact between the fibre and the dirt.

Similar efforts have been made by Xu et al. (Xu et al., 2005) who additionally took into consideration the influence of particle size ratio to the thickness of the fluid film on the hydrodynamic drag force. This was facilitated by introducing the concept of a lubrication model. (Xu et al., 2005). It was concluded that the drag force drastically increases as the particle diameter approaches the thickness of the cleaning fluids (Xu et al., 2005, Xu et al., 2004).

Verkouteren et al. (2008) and later Koh (2009) worked on the analysis of particle removal using nonwoven fabrics as wipe substrates. According to their findings, the acting forces on adhering particles are mainly reliant on van der Waals, electrostatic and capillary forces, depending on the wiping environment. They also added a load force, which is applied by the fabric or substrate, and the force of gravity (Verkouteren et al., 2008, Koh, 2009).

The adoption of similar analyses in different disciplines demonstrates their validity and indicates potential as a platform on which to build a model for baby wipe BM removal. It is important, however, to account for the difference in dirt composition between previous work and the present study. All previous studies have investigated the removal of dirt as solid particles, whereas baby BM consists of biological excrement, and although it may contain solid particles, this does not represent the entire mass composition of BM.

Burdick et al. presented a study utilising the critical particle Reynolds number approach to assess the mechanisms of particle removal by hydrodynamic flow. There was a critical ratio of particle size to the surface roughness below which particle removal could not be achieved by hydrodynamic flow. The study was carried out on glass particles adhering to a glass surface in laminar flow. (Burdick et al., 2001). In their later work, (Burdick et al., 2003a), (Burdick et al., 2003b) and (Burdick et al., 2003c), their model was used to assess whether or not hydrodynamic flow is sufficient to remove particles or if contact between the wipe element and the particles is required. It was concluded that physical contact is required for complete particle removal. While these results are relevant to the present research, the simplifying assumptions made by

Burdick et al. and the use of a critical particle Reynolds number are difficult to implement given the complex nature of BM.

Several other studies address the modelling of particle removal from surfaces, (Huang et al., 2011a) and (Huang et al., 2011b) but there is a dearth of studies dealing directly with the influence of the structural parameters of the cleaning element, and the wiping material in particular, on cleaning performance. However, some principles relating to the geometrical shape of wiping elements have been discussed and these are considered further in CHAPTER 6.

Previous studies strongly indicate that surface features and fabric structure characteristics impact the removal efficiency of materials from surfaces (Bahners et al., 2006, Koh, 2009). Scientists in P&G have also acknowledged the importance of surface structure in terms of removing materials from surfaces by specifically designing the surface topography to shear through the material and create mechanical interlocking which improves the removal efficiency. They suggested that introducing raised areas to the surface of the wipe which have adequate stiffness and density should allow higher cleaning efficiency due to higher localized pressure. A concept of geometrically designed raised surfaces featuring a “shovel effect” to act as mini shovels were introduced in his work, Figure 2.5. (Mason, Procter & Gamble Internal Communications).

The mini-shovel idea is in agreement with the theory presented in this section. However, there is little to no evidence as to whether it has a significant influence on wiping efficiency and there is no existing experimental work to confirm its impact in relation to BM slurry removal.

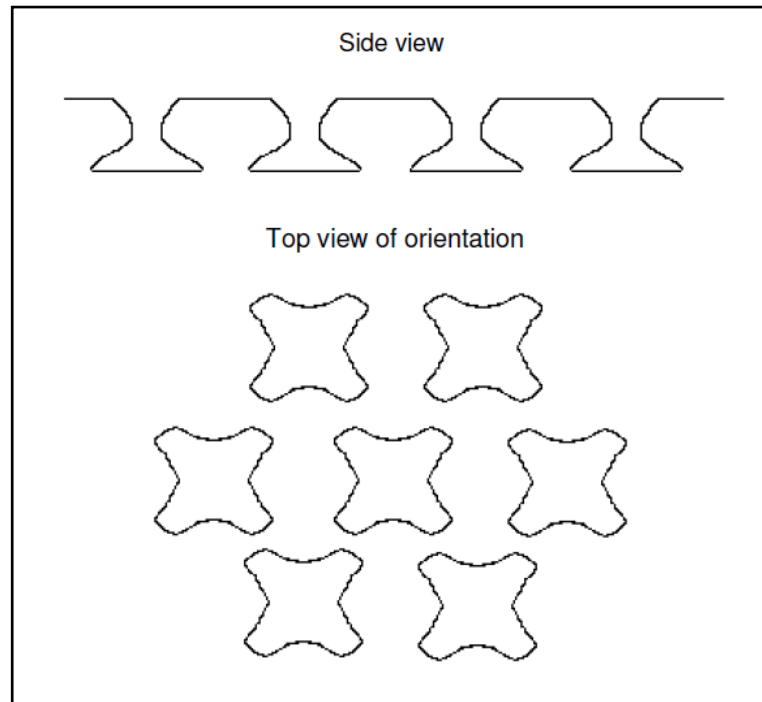


Figure 2.5: Raised surfaces of the wipe designed to maximize the „shovel effect“  
(Mason, Procter & Gamble Internal Communications)

### 2.3.3 Shearing Elements

For a shovel-like fibrous structural feature to shear through the BM slurry, it needs to have a geometry that is sharp enough to allow a smooth penetration yet stiff enough to resist deformation due to the resistance of BM. Geometrical properties include area, depth and shape.

#### 2.3.3.1 Area of Shearing Elements

This parameter refers to the area of a single shearing element in the plane of the fabric (x,y). The upper boundary of this parameter is the minimum distance covered during a single swipe which can also be related to the size of the average fingerprint. For an efficient shearing process, any single swipe must expose the skin surface to at least one complete shearing element. Therefore, the maximum shearing element size was set to be repeated each 5 mm. The lower level of this parameter is limited by the manufacturing process capabilities as well as the largest used fibre diameter. For example, in hydroentanglement, a minimum of 1 mm would be most efficient for a repeated pattern. While in electrospinning, the minimum could be as small as 50 nm.

### **2.3.3.2 *Depth of Shearing Elements***

For the purpose of illustration, Figure 2.6 shows the shearing elements on a broach. The depth of a shearing element represents the length of a tooth on the broach. In the prototypes, the upper level of this parameter is limited by the wipe's thickness. Any design of shearing elements that has a higher depth than the fabric's thickness is likely to be reduced during the wiping process due to the applied pressure. Currently used wipe thicknesses range between 850-1300  $\mu\text{m}$ . The upper level was, therefore, set to 1300  $\mu\text{m}$ .

### **2.3.3.3 *Shape of Shearing Elements***

Material removal in the processes of milling and machining has been extensively studied. Additionally, the studying of abrasive surfaces has been done thoroughly in fields other than wiping and a lot of efforts have been made in modelling and designing of abrasive surfaces. The shape of a cutting tool could be designed for the optimum efficiency. It depends on factors like the tools and materials hardness and moduli and the speed of cutting. The angles of a cutting tool help to manage the removed material and affect the forces required and the removal efficiency. Figure 2.7 explains the angles of a cutting tool. The prototyping process will attempt to introduce shearing elements with defined rake and clearance angles. The nominal rake angle levels will be  $1^\circ$ . The positive rake angle is believed to be more efficient according to (Butler-Smith et al., 2011), but it is more difficult to achieve due to the need of introducing an undercut to the substrate's surface. The clearance angle affects the strength of the shearing element and the removal efficiency. A low clearance angle leads to strong shearing elements but low removal efficiency. Conversely, a high clearance angle leads to weak shearing elements but high removal efficiency. The clearance angle for the prototypes will be set to  $4.5^\circ$  to maintain the strength of the shearing elements.

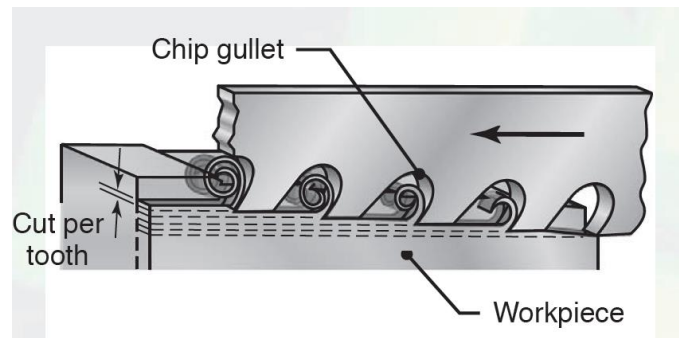


Figure 2.6: a series of shearing elements on a metal cutting tool (broach)(Kalpakjian and Schmid, 2008)

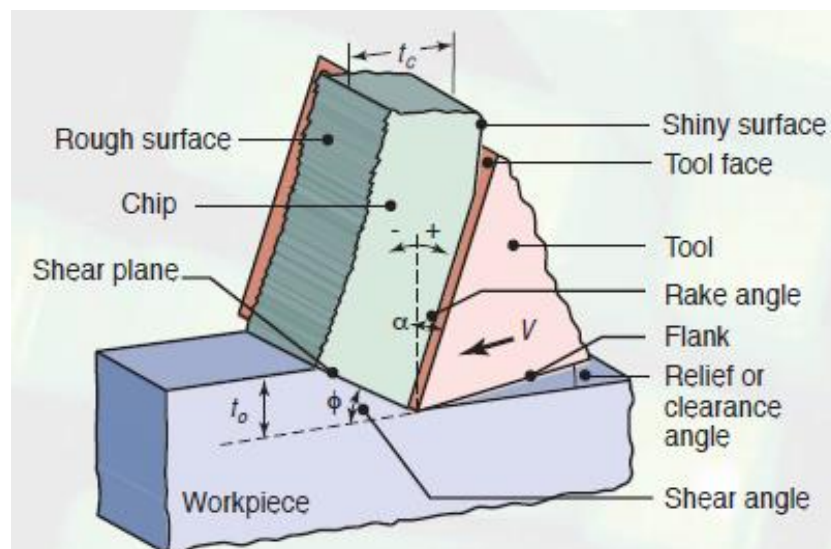


Figure 2.7: Rake angle and relief angle (clearance angle) in metal cutting tools (Kalpakjian and Schmid, 2008)

The angles between the surfaces of the shearing element as well as with the surface of the work piece have a great importance on the performance and cutting efficiency regarding cutting forces and friction (Wang et al., 2012, Ng et al., 2006). The design is precisely chosen in order to efficiently scoop material from the surface of the work piece, minimising energy dissipation and any resistance such as friction. It is possible for such design of a cutting element to be useful to a certain extent when extrapolating the mechanics of this process to a lower level of material moduli and hardness such as the ones of a conventional nonwoven wipe fabric, baby skin and the bowel movement.

#### 2.3.3.4 *Density of Shearing Elements*

The lower level of this parameter is limited by the upper level of the area of the shearing elements. The largest shearing element could have the area of  $25 \text{ mm}^2$  and therefore the minimum number of shearing elements per unit area is  $4 \text{ cm}^{-2}$ . The upper level is limited by the manufacturing process and fibre diameter. For example, in hydroentanglement, the efficient maximum would be  $100 \text{ cm}^{-2}$ , while for electrospinning, the maximum could be  $4 \times 10^{10} \text{ cm}^{-2}$ .

#### 2.3.3.5 *Arrangement of the Shearing Elements*

There are three levels for this parameter, they are shown in Figure 2.8. In the straight arrangement, the elements are ordered in rows and columns, in the offset arrangement, the elements are ordered in columns that have an offset smaller than half of the repetition distance and in the checkers arrangement, the offset of the columns is exactly half of the repetition distance.

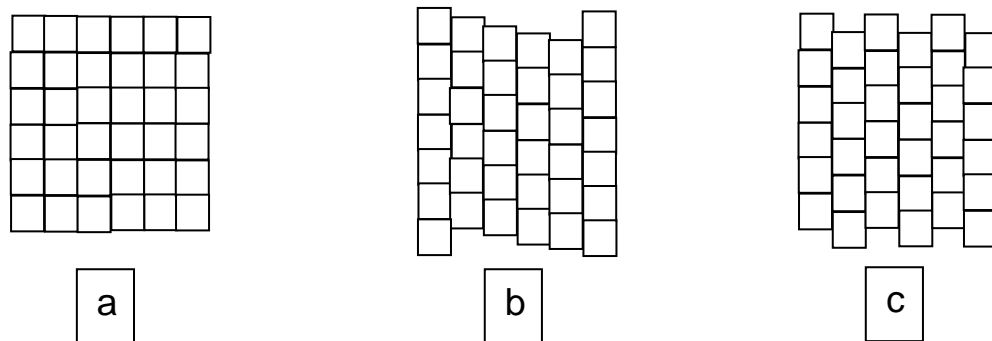


*Figure 2.8: Different arrangements of shearing elements, a) straight alignment, b) offset alignment, c) checkers alignment*

It has been demonstrated that an organised arrangement of abrasive crystals on the surface can lead to a more efficient removal of the surface layers. Using the designed arrangement of micro shearing elements instead of a random distribution also improves the performance, this is utilised in the design of diamond grinding wheels, Figure 2.9 (Butler-Smith et al., 2011).

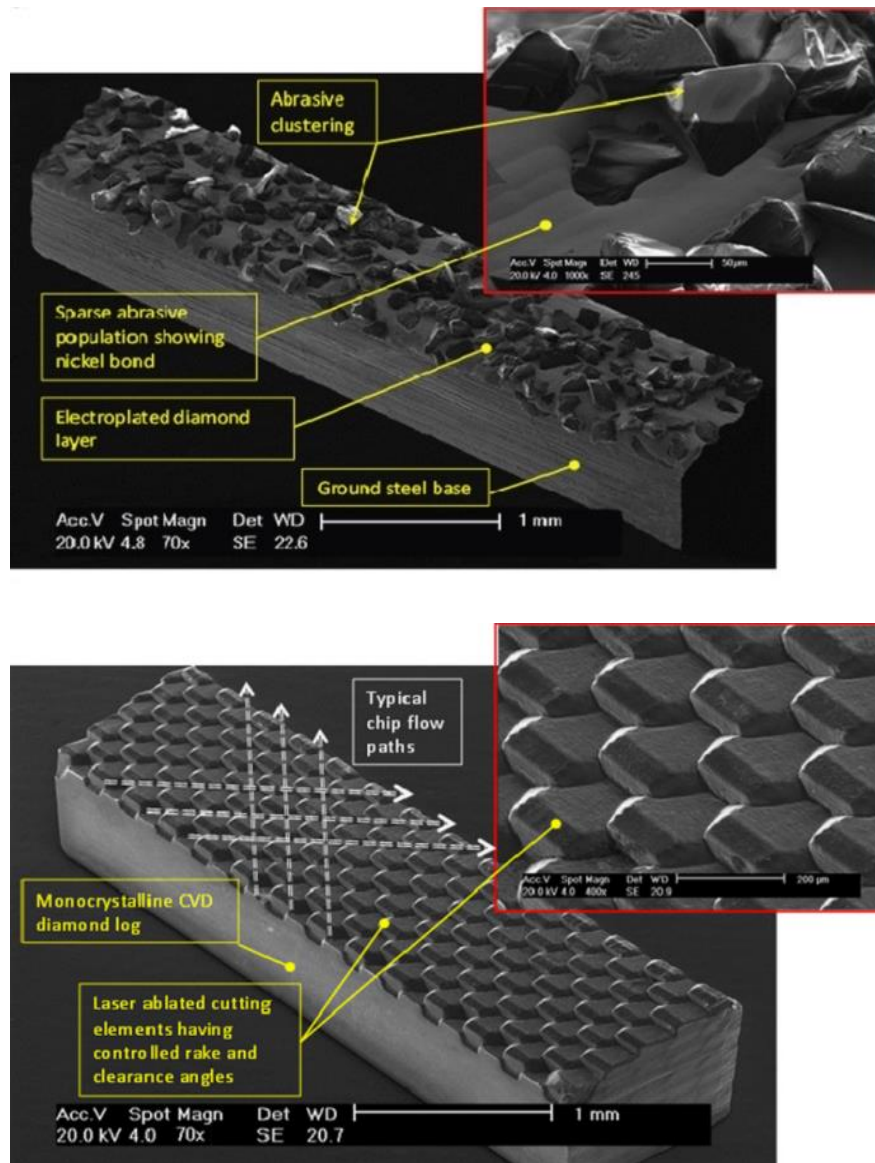


Figure 2.9: Surface of diamond grinding wheels, Top: random arrangement, bottom: ordered micro-arrays (Butler-Smith et al., 2011)

### 2.3.4 Design of the Fabric's Structural Features

An attempt to manufacture one structural design was made using the parameter levels shown in Table 1.

Parameter	Area (mm <sup>2</sup> )	Number per unit area (mm <sup>-2</sup> )	Alignment	Depth (mm)	Rake angle	Clearance angle
Value	1	100	checkers	1	1°	4.5°

Table 1: Design specifications of the fabric's structural features

The same principles of shape and arrangement were used to design a new nonwoven substrate texture using 3D printed moulds.

The shearing element was designed using the software SolidWorks®. Shearing elements' shape (angles), size and arrangement were controlled using the 3D design software. Figure 2.10 shows concept designs of the single shearing element depending on the effective direction. The single direction design was adopted for the prototyping stage as the DCM method uses single directional wiping.

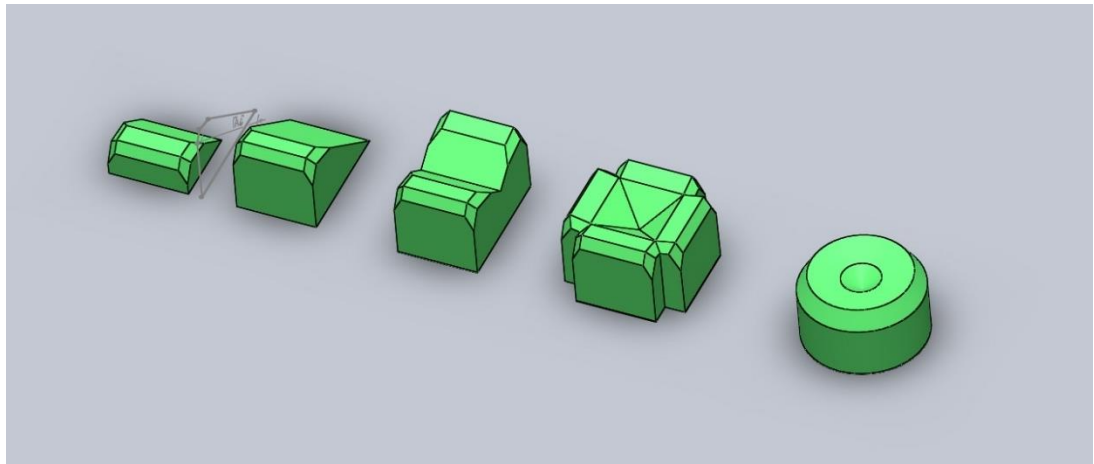


*Figure 2.10: 3D drawing of several designs of the shearing element. From left to right: initial design, shearing element design (single direction), shearing element design (double direction), shearing element design (quadriple direction) and shearing element design (all directions)*

Figure 2.11 shows 2D drawings of the shearing element's sides. Figure 2.12 is a rendered image of a 3D view of the shearing element.

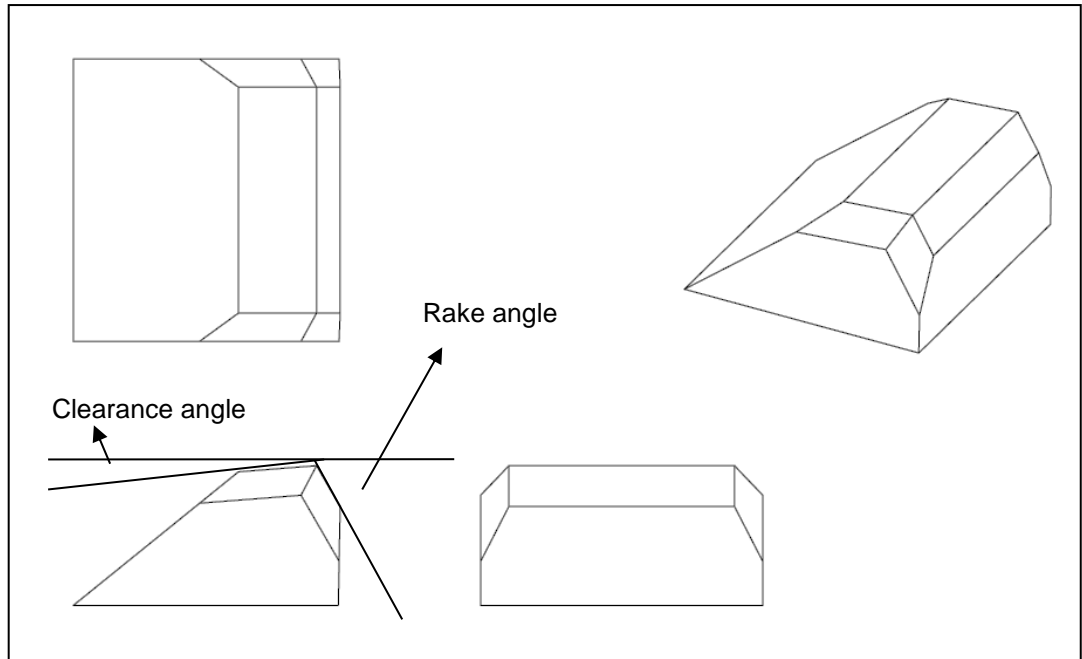


*Figure 2.11: Top, side and front views of the shearing element. The clearance angle and rake angles are shown. They have a great importance on the performance and cutting efficiency regarding cutting forces and friction*

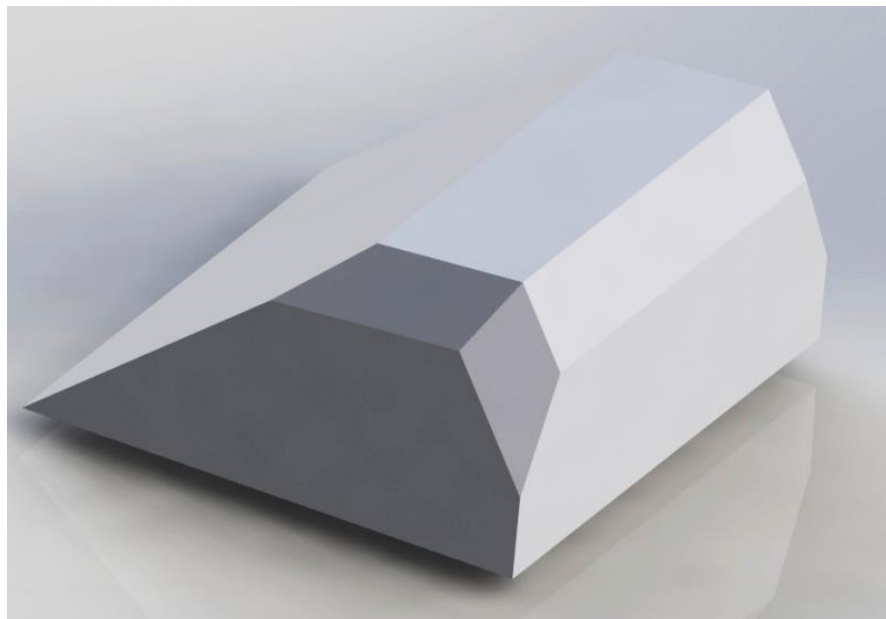


*Figure 2.12: 3D drawing of the single shearing element*

An array of shearing elements was created via the design software SolidWorks® in a checkers arrangement as explained in section 2.3.3.5. The arrangement pattern was repeated over an area equal to the area of a wipe which guaranteed an efficient coverage of the area of interest. Part of the array design is shown in Figure 2.13.

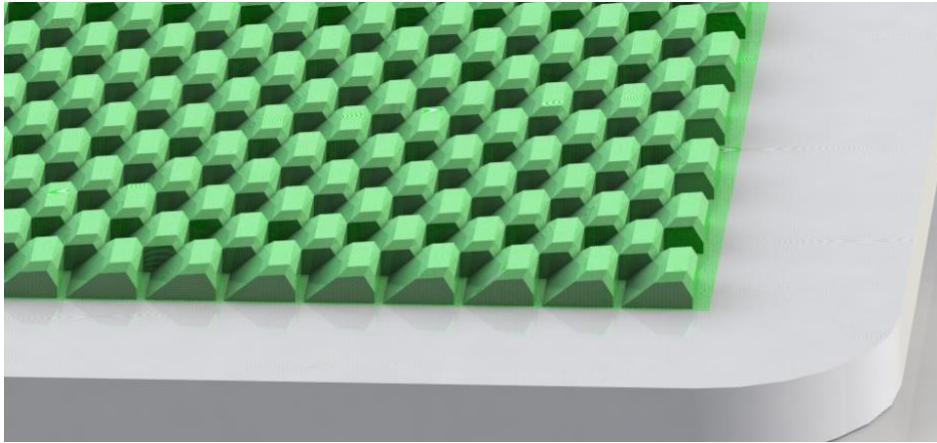


Figure 2.13: An array of repeated shearing elements in checkers arrangement.

### 2.3.5 Capture of BM by a Fabric

After BM removal, it must be captured on the surface of the fabric or within its pore volume. Capture refers to the retention of BM and slurry by the wipe and lotion after separating the wipe from the skin. The suggested situations in which BM capture happens are:

**Slurry absorption:** the soluble or dispersible part of the BM which, together with the lotion, forms the slurry must be absorbed by the wipe. Absorption behaviour is represented by absorption capacity and absorption rate within the timeframe of an average swipe.

Whilst various studies have reported the influence of global fabric porosity on absorptive capacity in nonwovens (Chatterjee, 1985, Mao and Russell, 2008, Chatterjee and Gupta, 2002b, Chatterjee and Gupta, 2002a), there have been no major studies in the public domain focused on BM slurry absorption. The degree to which porosity influences BM slurry absorption, particularly in relation to the absorption kinetics, therefore, remains largely unreported. Given the differences that exist between water and BM slurry in terms of chemistry, rheology and morphology, it is important to understand how absorption behaviour could differ when nonwoven fabrics are brought in to contact with this specific type of fluid medium. Absorption volume has a linear relationship with the square root of time according to Gane et al. for a certain range of pore size and porosities of 60% and 95% (Gane et al., 2004). The

relationship between the weight of absorbed BM slurry and time is therefore addressed in this experiment.

Additionally, the influence of porosity on the gravimetric absorption behaviour of nonwoven wipe samples is systematically investigated. To facilitate this, an experimental methodology was developed to enable real time measurement of slurry weight absorption enabling the studying of absorption kinetics.

Data acquired from consumer studies about the duration of an average single wipe using a baby wipe indicate the time window in which absorption behaviour is most critical to the process of wiping. Between a minimum of 0.39 s and a maximum of 3.10 s, the average wipe duration was shown to be 1.08 s. This means that the first few seconds of contact between the wipe and BM are of high importance.

Bearing in mind the dimensions of an average, commercially-available, wipe, the monitoring of BM absorption behaviour of fabrics within such boundary conditions is challenging using conventional test methods. This necessitated the design of a new experimental approach capable of recording liquid weights in the fabric sensitively enough to distinguish the small changes occurring during BM absorption.

**Particle/bulk entrapment:** the insoluble part of the BM as well as the soluble part that does not dissolve in the lotion due to a lack of lotion or lack of dissolution time must be entrapped within the nonwoven fibre matrix or adhered to its surface.

The capture of BM is relevant to mechanisms of liquid absorption, and capture may also be explained in terms of liquid filtration mechanisms in porous fibrous media. In the specific case of pre-moistened wipes, the capacity to absorb liquids is also influenced by the fact that they are pre-moistened with lotion. However, a baby wipe is generally not pre-moistened to the level of saturation and therefore in theory still has the capacity to absorb additional liquid. Absorbent capacity and rate of absorption are significantly influenced by the porosity as well as the structure and composition of the fabric (Das et al., 2012). Interestingly however, it cannot be assumed that increasing the

absorbent capacity of a baby wipe would improve its performance since it is necessary for the lotion to be partially deposited to deliver skin care substances.

In the scope of understanding dirt capture through filtration theories, liquid filtration efficiency may be relevant to understanding dirt capture efficiency. The efficiency depends on several parameters including dirt particle size, flow rate through the filter medium, fibre diameter and porosity (Dhaniyala and Liu, 2001). Obviously other factors affecting dirt capture may include fibre properties such as fibre surface area per unit volume (Rodman, 1990), surface tension and hydrophobicity of the fluids and solids involved.

Capture mechanisms include sieving, blocked pore capture, particle capture by fibres and particle re-entrainment. The latter two mechanisms are dominated by adhesion forces, which are mainly van der Waals forces. Particle capture by fibres and related mechanisms are extensively addressed in the literature (Grant et al., 1989) and classified in terms of direct interception, inertial impaction, gravitational deposition and diffusional deposition (Shimeta and Jumars, 1991, Yamamoto et al., 2005). However, according to Destephen and Choi gravity is of limited importance in relation to small particles (Destephen and Choi, 1996). Dhaniyala and Liu (Dhaniyala and Liu, 1997) confirmed the importance of the relationship between particle size and pore size distribution in terms of overall capture efficiency (Cieslicki, 1988). It is also possible that the internal structure of the nonwoven fabric, particularly the pore size, can influence the structure of the lotion itself, which is commonly prepared in the form of an emulsion rather than a solution (Bansal et al., 2011).

BM does not only consist of solid particles but also has a liquid phase (Lentner and Pharmaceuticals, 1981, Roe, Procter & Gamble Internal Communications), such that it has the characteristics of a viscous liquid at room temperature. Therefore, liquid absorption behaviour is likely to be an important part of the overall capture mechanism. Fluid transport through porous and fibrous media has been extensively studied (Pan and Gibson, 2006, Pan and Zhong, 2006, Patnaik et al., 2006), particularly in relation to

water and other common fluids from which it is known that the structural properties of fabrics can influence absorption behaviour. (Chatterjee, 1985, Chatterjee and Gupta, 2002a), (Masoodi et al., 2007) (Fan et al., 2007). However, these published studies have not extended to investigating the absorption of BM.

## **2.4 Wiping Evaluation Methods**

There have been substantial efforts to test and evaluate the performance of wipes and the wiping process (Bhattacharjee et al., 1993) (Atterbury et al., 1997) (Bhattacharjee and Paley, 1997) (Bhattacharjee and Paley, 1998) (Oathout and Mattina, 1998) (Diab-Elschahawi et al., 2010) (Shiue et al., 2011). Of these, the most relevant is the research published by Oathout (Oathout, 1999), which concentrated specifically on development of test methods for characterising the performance of nonwoven wipe substrates in both dry and pre-moistened formats.

### **2.4.1 Sled Methods**

In the test method used by Oathout (2000) which was later presented by Chatterjee (2002), the wiping efficiency apparatus consisted of a sled that allows a wipe to be placed beneath it. The wiping mechanism is based on pulling the sled with a certain speed using an electric motor until the sled with the wipe beneath it passes over the contaminated area, Figure 2.14. This method was later adopted by Koh (2009) after adding further modification, particularly in the soil composition and means of measuring the wiping forces.

The sled methods focus mainly on dry wipes intended for the removal of solid or liquid substances (Oathout, 1999, Oathout, 2000, Verkouteren et al., 2008, Koh, 2009). Such methods normally measure the wipe's capability of removing the soil from a surface, whether this soil is dry solid material or liquid. In the case of wet (pre-moistened) wipes, the wiping efficiency test has to be slightly different, because they are required to deposit a volume of liquid on the surface, in this case the skin, and remove the dirt from it. This limits the potential for a gravimetric assessment of cleaning efficiency.

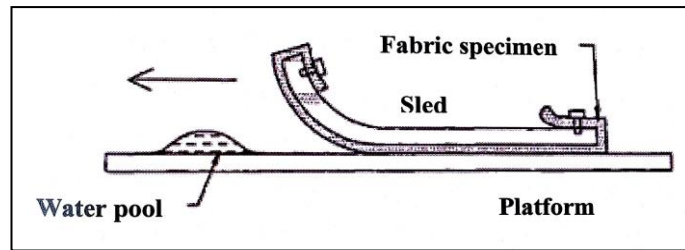


*Figure 2.14: Sled method apparatus  
(Chatterjee, 2002)*

The sled method was designed to assess the dynamic efficiency of fabrics in absorbing liquids and removing particles from a surface. The novelty of this method concerns the inclusion of a linear horizontal movement during the motion of wiping, rather than relying on a static absorbency test. This has allowed comparison of the wiping performance of different paper and nonwoven substrates and introduced a measure of cleaning in terms of the dynamic wiping efficiency at a defined pressure (Memari, 2011).

#### **2.4.2 Rotary Dynamic Cleaning Method (DCM)**

In judging the relevance of the sled method for the study of wiping using baby wipes, it might be worth reflecting on the fashion in which a parent might move their hand while holding the baby wipe. The position of a wipe at the beginning of the wiping process is fairly similar to that simulated in the sled method, and this may also apply as the parent commences the hand movement and until the point of contact between the wipe and the dirty area. At that point, parents tend to avoid the situation where part of the wipe is loaded with MB and yet is still in contact with the baby's skin. Consequently, they tend to twist their hand in a rotational movement taking the dirty part of the wipe away from the skin and thereby presenting clean areas of the wipe surface, and by doing so, they avoid smearing BM on to clean areas of the skin as the wipe is pulled across. As a result of these observations, the Rotary Dynamic Cleaning Method was developed by P&G as an advancement of the standard sled test methodology.

Figure 2.15 is a simplified schematic to explain how the rotational wiping movement functions in the DCM methodology.

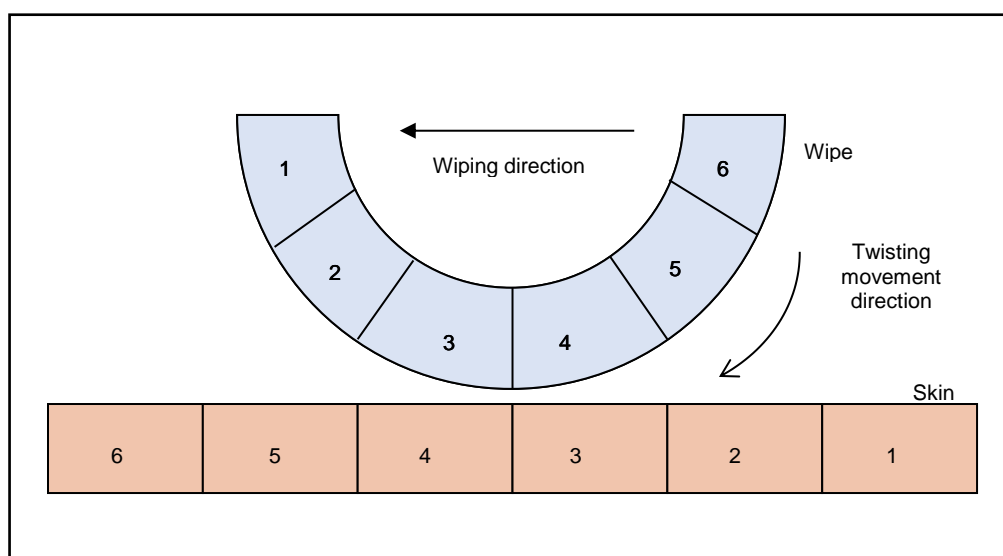


*Figure 2.15: Areas of contact between the wipe and the skin. Matching numbers indicate which area of the skin is wiped by which area of the wipe*

The motivation for developing the DCM approach arose from the desire to introduce a method specifically designed for evaluation of pre-moistened wipe cleaning efficiency. The aspects considered in its design include the nature and design of the wipe as a pre-moistened fabric, the composition of the dirt, which in this case was BM, and the real-world dynamics of the wiping process.

The development of the dynamic cleaning test method (DCM) was specific to the testing of baby wipes. The objective was to create a holistic test method that simulates, to the most reasonable extent, the real wiping process that occurs generally during a baby diaper change. The development of an artificial bowel movement (BM) was also one of the cornerstones on which the development of the dynamic cleaning test method depended. Another cornerstone was the design of a test rig to simulate the dynamics of the wiping process (Memari, 2011).

Dry wipes were tested in the majority of the cases where the sled method has been used, which means any liquid on the contaminated surface would be absorbed into the wipe carrying the solid particles along and thus the likelihood of smearing would be minimised. In the case of pre-moistened

wipes however, the absorption rate can be expected to be markedly lower, increasing the potential for smearing across the surface.

As the wiping process progresses during wiping, and reaches the end a complete separation of the wipe and skin will take place. It is not clear whether this phase is replicated in the sled method as the wipe is always in continuous contact with the surface until the sled is stopped, and then it is manually pulled away.

To simulate the parent's hand movement, overcoming the challenge of smearing, a cylindrically shaped object can be used as the wipe holder. Rotating this cylinder during the wiping process makes sure there will be new and clean areas of the wipe in contact with the test surface. Such a device was reported by Oh (2006) as part of a wiping test apparatus for assessing the efficiency of wipes, see Figure 2.16. The concept of a twisting movement during wiping was also introduced. However, it was not entirely explained in Oh's paper why this mechanism was adopted rather than the sled method.

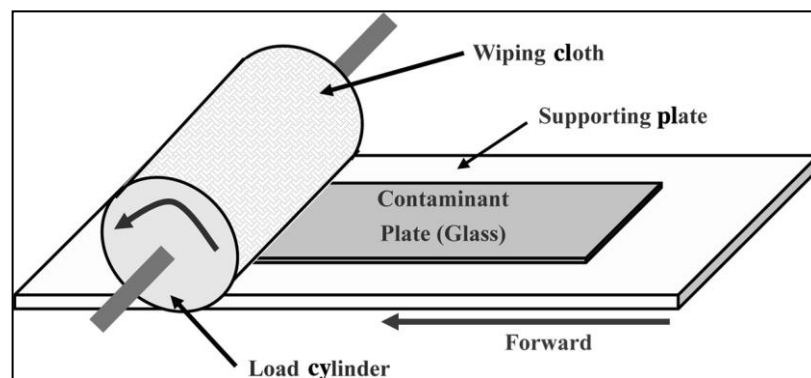


*Figure 2.16: Wiping test apparatus using a rotating cylinder as the wipe holder*

In Figure 2.16, the contaminated plate is the moving part in the apparatus, but this does not influence the dynamics of wiping because the relative motion of the wipe over the surface is the same whether the cylinder is moving or the surface. The surface material used in this method was transparent glass and the dirt or contaminant that was used comprised silicone oils. The dirt was spread on the glass plate and then pushed under the rotating cylinder with the wipe mounted upon it. The wiped glass plate was then placed in a commercial scanner to take an image of the surface and later analysed to obtain the

integrated value of the pixel greyscale values. Addition of carbon black mixed with the silicone oil produced sufficient contrast for it to be detectable by the scanner (Oh, 2006).

The introduction of the rotational movement of the wipe holder in this method brought wipe testing closer to simulating the hand movement of a parent, and therefore more relevant to testing baby wipes. However, it did not completely conform to the requirements of a test method because of the lack of a suitable BM contaminant composition that is easily detected (Memari, 2011). The simulated synthetic BM previously developed by companies such as P&G for in-house evaluation of wipes, was not originally intended for use in wipe test methods such as this, where digital scanning is used to detect residual contaminant levels. In this particular wiping method, the mode of controlling the separation of the wipe from the glass plate was also not clearly elucidated.

The latest DCM method has been developed for the specific purpose of testing baby wipes and was designed to address all the requirements of assessing wiping efficiency. Details of this system, which was developed by the author at P&G have been previously reported (Memari, 2011). The purpose of the DCM rig was mainly to simulate wiping dynamics, particularly the motion and force applied. The DCM involves the use of a moving object on which the wipe is mounted and it automatically performs three types of movement:

1. Horizontal motion when in contact with the surface to be cleaned.
2. Vertical motion, downwards on the approach to the surface to be cleaned and later an upwards motion after pickup.
3. Rotational (twisting) motion around an axis parallel to the surface to be cleaned, and perpendicular to the motion in the horizontal direction.

In addition, there is the ability to apply a force to the surface via the wipe to simulate the hand pressure applied during wiping, and the force is adjustable.

The DCM rig, shown in Figure 2.17, has a moving element, which is a metal cylinder that has the capability of having a variety of pre-moistened wipe sizes wrapped and fixed upon its surface. The DCM is capable of moving the

cleaning element in three different types of motion: linear horizontal, linear vertical and rotational.

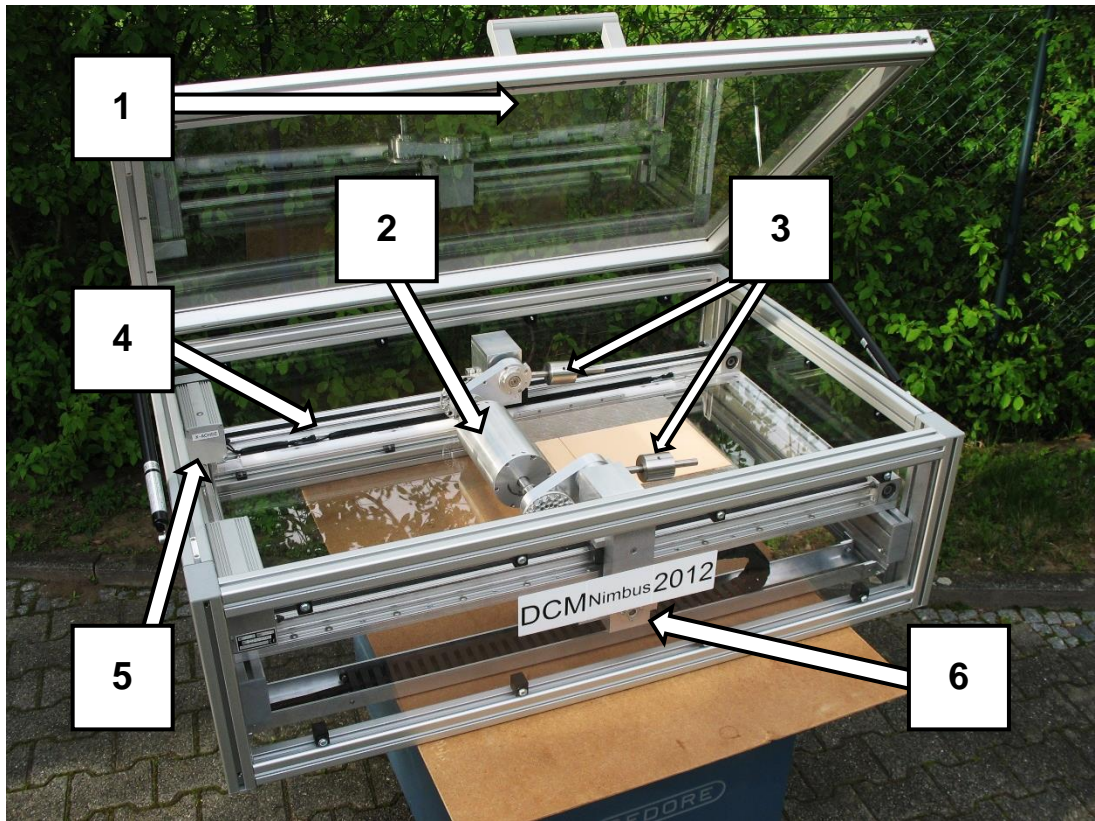


*Figure 2.17: Dynamic Cleaning Method rig used to assess the wiping efficiency. 1: lid, 2: aluminium cylinder to hold the sample, 3: weights to control wiping pressure, 4: rails to guide the cylinder's horizontal motion, 5: servo-motor for linear motion, 6: servo-motor for rotational motion*

The linear horizontal motion is achieved by mounting the cylinder on a bridge that moves on two guiding rails along the length of the machine. Motion is transferred from the servomotor to the bridge by a couple of conveyor belts on each guiding rail on the sides of the machine. Figure 2.18 shows the mechanisms used to achieve this movement.

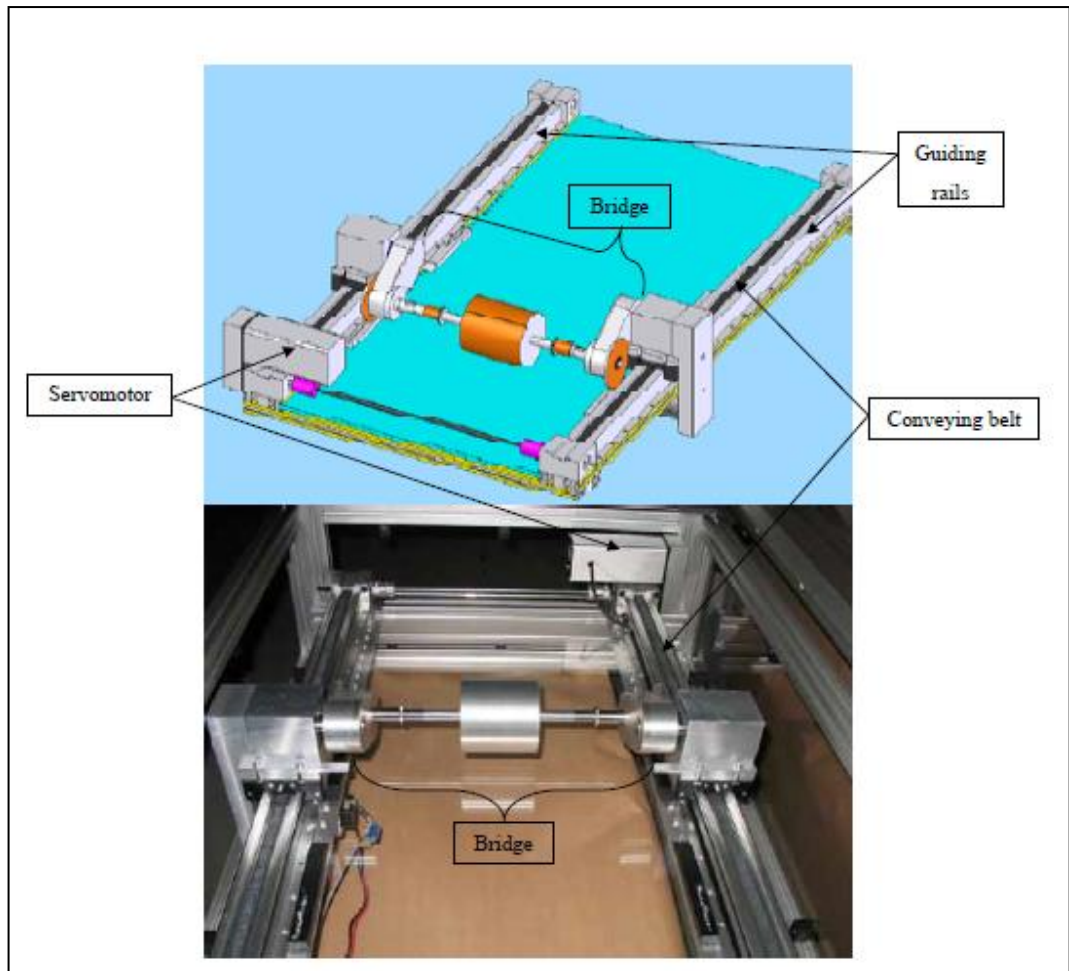


Figure 2.18: DCM linear horizontal motion mechanism

To obtain the linear vertical motion, the bridge is assembled in a way that enables it to freely rotate around an imaginary axis (A), see Figure 2.19, or in other words, the bridge is working like a rotation-free double elbow shaft.

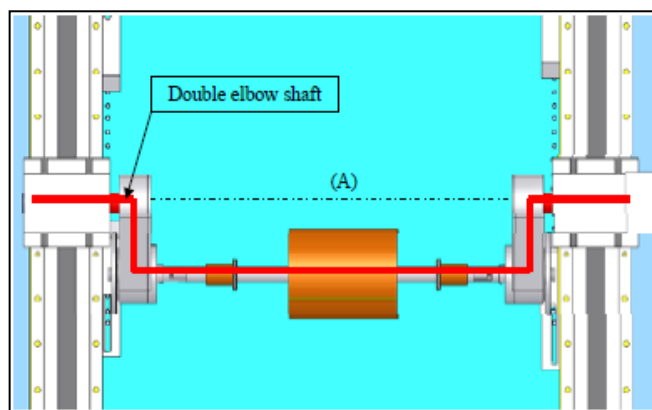
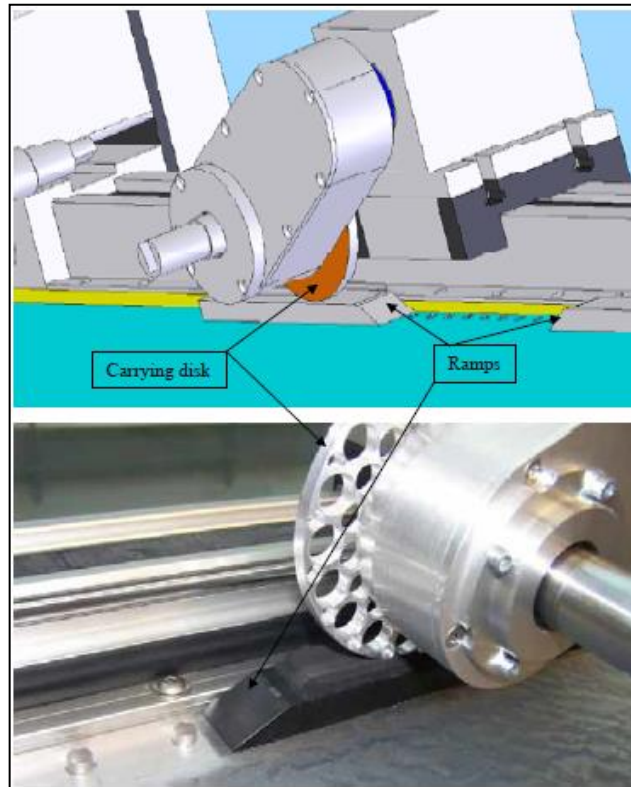


Figure 2.19: Top view of the bridge with the double elbow shaft marked in red

This shaft is carried by two disks, one from each side. The disks roll on special plastic tracks that include ramps, Figure 2.20, like a cam, this way the disks guide the height of the bridge from the base board.



*Figure 2.20: DCM bridge disks and the ramps*

To create the rotational motion of the moving cylinder a second servomotor is mounted on one side of the bridge, so that it moves with it, Figure 2.21.

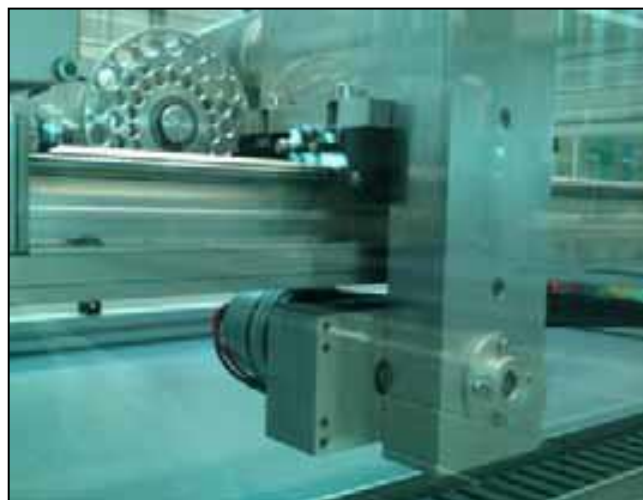


*Figure 2.21: Second servo motor attached to the bridge to provide the rotational movement to the cylinder*

For the wiping pressure control, when the carrying disks roll down the ramps, the cylinder comes in to contact with the sample placed on the base board. Starting from this contact point the pressure that is applied on the sample is determined by the weight of the cylinder. This pressure can be measured by using a spring balance and can be controlled by changing the torque around the axis of the double elbow shaft.

The machine is powered and controlled by an external control unit, which runs a software that allows the operator to adjust the motion parameters.

The motion parameters include the speed of the two servo motors, the positions where to start and stop the motion and the direction of motion.

## **2.5 Artificial Bowel Movement Material**

BM removal and capture by wipes cannot be fully understood without understanding how BM behaves during the wiping process. This requires a good knowledge of BM properties. Relevant properties relate to the chemical composition and the mechanical and rheological behaviour.

### **2.5.1 Chemical Composition of BM**

Faeces are a complex mixture of food residues excreted by the gastrointestinal system. According to Geigy Pharmaceuticals (Lentner and Pharmaceuticals, 1981), the water content of baby BM ranges between 38 – 92 %, and subsequently the dry mass ranges between 8 – 62 %. The dry mass contains organic and inorganic materials. Inorganic content ranges between 4 – 20 % of the dry mass. Inorganic substances found in BM include bicarbonate, chloride, phosphorus, fluoride, iodine, potassium, sodium, calcium, magnesium, iron, copper, manganese, zinc, lead, cadmium, chromium, cobalt, molybdenum, nickel, selenium, titanium, vanadium and tin. Nitrogenous substances include nitrogen, ammonia, urea, amino acids, amines, porphyrins, bilirubin, urobilinogen, purine base nitrogen, protein and enzymes. Non-nitrogenous substances include carbohydrates, organic acids, lipids, total fats, fatty acids, phospholipids and sterols. Other substances such as vitamins, bacteria and blood can also be found (Lentner and

Pharmaceuticals, 1981). The aforementioned substances may be found in the form of mucins, fibre, fats, soaps, short chains fatty acids, bile salts, enzymes, minerals/ions, urea and aromatics (Roe, Procter & Gamble Internal Communications).

Other properties summarized in Geigy Scientific Tables include the relative density ( $d_4^{25} = 1.09$ ), osmolality relative to water in dialysate ranging between 284 - 430 mmol/kg and pH ranging between 4 - 7.5 (Lentner and Pharmaceuticals, 1981).

### **2.5.2 Mechanical and Rheological Properties of BM**

Geigy Scientific classifies BM according to its appearance into three groups: meconium, soft, sticky and homogeneous with a greenish brown to black colour; infant BM, golden yellow with breast feeding, green after prolonged standing and brown for cow milk diets; adult BM is depending on the diet, darker colour with animal diets and lighter with vegetarian diets (Lentner and Pharmaceuticals, 1981). Many efforts have been made to study the structure and consistency of baby BM by scientists at Procter & Gamble, with a view to producing a synthetic substitute suitable to allow laboratory testing of wiping performance, and the most relevant work is summarised in this section.

- Baby BM can be qualitatively classified into four groups according to its consistency and appearance.
- Runny/watery: features high mucus content and presence of curds;
- Soft: similar to pasty but softer;
- Pasty: no defined shape but not mobile under influence of gravity;
- Firm: has a defined shape and notable resistance to deformation.

These consistency groups highly depend on the diet and Figure 2.22 shows the distribution of BM consistencies by diet (Roe et al., Procter & Gamble Internal Communications).

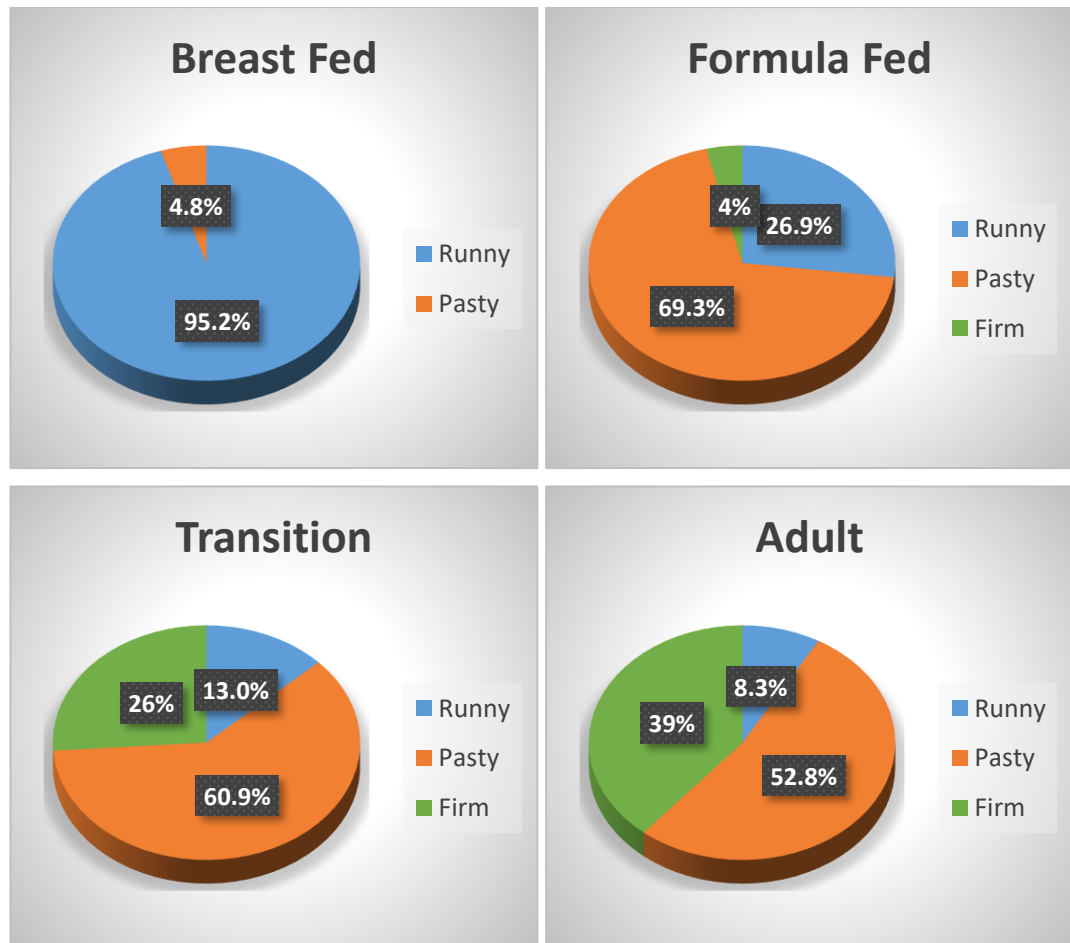


Figure 2.22: Distribution of BM consistencies by diet. Charts reproduced from P&G private communications

(Roe et al., Procter & Gamble Internal Communications)

BM consistency depends on its water content. However, it is possible that BMs of different consistency can have similar total water contents. Apparently, the way in which the water content is held within the material can vary in these visually distinct types of BM. The composition of BM for different diets and stages of baby development suggests that water can be either free, associated with bound water, bound, or entrapped in bacteria. Mucus is another water binding medium. Osmotic effect is one of the key water binding mechanisms in BM and is driven by polysaccharide content and other ionic species (Roe et al., Procter & Gamble Internal Communications, Holmes, 1986).

The water loss rate in drying experiments is significantly higher for watery BMs (including the diarrhea cases) versus runny/soft/pasty/firm BMs at the same

absolute water content (e.g., 25%). This is further evidence of differences in internal structure for the various BM types. The solids in watery BM are less structured than in the other types. Many runny BMs exhibit a lower water loss rate at a given water content than some pasty BMs, providing evidence in support of a hypothesized higher biopolymer content in these BMs (Roe et al., Procter & Gamble Internal Communications).

Understanding the behaviour of BM requires not only considering the structure and consistency, but also the mechanical properties, such as hardness, elasticity and viscosity. BM hardness is one of the main mechanical properties to consider. It can be measured by texture profile analysis (TPA). TPA hardness measures the relative stiffness of the BM (the peak force measured during the penetration of a 12.5 mm diameter spherical probe into the BM sample to a depth of 5 mm) and is a standard measure in the foods industry (Friedman et al., 1963, Bourne, 1968, Rosenthal, 2010). Baby BM has a wide range of hardness values from less than 10 g to more than 3000 g. Elastic recovery is the tendency of a material to recover from its deformation after an applied stress is removed. The majority of BMs have an elastic recovery between 60 – 80 % (Qin, Procter & Gamble Internal Communications, Roe et al., Procter & Gamble Internal Communications). The complex modulus of BM correlates to its hardness and consistency, but not necessarily to its water content. It is relatively low for runny BMs and increases towards firmer consistencies up to  $118 \cdot 10^3$  Pa. BMs are non-Newtonian substances, they demonstrate a high rate of shear thinning. Their zero-viscosity values range between  $<10^4 - 10^{11}$  cP. Rate index ranges between 0.05 – 0.21 and consistency index between  $<10^4 - 10^7$  cP.sec<sup>-1</sup> (Roe et al., Procter & Gamble Internal Communications). Table 2 summarizes BM properties including TPA stickiness and pH values, as reported by Procter & Gamble.

Property	Water content (%)	Hardness (g)	Elastic Recovery (%)	Complex Modulus (Pa)	Zero Viscosity (cP)	Rate Index	TPA Stickiness (g)	pH
Minimum	38	<10	60	$< 4 \times 10^3$	$< 10^4$	0.05	30	4.4
Maximum	92	>3000	80	$118 \times 10^3$	$10^{11}$	0.21	60	8.5

*Table 2: Baby Bowel Movement (BM) Properties*

Knowing these properties is essential to understand BM dynamic behaviour during the wiping process. Furthermore, this data also helps to define boundary conditions for the removal and capture of BM once a cleaning model has been proposed.

### **2.5.3 Preparation of Artificial BM**

It was essential to prepare a simulated BM material that could be safely used for experimental study. Real baby bowel movement is not suitable for this task for several reasons. It has a high variability in its mechanical, chemical and physical properties due to its dependence on diet, stage of growth and health conditions. An artificial bowel movement developed at P&G was adopted for use in this research, which comprises ubiquitous raw materials derived from vegetables, fats, water, yeast and yeast products, citric acid and preservatives.

The preparation procedure for artificial BM consists of three main stages. In the first stage, the solid part is prepared. This is done by mixing vegetable powder, fats and fat soaps together with yeast and yeast products. The product of this stage is a dry powder mix, the exact proportions and compositions were not provided by P&G due to the sensitivity of the information. In the second stage, the liquid part is prepared. 90% of the liquid's weight is water, whereas other ingredients or additives may be viscosity and consistency modifiers, citric acid and preservatives. This forms the solution which during the last stage is mixed with the powder and steam cooked for 40 min and then allowed to cool down in room temperature.

The nature of the artificial BM's ingredients and preparation makes it acceptably similar to real BM. The chemical composition resembles that resulting from an average diet digestive system of babies. The mechanical and rheological properties have been tested and confirmed to be relevant to real BM in an earlier study (Memari, 2011). Figure 2.23 shows a diagram of a dynamic mechanical analysis (DMA) test comparing the shear storage modulus of the artificial BM with several samples of BM plotted against the shear stress (Qin, Procter & Gamble Internal Communications).

As the BM composition and structure varies according to diet, age and health condition, it is important to have artificial BM properties that is representative of the real range. The artificial BM preparation method can be modified to achieve certain texture and consistencies, these two properties can be significantly influenced by the proportion of solution in the composition.

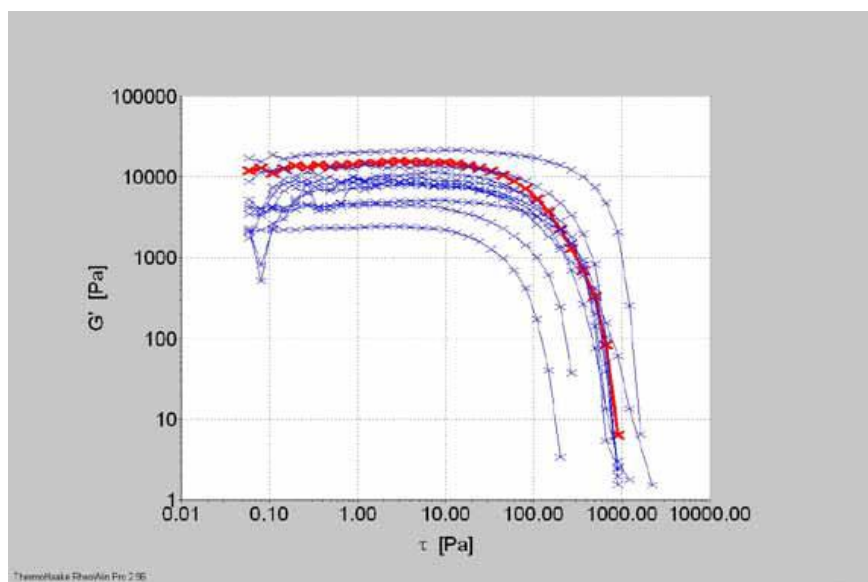


*Figure 2.23: Comparison of shear storage modulus vs. shear stress curves for artificial BM and real BM obtained by Dynamic mechanical analysis (DMA). Red curve: artificial BM, Blue curves: real BM samples. (Qin, Procter & Gamble Internal Communications)*

One of the most important advantages of artificial BM is its ability to be detected using conventional analytical methods. Vegetable powders and yeast are fluorescent when excited by ultraviolet light, which makes them visible when examined under fluorescence imaging systems or microscopes. They are also a source of Adenosine Triphosphate (ATP), which makes them detectable by conventional ATP concentration measurement devices. These are typically used by food and cleanroom industries to detect levels of contamination on surfaces. The natural colour of artificial BM is similar to real BM and gives a relatively good contrast with the surface of a baby wipe, making it convenient to examine using light microscopy.

The artificial BM was prepared from 65% aqueous solution and 35% of solid BM powder. The artificial BM powder mix was prepared and supplied by P&G's analytical laboratories in Cincinnati, USA. After thorough mixing of the

powder and the distilled-water-based solution, the formulation is steam cooked for 40 min at 100 °C and then left on the counter to cool down at room temperature. Once at room temperature, the artificial BM was ready for use. For the absorption experiments, the artificial BM was mixed with baby wipe lotion at a weight ratio of 1:1 to form the BM slurry, wherein the proprietary aqueous-based lotion was supplied by P&G (Pampers® Sensitive lotion).

## **2.6 Skin Biology, Structure and Morphology**

In the wiping process, the skin is the surface being wiped. Understanding skin properties is therefore part of understanding the whole process. Skin properties of most relevance are the mechanical properties, surface topography and surface chemistry. The skin is composed of three main layers, the epidermis, the fibrous dermis and the hypodermis, in other references they may be called epidermis, dermis and subcutaneous tissue (Reiger, 2000). Protection from the environment is the task of the epidermis and mainly the outermost layer of it, namely the stratum corneum. The mechanical resistance of the skin is mainly dominated by the fibrous dermis and hypodermis (Escoffier et al., 1989).

### **2.6.1 Skin's Mechanical Properties**

The mechanical properties of the *in vivo* dermis has been measured by many scientists (Agache et al., 1980) (Bader and Bowker, 1983) (Escoffier et al., 1989) (Makhsous and Lin, 2009) (Berardesca, 2001) (Visscher et al., 2009) (Koenig et al., 2013) (Sandford et al., 2013).

There are many methods of testing the mechanical properties of the skin such as suction and indentation, Table 3.

method	Modulus [MPa]	test region
tensile	$E_{\parallel} = 20$	leg
	$E_{\perp} = 4.6$	leg
torsion	$E = 0.42$	dorsal forearm (<30 yr)
	$E = 0.85$	dorsal forearm (>30 yr)
	$E = 1.12$	ventral forearm
suction	$E = 0.13-0.26$	various anatomical sites
indentation	$E = 1.99 \cdot 10^{-3}$	male thigh
	$E = 1.51 \cdot 10^{-3}$	male forearm
	$E = 1.09 \cdot 10^{-3}$	female forearm

*Table 3: Summary of in vivo Young's moduli of human skin (Hendriks, 2005)*

## 2.6.2 Surface Morphology

Cell margins are often difficult to see as adjacent cells appear to merge because of their close apposition. Consequently, desmosomal contacts are only occasionally visible at the cell margins. Mean cell size (horizontal diameter across the centre of the cell) in surface biopsies from normal skin has been found to be about 45µm (Dawber et al., 1972).

The outermost layer of the epidermis is the stratum corneum, which is the top layer of human skin and therefore is the surface which would be in direct contact with BM and the wipe. It is normally comprised of several layers of mature corneocytes and its thickness is roughly 10 – 25 µm in most body sites. Corneocytes are normally hexagonal and their thickness ranges between 0.3 – 0.8 µm and their diameter ranges between 30 – 35 µm. The corneocytes are linked with each other by intercellular lipids and corneodesmosomes. These linkages degrade with time and the fully mature corneocyte separates from the stratum corneum as it reaches the skin surface (Levi, 2009, Kolarsick et al., 2011). This is the process with which the epidermis renews its stratum corneum structure, Figure 2.24 shows a schematic of this process.

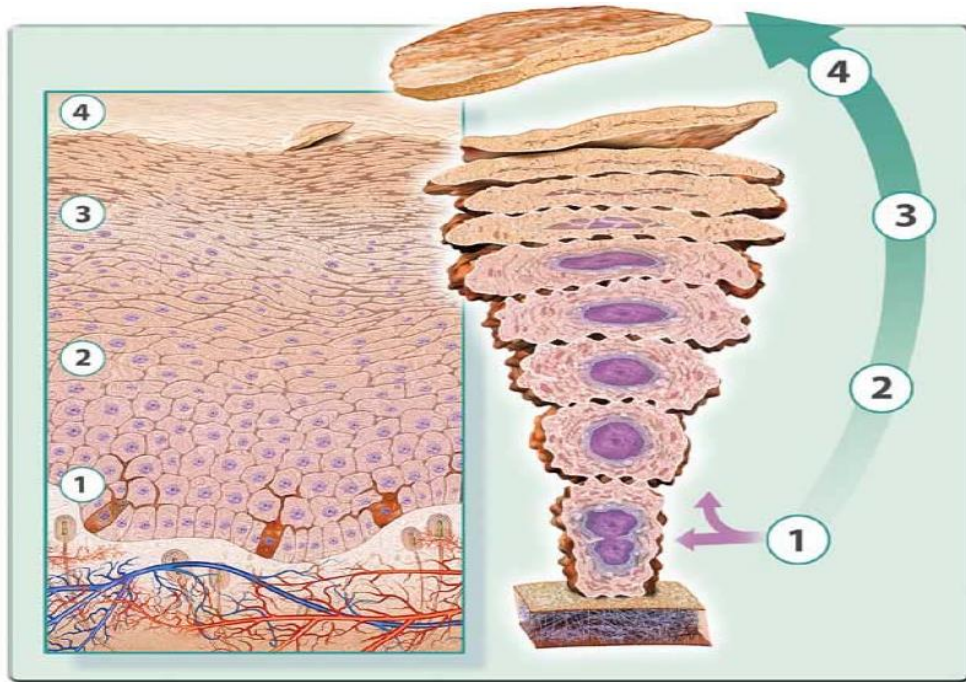


Figure 2.24: Schematic of the cross section of stratum corneum. The process of corneocyte renewal (Levi, 2009)

### 2.6.3 Surface Chemistry

The surface of the skin is made of fully matured keratinocytes (corneocytes). The cell envelope (cell membrane) consists of lipids. The intercellular lipids that are found between the corneocytes are a major contributor to the skin's resistance to water transport. This makes the stratum corneum the most water-resistant layer of the skin. However, water in the stratum corneum is in dynamic equilibrium with that in the other epidermal layers and that in the environment (dermatology.about.com, 2013). The composition of the skin's outermost layer leads to the hypothesis that it is hydrophobic, however water exchange can still happen between the skin and the environment to maintain the dynamic equilibrium. This means the skin maybe considered water absorbent or permeable and in sometimes water excreting, this depends on the direction of water transport. Besides loose corneocytes, which are released with a rate of about 1300 corneocytes per square centimetre per hour on the surface of the skin, other substances are present, such as sebum, sweat and bacteria.

## 2.7 Summary

In this chapter, the mechanics of wiping and the mechanisms of dirt removal and dirt capture are reviewed in relation to the cleaning of human skin contaminated with BM. This provides an essential platform on which hypotheses and an experimental plan can be developed for the assessment of BM removal from skin-like surfaces. The necessary knowledge about baby BM, skin composition and properties has also been established. Furthermore, the development of a method to test the dynamic wiping efficiency has been made by the author in earlier work in the form of the DCM. This test method is an essential tool for the rest of the experimental work presented herein. It is recognised that the DCM is also a method that could be further refined and improved. In particular, the way in which the BM is applied onto skin remains operator dependent and thus, is a potential source of experimental error. A modified approach is therefore required to improve robustness. A new way of BM application that eliminates the operator dependence and improves the method's sensitivity is important. Additionally, to enable experimental work, it is necessary to prepare prototype baby wipe fabric structures based on a knowledge of current wipe substrates relevant to industry.

# CHAPTER 3

## Materials and Methodology

This chapter describes the main definitions, raw materials and approaches used in the experimental chapters that follow. Specific experimental conditions and characterisation methods are reported in each experimental chapter, where required.

### 3.1 Manufacture of Nonwoven Fabric Samples

The manufacture of wipes samples for the experiments presented in this thesis was done using certain material properties and process parameters which aimed to achieve the production of prototypes comparable to the market-leading baby wipes product, namely Pampers® Sensitive. The manufactured nonwoven fabrics were, therefore, dry-laid (parallel carded) and hydroentangled. Further details of the properties and parameters are presented in the following sections (3.1.1 to 3.1.4).

#### 3.1.1 Fibre Opening and Blending

The fibre selection and blend ratios were chosen to match those of the control sample, a nonwoven substrate used to make the P&G commercial product (Pampers® Baby Wipes Sensitive). The blend used to prepare experimental samples consisted of 60% by weight of 1.0 dtex, 38 mm trilobal polypropylene fibres (supplier: FiberVisions Corporation); 20% by weight of 3.3 dtex trilobal polypropylene fibres (supplier: FiberVisions Corporation); 20 % by weight of 1.7 dtex viscose fibres (supplier: Lenzing Aktiengesellschaft).

Fibres were conditioned and weighed. The fibre types were then independently run through a 0.5m wide single cylinder Fearnought opening line, feeding a blending bin. Each of the opened fibre types was then divided into four quarters. Inside a large plastic tub, one quarter from each of the three fibre types was manually and homogeneously distributed over the base area of the tub. This eventually made a sandwich of three horizontal layers, each layer of a different fibre type. The other three quarters of each fibre type were

spread similarly to make three more sandwiches lying over the first one as shown in Figure 3.1. The layers were then manually mixed in a vertical fashion until a homogeneous mix was achieved. The mixed fibres were then fed to the fibre opener to ensure thorough blending was achieved prior to carding and fabric formation.

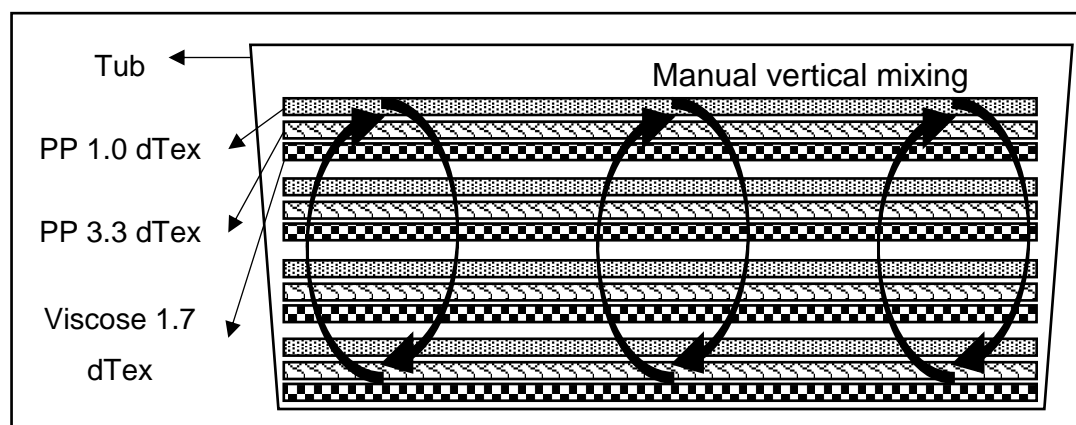


*Figure 3.1: Manual mixing of the fibre types in preparation for the blending phase. The fibres were laid over each other to make four equal sandwiches of the three fibre types. They were then mixed manually in a vertical fashion*

### **3.1.2 Carding and Web Formation**

Carding was initially used to further homogenise the blend. The whole amount of fibre blend was run through the card twice before the batts with defined weights were produced. After the first blending run, the batt was turned 90° and then fed into the card for the second blending run, this resulted in swapping MD and CD between the two runs which improves the blending efficiency and subsequently the homogeneity of the samples. Fibres were converted into parallel laid webs using a 0.5 m single cylinder card operating with three worker-stripper pairings and a single doffer. Lengths of 0.6 m webs were produced at a nominal basis weight of  $60 \pm 1 \text{ g.m}^{-2}$ , which yielded  $56 \text{ g.m}^{-2}$  after hydroentanglement to reproduce the value of the commercial control sample. The weights, areas and resulting basis weights of the batts are shown in Table 4.

Feed weight (g)	Batt area (m <sup>2</sup> )	Batt weight (g)	Basis weight (g.m <sup>-2</sup> )
19.5	0.3025	19.2	63.47
19.0	0.3025	18.0	59.50
18.8	0.3025	18.4	60.83
19.0	0.3025	18.4	60.83
18.9	0.3025	18.5	61.16
19.0	0.2915	18.5	63.46
18.8	0.3025	18.5	61.16
18.7	0.3025	18.2	60.17
19.0	0.3025	17.5	57.85
19.0	0.2964	18.3	61.74
19.0	0.3024	18.1	59.85
19.0	0.2912	17.3	59.41
19.2	0.2916	17.5	60.01
19.0	0.2915	17.2	59.01
19.4	0.3078	18.3	59.45
20.6	0.3360	20.0	59.52
20.5	0.3186	20.0	62.77
20.6	0.3240	19.1	58.95
20.6	0.3348	19.4	57.95

*Table 4: Resulting area, weight and basis weight of the carded batts*

### 3.1.3 Hydroentanglement and Pattern Application

Fibre bonding was achieved by hydroentanglement on a 0.5m wide Hydrolace pilot machine. Two groups of fabric were produced: plain and patterned. The carded web was passed first under a continuous curtain of water for pre-wetting on the woven conveyor belt and then subjected to alternate (face and back) hydroentanglement at a pressure of 40 bar to increase bonding. The hydroentanglement process for the plain and patterned fabrics is illustrated in Figure 3.2. For the patterned fabrics, screening meshes were applied to the conveyor to modify the texture and structure of the pre-bonded fabric samples. The conveyor speed was  $3 \text{ m}\cdot\text{min}^{-1}$ , the nozzle diameter was  $120 \mu\text{m}$  and the total specific energy was  $2.6 \text{ MJ/kg}$  throughout.

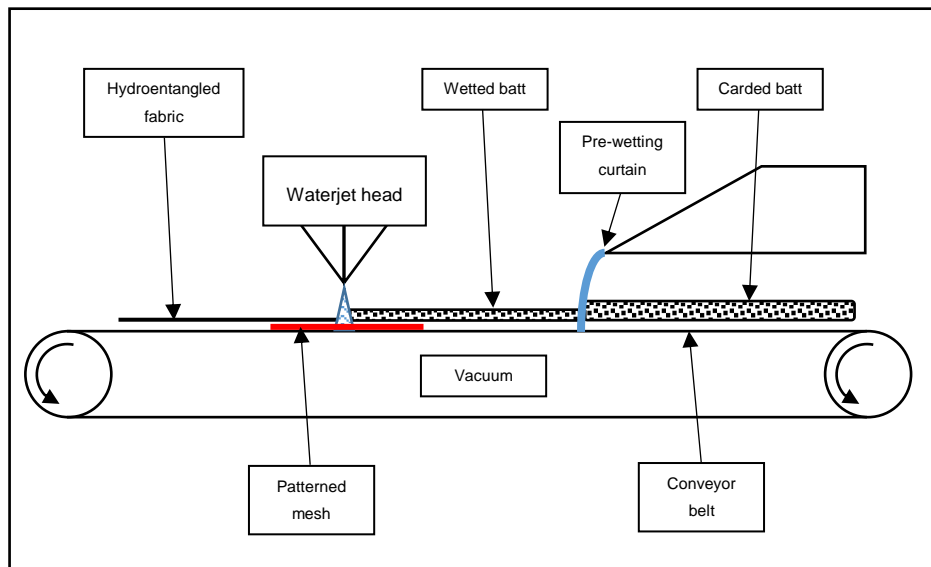


*Figure 3.2: Diagram of the hydroentanglement process for the preparation of fabric prototypes. Carded batts are pre-wetted then passed under the waterjet to produce the hydroentangled fabrics. During this process, a patterned mesh could be placed under the batts to imprint the pattern onto the fabrics*

Structural texture and surface features can be introduced in to hydroentangled fabrics using different techniques. Hydro-embossing is one of the most well-known methods in relation to wipes, and has been used for decades (Smith, 1971, Walton et al., 2010). Introducing such features during hydroentanglement to modulate wiping performance has been reported previously by various workers (Koh, 2009), (GKD, 2017, Saueressig, 2017). To introduce surface texture, apertures and combinations thereof, woven

polymer wire-meshes are routinely used by industry to introduce apertures and corrugated patterns in hydroentangled fabrics. Such wire meshes can be laid on top of webs or more usually, they are used underneath as a support conveyor. When the web supported by the mesh passes under the water jets, the interaction between the water, fibre and metal wire causes rearrangement of fibre segments, modulated by the design of the mesh. In this research, woven polymer wire-meshes were utilised supplied by GKD (Gebr. Kufferath AG, Dueren, Germany).

A control sample was prepared with no substantial texture or pattern. The web for the control sample was pre-wetted and then hydroentangled at a pressure of 40 bar, in an alternating water jet profile. All other hydroentangling conditions were as reported in section 3.1.

An apertured fabric was produced using a wire mesh with relatively large knuckles in the surface (Figure 3.3, GKD item no. 40565800). This was a plain woven, linear screen type 800, made of polyester (both warp and weft) with a wire diameter of 0.80 mm (both warp and weft) and thread count of 6.1 thread/cm (both warp and weft). To manufacture the fabric, the water jet pressure in pre-entanglement was 40 bar and for structuring, it was 60 bar.

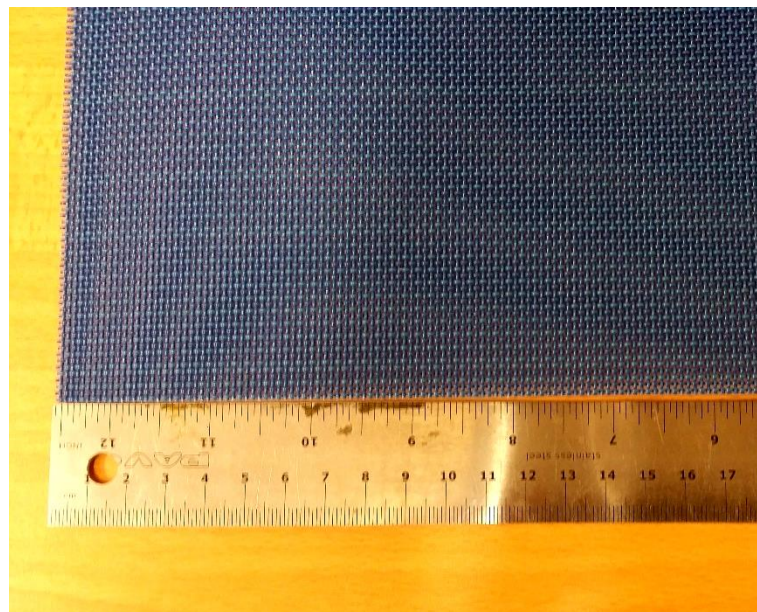


*Figure 3.3: Mesh used for the production of the apertured fabric. Manufacturer: GKD - Gebr. Kufferath AG, Dueren, Germany. Item ref. no. 40565800*

A fabric with a corrugated surface was produced using a different wire mesh. It had lower thread count, both warp and weft, and its topography was not as prominent as the one used for aperture. This was a GKD belt (no. 40560820), (Figure 3.4), with a plain woven linear screen type 3000, made of polyester (both warp and weft) and with a wire diameter of 1.00 mm (both warp and weft), a thread count of 2.7 thread/cm in the warp and 2.5 thread/cm in the weft. The water jet pressure used for pre-wetting and for structuring, was 40 bar.

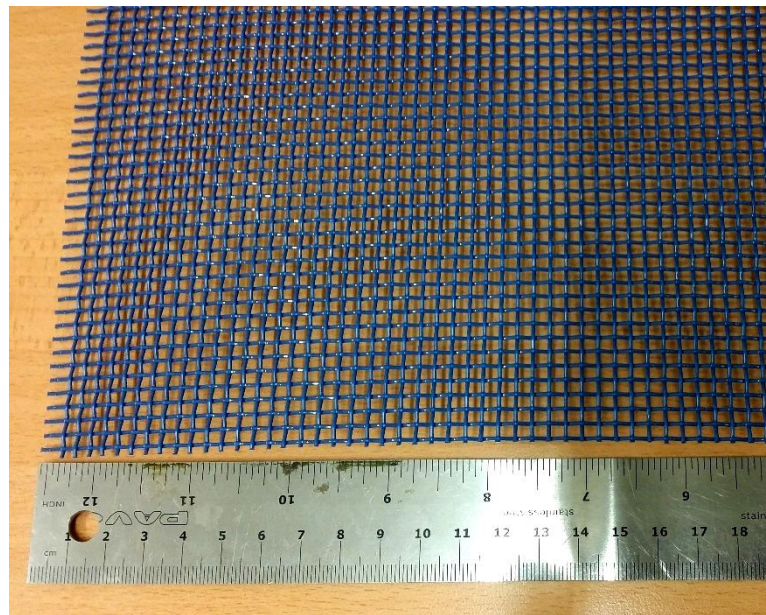


*Figure 3.4: Screening wire mesh used to make deep corrugations in the fabric.  
Manufacturer: GKD - Gebr. Kufferath AG, Dueren, Germany. Item ref. no.  
40560820*

Water jets were applied on the same side of the web in both the pre-entanglement, and structuring stages. The screening mesh was placed on the conveyor.

#### **3.1.4 Drying and Cutting:**

The hydroentangled fabrics were then placed in an electrically heated, 0.5m wide Spooner through-air drying oven for 20 min at a temperature of 75 °C. Wipes of 10 cm x 20 cm were cut and stored in sealable plastic bags for subsequent study.

## 3.2 Fabric Porosity

The manufactured fabrics had an average porosity of 95.6% as calculated using equation 3.1 (Chatterjee and Gupta, 2002a).

$$\phi = 1 - \frac{\rho_{bulk}}{\rho} \quad 3.1$$

Where  $\phi$  is the fabric porosity.  $\rho$  is the fibre density and is obtained from the manufacturer.  $\rho_{bulk}$  is the fabric density and is calculated from equation 3.2.

$$\rho_{bulk} = \frac{m_{bulk}}{V_{bulk}} \quad 3.2$$

Where  $m_{bulk}$  is the fabric mass.  $V_{bulk}$  is the fabric volume and is calculated from equation 3.3.

$$V_{bulk} = A_{bulk} \times h_{bulk} \quad 3.3$$

Where  $A_{bulk}$  is the fabric area.  $h_{bulk}$  is the fabric thickness. The fabric thickness was measured using Shirley Thickness Measurer and the standard EDANA method NWSP 120.6.R0 (15) (EDANA and INDA, 2015).

Randomly selected samples from the prototype fabric were compressed using a hydraulic press in order to change their thickness and subsequently their porosity. The compression setup is shown in Figure 3.5.

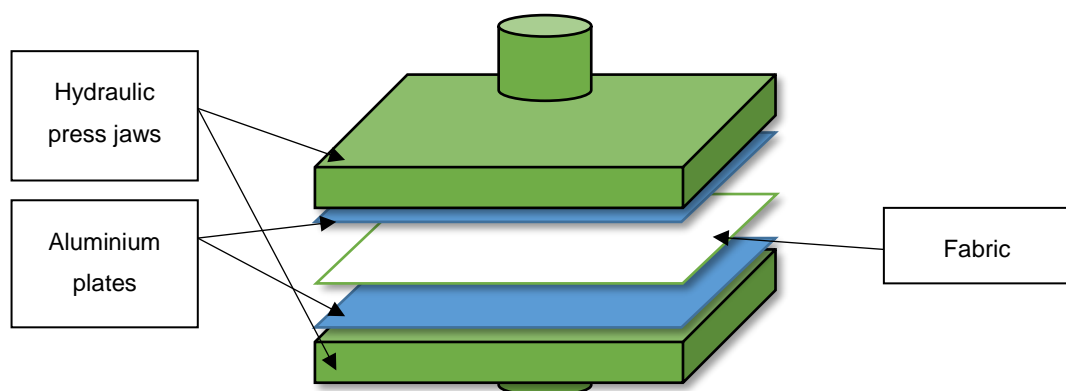


Figure 3.5: Schematic of the fabric compression set up using a hydraulic press

Aluminium plates were used to protect the fabrics from any damage by the jaws of the press. The applied pressure was modulated between 0.5 MPa and 1 MPa depending on the degree of thickness reduction required by the experiment.

### **3.3 Fabric Pre-Moistening**

The role played by the lotion in the wiping performance of pre-moistened wipes can be significant so it demands both accuracy and precision when applying lotion to a dry substrate for the purpose of assessing wiping efficiency. Therefore, it was necessary to develop a robust method. Commercially, lotion loads for baby wipes vary between products, but in the present study, samples were loaded with the same lotion load as the control product sample, namely Pampers® Sensitive, which is 440% by weight. This allows for the results to be useful in the comparison with the leading commercial wipes. Therefore, a lotion loading of 440% was targeted with a coefficient of variation (CV%) of less than 5%.

#### **3.3.1 Materials and Methods**

The dry 56 g.m<sup>2</sup> hydroentangled substrates used for the development of the lotion loading method comprised polypropylene/viscose in the blend proportions reported in Section 3.1. The lotion was supplied by P&G (Pampers® Sensitive lotion). Both the nonwoven substrate and the lotion were considered as control materials.

#### **3.3.2 Development of the Lotion Loading Procedure**

##### **3.3.2.1 Method**

Wipes were conditioned in a standard textile testing environment and weighed. When on the balance tray, lotion was dropped on to the wipe surface from a burette until the desired weight was reached. The desired weight was calculated from the original dry weight of the wipe, equation 3.4.

$$\text{Wet wipe weight} = \text{Dry wipe weight} + (4.4 \times \text{Dry wipe weight}) \quad 3.4$$

The lotion did not entirely wet the wipe. Although it slowly spread, some areas remained dry after 10 min after dropping the lotion, with some lotion remaining on the tray.

Capillary forces were apparently not strong enough to spread the lotion throughout the fabric. Since this method was not suitable for the purpose, regardless of how long the lotion was allowed to wick through the fabric, no repetitions were made and another method was needed.

To overcome this limitation, the fabric was first impregnated with lotion to achieve maximal loading and then a proportion of the lotion was removed in the roller nip of a pad mangle (Xiamen Rapid Co. Ltd P-B0). By modulating the nip pressure, lotion loading could be modulated. Lotion loading was calculated as in equation 3.5.

$$\frac{\text{Wet weight} - \text{Dry weight}}{\text{Dry weight}} \times 100\% \quad 3.5$$

The nip pressure was varied in order to attempt to achieve the desired lotion load of 440%. At least 3 repetitions were done for each pressure level. The lowest pressure level feasible in this method was attempted and repeated 20 times to try and achieve a high enough lotion load. However, as indicated in Figure 3.6, lotion loadings could only be achieved between 280-364%. The raw data are shown in Appendix 1, Table 12.

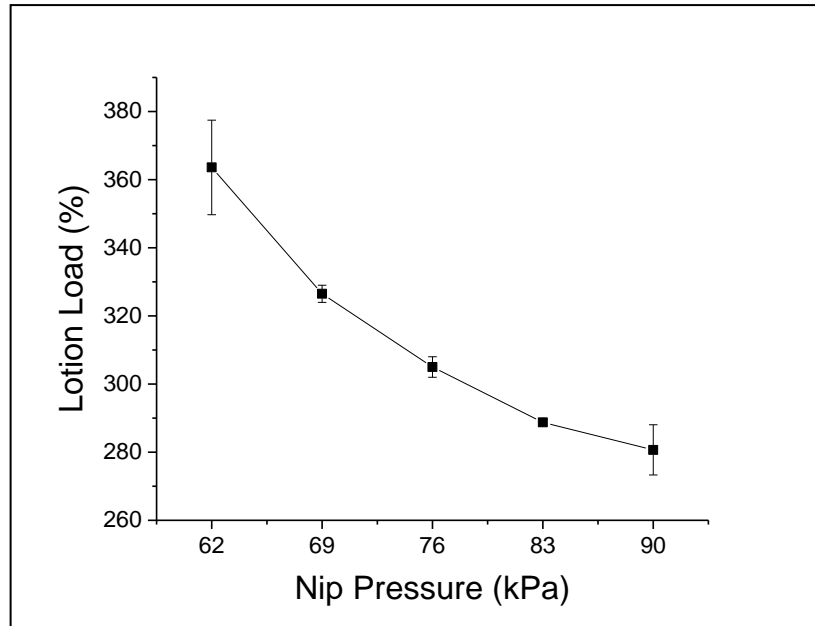


*Figure 3.6: Lotion loading as function of Nip Pressure using Xiamen Rapid Co. Ltd P-B0*

A very low nip pressure was therefore required to obtain the required lotion loading target and to this end, a hand mangle was utilised instead. The dry fabric was first impregnated in the lotion bath for 10 s and then manually passed through the hand mangle. Twenty repetitions were made to determine variance. The lotion load was calculated as in equation 3.5. The lotion load results are shown in Table 5. The coefficient of variation was 3.2 CV%, confirming results fell within the acceptable range (<5 CV%). The details of the raw data can be found in Appendix 2, Table 13.

Mean Lotion Load (%)	439
Standard Deviation (%)	14.15
Coefficient of Variation (CV%)	3.2

*Table 5: Variation of lotion loading results using the hand mangle method*

The hand mangle method therefore proved to be capable of delivering the desired lotion loading with acceptably low variation. This method has been selected to be used for the production of samples used in the experiments presented in this thesis.

### **3.4 Measurement of BM Wiping Efficiency**

The DCM system described in Section 2.2.2 originally developed by the author was used throughout. Fabric samples of 10 mm x 20 mm were mounted on the roller prior to testing. The leading edge was fixed on the roller by wedging it with a stainless-steel bar. The fabric samples were wrapped around the roller and the trailing edge was fixed with an adhesive tape without exerting any force to cause the stretching of the samples. The skin mimic used was d-c-fix Snow (supplier: Konrad Hornschuch AG). The linear wiping speed was set to 0.1 m.s<sup>-1</sup>. The rotational speed was set so that the speed at the surface of the roller would be 0.1 m.s<sup>-1</sup>. The wiping pressure was 2 psi which is equal to 13.79 kPa. The length covered by a single swipe was 0.1 m. At least 3 replicates were assessed to obtain statistical information about the sample. Skin mimic was fixed on the wiping board using adhesive tape.

### **3.5 Image Processing and Analysis**

To enable assessment of BM cleaning efficiency, a fluorescence imaging system was dedicated to this project. Generation of luminescence through excitation of a molecule by ultraviolet or visible light photons is a phenomenon termed photoluminescence. Fluorescence is the behaviour of some atoms and molecules where they absorb light at a particular wavelength and then emit light of longer wavelength after a brief interval, called the fluorescence lifetime (Herman, 2015). A typical imaging system consists of the following main elements:

- Excitation source
- Light delivery optics
- Light collection optics
- Filtration of the emitted light
- Detection, amplification and digitisation

The system used herein to detect BM contamination was an AlphaImager™ 3400 digital imaging system, which takes instant photographs of contaminated samples using a charge coupled device (CCD) camera under UV-illuminated

conditions. This system produces photographs which are 256-level greyscale images.

The quantitative image analysis method used is based on calculating the integrated density value of all the pixels in a defined area of interest (AOI) and comparing it to a control area, referred to as the background. Templates of the AOI and background were prepared and saved during the development of the dynamic cleaning method. The same templates were used to compare different samples. Once the AOI and background frames were drawn or loaded from a saved template, the software automatically calculated and displayed the density data. An example is shown in Figure 3.7. The numbers 1n to 9n represent the different AOIs, the IDV column shows the integrated density values for the respective AOIs. The Integrated Density Value (IDV) is the sum of all the pixel values after background correction (BACK), calculated using equation 3.6. Greyscale images consist of pixels, each pixel ranges on the greyscale which is represented in a number between 0 for completely black and 255 for completely white. The column titled % shows the proportion of the respective IDV compared to the sum of the IDVs of all AOIs. The area column shows the areas of the respective AOIs measured in the number of pixels. The column titled AVG shows the respective average value for each pixel in the AOI. The column titled BACK shows the IDV of the reference area which is normally selected to be a clean area on the specimen. The software calculates the background value automatically from the defined background frame. It calculates the average density for the background pixels and subtracts this value from each pixel in the AOI as in equation 3.6. The IDV is directly related to the fluorescence of each AOI which, in turn, is proportional to the amount of fluorescent contaminant in the AOI. This makes this method suitable for the assessment of the wiping efficiency. The method has been assessed and validated in earlier work at P&G's laboratories (Memari, 2011).

$$IDV = \sum \text{each pixel value} - BACK \quad 3.6$$

#	IDV	%*	AREA	AVG	BACK
1n	13775625	7.8	1975	6975	25045
2n	3876075	2.2	1725	2247	25045
3n	9922525	5.6	1825	5437	25045
4n	25137496	14.2	2387	10531	25045
5n	21587068	12.2	2511	8597	25045
6n	28139034	15.9	2541	11074	25578
7n	33589220	19.0	2765	12148	25578
8n	13156500	7.4	2625	5012	26812
9n	27678316	15.6	2555	10833	26812

IDV=Integrated Density Value  
\* based on Integrated Density Value

Figure 3.7: Example of the density data window in which the resulting IDVs of an image are displayed

### 3.6 Experimental Design

Chapters 4 to 6 present the experimental work done in this thesis. The chart below, Figure 3.8, shows the system in which experiments were structured.

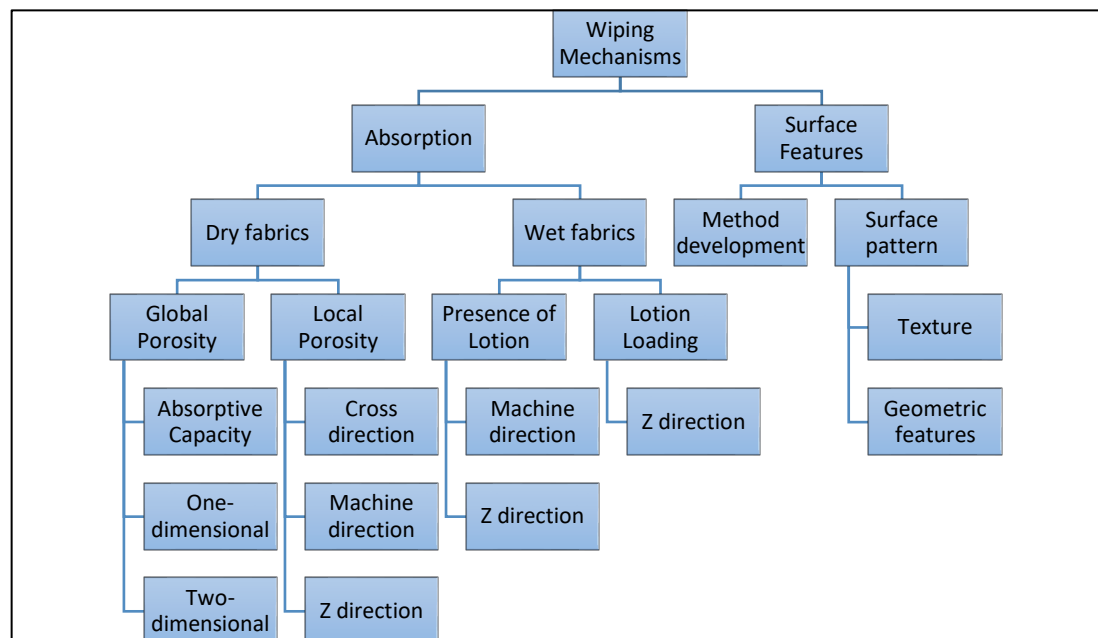


Figure 3.8: Diagram showing the experimental structure of the work presented in chapters 4 to 6.

Chapters 4 and 5 contain the experimental work addressing the absorption mechanism while chapter 6 addresses the dynamic removal of BM.

Experiments in Chapter 4 address the absorption mechanism of dry nonwoven fabrics and the influence of porosity, global and local, on the absorption behaviour. Variations in porosity in MD, CD and ZD are considered and the respective absorption behaviours were measured.

Chapter 5 addresses the influence of lotion on the absorption behaviour. On one hand, the presence of lotion was investigated by comparing the absorption behaviour of dry and wet fabrics. On the other hand, the influence of the amount of lotion loading on the absorption behaviour was investigated by comparing the behaviour of samples loaded with different amounts of lotion.

Chapter 6 contains the experimental work addressing the removal of BM by the dynamic movement of the wipe and the influence of fabric texture and engineered surface features on the efficiency of dynamic wiping. Initially, fabric prototypes were made using existing texture patterns and the dynamic cleaning performance was assessed. Then the experimental work addresses the influence of specific surface features, which were designed for high efficiency cleaning, on the dynamic cleaning performance.

# **CHAPTER 4**

## **Artificial Bowel Movement (BM)**

### **Absorption by Wipes**

#### **4.1 Introduction**

As discussed in Section 2.3.2 and illustrated in Figure 2.2(a), a proportion of BM is dissolved or dispersed in the lotion during the wiping process. The resulting solution is referred to as BM slurry and its absorption behaviour has not previously been reported in the literature. BM slurry differs from entirely aqueous media in that it contains biological substances (Lentner and Pharmaceuticals, 1981). Some of these components are water insoluble and their concentrations can vary. Another difference is BM consistency, which also varies depending on its composition and water content (Roe, Procter & Gamble Internal Communications, Mason, Procter & Gamble Internal Communications). BM also contains solid particles, which vary in size and chemistry (Meeker et al., 2004, Roe et al., Procter & Gamble Internal Communications, Mason, Procter & Gamble Internal Communications). The aforementioned factors are likely to contribute to complex absorption behaviour and there is therefore a need to develop a better understanding of how BM interacts with nonwoven substrates. This chapter reports experiments on BM slurry absorption behaviour and how it is influenced by various parameters.

#### **4.2 Influence of Global Porosity on BM Absorptive Capacity**

##### **4.2.1 Introduction**

Liquid absorptive capacity (LAC) is one of the most commonly used standard absorption methods used to assess nonwoven fabrics and is undertaken following standard methods NWSP 010.1.R0 (15) and ISO 9073-6 2000. (EDANA and INDA, 2015). The EDANA standard liquid absorptive capacity

test procedure was followed to study slurry absorption capacity in two nonwoven substrates differing in porosity.

#### 4.2.2 Materials and Methodology

All fabric samples were prepared from the same ternary fibre blend of 60% 3.3 dtex trilobal polypropylene; 20% 1.0 dtex trilobal polypropylene and 20% 1.7 dtex viscose reported in section 3.1. Fabric samples were manufactured in low (90.2%) and high (95.6%) porosity variants using the procedure described in section 3.2. While the porosity levels seem to differ only slightly, they reflect a significant difference in the void volume between the two samples. Considering that the fibres' densities, the samples' area and therefore, the fibres' volume are the equal between the two samples, the change in thickness from 1.2 mm for the high porosity sample to 0.64 mm for the low porosity sample led to a reduction of the void volume with a ratio of 2:1.

BM slurry was prepared by mixing the lotion with BM in the weight ratio of 1:1. The making of BM and BM slurry was as reported in section 2.5.3. 50 ml of the BM slurry was placed in a container. Three square fabric specimens of 100 mm x 100 mm were cut from each sample, conditioned and weighed.

Each of the specimens was then immersed in the slurry solution and hung vertically to drip excess amounts of slurry in accordance with EDANA method NWSP 010.1.R0 (15) (EDANA and INDA, 2015).

After the dripping phase, the saturated specimens were weighed and the liquid absorptive capacity was calculated as in equation 4.1.

$$LAC\% = \frac{(M_n - M_k)}{M_k} \times 100\% \quad 4.1$$

Where,

$M_n$ : Mass in grams of the wet test piece,

$M_k$ : Mass in grams of the dry test piece.

### 4.2.3 Results

Using the results of  $M_k$  and  $M_n$  for each of the samples, it was possible to calculate LAC by applying equation 4.1. The results are shown in Figure 4.1 and Table 6.

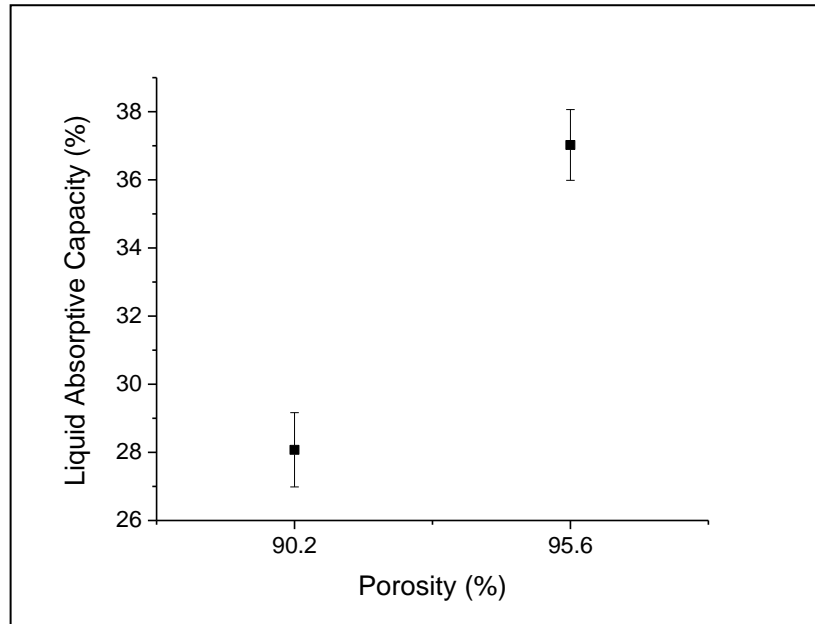


Figure 4.1: Liquid absorptive capacity for the high porosity (95.6%) and low porosity (90.2%) samples

Sample	Liquid Absorptive Capacity (%)
High Porosity (95.6%)	3702
Low Porosity (90.2%)	2808

Table 6: Liquid absorptive capacity (LAC) for samples of high (95.6%) and low (90.2%) porosities

A higher BM absorptive capacity was obtained for the high porosity sample, which is consistent with the hypothesis presented in section 4.2.1. This result is the first relating to BM slurry absorption. It raises a question about the manner in which a sample with areas of local porosities would absorb BM slurry and whether it would affect the distribution of the absorbed BM slurry. And would several levels of porosities behave similarly? A porosity gradient

profile is therefore a subject of the experimental investigation and is presented in section 4.8.

But first, to gain a fuller understanding of BM absorption behaviour, it is important to investigate the absorption rate. This is particularly relevant because the process of wiping occurs in a relatively limited timeframe, compared to the time it may take to fully saturate a nonwoven with the BM liquid.

### 4.3 Influence of Global Porosity on the BM Absorption Rate

The BM slurry absorption rate is the amount of slurry absorbed per unit time and can be expected to depend on several factors, particularly the porosity and other quantities such as pore size, pore size distribution and pore geometry because of their potential influence of capillary driving forces.

Hypothetically, the fabric samples with different porosities, the making of which has been explained in section 3.2, differ in their respective equivalent capillary radius. This is due to the compression method used in their making. Absorption is proportional to the square root of time according to Washburn's equation, equation 4.2 (Washburn, 1921). If the hypothesis is correct, then the sample with lower porosity would show a higher absorption rate and vice versa.

$$L = \sqrt{\frac{r_c \gamma \cos \theta}{2\eta}} t^{1/2} = k_0 t^{1/2} \quad 4.2$$

Where  $k_0$  is a constant,  $r_c$  is the capillary radius,  $\eta$  is the fluid viscosity,  $L$  is the wetted length,  $\gamma$  is the surface tension of the advancing liquid and  $\theta$  is the contact angle at the liquid-solid-air interface.

#### 4.3.1 Materials and Methodology

To study the BM absorption rate in the same 90.2% and 95.6% porosity fabrics described in section 4.2.2, video recording of the dynamic absorption process

was implemented followed by image analysis to quantify the amount of slurry absorbed as a function of time. Two setups were evaluated to undertake the experiment. In the first, a droplet of slurry was placed on top of the fabric sample and video recorded for 2 min as the slurry penetrated the fabric surface, using only gravity as a driving force. In the second, the slurry was placed on a plastic plate and the fabric sample was placed upon it such that absorption could be studied in real-time.

#### 4.3.1.1 **Method 1: BM Slurry Droplet Above**

The CCD video camera set up is shown in Figure 4.2. The fabric was placed on top of a plastic plate under the camera, which faced immediately down towards the subject illuminated by incident light.

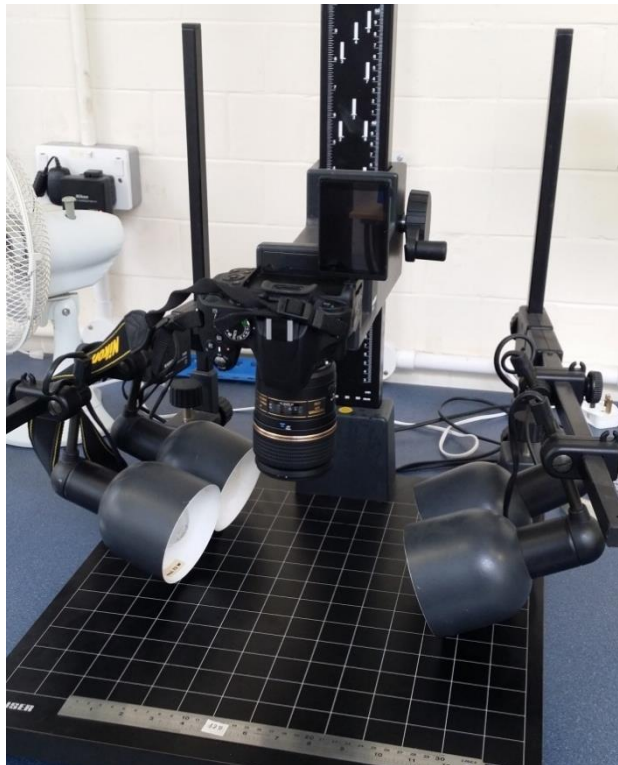


*Figure 4.2: Test setup for the capture of BM slurry absorption. The camera is mounted vertically above the test table facing downwards. Incident lighting is provided from both sides left and right.*

A droplet of slurry (approx. 0.1 ml) was placed on the upper surface of each of the two fabrics (low and high porosity) as shown in Figure 4.3.

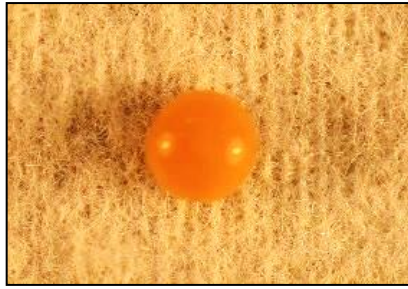


*Figure 4.3: Droplet of slurry placed on top of the high porosity (95.6%) fabric sample*

Real-time recording of dynamic slurry absorption behaviour over a period of 2 min was undertaken for each fabric.

#### **4.3.1.2 Method 2: BM Slurry Droplet Below**

The same camera setup shown in Figure 4.2 and explained in 4.3.1.1 was adopted. A pool of slurry was prepared on a clean polyethylene plate as shown in Figure 4.4. The amount of slurry was 0.2 ml.

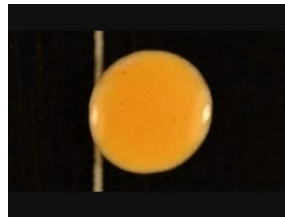


*Figure 4.4: Pool of slurry on the polyethylene plate*

Each of the low and high porosity fabrics was then placed on top of the pool of slurry for 2 min, such that liquid absorption occurred, Figure 4.5.

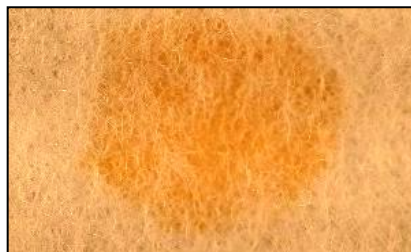


*Figure 4.5: High porosity (95.6%) fabric sample placed over the pool of slurry; duration: 2 min*

#### 4.3.1.3 **Experiment Procedures**

Footage was captured at 25 frames per second (fps) starting from the initial point of BM slurry droplet contact with the fabric's surface. These images were processed to obtain the integrated density values (IDV). The IDVs for each uncontaminated fabric were subtracted so that only data relating to the BM could be obtained. The corrected values were then plotted against time to illustrate the rate of BM absorption.

#### 4.3.1.4 **Image Analysis**

The images were processed using ImageJ software. They were cropped to the suitable size then their colours were inverted. This step inverts the contrast between the background (fabric surface) and the contamination (BM slurry). The resulting images showed the BM slurry in bright colour compared to the background (fabric surface). The brighter the colour the higher the IDV, hence the IDV represents the amount of BM slurry. Figure 4.6 and Figure 4.7 show examples of the cropped and inverted images for method 1 and method 2 respectively.

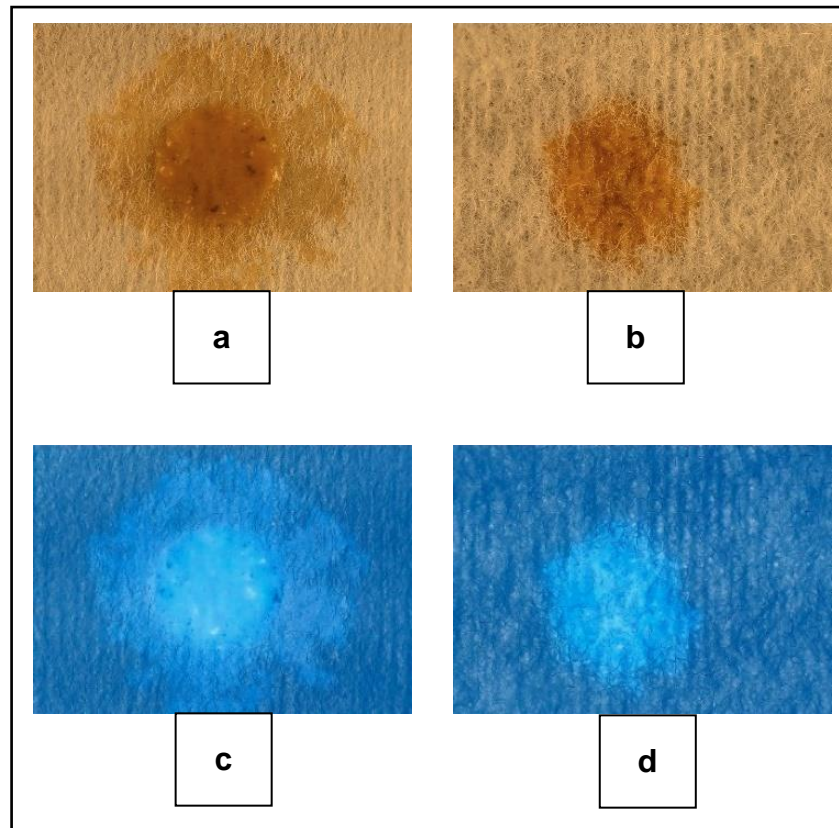


*Figure 4.6: Image processing of the video frames captured during method 1 experiment at  $t = 120$  s. a: image of low porosity sample (90.2%). b: image of high porosity sample (95.6%). c: inverted image of low porosity sample (90.2%). d: inverted image of high porosity sample (95.6%)*

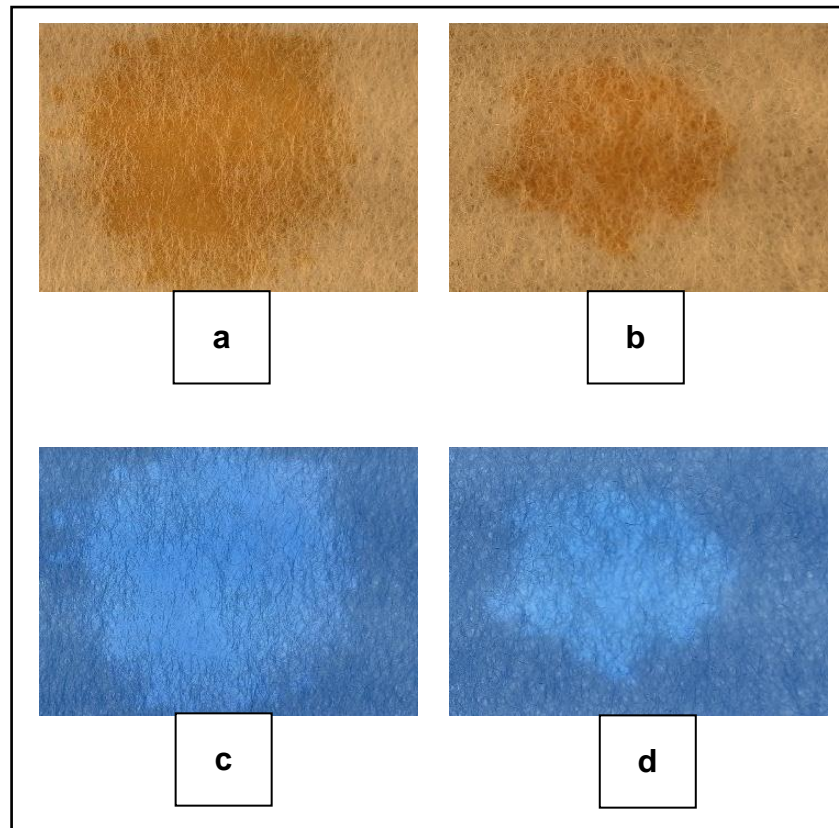


*Figure 4.7: Image processing of the video frames captured during method 2 experiment at  $t = 120$  s. a: image of low porosity sample (90.2%). b: image of high porosity sample (95.6%). c: inverted image of low porosity sample (90.2%). d: inverted image of high porosity sample (95.6%)*

#### 4.3.1.5 **Data Correction**

The IDV results are a representation of the spread of BM slurry over an area of fabric. Processed images from which IDVs were obtained are two-dimensional media. A three-dimensional measurement is required to obtain a representation of the slurry volume. Based on the evaluation only on the images would mean to ignore the third dimension which is the thickness of the fabric (the Z-direction). To achieve a more accurate description of the difference in BM slurry absorption rate behaviour between the two fabrics, a correction factor was applied to the resulting IDVs. By multiplying the IDVs of each fabric with its associated thickness in millimetres (section 3.2), a new set of data is produced.

### 4.3.2 Results

Since in a typical wiping cycle, the duration of contact with the skin is likely to be less than 10 s, it is instructive to consider the short and longer-term BM absorption rates.

#### 4.3.2.1 Method 1: BM Slurry Droplet Above

Figure 4.8 shows the short-term response (up to 10 s) and the long-term absorption (up to 120 s) is shown in Figure 4.9.

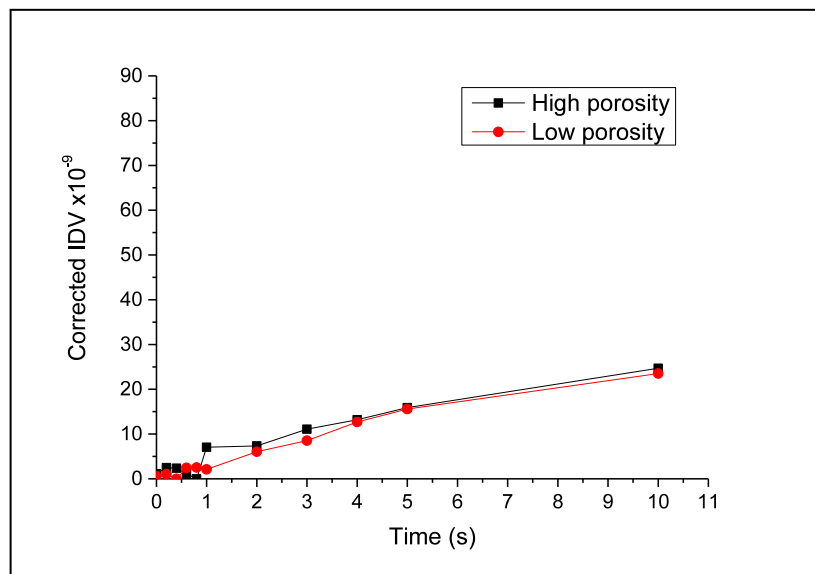


Figure 4.8: IDV data for the low (90.2%) and high (95.6%) porosity fabrics; duration: 10 s

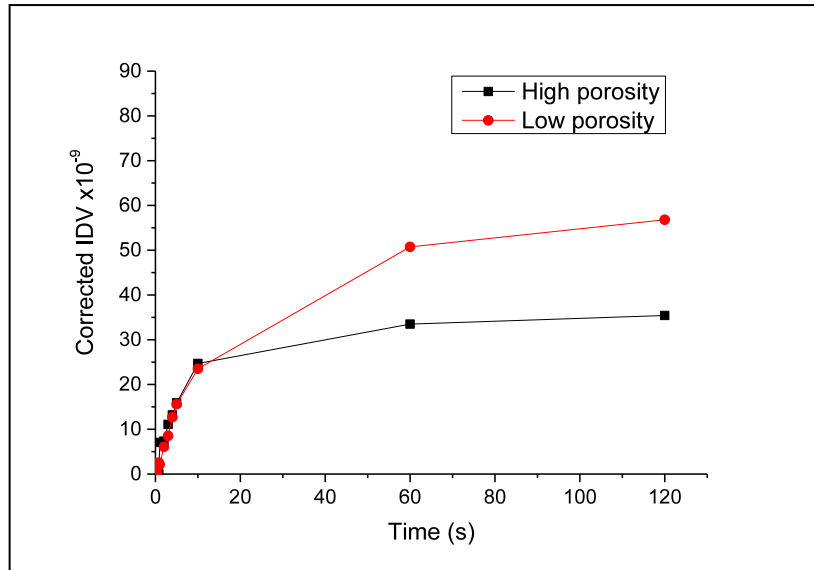


Figure 4.9: IDV data for the low (90.2%) and high (95.6%) porosity fabrics; duration: 120 s (2 min)

#### 4.3.2.2 Method 2: BM Slurry Droplet Below

The same approach was implemented for the second method as shown in Figure 4.10 and Figure 4.11.

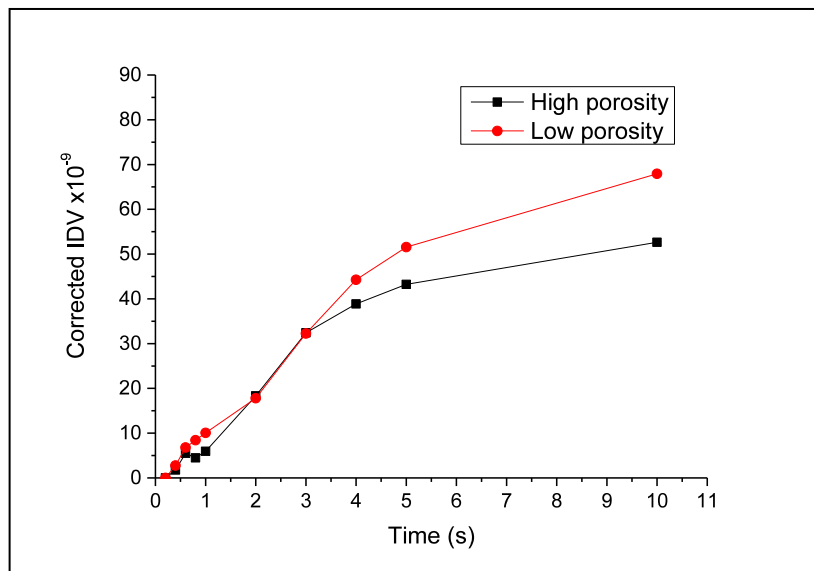


Figure 4.10: IDV data for the low (90.2%) and high (95.6%) porosity fabrics; duration: 10 s

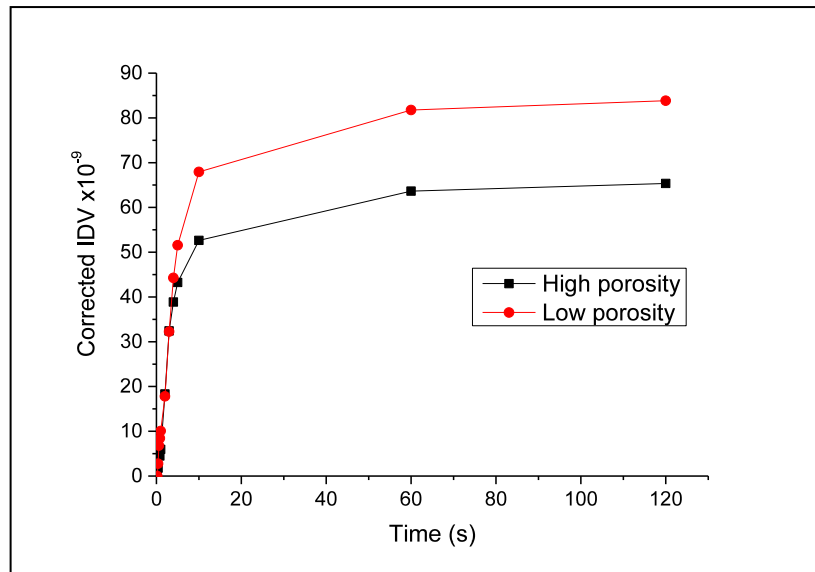
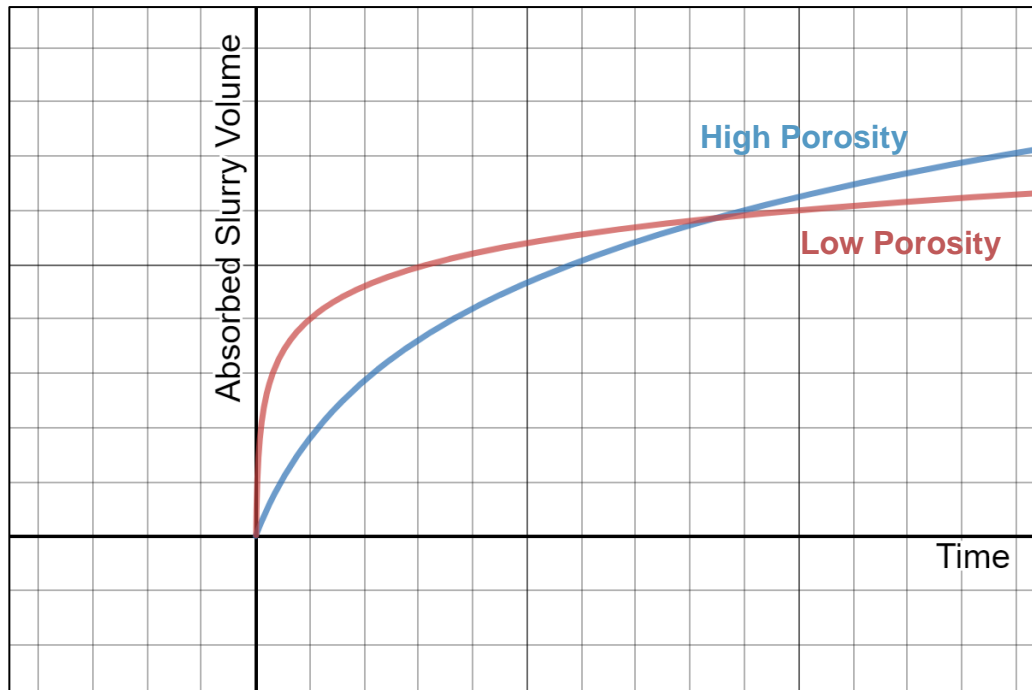


Figure 4.11: IDV data for the low (90.2%) and high (95.6%) porosity fabrics; duration: 120 s (2 min)

### 4.3.3 Discussion

In all the short-term BM absorption rate data (up to 10 s), the rate of change for the low porosity (90.2%) fabrics was similar or higher than the high porosity fabric (95.6%). This result corresponds with what might be expected in theory for low and high porosity fabrics (Figure 4.8 and Figure 4.10). Wherein in section 4.2, the sample with high porosity had a higher absorption capacity than that of a low porosity. However, it is expected that on the short timescale the sample with low porosity is expected to have a higher absorption rate compared to the high porosity sample. This is because capillary pressure is expected to be higher in the low porosity sample. Additionally, when porosity is lower, less volume of slurry is required to fill a given area of fabric, which leads to a faster spread of slurry to fill the same area. Accordingly, the hypothetical absorption curves of the two samples should look like Figure 4.12.



*Figure 4.12: Hypothetical graph of absorption behaviour curves of two fabric samples which differ in porosity but identical in other properties. Blue curve: high porosity sample, red curve: low porosity sample*

However, this trend did not apparently change over longer periods up to 2 min (Figure 4.9 and Figure 4.11), unlike what might be hypothesised. The resulting absorption rate curves do not substantially cross except for a short period of time,  $t = 1 \text{ s} \rightarrow t = 5 \text{ s}$  in Figure 4.8 and  $t = 1 \text{ s} \rightarrow t = 2 \text{ s}$  in Figure 4.10, after which they cross again to return to their original positions where low porosity sample (90.2%) appears to absorb more than high porosity sample (95.6%). The results in Figure 4.9 and Figure 4.11 indicate that BM slurry absorption and spreading is faster in the low porosity samples (90.2%) compared to the high porosity samples (95.6%). This is despite the data correction for fabric thickness explained in 4.3.1.5.

The porosity correction step was made based on the assumption that absorption in the Z-direction is homogeneous and that BM slurry is a homogeneous medium throughout the absorption process. Observation of the slurry spread in the samples after the experiment (Figure 4.13), agree with the findings of the image analysis but it was also noticeable in the low porosity samples (90.2%), that the volumetric spread was not homogeneous as was assumed, as in Figure 4.13 top. The slurry appeared to have been separated

into two distinct phases, liquid and solid. It appeared that the solid and insoluble phase of the slurry was concentrated in the centre where the droplet was originally in contact with the fabric surface, whereas the liquid phase spread to a wider radius, beyond this region. This does not contradict the rate of BM spreading indicated by the data collected from the image processing. However, based on these observations evaluating absorption rate is not entirely reliable using this method because it is neither possible to assume a homogeneous spread of slurry, nor is it possible to assume that phase separation would not occur.



*Figure 4.13: Spread of BM slurry in 90.2% low porosity fabric (top) and 95.6% high porosity fabric (bottom) showing heterogeneous phase separation in the low porosity fabric*

Additional experimental methods are therefore required that enable measurements of absorbed BM slurry volume or slurry weight per unit time to be obtained. Accordingly, a further method was investigated to determine the influence of global porosity on BM slurry absorption.

## 4.4 Influence of Global Porosity on Slurry Absorption

### 4.4.1 Absorption Behaviour using Tensiometry

Standard methods are conventionally used to measure absorptive capacity and absorption rate in nonwovens using for example internationally recommended procedures jointly agreed by EDANA and INDA referred to as nonwovens standard procedures (NWSP), particularly NWSP 010.1.R0 (15), NWSP 010.2.R1 (15) and NWSP 010.3.R0 (15) which describe absorption test methods and comply with ISO 9073-6: 2000 and ISO 9073-12: 2002 (Mao, 2016, EDANA and INDA, 2015). These methods do not, however, allow for the gravimetric assessment of liquid uptake as a function of time, which is a key indicator of the performance of a baby wipe. Accordingly, it was necessary to develop an alternative approach that enabled the weight of BM slurry absorbed by a wipe to be evaluated.

Although many questions have been raised about pore geometry calculations and the possibility to use Washburn's equation to calculate contact angle (Dullien, 1992a, Dullien, 1992b, Mittal, 2006), it has been used in many studies to describe capillary flow in textiles. This suggests that liquid absorption in porous media is significantly influenced by capillary pressure and the liquid's surface tension. The forces associated with the capillary behaviour are a function of a number of factors as indicated by Washburn's equation 4.2 (Washburn, 1921).

Washburn's equation of capillary flow describes the penetration distance by liquid's flow front as a function of time, capillary radius, liquid's surface tension, liquid's dynamic viscosity and contact angle between the liquid and capillary. Washburn used Poiseuille's law in the case of circular tube as in equation 4.3, (Chatterjee and Gupta, 2002a).

$$q = \left( \frac{r_c^2}{8\eta} \right) \frac{\Delta P}{L} \quad 4.3$$

Where,  $q$  is the volume flux and  $\Delta P$  is the net driving pressure or pressure drop.

Washburn replaced  $\Delta P$  with capillary pressure calculated by Laplace from equation 4.4, (Chatterjee and Gupta, 2002a).

$$p = \frac{2\gamma \cos \theta}{r_c} \quad 4.4$$

Where  $p$  is the capillary pressure,  $r_c$  is the capillary radius,  $\gamma$  is the surface tension of the advancing liquid and  $\theta$  is the contact angle at the liquid-solid-air interface.

Conventionally, capillarity is assessed using methods such as vertical wicking (Chatterjee and Gupta, 2002a) but this does not provide gravimetric data indicating the amount of liquid absorbed by the sample. To enable a detailed picture of the forces generated between the fluid and the fabric from the point they first come into contact to the point of equilibrium absorption requires a highly sensitive system of force measurement.

Measuring forces of the scale of surface tension is possible using Kruss® tensiometry, Figure 4.14. Such tensiometers are capable of measuring surface tension and surface energy, in addition to contact angle and sorption kinetics. Measurements can be made with a resolution of  $\pm 5 \cdot 10^{-6}$  g in real time with frequencies up to 30 Hz.

In the present work, a Kruss® tensiometer (K100SF/20000204) was utilised to monitor the forces acting between nonwoven specimens and BM slurry from the point of initial contact to infiltration and uptake of liquid into the internal pore volume. The Kruss® instrument enables automatic detection of liquid surface when a test specimen comes in contact with it by monitoring the changes in interfacial forces during the liquid approach phase.

Upon contact, the wetting process begins. When one of the phases is wetted by the other, energy is released due to the disappearance of the two previously existing surfaces and subsequently the respective surface tensions  $\sigma_1$  and  $\sigma_2$ . Consequently, work has to take place to form the new interface between the two phases and its respective interfacial tension  $\sigma_{12}$ . The sum of the aforementioned tensions is called the work of adhesion  $W_{12}$ , (Kruss-

GmbH). This approach can be used to determine the work of adhesion  $\text{J}\cdot\text{m}^{-2}$  between a solid and a liquid  $W_{ls}$ , see equation 4.5.

$$W_{ls} = \sigma_1 + \sigma_2 - \sigma_{12} \quad 4.5$$

The work of adhesion is the work required to separate two adjacent phases, 1 and 2, of a liquid-solid phase boundary from one another. This is equivalent to the energy released during wetting. It can be expressed as given in equation 4.6.

$$W_{12} = \sigma_1(1 + \cos \theta) \quad 4.6$$

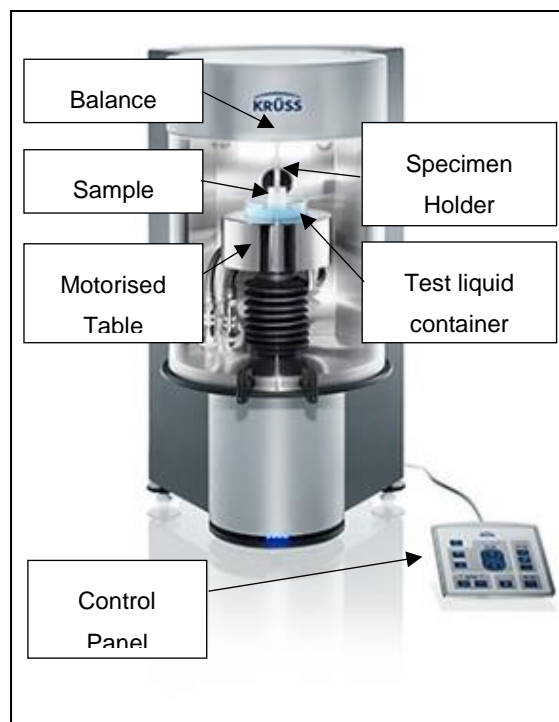


*Figure 4.14: Kruss Force Tensiometer K100 (Kruss-GmbH)*

If appropriately configured during testing, data produced by a tensiometer can be interpreted into terms of absorption behaviour. In this type of tensiometer system, a fabric specimen is lowered into a container of the test liquid and hence, wetting and absorption are initiated. Factors influencing the absorption behaviour of a fabric specimen will include the surface properties of both the porous medium (or fabric) and the liquid, followed by transport via capillary pressure. To the author's knowledge, BM slurry has not been previously

studied using a tensiometer. It was reasoned that a tensiometer could allow monitoring of the weight of slurry absorbed by a fabric specimen as the experiment progresses. The weight of slurry absorbed per second could then be used to characterise the absorption rate.

#### 4.4.2 Materials and Methodology

A diagrammatic representation of the experimental set up is shown in Figure 4.15. A picture showing the test setup is shown in Figure 4.16.

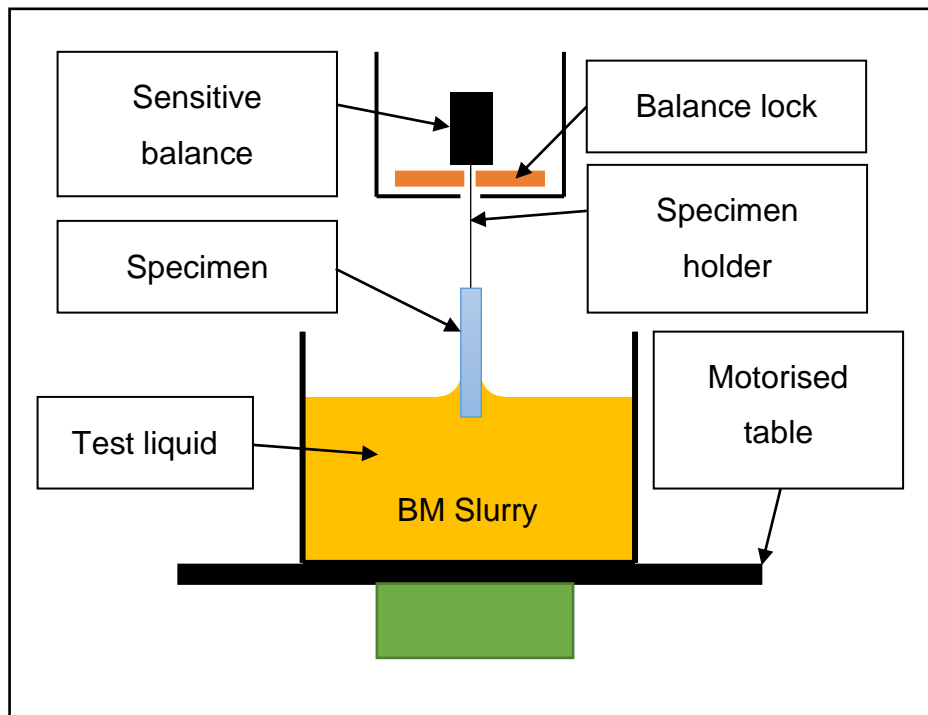


Figure 4.15: Schematic of the main parts of the tensiometer. Control of immersion is via the motorised table.

With reference to Figure 4.17, specimens of high (95.6%) and low (90.2%) porosity nonwoven fabrics of the width 20 mm were carefully cut from the previously prepared fabrics (sections 3.1 and 3.2) using a template. After the tensiometer calibration process, a fabric specimen was mounted in the tensiometer using the specimen holder. The specimen holder can be easily removed from the elastic grip of the upper jaws by pulling it downwards manually. The holder is used carefully to clip the specimen making sure the lower (leading) edge of it is perpendicular to the axis of the holder, it can then be put back in the upper jaws of the tensiometer, along with the specimen by

simply pushing the back end of the specimen holder between the elastic jaws. After mounting the specimen in the tensiometer its lower (leading) edge is checked again to confirm it is still perpendicular to the holder's axis and is itself horizontal.

BM slurry was prepared by mixing the lotion with BM (65% water content) in a weight ratio of 1:1. 30 ml of the BM slurry was placed in the container (shown in Figure 4.14 and Figure 4.15).

To conduct the measurement, the vessel containing the slurry was raised by the motorised table towards the lower (leading) edge of the specimen such that 0.5 mm of the fabric was fully immersed and wetted out at a rate of 10 mm/min. Measurement starts as soon as immersion depth is achieved and the distance between the specimen holder and the motorised table will be locked for the set duration of the test which is 60 s.

During the experiment, data is recorded where the balance readings are logged into the data sheet at a predefined rate. In this experiment, the balance reading rate was 10 Hz with the exception of the first second where it was set to 30 Hz. This is due to the importance of the immediate contact response between the nonwoven fabric and the BM slurry. After 60 s, the measurement stopped automatically, and the balance was locked.

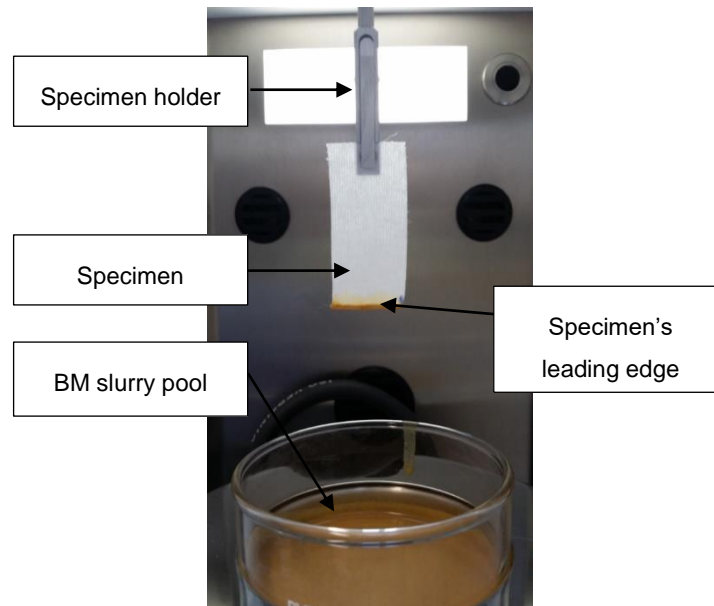


*Figure 4.16: BM Slurry absorption using the tensiometer showing the final specimen position after the experiment and the end of the fabric wetted with BM slurry*

Based on conventional theory, fabrics with higher porosity can be expected to provide an overall greater void volume per unit area than those of lower porosity (Russell, 2007). When comparing two fabric samples that differ in their porosity, it is expected that a sample of higher porosity will therefore exhibit higher absorptive capacity. However, the converse may be expected in terms of absorption rate because in high porosity fabrics, the capillaries will be of larger average radius (or equivalent diameter), such that capillary pressure will be reduced. Equation 4.4 (shown in section 4.4.1) shows the relation between capillary pressure and pore radius (Gane et al., 2004).

#### **4.4.2.1 Sample Preparation**

All fabric samples were prepared from the same ternary fibre blend of 60% 3.3 dtex trilobal polypropylene; 20% 1.0 dtex trilobal polypropylene and 20% 1.7 dtex viscose reported in section 3.1. Fabric samples were manufactured in low (90.2%) and high (95.6%) porosity variants using the procedure described in section 3.1 and 3.2, see Figure 4.17.

Three specimens were tested for each sample. The resulting curves were then averaged and plotted in the results section 4.4.3.

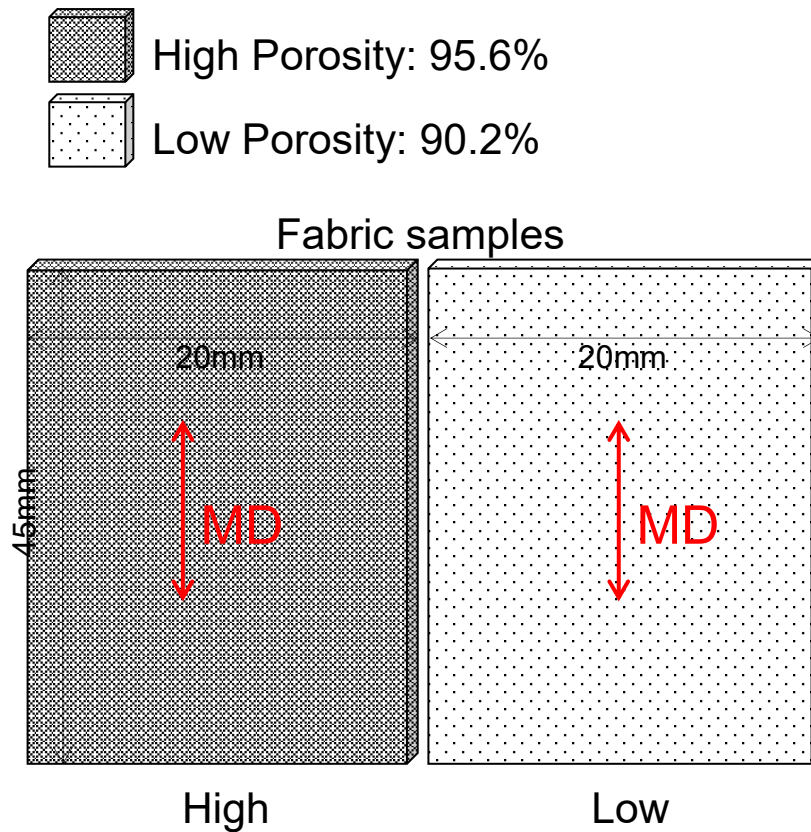


*Figure 4.17: Sample preparation. Specimens were cut in the dimensions 45 x 20 (mm) such that the MD was vertically aligned prior to immersion of 0.5 mm of the lower edge being immersed in the BM slurry for absorption measurement.*

To ensure anisotropy effects were accounted for, the machine and cross directions (MD and CD respectively) were recorded in all the specimens.

#### 4.4.2.2 **Data Recording**

The parameters used in these experiments are summarised in Figure 4.18.

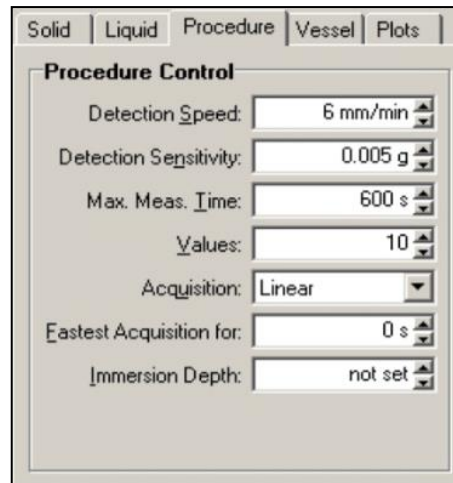


Figure 4.18: Summary of conditions used during tensiometry measurements.

Detection speed refers to the speed of the sample holder as it approaches the liquid surface prior to contact with the specimen. It influences the accuracy of measurements. Upon contact with the test liquid surface wetting is initiated and the work of adhesion done at the interface can be detected by the sensitive scale of the tensiometer. Detection sensitivity is the necessary change of force during the approach phase in order to trigger the measurement phase. This occurs as a result of the fabric edge coming into contact with the BM slurry. Default values for detection speed and sensitivity are set to 6 mm/min and  $5 \times 10^{-3}$  g respectively as shown in Figure 4.18. There are no standards for these values as they depend on the nature of the test material and liquid. Default values have been used in this experiment and shown to be suitable for use with the sample fabrics and BM slurry.

Given that in the case of a baby wipe the total use period is known to be  $\leq 60$ s, this was set as the cut off time point following immersion. A nominal frequency of readings of 10 Hz was set. To maximise the resolution of initial measurements made at the point the fabric sample comes in to contact with the BM slurry, the fastest acquisition time was set for the first second of contact, which meant recording 30 readings in the first second.

#### 4.4.3 Results and Discussion

The results of this experiment are reported as absorbed slurry weight vs. time. The absorption rate can then be determined from either the slope of the tangent of the resulting curve at the desired time point or by linear fitting of the

slope of the resulting absorption curve between two time points. Absorption capacity could also be obtained although it does not involve full immersion of the specimen unlike standard EDANA methods, NWSP 010.1.R0 (15) (EDANA and INDA, 2015).

At a certain point during a test, the specimen takes up liquid mass against which gravity acts, equal to the capillary forces that drive liquid transport. This eventually leads to a plateau-like curve, which in the present experiments using BM slurry was reached in  $\leq 1$  min from the test start time. The force value obtained at this time point is related to the absorbed capacity or the total weight of fluid absorbed by the fabric.

The absorption curves for the high porosity (95.6%) specimens are shown in Figure 4.19 whereas the absorption curves for the low porosity (90.2%) specimens are shown in Figure 4.20. Average curves were calculated for low porosity specimens and the high porosity specimens and then plotted against each other Figure 4.21. Substantial differences were observed in both the total weight of absorbed fluid and the rates of absorption, which is consistent with the differences in fabric porosity. Porosity is the ratio of the void volume to the fabric bulk volume. This means that in two identical samples, which only differ in their levels of porosity, the one with higher porosity will have a greater void volume providing more void volume to contain BM slurry.

In Figure 4.21, the curves reveal the absorption rate behaviour. Referring to the absorption curve of the low porosity (90.2%) sample, a near plateau is reached after about 25 s, where at the same time, the absorption curve of the high porosity sample (95.6%) continues to rise up to 60 s. Thus, in the low porosity sample (90.2%) a balance of forces was reached after a relatively short time, that prevented further fluid absorption. Such forces are capillary forces acting on absorbing BM slurry into the fabric, gravity force which opposes the capillary forces and the loss of liquid mass due to evaporation. Theoretical models developed by Masoodi et al. (Masoodi and Pillai, 2012) illustrate how porosity is proportional to the amount of liquid absorbed by a porous medium at a steady state when the liquid weight balances the capillary forces, equation 4.7 from the definition of porosity of a wick.

$$\varepsilon = \frac{m_{sat}}{\rho A_{cs} L_{ss}} \quad 4.7$$

Where:

$\varepsilon$  is porosity of the wick

$m_{sat}$  is the mass of liquid in the fully saturated wick

$\rho$  is the density of the liquid

$A_{cs}$  is the cross-sectional area of the wick

$L_{ss}$  is the steady state location the liquid front reaches

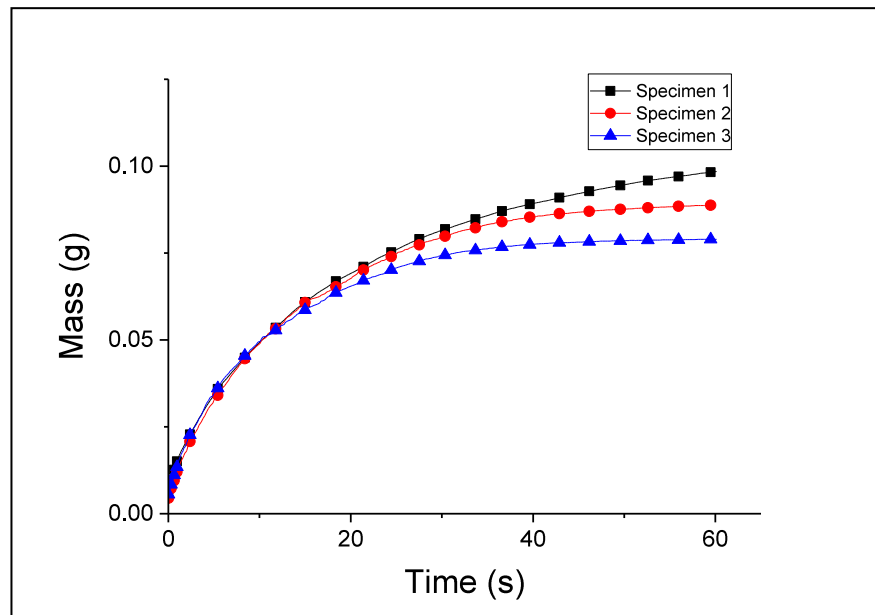


Figure 4.19: BM slurry absorption curves for the high porosity (95.6%) sample in the MD determined by tensiometry

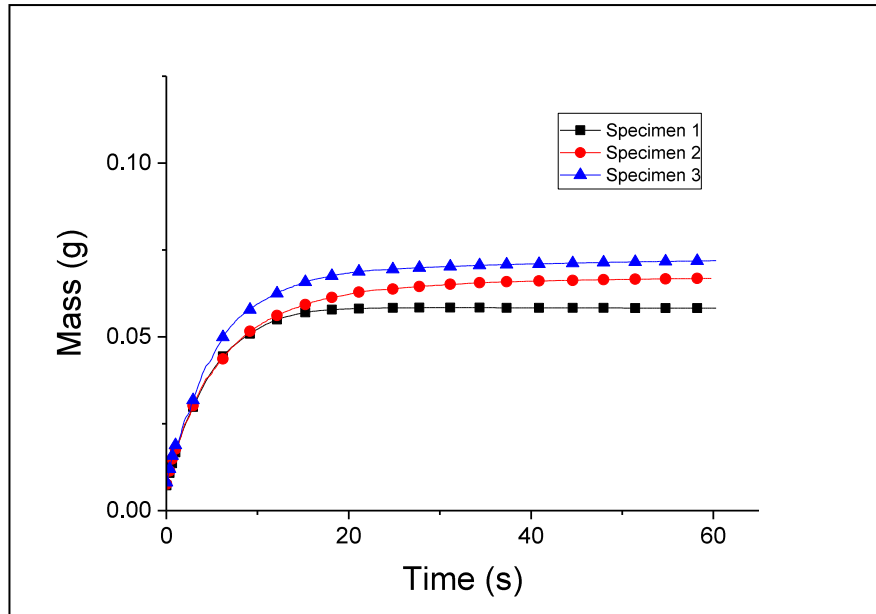


Figure 4.20: BM slurry absorption curves for the low porosity (90.2%) sample in the MD determined by tensiometry

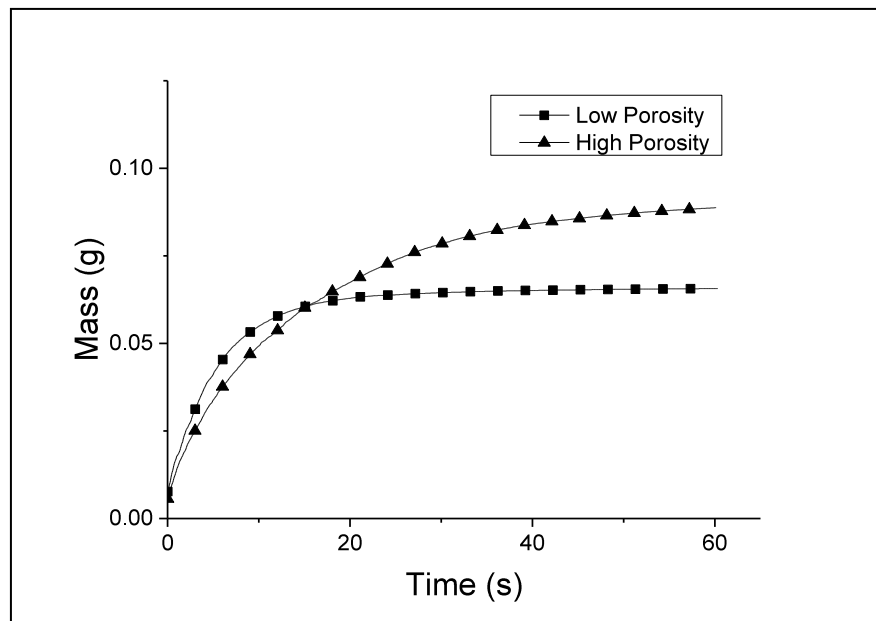
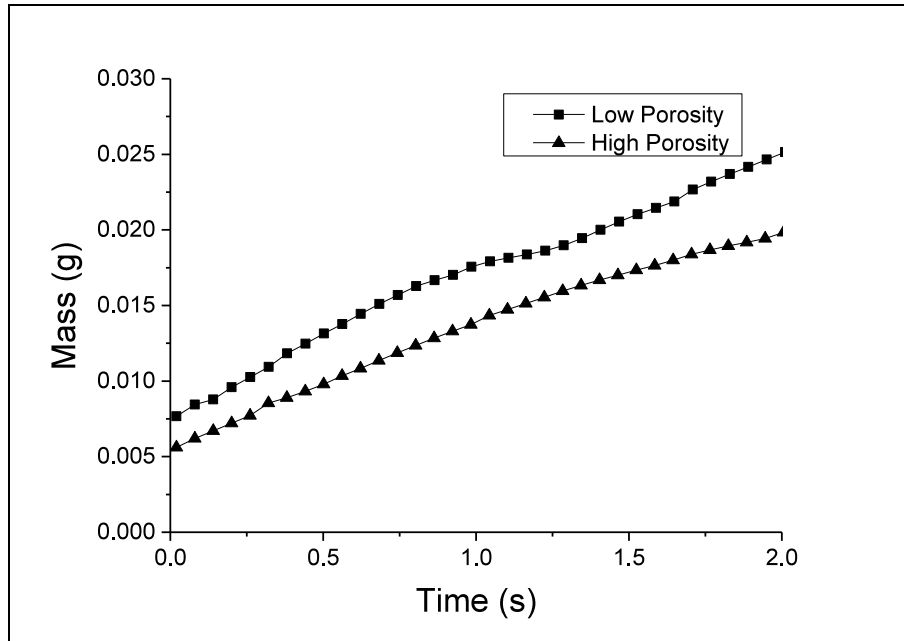


Figure 4.21: BM slurry absorption curves for high (95.6%) and low (90.2%) porosity samples in the MD determined by tensiometry

In practice, it is known that a baby wipe has to perform most effectively in a short time frame after a contact time that may be of only 2 s on average, consistent with the mode of use by the consumer. Average absorption rates were therefore calculated for each sample from the initial absorption curves based on the first two-second response, Figure 4.22.



*Figure 4.22: A plot of the tensiometer absorption curves for high (95.6%) and low (90.2%) porosity samples during the first two seconds of contact with BM slurry.*

The initial sections of each curve are shown in Figure 4.22, for the low and high porosity samples, which increasingly diverge as time approaches 2 s. To calculate the absorption rate over this short 2 s period, the slope was fitted to a linear model for each specimen of the two samples. The resulting slopes were compared to characterise the weight of BM slurry absorbed per unit time. A comparison of the slopes means for the two samples are shown in Figure 4.23. The statistical test showed that the two means are significantly different at a confidence level of 95%.

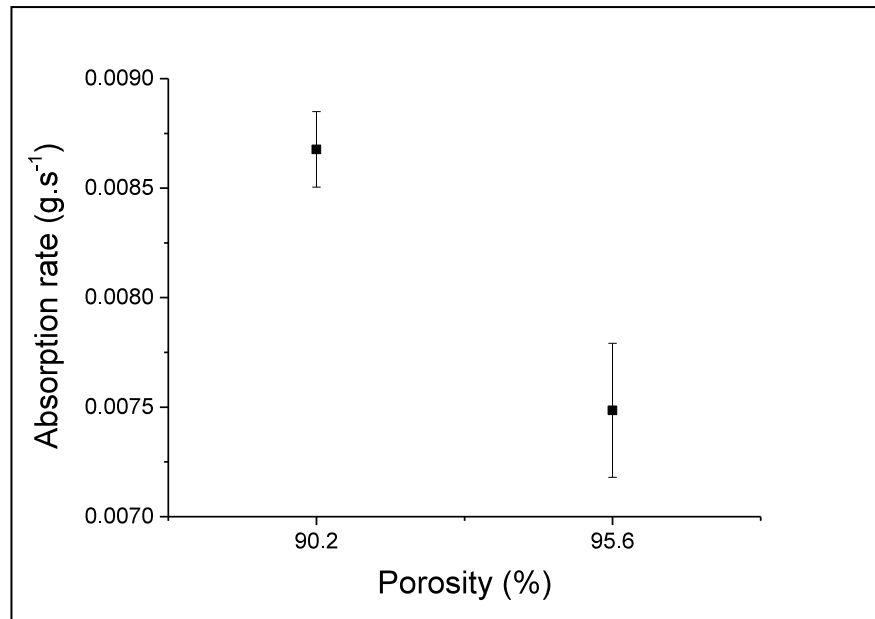


*Figure 4.23: BM slurry weight absorption gradient for the first two seconds in MD*

As hypothesised in section 4.3, the slurry absorption rates for each sample differed according to the respective global porosity.

BM absorption capacity data was also measured after 60 s, as the total weight absorbed in each of the two samples. The higher porosity sample (95.6%) absorbed about 69% more BM than that of the lower porosity sample which demonstrated plateau-like sorption behaviour after only 25 s, which can be explained by the difference in fabric void volume.

Both the Washburn's equation 4.2 and Hagen-Poiseuille's equation 4.3 express the proportional relation between the absorbed quantity of liquid ( $L$  in Washburn's and  $q$  in Hagen-Poiseuille's) and the average pore size (represented by the capillary radius in both equations  $r_c$ ). Other parameters in these two equations such as the surface tension  $\gamma$ , viscosity  $\eta$  and contact angle  $\theta$  will all be different for BM compared to water alone.

Regarding absorption rate, capillary pressure can be expected to be higher in fabrics of lower porosity where mean pore radius is relatively small (Masoodi et al, 2012). However, this does not necessarily mean the overall weight of liquid uptake will be very high, as indicated in Figure 4.21, since the overall pore volume is low. Even over a very short wiping time period of only 2 s,

Figure 4.22 indicates marked differences in BM slurry uptake between high and low porosity fabrics, which increases further up to 60 s.

## **4.5 Influence of Local Porosity on BM Slurry Absorption**

### **4.5.1 Introduction**

As reported in section 4.4, BM slurry absorption behaviour is dependent on global porosity. Optimising the global porosity in a wipe substrate that is expected to remove the largest possible quantity of BM in a short period of time of only ~ 2 s means balancing absorptive capacity and absorption rate. By manipulating the distribution of porosity within a porous medium it is possible to produce structures with absorption behaviour that deviates from what would be predicted by the classical Washburn equation (Chatterjee and Gupta, 2002a). For example, with a constant global porosity, Ridgeway et al. demonstrated how the internal pore geometry, aspect ratio and pore size distribution may be modulated such that that variations in liquid absorption behaviour can be obtained (Ridgway and Gane, 2002, Ridgway et al., 2002). It has been suggested that absorption rate in porous media can be enhanced by broadening the pore size distribution, which does not necessarily mean changing the global porosity, and that local porosity and equivalent hydraulic radius can affect absorption rate (Gane et al., 2004). In other words, the nature of the porosity is also important. Other studies have suggested that absorption capacity can be improved by implementing certain structural designs without compromising the absorption rate (Ridgway et al., 2006).

It is also known that in some porous media, such as coated substrates, the absorption behaviour over short timescales, which is most relevant to baby wipes, does not necessarily follow classical Lucas-Washburn predictions (Rioux, 2003) and (Gane et al., 1999). Similar observations have been made when studying liquid interactions with porous media over short time periods by Ridgeway et al. and by Bosanquet, which was published two years after Washburn's research (Ridgway et al., 2001, Bosanquet, 1923).

Interestingly, these previous studies, have relied upon proposed theoretical models and/or experimental results based on a small selection of materials and liquids. However, the work has not been extended to study of nonwoven fabrics over very short liquid contact time periods. It is therefore of interest to determine the extent to which similar dimensional modifications to a nonwoven fabric by variations in local porosity, for example, can potentially influence BM absorption behaviour.

#### 4.5.2 Experimental Design

Figure 4.24 summarises the approaches evaluated in the preparation of customised nonwoven structures for experimental study with varying local porosities and the methods used for BM slurry absorption.

The approach to manufacturing nonwoven fabrics with different combinations of local porosity has to be carefully considered since other structural changes may inadvertently be introduced at the same time, influencing BM slurry absorption.

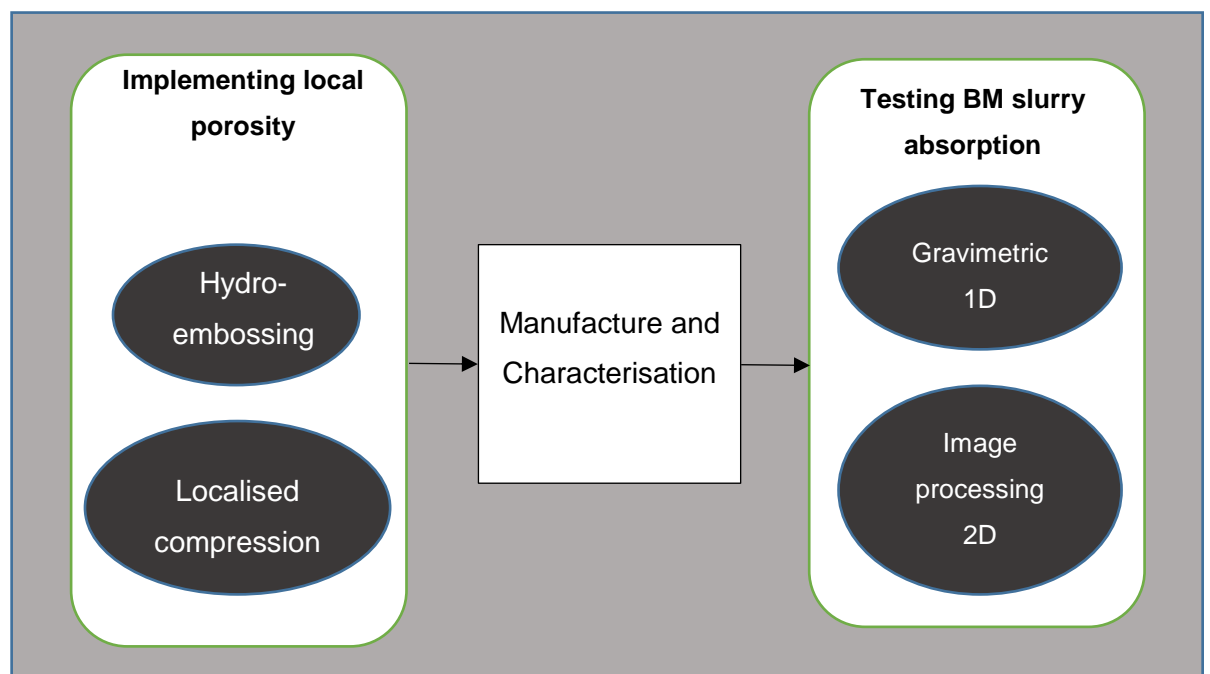


*Figure 4.24: Summary of experimental approaches used to modulate variations in local porosity and to determine resultant BM slurry absorption behaviour*

Changing process conditions during hydroentangling (section 3.1) to introduce regions in the fabric with different levels of porosity can be achieved

by hydro-embossing, as described in section 3.1.3, which produces spatially distributed structural patterns in which porosity, fibre orientation, thickness and fabric density may be affected. While this method is quite convenient from a manufacturing point of view it is inconvenient for the purpose of this experiment, because fibre arrangement is affected not just consolidation. During hydro-embossing, fibres are rearranged such that their local orientation and spatial position in the fabric are modified.

The second approach is to modify the hydroentangled fabric after it is manufactured such that only fabric thickness and consolidation are changed. By decreasing the fabric thickness using compression applied to discrete areas across the sample, local variations in porosity can be introduced without substantially changing fibre orientation. This is therefore a convenient way of studying the effects of local porosity variations on BM slurry absorption. The following section describes how the compression approach was used.

#### **4.5.2.1 *Design of the Compression Moulds***

To enable precise patterning of the fabric during compression, moulds were produced. Three geometrical aspects were taken into consideration. Pattern shape, distribution of repeated element, and size of the compression areas. The pattern shape took the form of a number of repeated squares. This had the benefit of eliminating complexities that could arise from implementing other shapes. A square, or a rectangle, has right angles, this simplifies the study of planar absorption when using the conventional Cartesian coordinate system. It also simplifies the experimental design to investigate the influence of fibre orientation on planar absorption. These squares were distributed in a pattern of rows and columns. The squares in each row were separated by a distance of one square and the rows were repeated with an offset of half the size of the repeated pattern i.e. the size of one square. This distribution design results in a chequered pattern that guarantees the succession of the repeated pattern in each row and each column. Each row was separated from the adjacent ones by a defined distance to maintain the integrity of the mould. Regarding the size of these rectangular areas, a range of sizes was selected to test the applicability of the mould on the sample fabric, taking into consideration the dimensional boundary conditions. The upper boundary

being derived from consumer studies of the typical distance covered by a single wipe and the average size of an adult hand. The lower boundary being defined by the limits of the prototyping machine which is explained next. A drawing of the mould design is shown in Figure 4.25.

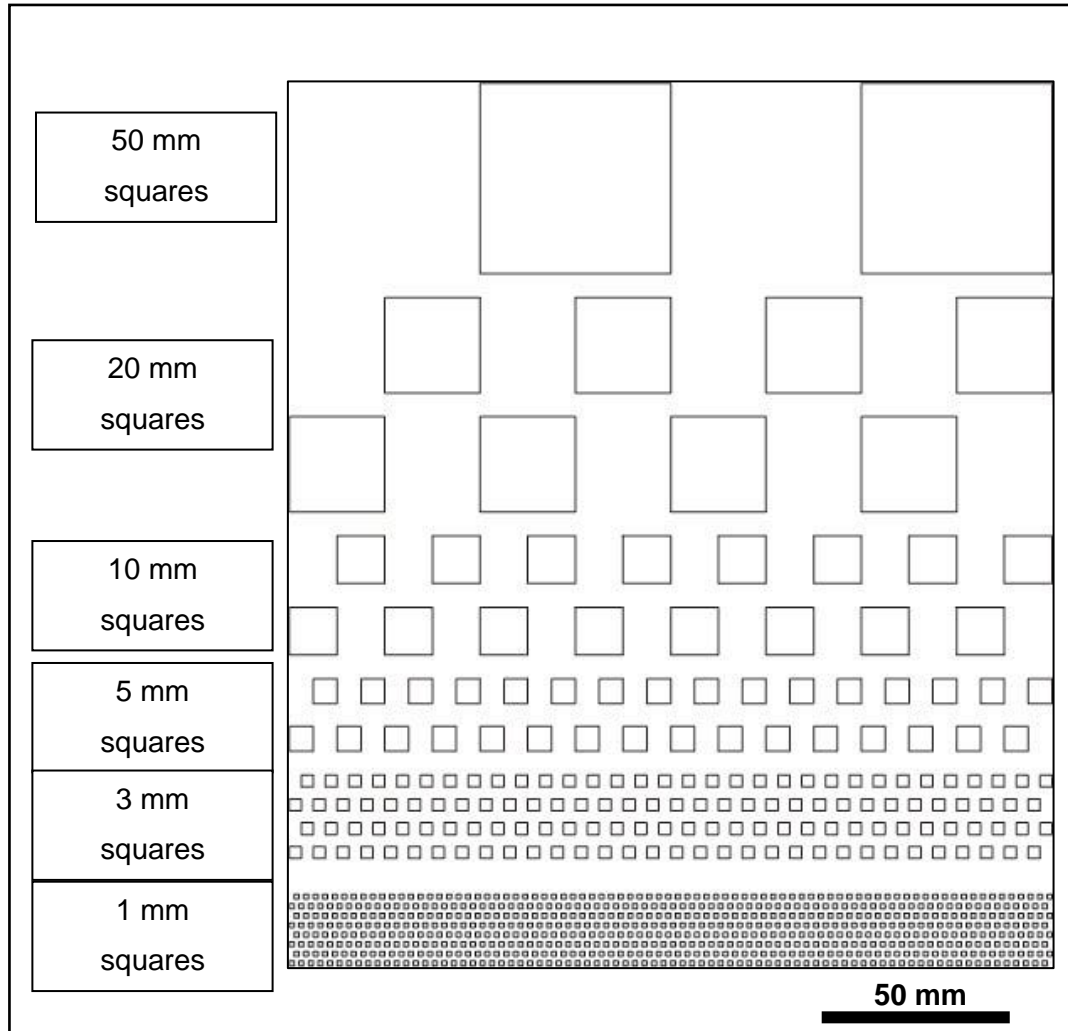


*Figure 4.25: Illustrator drawing of the mould design showing the different sizes of the local compression areas*

The material used to produce the mould comprised 3 mm thick, cast sheet of PMMA (Poly methyl methacrylate) made by Lucite International under the trade mark Perspex® with the product code, Black 962. To cut out the designed patterns a laser cutting machine was used (CAD-CAM Technology (UK) 50 W FB Series laser cutter). The diameter of the laser beam was 100 µm, therefore, the smallest square size selected in the designed range was 1 mm<sup>2</sup>. Figure 4.26 shows the prototype mould.

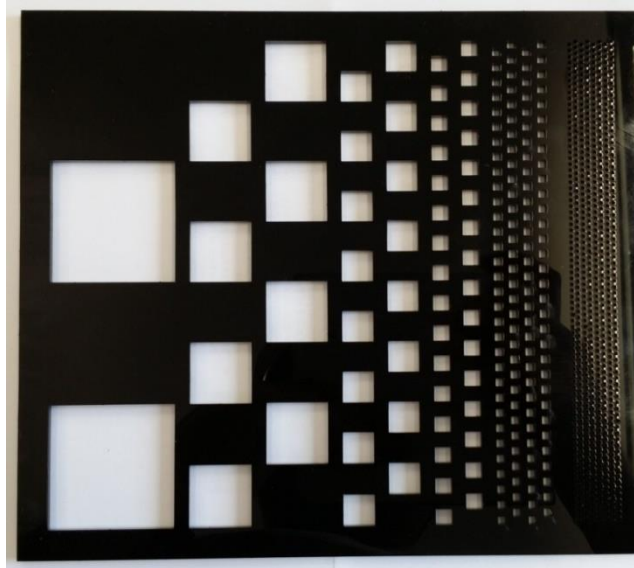


Figure 4.26: Mould template. The square side lengths are from left to right: 50 mm, 20 mm, 10 mm, 5 mm, 3 mm and 1mm

#### 4.5.2.2 Fabric Compression and Resulting Characteristics

The hydroentangled fabric sample used in this experiment was prepared as explained in section 3.1. The mould was laid on top of the fabric and both were laid between two aluminium plates. These two plates were then horizontally placed between the two jaws of a hydraulic press, Figure 4.27.

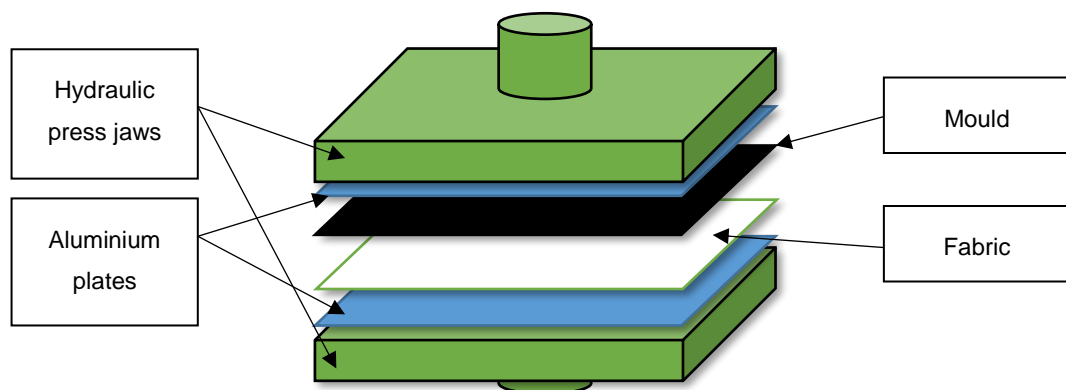
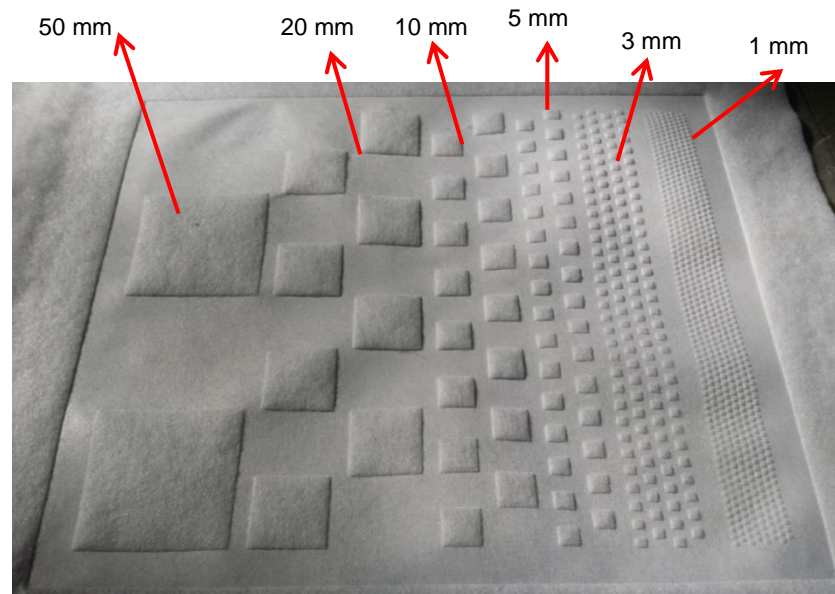


Figure 4.27: Schematic of the fabric compression set up using the prototype mould to introduce areas of different local porosities to the sample.

The pressure was set to  $7.6 \text{ kgf.cm}^{-2}$  which is approximately  $0.745 \text{ MPa}$ . The sample was left under the aforementioned pressure for 20 min. After compression, the appearance of the fabric is illustrated in Figure 4.28.



*Figure 4.28: Nonwoven fabric after compression using the mould template for 20 min at a pressure of  $0.745 \text{ MPa}$ .*

The fabric thickness was measured and the resulting local porosity was calculated for both the compressed and non-compressed areas. For measuring the fabric thickness, the method described in section 3.2 was used. Porosity was calculated by equation 3.1 (Chatterjee and Gupta, 2002b), and the resulting values were  $\Phi_{\text{high}} = 95.6\%$  for the non-compressed sample and  $\Phi_{\text{low}} = 90.2\%$  for the compressed sample.

The different square sizes shown in Figure 4.28 are all achieved using the compression approach presented in Figure 4.24. Reproducible changes in porosity could be obtained for each mould dimension and the resulting effects on BM slurry absorption behaviour were investigated.

### **4.5.3 Testing BM Slurry Absorption**

In this section, the investigation of BM slurry absorption by the prototype fabric is presented. Initially, the absorption behaviour in one dimension was investigated. Absorption behaviour was evaluated gravimetrically. Two-dimensional observations were also made in which evaluation was carried out

using image analysis. The purpose of these observations is to improve the understanding of BM slurry flow through nonwoven fabrics with local porosities. Only one run was conducted in each test and the results were not used to define the settings for the experimental work in the following sections 4.6 to 4.8.

#### 4.5.3.1 **Gravimetric Evaluation (1-Dimensional spread)**

Sampling for this experiment was performed by cutting out a piece of the compressed fabric which contained two areas of different porosity (compressed and uncompressed regions). The porosity borderline extended in parallel to the direction of absorption. Theoretically, in this case, liquid absorption in each of the local porosity areas could be described as one-dimensional unsteady-state transport in a homogeneous anisotropic nonwoven in the horizontal direction, as explained by Mao (2009b).

#### 4.5.3.2 **Test Procedure**

The fabric sample was placed horizontally on a smooth glass plate. Then a 2 ml pool of slurry (prepared using the method in section 2.5.3) was introduced at the edge of the fabric sample in a way that covered both sides of the porosity border line as in Figure 4.29, (left). The slurry was introduced from the edge of the fabric for the purpose of observing one dimensional spread of BM slurry. After two minutes, the fabric sample was separated from the slurry and its appearance is shown in Figure 4.29, (right). The two porosity areas were then cut apart and weighed. Their weight was then compared to the weights of an identical sample of fabric without slurry.

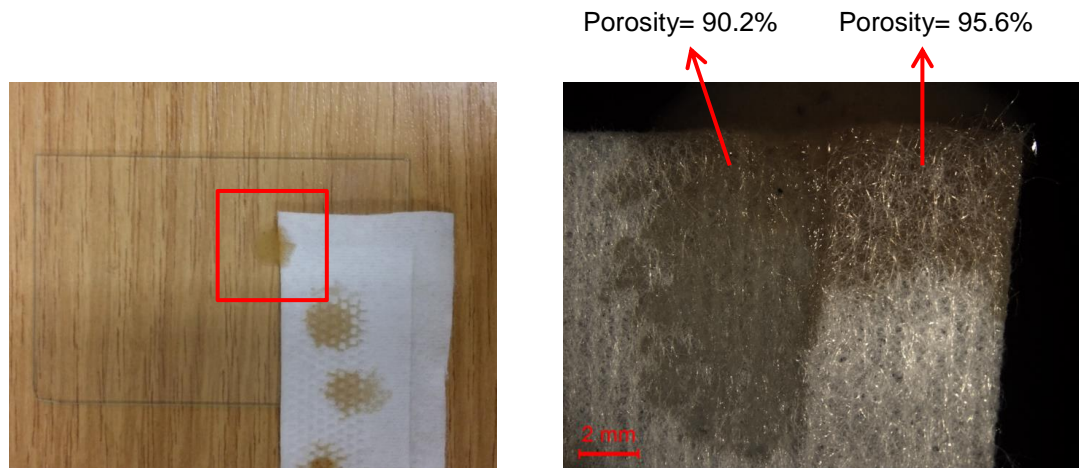


*Figure 4.29: Slurry absorption in 1D as it occurs in parallel to the porosity borderline. Left: introduction of slurry to the edge of the fabric sample, right: magnified image of the sample after 2 min*

#### 4.5.3.3 **Results and Discussion**

By examining Figure 4.29, (right), the differential spread of slurry associated with differences in local porosity can be observed. As expected, due to the differences in the void volume, the area covered by slurry in the low porosity region is larger than that in the high region. This reinforces the findings in section 4.4, in relation to global porosity. What could not be explained in the global porosity experiments, however, is how local porosity variations influence local BM slurry spreading behaviour, Figure 4.30, image 1. By examining the flow front profile of the BM slurry, particularly in the high porosity area, the shape of the leading edge can be discerned, as illustrated in Figure 4.30, image 2 where the direction of BM absorption is indicated by the arrow D.

Curve A represents the flow front. It shows that BM slurry did not penetrate the fabric at the same rate across the width of the fabric, and appeared to have advanced at the sides more than in the middle. The advancement on the side B can be explained by the different porosities on its sides. The line B represents the porosity borderline, and on the other side of it lies the low porosity area where it has been demonstrated (section 4.4.3) that the slurry absorption rate is expected to be higher. This means that by the time the flow front in the high porosity area reaches a defined point on the porosity

borderline, the slurry would have already wetted that point from the low porosity area. This makes line B a source of earlier occurrence of slurry influx towards the high porosity area than the flow front of that area itself. Line C represents the edge of the fabric sample which was cut using scissors. At this line, the fibres are probably sheared and most likely physically bound together due to shearing, subsequently, structural properties in this region are different. This explains the different absorption behaviour along this line. Referring to curve A, it is reasonable to consider that line B is where the maximum absorption spread happens. In other words, in the high porosity area, absorption is fastest at the porosity borderline.

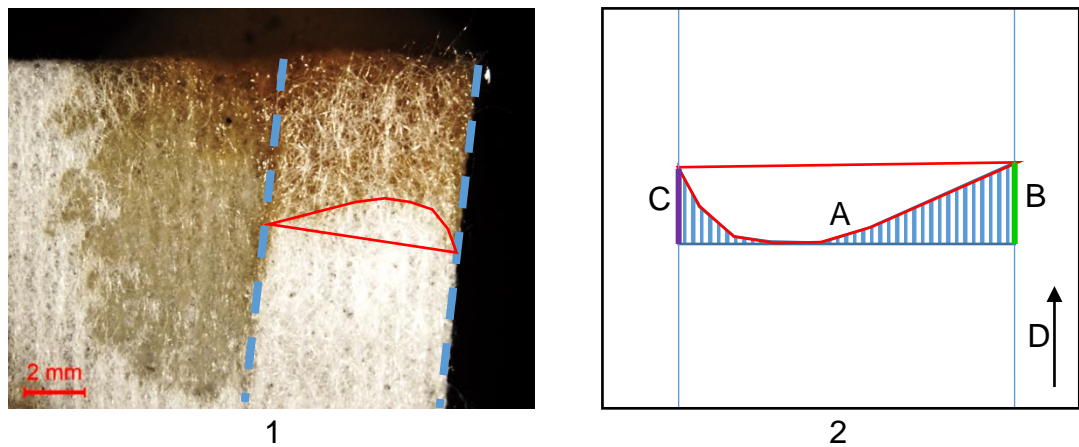


*Figure 4.30: 1: Enhanced image of 1D BM absorption sample after 2 min  
2: corresponding flow front of the BM slurry in the high porosity area*

This conclusion, however, does not explain why a sample with low global porosity would show an overall higher absorption behaviour. This is why a quantitative assessment was also made to obtain gravimetric data, Figure 4.31.

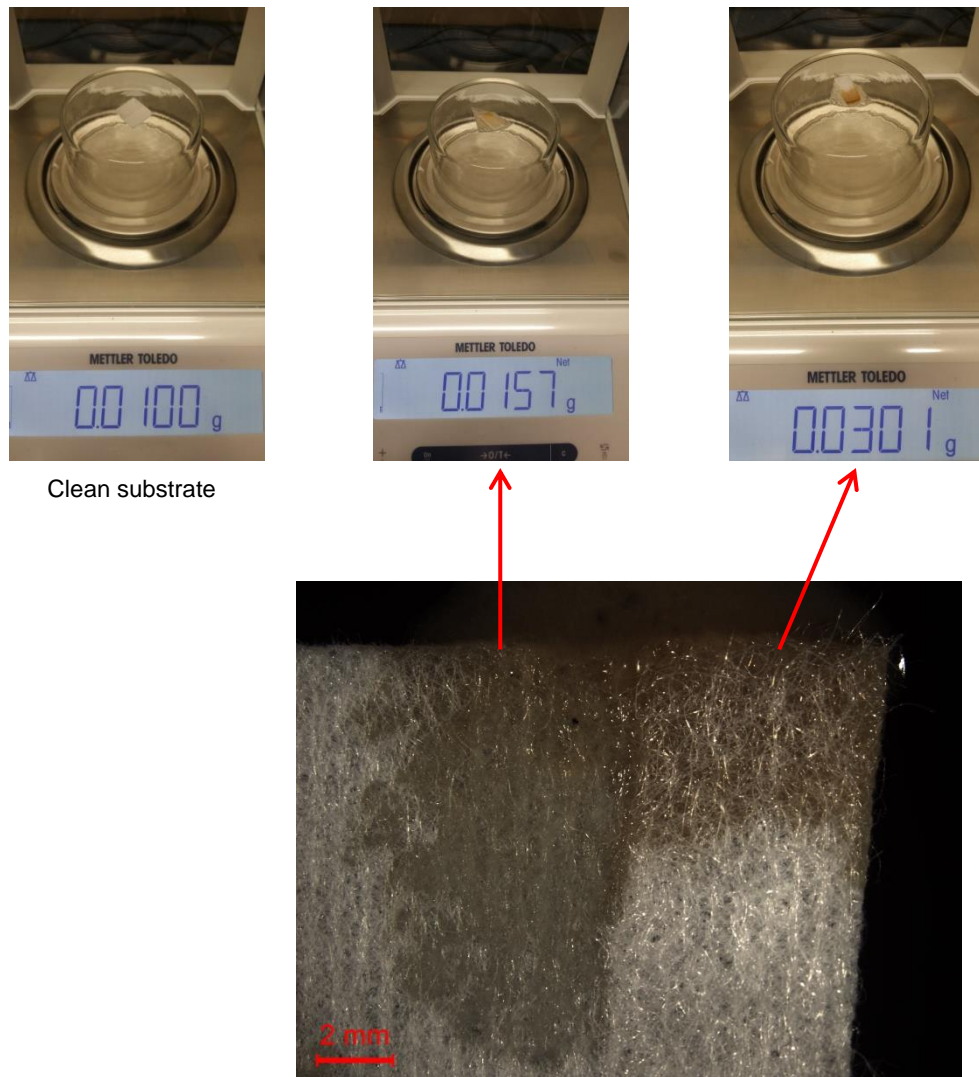


Figure 4.31: Gravimetric data for each region in the 1D BM absorption experiment

The overall weight reading for the BM containing fabric sample ( $m_f$ ) was:

$$m_f = 100 \times 10^{-4} \text{ g}$$

The weight reading for the low porosity region of the fabric sample containing BM slurry, ( $m_1$ ), was:

$$m_1 = (m_f/2) + m_{l.sl} = 157 \times 10^{-4} \text{ g} \rightarrow m_{l.sl} = 107 \times 10^{-4} \text{ g}$$

Where  $m_{l.sl}$  is the weight of BM slurry absorbed by the low porosity region of the sample. The weight reading of the high porosity part of the fabric sample with BM slurry, namely ( $m_2$ ), was:

$$m_2 = (m_f/2) + m_{h.sl} = 301 \times 10^{-4} \text{ g} \rightarrow m_{h.sl} = 251 \times 10^{-4} \text{ g}$$

Where  $m_{h.sl}$  is the weight of BM slurry absorbed by the high porosity region of the sample.

$$m_{h.sl} / m_{l.sl} = 2.35$$

The weight results illustrate that although the high porosity area, does not enable a high spread of BM slurry, it absorbed more than twice the amount of BM slurry as the low porosity area which, during the same period of time, spreads the BM slurry over a larger area of fabric, in addition to increasing the amount of BM slurry absorbed by the high porosity area. This is evidence that slurry absorption behaviour can be positively influenced by both the high and low porosity areas within the same fabric sample.

#### **4.5.3.4 *Evaluation Using Image Processing (2-Dimensional spread)***

The one-dimensional analysis suggests that the BM slurry absorption behaviour in one direction is enhanced by the presence of a porosity borderline. In a 2-dimensional BM slurry absorption experiment, the porosity borderline is not a simple straight line but has a shape. This shape, along with its size and distribution pattern, have been discussed in section 4.5.2.1. This section investigates the absorption behaviour of BM slurry as it spreads in two dimensions through a fabric sample that contains areas of different local porosity levels.

Selecting the appropriate square pattern size from the range produced on the sample was based on the following criterion. The maximum pattern size to be tested was determined by the application of these nonwoven fabrics as baby wipes. This means, in order for the experiment to be relevant to the application, the repeated pattern must occur at least one time during a single wipe cycle. Considering the smallest possible single wipe cycle is equal to the size of a small size fingertip (Hohendorff et al., 2010, TheAverageBody.com, 2012). Patterns that have squares of the size of 5 mm and higher have repeated elements of 10 mm and higher, and this does not guarantee the occurrence of a complete repeated element which means they do not meet the criterion, therefore, they were not selected for this particular study.

#### 4.5.3.5 *Measuring Procedure*

BM slurry was prepared for this test the same way explained in Section 2.5.3. The fabric samples were cut out of the nonwoven fabric for each of the pattern sizes, 1 mm and 3 mm. Each sample was laid on a microscope slide and then mounted on an optical microscope sample holder (Leica M205 C microscope). Under reflected light, images were recorded using Leica Application Suite v4.1. A single droplet of 2 ml of BM slurry was dropped on to the centre of the sample. At this point a second image was captured and saved to record the size and shape of the droplet. BM slurry was left to be absorbed by the patterned fabric for 2 min. A third image was captured and saved after 2 min had elapsed.

#### 4.5.3.6 *Image Analysis*

The images were processed using the open source software ImageJ. Image processing was performed to isolate the areas of the fabric containing absorbed BM slurry. The first and third images containing pattern sizes of 1 mm were transformed into greyscale in order to eliminate contrast variations originating from the inhomogeneity of the slurry. A greyscale image is a 2D map of pixels in which each pixel carries intensity information. This data ranges from 0, which means complete black to 255, which means complete white. Since the slurry in the images appeared as darker areas, it made sense to invert the images such that the clean areas were converted to dark black, and the BM slurry areas into bright white. Once the two images were inverted, the first image was subtracted from the third image. This omitted the clean areas from the third image and resulted in an image showing only the slurry represented by pixel brightness. The resulting images are shown in Figure 4.32. The same procedure was performed for the 3 mm pattern size 3 mm as indicated in Figure 4.33.

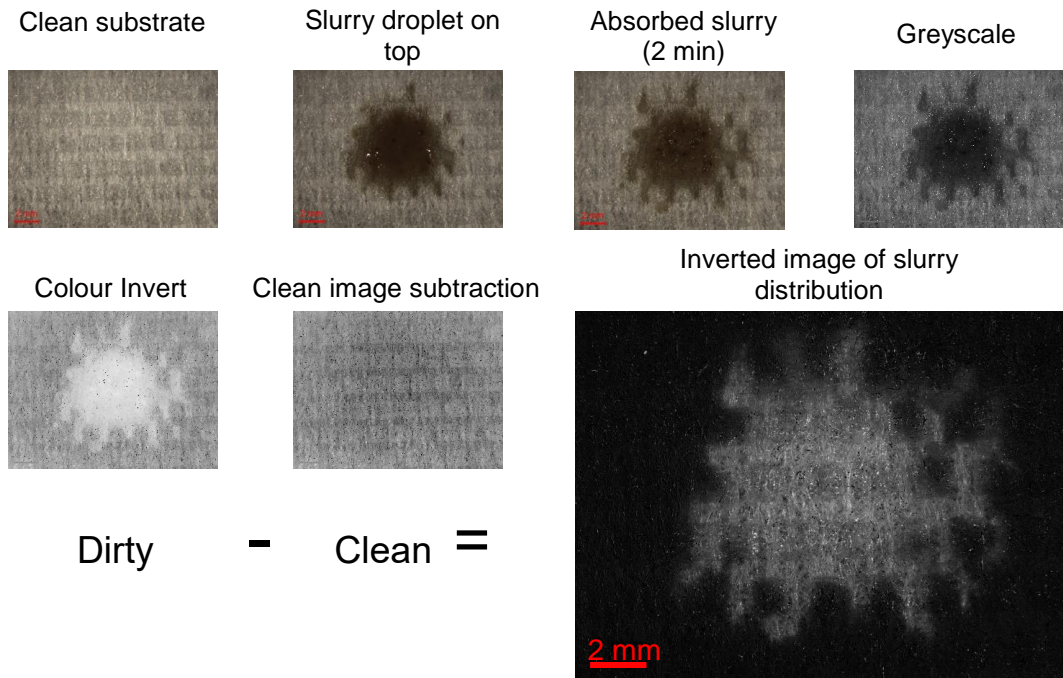


Figure 4.32: Image processing steps of the 1 mm pattern. This sample was taken from the part of the fabric to which local porosity areas of  $1 \text{ mm}^2$  were introduced. The images were converted to greyscale then their colours were inverted. Both the clean image when  $t = 0 \text{ s}$  (background) and the image taken at  $t = 120 \text{ s}$  (2 min) underwent those two image processing steps. The final image is the result of subtracting the two images taken at  $t = 120 \text{ s}$  and  $t = 0 \text{ s}$  respectively.

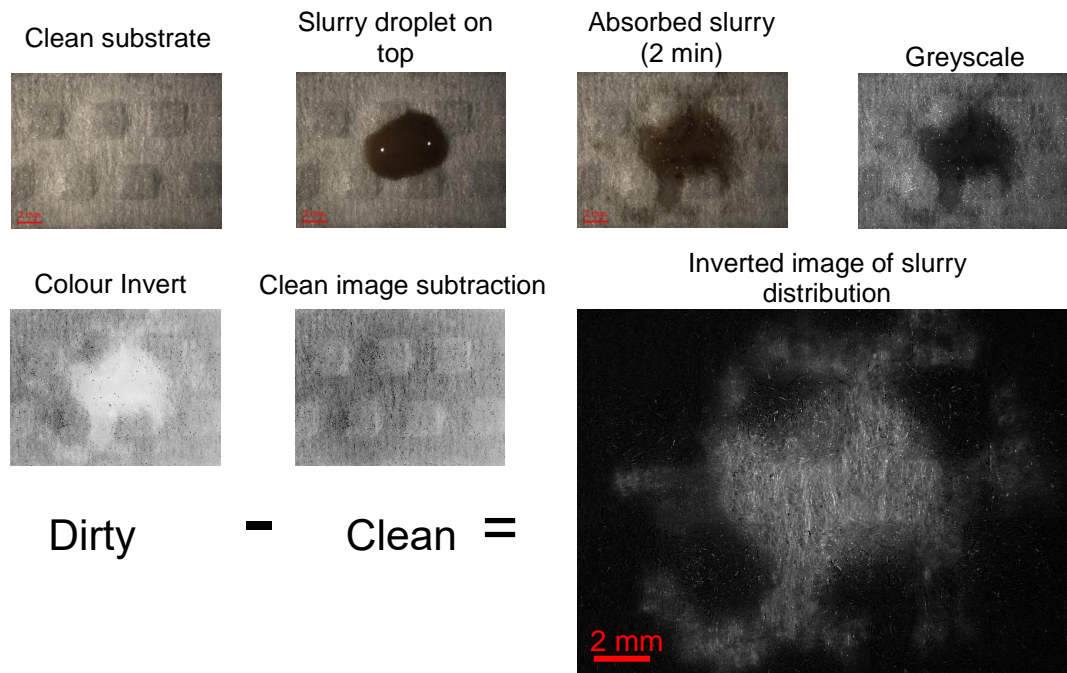
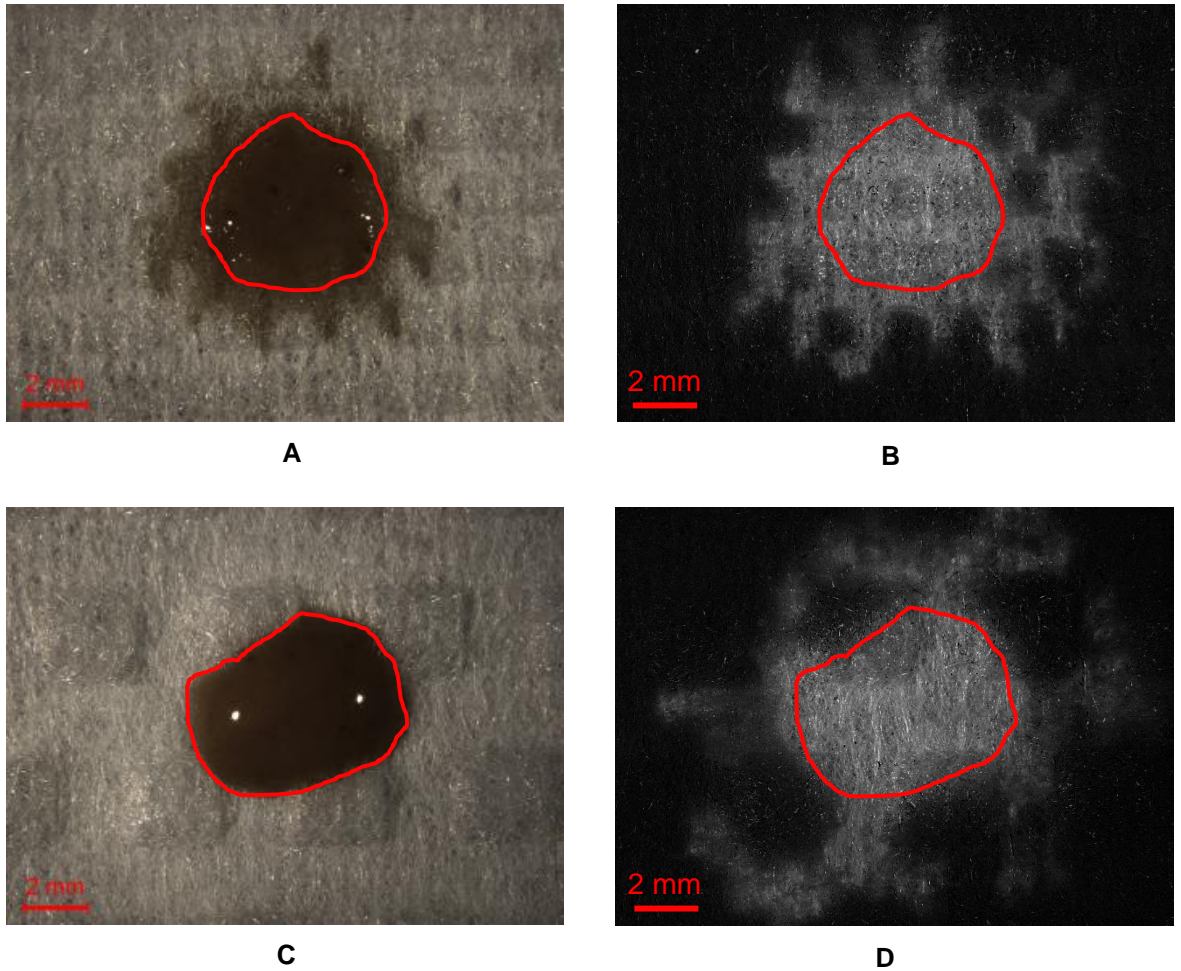


Figure 4.33: Image processing steps of the 3 mm pattern. This sample was taken from the part of the fabric to which local porosity areas of  $9 \text{ mm}^2$  (3-mm-sided squares) were introduced. The images were converted to greyscale then their colours were inverted. Both the clean image when  $t = 0 \text{ s}$  (background) and the image taken at  $t = 120 \text{ s}$  (2 min) underwent those two image processing steps. The final image is the result of subtracting the two images taken at  $t = 120 \text{ s}$  and  $t = 0 \text{ s}$  respectively.

#### 4.5.3.7 Results and Discussion

The size and shape of the BM slurry outline, represents the spreading behaviour. Referring to Figure 4.34, it is clear that the BM slurry spread in an irregular manner such that the response could not be considered isotropic. The outlined leading edge of the BM slurry absorbed by the patterned fabrics, represented by the high intensity pixels shown in Figure 4.34, images B and D, deviates significantly from a circle or from the original shape of the droplet. This is due to the BM slurry transporting faster through certain regions than others, a phenomenon discussed by Ridgway et al. (2002) about the behaviour of liquids in porous media (section 4.5.1).



*Figure 4.34: Comparing the initial shape of the slurry drop with the shape of its spread within the patterned nonwoven fabric after 2 min.*

**A:** 1 mm patterned fabric (Figure 4.32) at  $t = 0$  s. **B:** processed image of A. **C:** 3 mm patterned fabric (Figure 4.33) at  $t = 0$  s. **D:** processed image of C.

Clearly, the patterning of the fabric and the provision of discrete regions of low and high porosity introduces dimensional heterogeneity, which means a modification in both the local porosity and the local resistance to flow (permeability) in the nonwoven. It is apparent from the shape of the BM fluid front, that this affects local liquid transport, and therefore can be modulated to customise the way in which BM slurry is absorbed by the fabric.

## **4.6 Influence of Local Porosity Profiles in the Fabric Cross Direction on BM Slurry Absorption**

### **4.6.1 Introduction**

Initial investigations of the effect of local porosity regions the hydroentangled fabric samples confirmed its influence on the absorption behaviour of BM slurry, as discussed in sections 4.5.3.3 and 4.5.3.7. The absorption rate in the presence of a porosity borderline is particularly important in order to understand how absorption behaviour changes with time (unsteady-state fluid flow), particularly in the first few seconds of BM absorption.

The porosity borderline can be defined as the sum of locations within the fibrous structure of the fabric where the level of porosity substantially changes such that a separating boundary is present between the two areas. A fabric with a porosity borderline parallel to the direction of BM absorption can demonstrate behaviour that deviates from the conventional Lucas-Washburn equation. Mao concluded that the global permeability of a patterned nonwoven fabric is a function of the permeability of its local homogeneous areas, which in turn, is influenced by the local porosity of these areas. In other words, nonwoven fabrics with heterogeneous structures, having dual porosity properties arranged in patterns, have been mathematically demonstrated to have unconventional liquid permeability (Mao, 2009a).

The structural properties of porous media and their influence on liquid absorption behaviour have been studied theoretically and experimentally and this has enabled a thorough understanding of the fundamental mechanisms to be established (Chatterjee, 1985, Chatterjee and Gupta, 2002a, Bal et al., 2011, Gane et al., 2004, Kim and Kim, 2012, Mittal, 2006, Ridgway et al., 2002). Specifically, liquid absorption in fibrous media, particularly nonwoven fabrics has been studied, and the influence of fibre arrangement has been intensively investigated (Das et al., 2012, Landeryou et al., 2005, Landeryou et al., 2003, Manas et al., 2007, Mao, 2000, Mao and Russell, 2003b, Mao and Russell, 2010, Pan and Zhong, 2006, Patnaik et al., 2006, Tang et al., 2015a, Tang et al., 2015b, Mao and Russell, 2003a, Mao and Russell, 2008).

While absorption in inhomogeneous porous media has been both theoretically and experimentally modelled (Bal et al., 2011, Gerke and van Genuchten, 1993, Ridgway et al., 2006, Gerke and van Genuchten, 1996, Kim et al., 2015), studies of liquid absorption in inhomogeneous fibrous media is rather limited to theoretical modelling and relatively little experimental work (Čiegis and Zemitis, 1997, Hall et al., 1996, Holzel et al., 2007, Mao, 2009b, Mao, 2009a, Mao and Russell, 2000a, Mao and Russell, 2000b, Mao and Russell, 2010).

The modelling work of Mao (2009a, 2009b), concluded that there is a rapid increase of capillary pressure and velocity in high porosity areas and a relatively slow increase in the low porosity areas (Mao, 2009b). What was not addressed in Mao's work is how liquid flow behaviour in patterned nonwoven fabrics compares to that in homogeneous nonwoven fabrics. Mao's results, however, reveal the dependence of global permeability of dual porosity patterned nonwoven fabrics on the ratio of dimensions for their local porosity areas and not by their absolute values (Mao, 2009a). Although no validation of Mao's models has yet been reported, neither by simulation nor experimentation, it provides a state of the art modelling approach describing the absorption behaviour of anisotropic patterned nonwoven fabrics.

Liquid flow in unsaturated nonwoven fabrics is example of unsteady-state flow. In such flow conditions, the characteristics of flow depend on time. To understand the function of dual porosity patterned nonwoven fabrics in absorbing liquids, this flow must be predicted. The relationship between the unsteady flow and the structural properties of dual porosity patterned nonwoven fabrics has been modelled by Mao (2009b). Homogeneous anisotropic nonwoven fabrics were studied together with patterned homogeneous anisotropic nonwoven fabrics. This unsteady-state flow in patterned nonwoven fabrics has also been modelled using dual permeability models (Mao, 2009b).

Patterns on nonwoven fabrics are local areas of different structural properties where the differences might be introduced during the manufacturing process or by the presence of binders, apertures or local differences in packing density

(Russell, 2007). Patterned nonwoven fabrics are frequently used as hygiene products such as wipes or as medical absorbent fabrics (Mao, 2009a). The use of certain patterns in the fabric has been for the purpose of modifying aesthetics, mechanical properties or as means of joining two functionally different product parts by, for example, lamination (Russell, 2007). While the liquid flow through such fabrics has been studied and modelled, it has been merely for the purpose of understanding product behaviour. It has not been utilised to enhance the performance of a nonwoven wipe. The reason this is most likely due to the reasonable assumption that enhancing the absorptive capacity will adversely affect the absorption rate, or vice versa, as explained in section 4.4.3.

There is reason to believe certain structural or dimensional properties of the fabric could enhance overall BM slurry absorption performance. Recent work on porous media other than textiles has shown interesting results. Sun et al, (Sun et al., 2016), developed a model to simulate flow of aqueous liquids in porous media and used it to predict the imbibition dynamics of such liquids in pore networks with bimodal pore size distribution. Sun et al. concluded that imbibition rate depended strongly on the orientation of pore arrangement, their continuity and cluster distribution, which cannot be described by Lucas-Washburn (Sun et al., 2016). However, their work on bimodal pore size distribution networks was only based on simulations and no experimental results based on sample measurements were presented. Additionally, Gane et al. (2004) argued that in addition to porosity, a structural complexity descriptor representing additional parameters such as pore size distribution, pore shape, pore shape distribution, tortuosity and connectivity should be considered. They then demonstrated mathematically that this complexity descriptor is one of the main factors affecting liquid absorption. No previous work dealing with the absorption behaviour of BM slurry as it relates to wipes is available in the academic literature. It is therefore of interest to explore this aspect in greater detail.

#### **4.6.2 Experimental Aim**

The purpose was to explore the influence of local porosity as a potential factor influencing BM slurry absorption in hydroentangled nonwoven fabrics. While

in the previous experiment discussed in section 4.5.3, the fabric samples were presented horizontally to the BM slurry, and there was no influence of gravity, the present experiment was designed differently. Because of the necessity to measure the absorbed BM slurry weight in real time, the nonwoven fabric specimens with different porosities were held vertically during testing. The weight of the BM slurry was measured as it penetrated the nonwoven fabric sample upwards against gravity. Measurements were obtained using the tensiometry procedure described in section 4.4.1.

### **4.6.3 BM Slurry Absorption Behaviour Using Tensiometry**

The test method was based on the use of tensiometry (Kruss tensiometer, K100SF). Details of the method are explained in section 4.4.1. The tensiometer settings and BM slurry sampling were not changed. To obtain porosity profiles in the fabric's cross direction, the compression method using a plastic mould explained in 4.5.2 was used.

### **4.6.4 Materials and Methodology**

With reference to Figure 4.35, specimens of hydroentangled nonwoven fabric with different porosities (specifications summarised in 4.5.2.2) of dimensions 20 mm x 45 mm were carefully cut using a rigid template. After the tensiometer calibration process as detailed in section 4.4.1, a specimen was mounted in the tensiometer jaws of the specimen holder. BM slurry was prepared by mixing the lotion with BM (65% water content), as explained in section 2.5.3, with a weight ratio of 1:1. A total volume of 30 ml of the BM slurry was placed in the container of the tensiometer.

To conduct the measurement, the container containing the BM slurry was raised by the motorised table towards the lower (leading) edge of the specimen such that 0.5 mm of the fabric was immersed and wetted out at a rate of 10 mm.min<sup>-1</sup>. Measurement was started as soon as the correct immersion depth was achieved and the distance between the specimen holder and the motorised table was then locked for the set duration of the measurement, which was 60 s. During the experiment, data is recorded where the balance readings were logged into the database at the predefined rate. In this experiment, the balance reading rate was 10 Hz with the exception of the

first second, where it was set to 30 Hz (see section 4.4.1). After 60 s, the measurements stop automatically and the balance was then locked.

Fabric samples were all prepared from the same ternary fibre blend of 60% 3.3 dtex trilobal polypropylene; 20% 1.0 dtex trilobal polypropylene and 20% 1.7 dtex viscose, as described in section 3.1. The procedure minimised any changes to fibre orientation or basis weight of the samples to aid interpretation of the results.

Each fabric sample was compressed under controlled conditions to achieve the required local porosity structure using the hydraulic press and the prepared mould as described in section 4.5.2.2. Then, the specimens were cut out of the compressed fabric using a rigid template. Two different patterns were cut as shown in Figure 4.35. Sample A contained two areas, one with high porosity (95.6%) and one with low porosity (90.2%). Both areas had the same width of 10 mm and this leading edge was the first region to come in to contact with the BM slurry surface. Sample B, on the other hand, contained four distinct regions, two of high porosity (95.6%) and two of low porosity (90.2%). Each of these regions had a width of 5 mm and therefore a leading edge of 5 mm. The total length of the leading edge for the high porosity areas was therefore 10 mm, and the same for the low porosity area, which was equal to that in Sample A. To calculate the global porosity of the samples, equation 4.8 was applied (Mao, 2009b). From a global porosity point of view, the two samples were also equal, as shown in equations 4.8 to 4.13.

$$\varepsilon = \psi_h \varepsilon_h + \psi_l \varepsilon_l \quad 4.8$$

Where  $\varepsilon$  is the sample's global porosity,  $\psi_h$  and  $\psi_l$  are the relative volumetric proportions of the high porosity and low porosity areas respectively,  $\varepsilon_h$  and  $\varepsilon_l$  are the local porosities of the high porosity and low porosity areas respectively.

Since the collective volume of the high and low porosity areas in sample A was equal to that of sample B, the volumetric proportions of the high and low porosity areas in samples A and B were equal, equations 4.9, 4.10 and 4.11.

$$\psi_{h_A} = \psi_{h_B} \quad 4.9$$

$$\psi_{l_A} = \psi_{l_B} \quad 4.10$$

Where  $\psi_{h_A}$  and  $\psi_{h_B}$  are the relative volumetric proportions of the high porosity areas in samples A and B respectively. By substituting local porosities with their values in equation 4.8 equations 4.11 and 4.12 are obtained, and by subtracting them and solving for either  $\varepsilon_A$  or  $\varepsilon_B$  we obtain equation 4.13.

$$\varepsilon_A = \psi_{h_A} \times 95.6 + \psi_{l_A} \times 90.2 \quad 4.11$$

$$\varepsilon_B = \psi_{h_B} \times 95.6 + \psi_{l_B} \times 90.2 \quad 4.12$$

$$\varepsilon_A = \varepsilon_B \quad 4.13$$

Where  $\varepsilon_A$  and  $\varepsilon_B$  are the global porosities for sample A and sample B respectively.

However, due to the expected differences in the BM slurry spreading the local porosity areas, sample B had three porosity borderlines, which was two borderlines greater than sample A, despite them having the same global porosity.

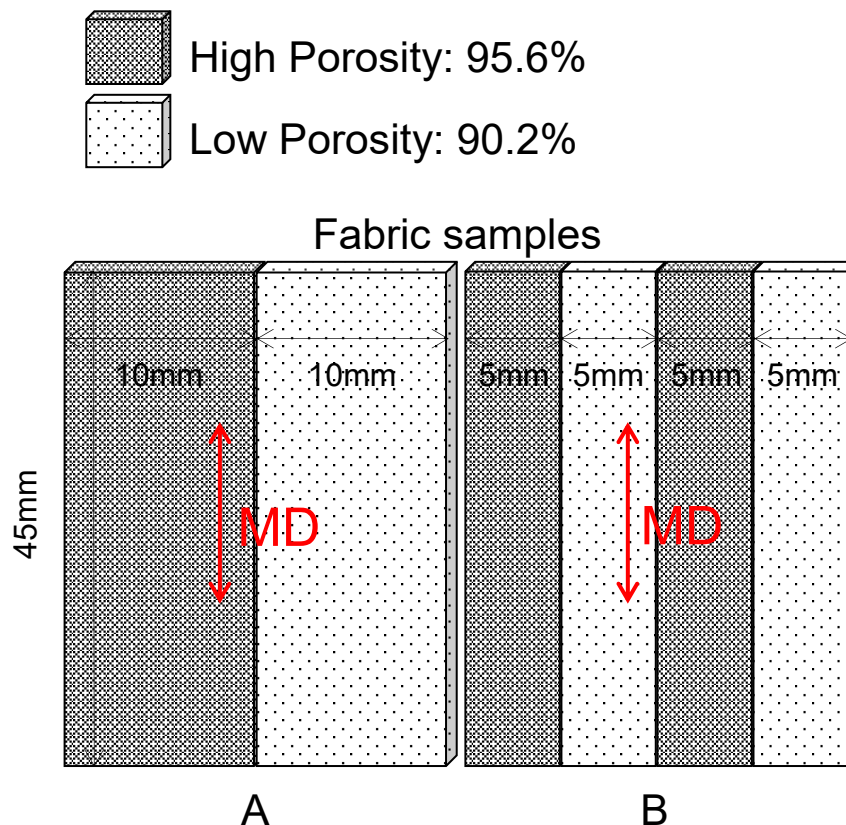


*Figure 4.35: Local porosity hydroentangled nonwoven fabric samples. A: Pattern A contains two equal areas which differ in porosity and are separated by a vertical porosity borderline. B: Pattern B contains four equal areas alternating in porosity between high (95.6%) and low (90.2%), and are separated by three vertical porosity borderlines*

The only difference between patterns A and B is in the distribution of local porosity areas. Ridgeway et al. found that porous media with identical porosity can display markedly different liquid absorption behaviour depending on internal structural properties, (Ridgeway et al., 2002). If this is true for BM slurry absorption by nonwoven fabrics, then sample A can be expected to behave differently to sample B.

#### 4.6.5 Results and Discussion

Figure 4.36 shows the absorption curves for nonwoven samples A and B for a duration of 60 s. These curves provide a general overview of the samples' BM slurry absorption behaviour, which appear to be similar for the two porosity

patterns. Focusing on the first 2 seconds of BM slurry absorption, which is of practical significance in wiping applications, the curves appear to be linear. A slight difference between the samples is noticeable, as shown in Figure 4.37. This difference did not prove to be statistically significant. However, absorption rate was calculated and compared with the global porosity samples, Figure 4.38. The rate of absorbed BM slurry weight per unit time is calculated by fitting the curves with a linear model. The linear fit calculation was applied to a duration of one second for  $t = 0 \rightarrow 1$  seconds and  $t = 1 \rightarrow 2$  seconds. All linear fit models had a good fit with  $R^2 > 0.99$  as shown in Figure 4.39, Figure 4.40, Figure 4.41 and Figure 4.42. For a complete comparison of BM slurry absorption rate in the first two seconds between the patterned porosity samples and the global porosity samples presented previously in section 4.4, Table 7 shows the resulting slopes for each of the models.

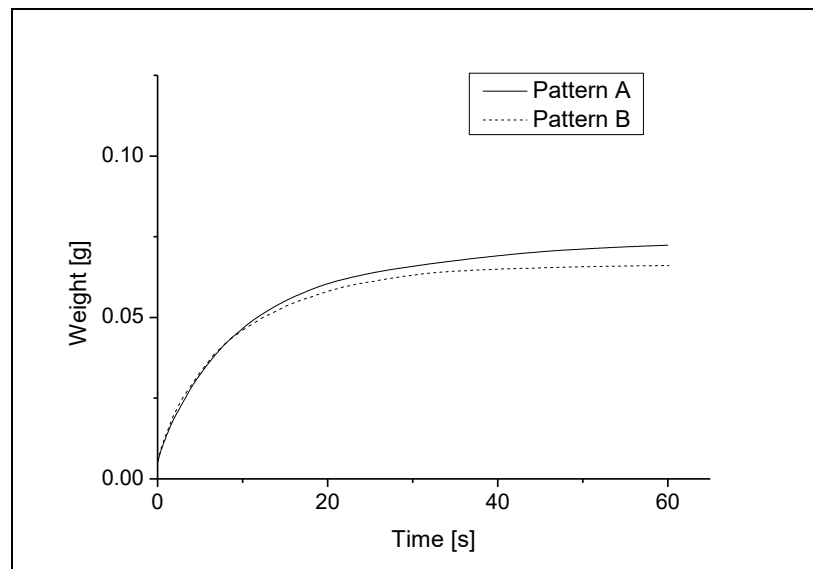


*Figure 4.36: Tensiometry BM slurry absorption curves for patterns A and B for a duration of 60 s*

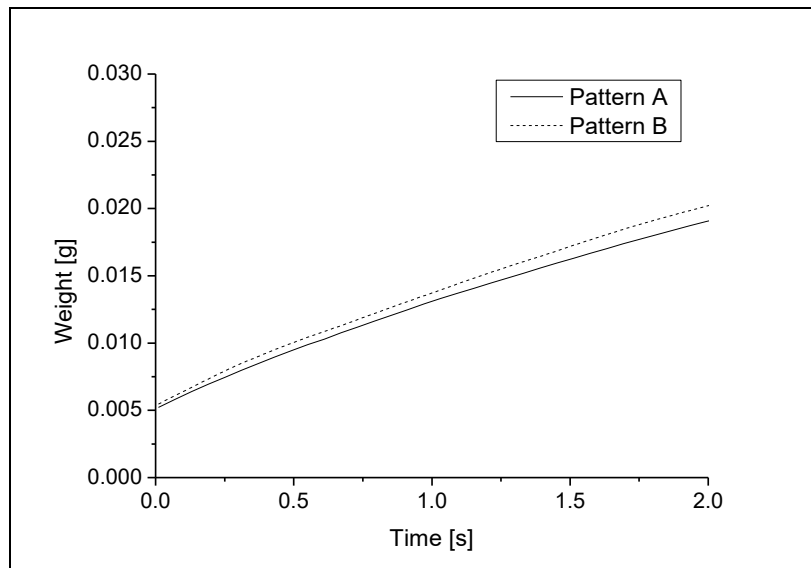


Figure 4.37: A plot of the tensiometer BM slurry absorption curves for patterns A and B during the first two seconds of contact with the BM slurry surface. The first 2 seconds of contact are of high importance when fabrics are used as baby wipes. The difference in the slopes of the curves represent the difference in the weight of BM slurry absorbed per unit time.

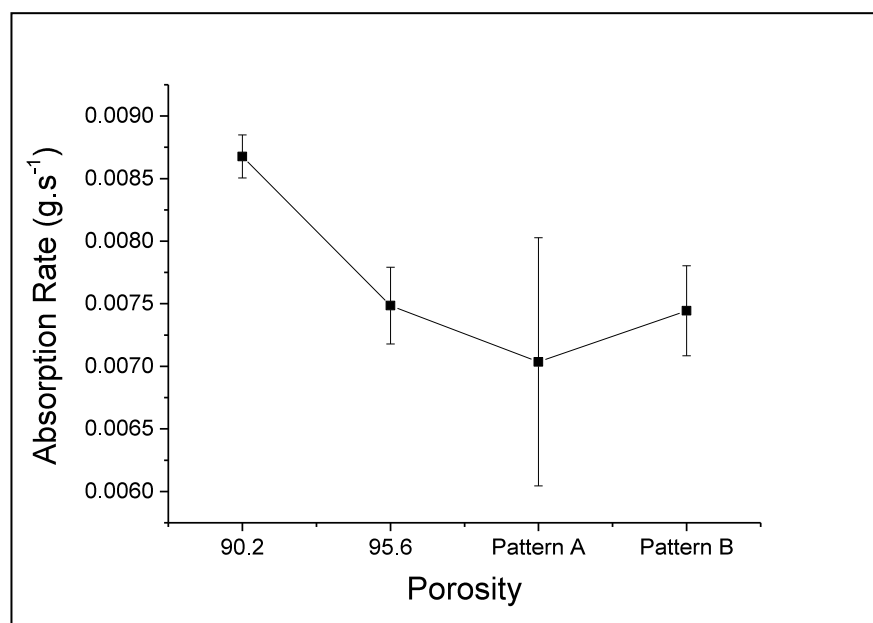


Figure 4.38: BM slurry absorption rate of the samples low porosity, high porosity, pattern A and pattern B for the first 2 s. Only the difference between the low porosity sample and pattern A proved to be statistically significant

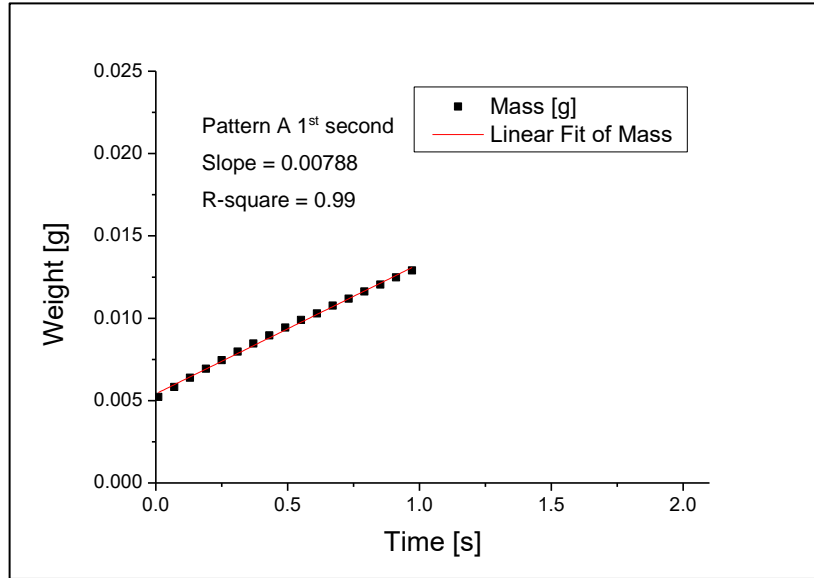


Figure 4.39: Linear fit result from the first second of the tensiometer BM slurry absorption curve of pattern A sample in MD. The fit model shows a value of  $R^2 = 0.99$

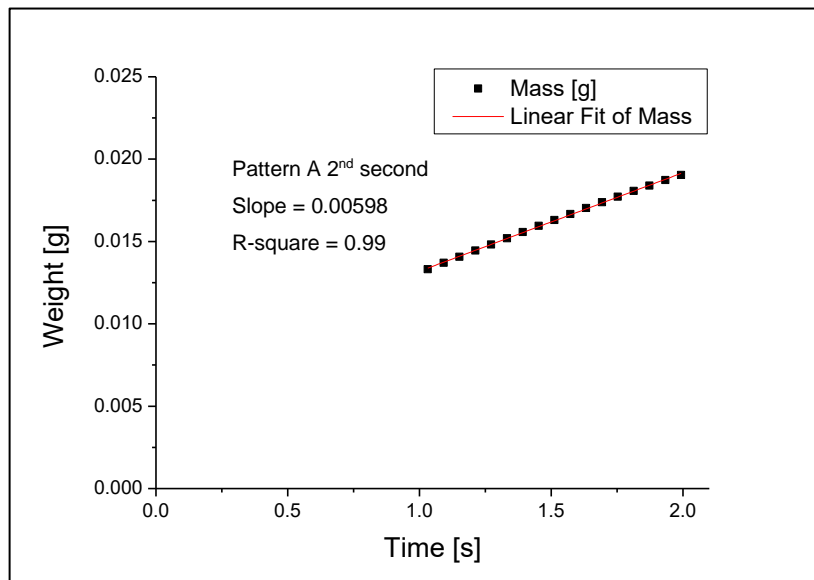


Figure 4.40: Linear fit result from the second second of the tensiometer BM slurry absorption curve of pattern A sample in MD. The fit model shows a value of  $R^2 = 0.99$

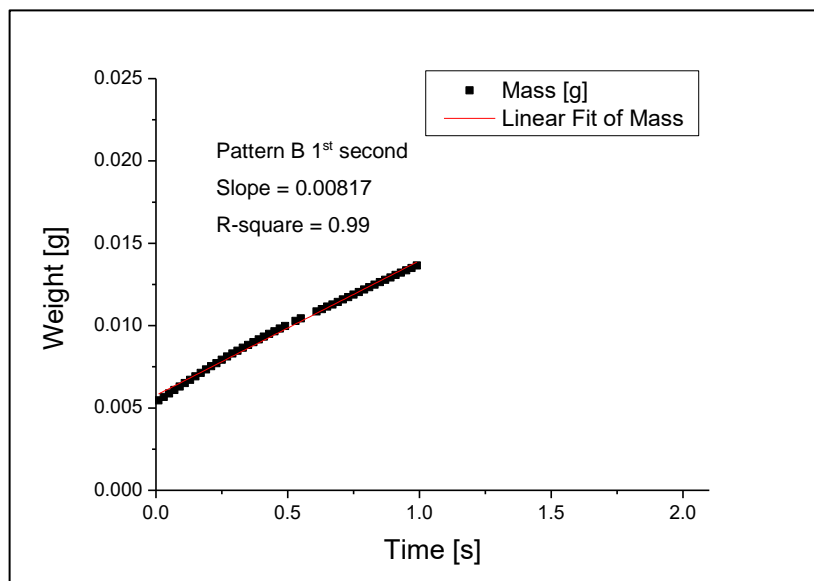


Figure 4.41: Linear fit result from the first second of the tensiometer BM slurry absorption curve of pattern B sample in MD. The fit model shows a value of  $R^2 = 0.99$

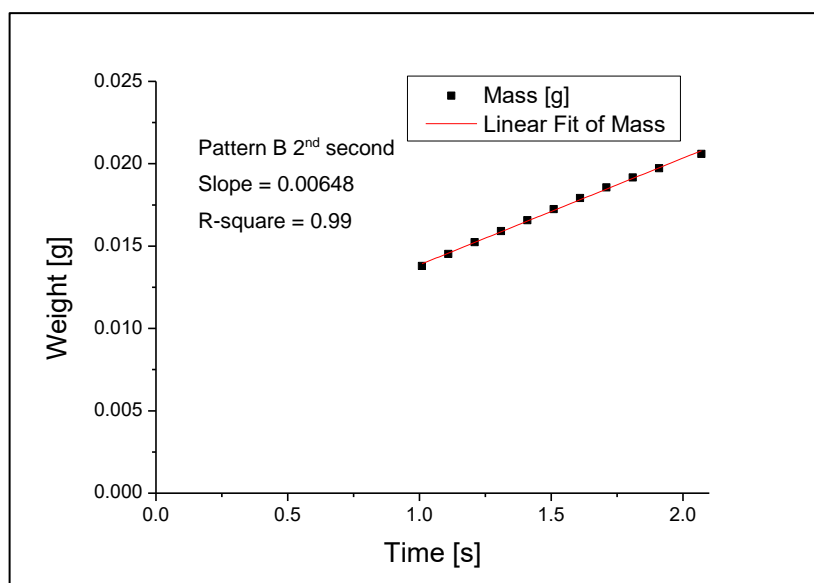


Figure 4.42: Linear fit result from the second second of the tensiometer BM slurry absorption curve of the pattern B sample in the MD, where  $R^2 = 0.99$

Sample	Linear fit model's slope (g.s <sup>-1</sup> )	
	1 <sup>st</sup> second	2 <sup>nd</sup> second
Low Porosity	9.52 x10 <sup>-3</sup>	7.67 x10 <sup>-3</sup>
High Porosity	8.63 x10 <sup>-3</sup>	5.46 x10 <sup>-3</sup>
Pattern A	7.88 x10 <sup>-3</sup>	5.98 x10 <sup>-3</sup>
Pattern B	8.17 x10 <sup>-3</sup>	6.48 x10 <sup>-3</sup>

*Table 7: Results of the linear fit model's slope of the 1<sup>st</sup> and 2<sup>nd</sup> seconds of the tensiometer BM slurry absorption curves for global porosity samples (high and low) and local porosity samples (patterns A and B).*

#### 4.6.5.1 **Local Porosity vs. Global Porosity**

In the first second, the low porosity sample absorbed BM slurry at a significantly higher rate than both local porosity patterns. This changed after a few additional seconds.

On the one hand, the local porosity samples produced a higher BM slurry absorption rate than the high global porosity sample. On the other hand, this BM slurry absorption rate was less than that of the low global porosity sample. This difference in BM absorption behaviour between the first and second seconds can be explained by the rise of BM slurry flow front through the fabric samples with time. This experiment was designed so that the change of porosity (i.e. the porosity profile) was arranged through the cross direction which was parallel to the BM slurry surface. The general absorption direction, however, is vertical (which is here parallel to the machine direction).

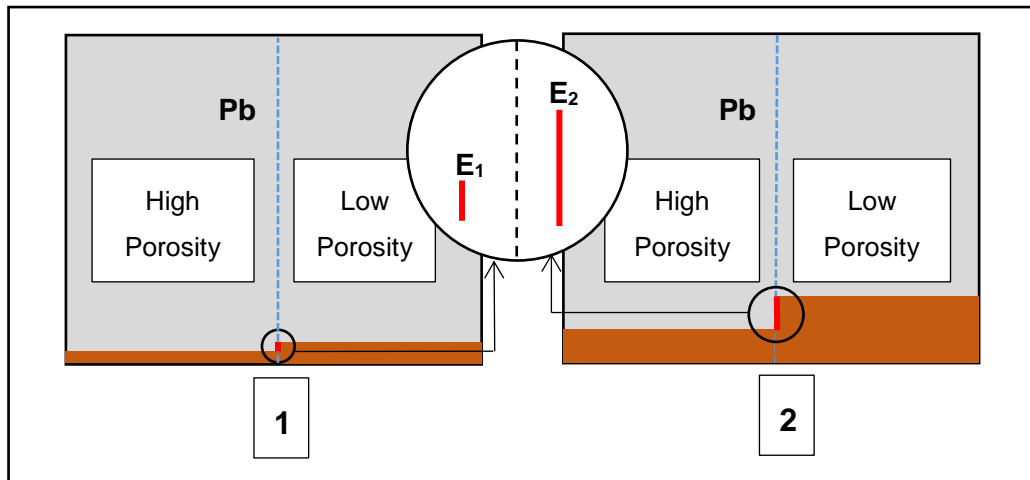


*Figure 4.43: Schematic illustrating the proposed influence of the two local porosity regions, separated by a porosity borderline (Pb) showing how the expected unequal spread of BM slurry in the local porosity areas can lead to an increase in the length of the effective porosity borderline (E) with time. 1: BM slurry spread at the 1<sup>st</sup> second where ( $E_1$ ) is relatively small. 2: BM slurry spread at the 2<sup>nd</sup> second where ( $E_2$ ) is relatively large*

Local porosity areas influence BM slurry absorption by exchanging the absorbed liquid due to the differences in the spreading rate between the different porosity regions, as explained in section 4.5.3.1. Though in order for this exchange to occur, some liquid has to be absorbed, at different rates, by the different local porosity areas. The slurry flow front advances through the fabric sample with time, and between the 1<sup>st</sup> and the 2<sup>nd</sup> seconds, the two different porosity levels will have absorbed more BM slurry, unequally. Hence the difference in BM slurry spread increases which, in turn, increases the length of the porosity borderline covered by the BM slurry along one of its sides, as reflected in Figure 4.43. This leads to an increase in the effect of local porosities on the BM absorption rate.

As time progresses and the BM slurry continues to spread at unequal rates in the different local porosity areas, the length of the effective porosity borderline continues to increase, thus more horizontal BM slurry exchange takes place. This suggests that, in this experiment, the effect of local porosity on the BM slurry absorption rate upon contact is minimal, but its effect increases gradually with time.

#### 4.6.5.2 **Local Porosity Pattern A vs. Pattern B**

The BM slurry absorption rate in the 1<sup>st</sup> and 2<sup>nd</sup> seconds for each of the two patterns are shown in Table 7. Pattern B appeared to absorb more BM slurry at a higher rate than pattern A at both the 1<sup>st</sup> and 2<sup>nd</sup> seconds. This can be explained by the difference in their structural design. As explained in section 4.6.4, the difference between pattern A and pattern B is merely the distribution of local porosity areas. Other characteristics are identical, including the global porosity. Pattern A has two areas separated by one porosity borderline, whereas pattern B has four areas separated by 3 porosity borderlines. The results show that the sample with more porosity borderlines has a relatively higher BM slurry absorption rate with an average of 0.00704 g.s<sup>-1</sup> for pattern A and 0.00744 g.s<sup>-1</sup> for pattern B. This difference in the means has not been proven to be statistically significant, therefore further investigations are necessary to make solid conclusions on this point. Figure 4.44 illustrates how the distribution of local porosity areas influences the effective porosity borderline and hypothetically the slurry absorption rate.

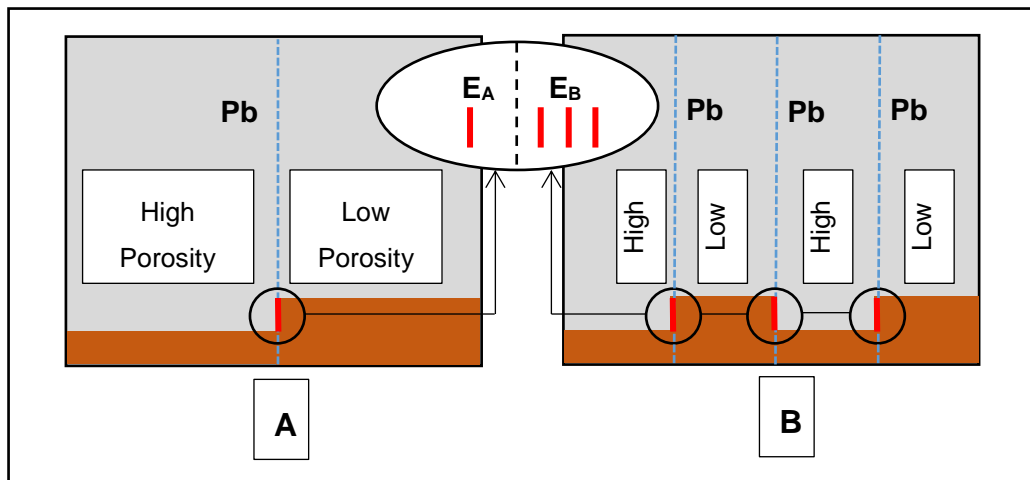


*Figure 4.44: A schematic showing the two local porosity patterns A and B where local porosities are separated by porosity borderlines (Pb) showing how different distributions of local porosity for samples of identical global porosity can lead to different total lengths of porosity borderlines and subsequently different lengths of effective porosity borderlines (E). Pattern A has one porosity borderline (Pb) and subsequently one effective porosity borderline (E<sub>A</sub>). Pattern B has three porosity borderlines (3 x Pb) and subsequently three effective porosity borderlines with a total length of (E<sub>B</sub> = 3 x E<sub>A</sub>).*

It must be noted that these findings need further supporting data under the experimental conditions and settings explained throughout section 4.6.

#### **4.6.6 Summary and Conclusions**

This experimental work sheds illustrates the potentially valuable effects of introducing local porosity areas within nonwoven fabrics in terms of one-dimensional BM slurry absorption behaviour. A comparison of the BM slurry absorption behaviour between global porosity samples and the patterned samples has been elucidated and explained in terms of the total length of the porosity borderlines.

When comparing global porosity samples and patterned ones, a trend in the BM slurry absorption behaviour was apparent during the first seconds of contact with the fabric. In conclusion, the experiments discussed in sections 4.4 and 4.5, as well as the present section have collectively demonstrated that relatively low porosity fabrics exhibit a BM slurry absorption behaviour characterised by a high absorption rate, compared to high porosity fabrics. In fabrics containing patterns, defined by variations in local porosity, there is BM slurry liquid exchange at the borderlines between the low and high porosity areas. This liquid exchange causes a deviation in the BM slurry absorption behaviour relative to what would be expected from the conventional theory of Lucas-Washburn. In other porous media, this deviation has been proven experimentally (Ridgway et al., 2002, Gane et al., 2004, Ridgway et al., 2006) and in textiles, and nonwovens in particular, it has been described theoretically (Mao, 2009b, Mao, 2009a). This experimental work provides additional evidence of the effect in nonwoven fabrics. Mao's conclusion about the absorption behaviour of patterned nonwoven fabrics is different to the work presented in this experiment. However, it should not be understood as a contradiction of results. While Mao found that there is increase of pressure and velocity in high porosity areas compared to the low porosity ones, the experiment presented herein shows a higher absorption rate in the low porosity areas. This apparent difference can be explained by the methods used to introduce these local porosity areas in the present work and in the work presented by Mao. As explained in section 4.5.2.2, the low porosity areas in this experiment were produced using compression which reduced fabrics

thickness. By contrast the low porosity areas in Mao's work was produced by print bonding, which involves both pressure and the application of chemical binder, which consequently reduces the permeability of the low porosity areas.

In the second experiment, the BM slurry absorption behaviour of two different porosity patterns was investigated. The difference between the two samples could be explained in terms of the total length of their porosity borderlines. The experimental data revealed that despite two fabric samples having identical fibre characteristics and global porosity, different BM slurry absorption behaviour was observed. It was shown that the BM slurry absorption rate increases with increasing the total length of the effective porosity borderline. Mao demonstrated that the global permeability of dual porosity patterned nonwoven fabrics depends on the ratio of dimensions for their local porosity areas and not on their absolute values (Mao, 2009a). This experiment further suggests that, even with equal dimensional ratio of the local porosity areas, fabrics can behave differently according to the distribution of these areas, which is, in this case, the total length of porosity borderlines. This finding also aligns with the observations of Gane et al. and Sun et al. regarding the influence of several structural properties on liquid absorption by porous media (Gane et al., 2004, Sun et al., 2016).

Therefore, it is apparent that vertical porosity borderlines influence vertical BM slurry absorption with time. The distribution of local porosity areas defines the length of porosity borderline in a sample which, in turn, influences the BM slurry absorption rate accordingly. The longer the vertical porosity borderline the higher the vertical absorption rate. Now that the effect of one dimensional changes local porosity is better understood, an attempt was made to understand two-dimensional changes in local porosity.

## **4.7 Influence of Local Porosity Profiles in the Machine Direction on BM Slurry Absorption**

### **4.7.1 Introduction**

Liquid absorption in inhomogeneous nonwovens in three-dimensions has not been thoroughly modelled as compared to one and two-dimensions, but there

are studies dealing with liquid transport in homogeneous nonwovens (Mao and Russell, 2003b). Absorption is usually studied in one-dimension for the purpose of simplifying the theoretical modelling and experimental measurements. In practice, BM slurry transports through a wipe fabric in all directions. As is often the case, planar absorption can be described in two-dimensional space (Mao and Russell, 2003b) and the third dimension represents the absorption through the fabric thickness, i.e. trans planar absorption. In 2D space, if each direction is described by a vector, then it can be represented by two Cartesian components (Kemmer, 1977). In all fabric samples in the present experiments, the Cartesian coordinates within the fabric plane were chosen to be aligned with the machine direction (MD) and cross direction (CD) of the fabric.

Describing the structure of porous media is a complex task, particularly when it comes to investigating its influence of liquid absorption (Gane et al., 2004). When investigating the influence of local porosity, we are particularly focusing on the transitional phases between areas of different porosities. In previous sections (sections 4.5 and 4.6) the term porosity borderline was introduced as the line separating areas of different local porosity. In a three-dimensional space, the geometrical characteristics of two adjacent spaces is a surface. For simplification purposes, such surfaces are assumed to be planes. Subsequently, in a two-dimensional space, these separating entities between two different areas are characterised as boundary lines, and for simplification they are assumed to be straight lines. This geometrical concept is reflected in a nonwoven fabric with areas of local porosities and simplified into areas of two dimensional characteristics separated by straight porosity lines. This further explains the design of the mould used to introduce local porosity areas onto the nonwoven prototypes. Porosity borderlines discussed in the previous experiments discussed in sections 4.5 and 4.6, as well as in the present one were represented by Cartesian coordinates (MD and CD). This way, and as illustrated in Figure 4.45, any hypothetical straight porosity borderline in the two-dimensional nonwoven fabric can be described by its Cartesian components.

The systematic investigation of BM slurry absorption in the presence of local porosity areas began by describing the in-plane BM slurry absorption as two-dimensional unsteady-state transport. To tackle the complexity of experimental investigations of multi-dimensional absorption, the absorption behaviour in each dimension was studied separately. The one-dimensional unsteady-state transport in homogeneous and inhomogeneous anisotropic nonwoven fabrics was used to explain BM slurry absorption in sections 4.4, 4.5 and 4.6 with reference to Mao (2009b). The case discussed in section 4.5 addressed the BM slurry one-dimensional in-plane absorption through horizontal fabric samples, which contained local porosity areas separated by what has been defined as porosity borderlines. The end-state BM slurry absorption was investigated, i.e. absorption after 120 seconds. In section 4.6, the BM slurry absorption rate was additionally investigated and, for that, the samples had to be held vertically, i.e. in presence of the gravity.

The porosity borderlines in sections 4.5.3.1, 4.5 and 4.6 were parallel to the direction of BM slurry absorption. In this section, study of one-dimensional unsteady-state transport in heterogeneous anisotropic nonwoven fabrics with borderlines perpendicular to the absorption direction was carried out.

Liquid exchange between the local porosity areas happens in a direction perpendicular to the porosity borderline. When the porosity borderline was parallel to the absorption direction in section 4.6, i.e. vertical, the BM slurry exchange was horizontal. In a case where the borderline is perpendicular to the absorption direction, liquid exchange is expected to happen in the same direction of absorption, i.e. vertical. This, in turn, is expected to have a relatively large influence on absorption measurements, particularly the absorption rate, compared to the former case.

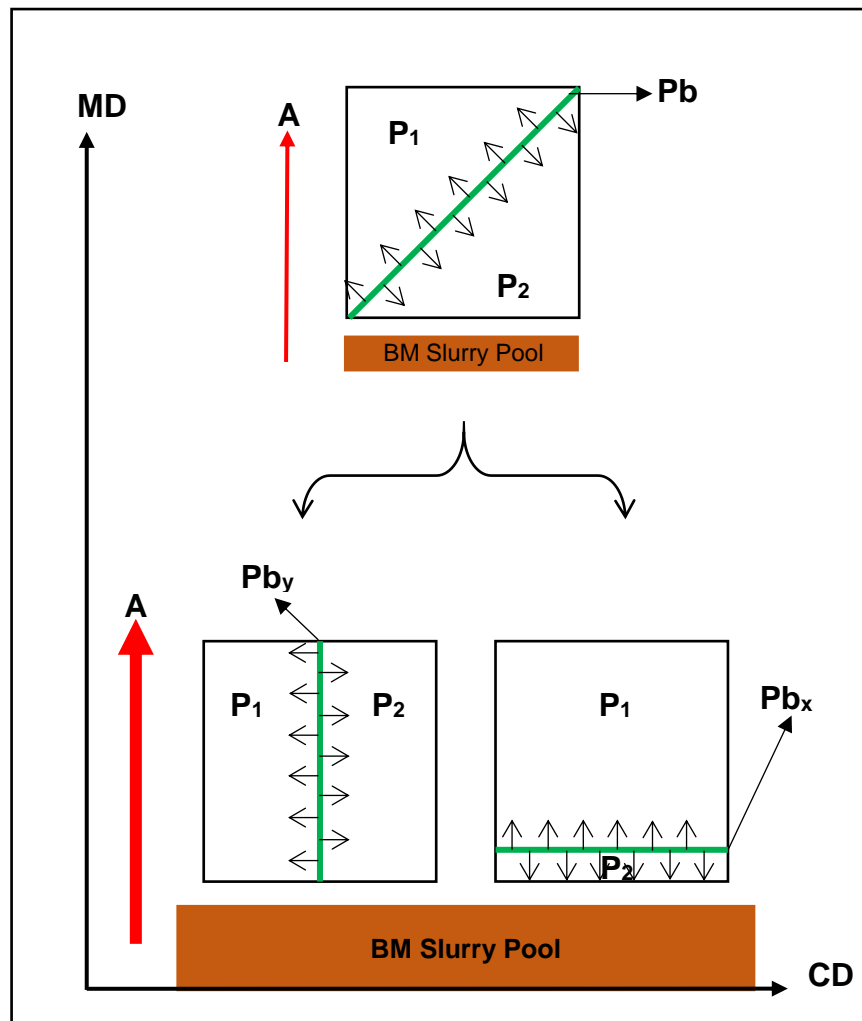


Figure 4.45: Schematic of the porosity borderline ( $B$ ) separating two areas of different porosities ( $P_1$ ) and ( $P_2$ ) and its representation into Cartesian components: ( $B_y$ ) parallel to the machine direction ( $MD$ ) and the absorption direction ( $A$ ), and ( $B_x$ ) parallel to the cross direction ( $CD$ ) and perpendicular to the absorption direction ( $A$ )

Previous theoretical work has suggested that the basic challenge of achieving high liquid absorption combined with a high absorption rate can be potentially obtained by engineering a heterogeneous fabric structure. The hypotheses was inspired by a theoretical model published by Shou et al. (2014b).

The two media modelled by Shou et al. (2014b) consisted of circular tubes, Figure 4.46 and porous layers, Figure 4.47. Both media have heterogeneous structures. The local differences are in the tube radii or the porosity and in the tube heights or the porous layer thicknesses.

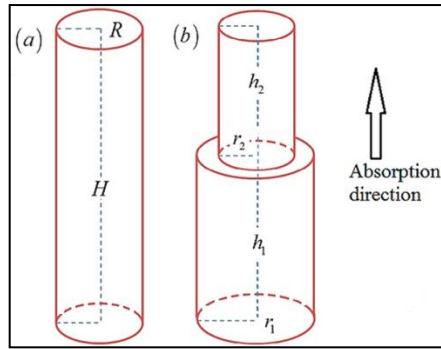


Figure 4.46: (a) uniform tube with height  $H$  and radius  $R$ , (b) heterogeneous tube with two sections of heights  $h_1$  and  $h_2$  and two radii  $r_1$  and  $r_2$  (Shou et al., 2014b)

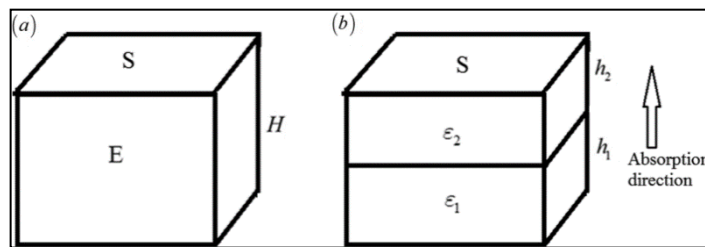


Figure 4.47: (a) uniform porous medium with a cross-sectional area  $S$ , porosity  $E$  and height  $H$ , (b) heterogeneous double-layered porous medium with a cross-sectional area  $S$ , porosities  $\epsilon_1$  and  $\epsilon_2$  and heights  $h_1$  and  $h_2$  for the respective layers (Shou et al., 2014b)

This theoretical model describes the calculated absorption rate in several cases. The sample porous medium used in the original study, shown in Figure 4.47, consists of two structurally different layers. The difference is based on the change in the layer's porosity and thickness. In each of the cases, the porous structure is controlled and the aforementioned two factors are altered. Shou et al. (2014b) compared their results to those of homogeneous structures which have equal total height and global porosity. The model was consistent with experimental results found in the literature (Shou et al., 2014b). However, the results were for water absorption, which may or may not differ from what would result when studying BM slurry absorption by heterogeneous nonwoven fabrics.

Fundamentally, capillary pressure, which is a primary driver of dynamic absorption, is inversely proportional to the pore size, while permeability is proportional to the square of the pore size. When optimising these two competing mechanisms of liquid absorption in heterogeneous porous

structures, the model predicted an increase the absorption rate up to 38% compared to that of homogeneous porous structures of equal global porosity (Shou et al., 2014b).

Shou et al. (2014b) modelled the double-layered porous medium at different levels of global porosities [0.4, 0.5 and 0.6] and local porosity ratios [0.5, 1 and 2] within a height ratio ranging from [0 – 3]. Figure 4.48 shows the normalised absorption time ( $t_p$ ) plotted against the layers' height ratio ( $n$ ).

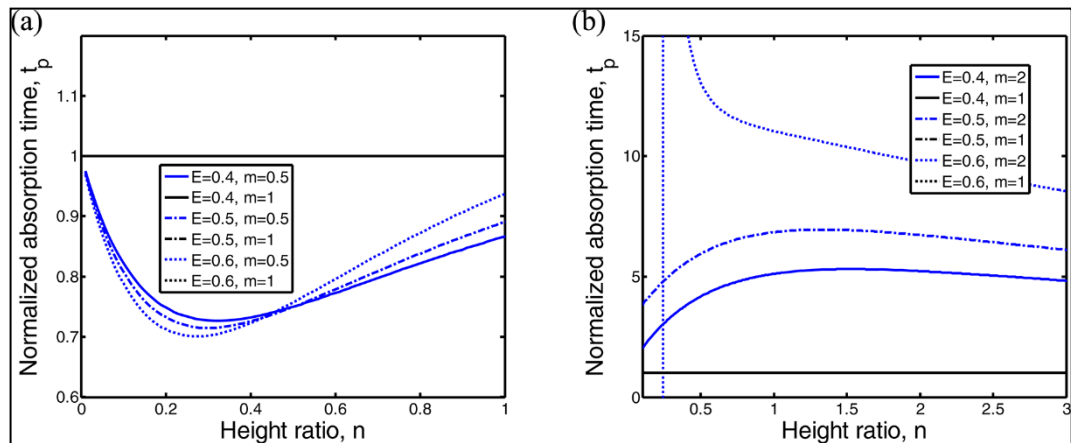


*Figure 4.48: Normalised absorption time ( $t_p$ ) in the heterogenous layered porous medium plotted against the layers' height ratio ( $n$ ) at different global porosities ( $E$ ) and local porosity ratios ( $m$ ) (Shou et al., 2014b)*

*a) Porosity ratio  $m \geq 1$  : negative porosity gradient*

*b) Porosity ratio  $m \leq 1$  : positive porosity gradient*

By examining the resulting curves of Shou's model Figure 4.48 at the porosity ratio 0.5 we can conclude that for height ratios  $n < 0.4$ , absorption time decreases with the global porosity. And for example, the absorption time could be reduced by as much as 30% for a global porosity of  $E = 0.6$ , a porosity ratio of  $m = 0.5$  and a height ratio of  $n = 0.25$ .

In further work, Shou et al. (2014a) used their model to describe water wicking through three different paper media. Compared to a homogeneous paper sample, Shou et al. (2014a) concluded that there is an optimum structure that absorbs the fastest.

Other studies focusing on the effect of changing local porosity on absorption rate, include that of (Kim et al., 2015, Ridgway et al., 2006) however, none of

these scientific studies have investigated BM-like liquids and their behaviour in nonwoven fabrics. Therefore, there is a need to explore the application of such theories for enhancing the performance of nonwoven wipes.

#### **4.7.2 Aims and Objectives**

The purpose of this experiment is to explore the effect of a porosity borderline that is perpendicular to the absorption direction.

#### **4.7.3 Materials and Methodology**

A test method was implemented based on tensiometry using a Kruss tensiometer (K100SF). Details of the basic method are explained in section 4.4.1. With reference to Figure 4.49, specimens of a nonwoven fabric of dimensions 20 mm x 45 mm were carefully cut using a template. After the tensiometer calibration process as detailed in section 4.4.1, a specimen was mounted in the tensiometer using the specimen holder. BM slurry was prepared by mixing the lotion with BM (65% water content), as explained in section 2.5.3, with the weight ratio of 1:1. 30 ml of the BM slurry was placed in the tensiometer container.

To conduct the measurement, the container containing the slurry was raised by the motorised table towards the lower (leading) edge of the specimen such that 0.5 mm of the fabric was immersed and wetted out at a rate of 10 mm.min<sup>-1</sup>. Measurements started as soon as the correct immersion depth was achieved and the distance between the specimen holder and the motorised table is then locked for the set duration of the measuring cycle which was 60 s. As in the procedures described in sections 04.4, 4.5 and 4.6, the balance reading rate was 10 Hz with the exception of the first second, where it was set to 30 Hz (see section 4.4.1). After 60 s, the measurements were stopped automatically and the balance was then locked.

Fabric samples were all prepared from the same ternary fibre blend of 60% 3.3 dtex trilobal polypropylene; 20% 1.0 dtex trilobal polypropylene and 20% 1.7 dtex viscose, and manufactured using the method described in section 3.1. The procedure was developed to minimise any changes to fibre orientation or basis weight of the samples to aid interpretation of the results.

Each sample was compressed under controlled conditions to achieve the required local porosity structure using the hydraulic press and the prepared mould as described in 4.5.2.2. Then the specimens were cut out of the compressed fabric using a template. Two different patterns were cut as shown in Figure 4.49.

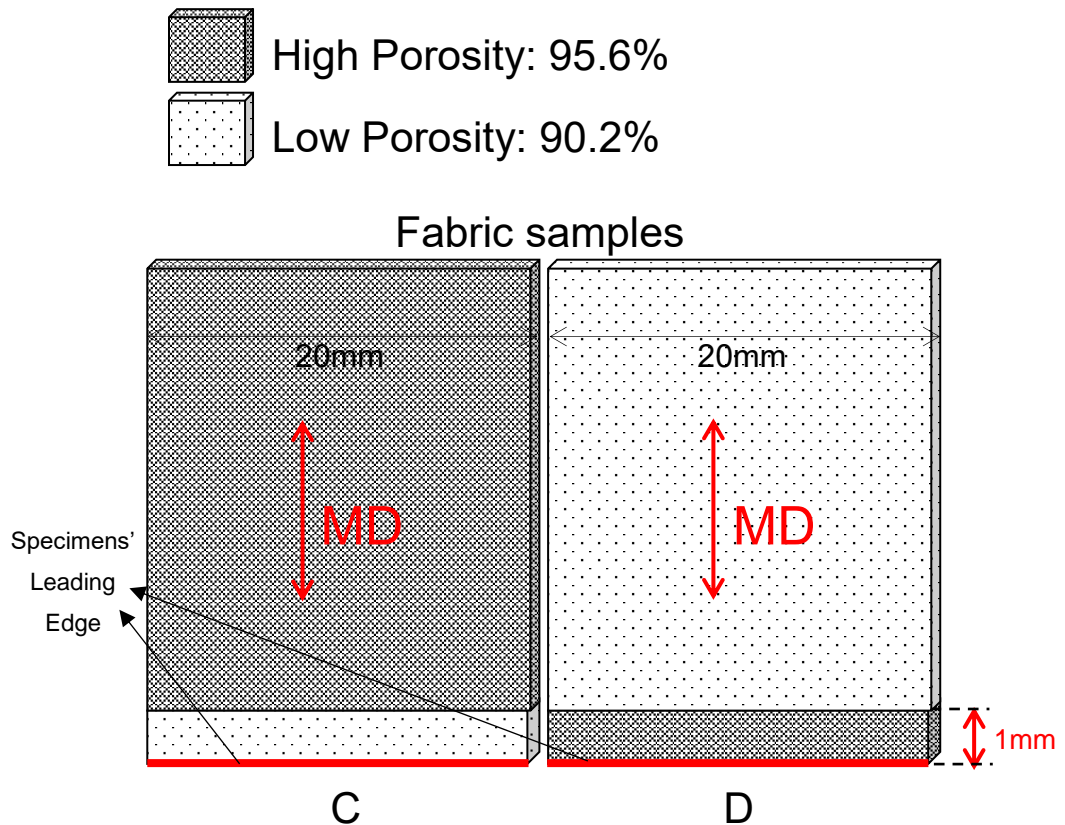


*Figure 4.49: Local porosity nonwoven fabric samples*

*C: Pattern C starts with a low porosity (90.2%) area from the leading edge with a height of 1mm, it then transitions to the high porosity area (95.6%) for the rest of the sample through a horizontal porosity borderline.*

*D: Pattern D starts with a high porosity (95.6%) area from the leading edge with a height of 1 mm, it then transitions to the low (90.2%) porosity area for the rest of the sample through a horizontal porosity borderline*

The specimens were cut so that their leading edge is 1 mm away from the porosity borderline. Since 0.5 mm will be immersed in the BM slurry, the porosity borderline will be 0.5 mm above the BM slurry surface. This relatively small distance allows the observation of the change in absorption behaviour

as the slurry is absorbed through from one porosity level to another within the measurement time.

#### 4.7.4 Results and Discussion

Figure 4.50 shows the BM slurry absorption curves for the patterned samples C and D for a duration of 60 s. These curves give a general overview of the samples' absorption behaviour which appeared to be similar for the two patterns. Focusing on the first two seconds of BM slurry absorption, which are of practical significance in wiping applications, the difference between the samples is noticeable (Figure 4.51), particularly around the points  $t = 0.7$  s where the slope of the rate curve for sample D decreased, and  $t = 1.4$  s where the two curves meet. The rate of absorbed BM slurry weight per unit time is calculated by fitting the curves with a linear model. The linear fit calculation was applied to a duration of one second for  $t = 0 \rightarrow 1$  s and  $t = 1 \rightarrow 2$  s. All linear fit models had a good fit with  $R^2 > 0.99$  as shown in Figure 4.53, Figure 4.54, Figure 4.55, and Figure 4.56. For a complete comparison of BM slurry absorption rate in the first two seconds with the patterned samples presented previously in section 4.6.5, Table 8 shows the resulting slopes for each of the linear fit models.

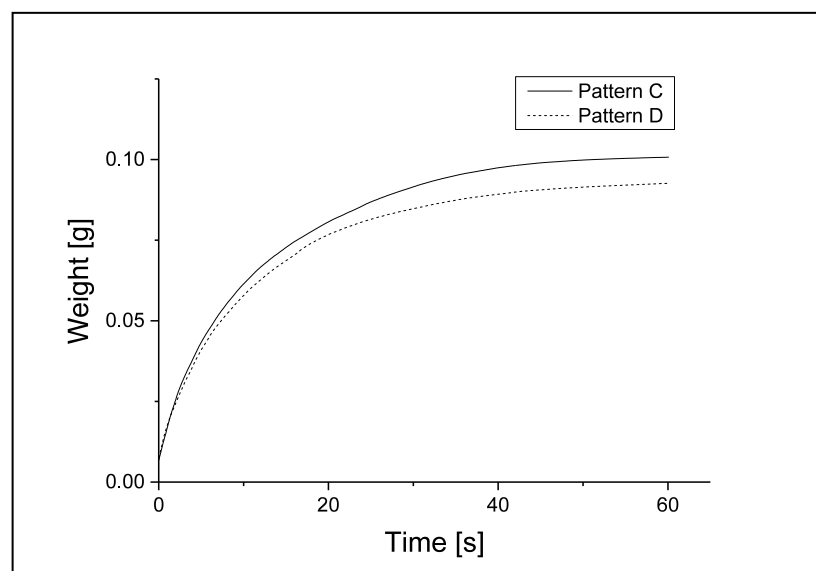


Figure 4.50: Tensiometry BM slurry absorption curves for samples C and D, with two different local porosity patterns for a duration of 60 s

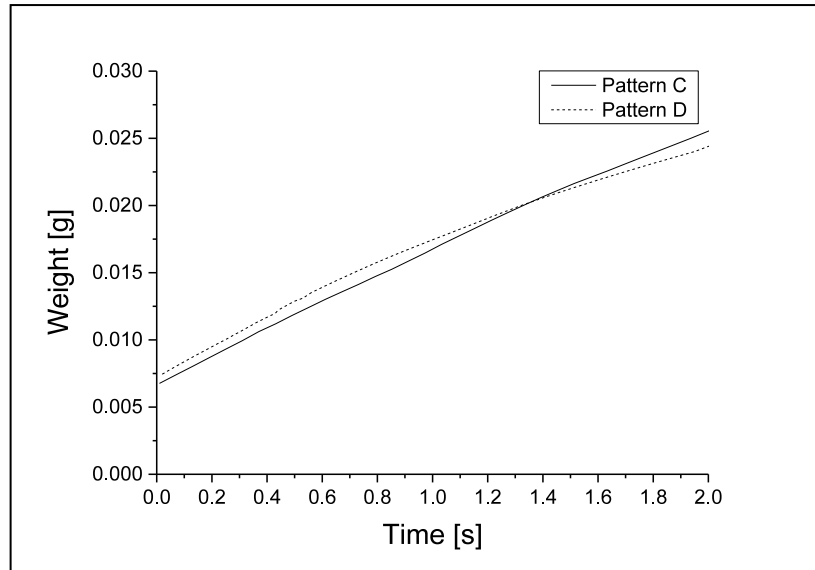


Figure 4.51: A plot of the tensiometer BM slurry absorption curves for patterns C and D during the first two seconds of contact with the BM slurry surface. The first 2 seconds of contact are of high importance when fabrics are used as baby wipes. The difference in the slopes of the curves represent the difference in the weight of slurry absorbed per unit time.

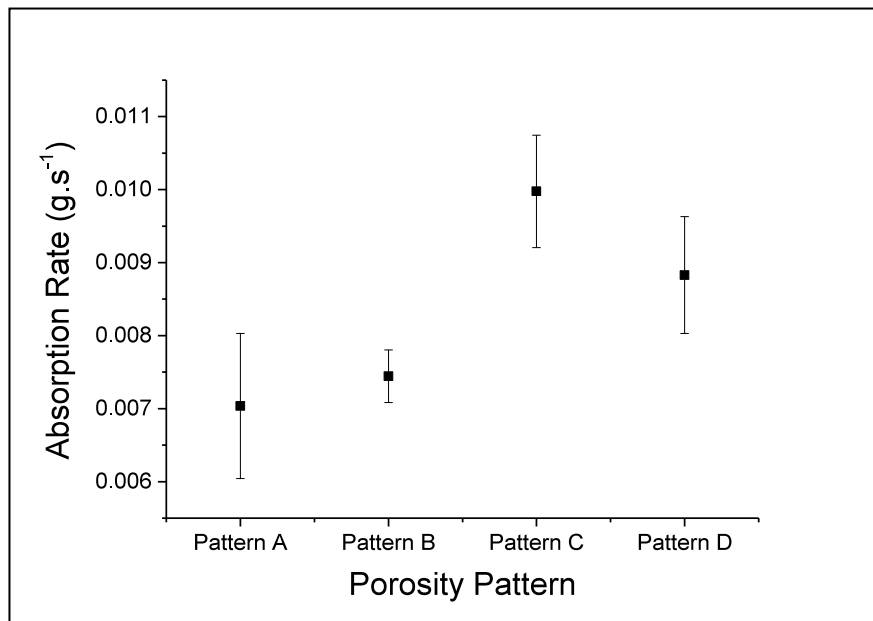


Figure 4.52: BM slurry absorption rate of the samples with porosity patterns A, B, C and D for the first 2 s. Only the differences between patterns C and A and between patterns C and B are statistically significant

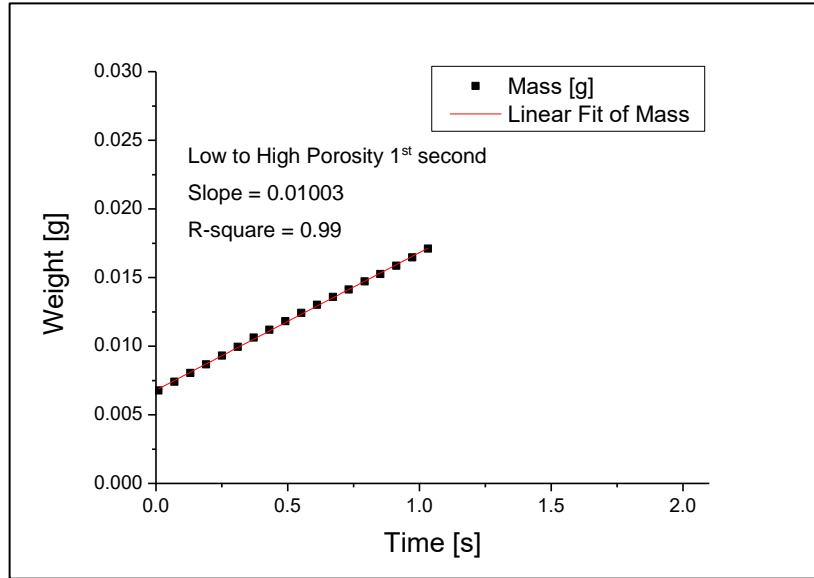


Figure 4.53: Linear fit result from the 1<sup>st</sup> second of the tensiometer BM slurry absorption curve of pattern C. The fit model shows a value of  $R^2 = 0.99$

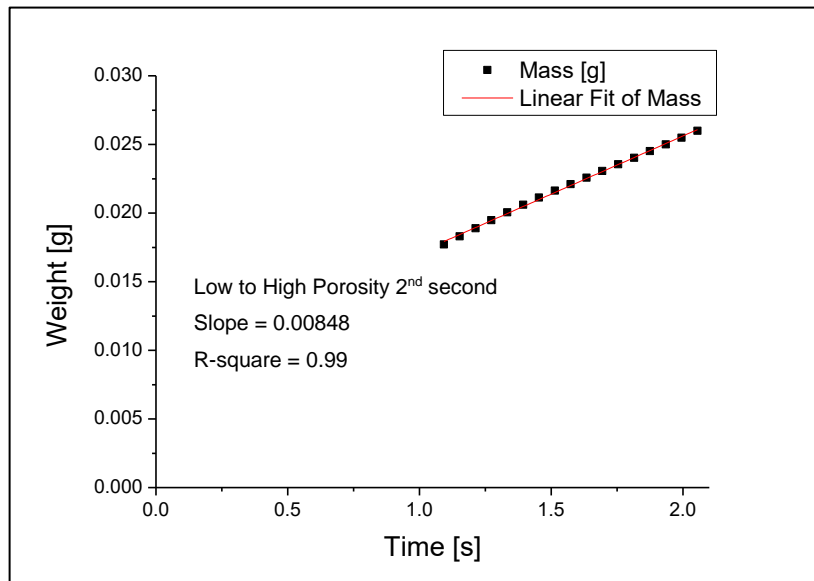


Figure 4.54: Linear fit result from the 2<sup>nd</sup> second of the tensiometer BM slurry absorption curve of pattern C. The fit model shows a value of  $R^2 = 0.99$

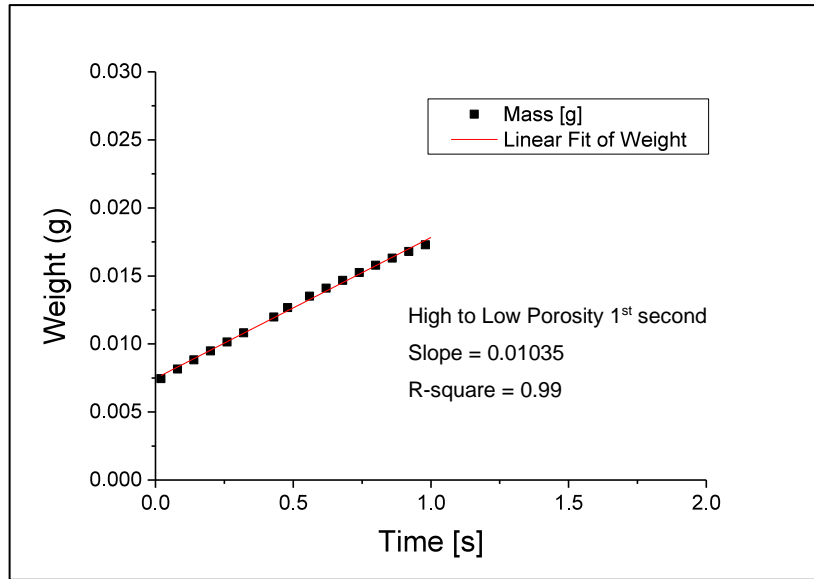


Figure 4.55: Linear fit result from the 1<sup>st</sup> second of the tensiometer BM slurry absorption curve of pattern D. The fit model shows a value of  $R^2 = 0.99$

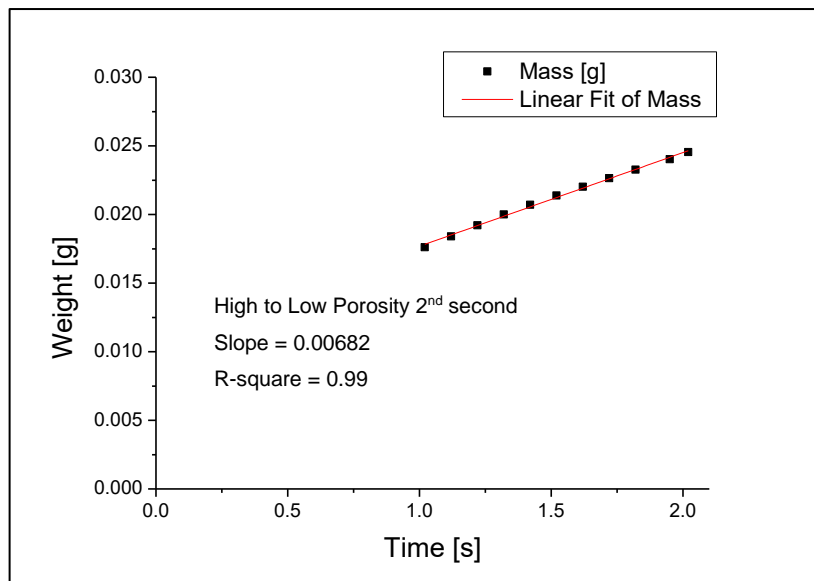


Figure 4.56: Linear fit result from the 2<sup>nd</sup> second of the tensiometer BM slurry absorption curve of pattern D. The fit model shows a value of  $R^2 = 0.99$

Sample	Slope of linear fit model (g.s <sup>-1</sup> )
--------	--

	1 <sup>st</sup> second	2 <sup>nd</sup> second
Pattern A	$7.88 \times 10^{-3}$	$5.98 \times 10^{-3}$
Pattern B	$8.17 \times 10^{-3}$	$6.48 \times 10^{-3}$
Pattern C	$10.35 \times 10^{-3}$	$6.82 \times 10^{-3}$
Pattern D	$10.03 \times 10^{-3}$	$8.48 \times 10^{-3}$

*Table 8: Results of the linear fit model slopes for the 1<sup>st</sup> and 2<sup>nd</sup> seconds of the tensiometer BM slurry absorption curves for patterns (A, B, C and D).*

The data in Table 8 shows the results of linear fit of the absorption curves for each of the patterns A, B, C, and D for the 1<sup>st</sup> and the 2<sup>nd</sup> seconds. The interpretation of these results is discussed in sections 4.7.4.1 and 4.7.4.2.

#### **4.7.4.1 Porosity Borderlines, Perpendicular vs. Parallel to Absorption Direction**

As explained in Figure 4.45, any porosity borderline can be represented by two components. When the BM slurry absorption occurs in the MD direction, it is parallel to the MD-direction component of the porosity borderline (discussed in section 4.6) and perpendicular to the CD-direction component of the porosity borderline discussed in this section. By the definition of the effective porosity borderline mentioned in section 4.6.5, the influence of the one perpendicular to the absorption direction is greater than that of the one parallel to it in the short timescale. This is particularly true because in the case of a porosity borderline parallel to the BM slurry absorption direction, the effective length is initially minimal and it increases with time until an ultimate length equal to the MD component. Whereas in the case of a porosity borderline perpendicular to absorption direction, the effective length is maximised and is equal to the CD component from the point of contact with the BM slurry flow front.

The results shown in Table 8 are consistent with this rationale as even in the case of a leading edge of high porosity level (as in sample D) whose BM slurry absorption rate was found to be relatively low (see 4.4.3, high porosity), the BM absorption rate was higher than that of either of the samples, A or B. Therefore, the first hypothesis mentioned in section 4.7.1 has been confirmed.

#### **4.7.4.2 *Negative Porosity Gradient vs. Positive Porosity Gradient***

The theoretical model of Shou et al. (2014b), which resulted in the plots shown in Figure 4.48, suggests that BM slurry absorption time of liquids transitioning from one local area in a porous medium to another, in a way that the porosity gradient is negative, is expected to be shorter than that where the porosity gradient is positive.

In the case of BM slurry absorption by heterogeneous anisotropic nonwoven fabrics with borderlines perpendicular to the absorption direction, sample C represents the case of a positive porosity gradient and sample D represents the case of a negative porosity gradient. Their BM slurry absorption rates, shown in Table 8, for the 1<sup>st</sup> and 2<sup>nd</sup> seconds follow a similar trend as that is suggested by Shou et al.

The BM slurry absorption rates of sample D at  $t = 0 \rightarrow 1 \text{ s}$  and  $t = 1 \rightarrow 2 \text{ s}$  are higher than those of sample C at the same times. This confirms the second hypothesis mentioned in section 4.7.1.

#### **4.7.5 Summary and Conclusions**

In this section, BM slurry absorption in the 2<sup>nd</sup> dimension was studied from a local porosity perspective. The porosity borderline was perpendicular to the BM slurry absorption direction. The results were compared to those of the case where the porosity borderline was parallel to the absorption direction. It can be concluded that the perpendicular component of a porosity borderline to the absorption direction has a greater influence on the BM slurry absorption rate than in the parallel case.

Two different samples were tested in this experiment, one where the porosity gradient was positive and one where it was negative. It can be concluded that the BM slurry transition from high porosity to low porosity, i.e. through a

negative porosity gradient, occurs at a higher rate than that from the lowest porosity to the highest one, i.e. through a positive porosity gradient.

In the experiments presented in section 4.6 and 4.7, the BM slurry absorption by nonwoven fabrics from the perspective of local porosity was investigated in two dimensions. This can be further used to explain planar BM slurry absorption by nonwoven fabrics in the presence of local porosity areas. It was also found that varying the distribution of local porosity areas and their dimensions could be used to design nonwoven fabrics with improved BM slurry absorption performance as compared to homogeneous structures.

Although modelling nonwovens' absorption in two dimensions has been well studied (Mao, 2009a, Mao, 2009b, Mao, 2000, Mao and Russell, 2003a, Mao and Russell, 2000b, Mao and Russell, 2000a), the interest in further understanding the 3D liquid absorption behaviour of nonwovens and other porous media and is evident from the studies of (Tang et al., 2015b, Tang et al., 2015a, Mao and Russell, 2008, Mao and Russell, 2003b). It is particularly important for the application of nonwoven wipes that the BM slurry absorption through the thickness of the fabric is understood, i.e. the transplanar absorption. This is because it is the desired direction of absorption for removal of bowel movement from a surface. Furthermore, to enhance the performance and efficiency of nonwoven wipes regarding BM slurry absorption, it is necessary to seek the use of the maximum volume possible and available in the wipe and that means including the third dimension, i.e. the fabrics' thickness, must be considered in the experimental investigations.

The next section addresses the investigation of transplanar absorption of BM slurry by nonwoven fabrics. It involves development of the test method, understanding the factors influencing measurements and the possibilities of improving it through an improved fabric design.

## **4.8 Influence of Local Porosity Profiles in the Z Direction on BM Slurry Absorption**

### **4.8.1 Background**

The positive results in section 4.7 are evidence that BM slurry absorption can be improved by introducing areas of locally varying porosity. The results were found to be consistent with the theoretical work presented in the literature (Ridgway et al., 2006, Shou et al., 2014a, Shou et al., 2014b, Kim et al., 2015, Shou and Fan, 2015). It is believed that absorption in the z-direction could also be improved by engineering the microstructure of nonwoven fabrics, for example by introducing local porosity profiles through the fabrics' thickness. This belief is also supported by theoretical and experimental work found in the recently published literature.

Mao et al. developed a model to predict directional permeability of a 3D nonwoven fabric considering the influence of fabric thickness and permeability in the z-direction (Mao and Russell, 2003b). Li et al. (2016) investigated the influence of structure parameters on the spontaneous imbibition of liquids in fractal tree-like network. The structure parameters they addressed were tube diameter, length and the branching number, i.e. the number of branches per tube. They concluded that the potential of imbibition rate is inversely proportional to the length ratio between adjacent branching levels, proportional to the diameter ratio and to both branching number and branching level. Furthermore, layered structures of capillaries or porous media with different porosity levels, as shown in Figure 4.46 and Figure 4.47, are suggested to increase the liquid absorption rate depending on the layers thicknesses, according to a theoretical model developed by Shou et al. (2014b). Recent work has studied the application of this theoretical model on soft solids to improve mass transport (Kim et al., 2015).

This approach was studied herein to investigate for nonwoven fabric behaviour in the absorption of BM slurry. If the model were to prove applicable for BM slurry absorption it could provide a means of improving the performance of wipes.

To enable such investigation, a suitable test method must be devised. The measurement of BM slurry absorption in the z-direction and the development of a suitable test method are discussed in the next section.

## **4.8.2 Measurement of BM Slurry Absorption in the Z Direction**

### **4.8.2.1 Suitability of the Tensiometry Test Method**

In the Z-direction BM slurry absorption test, the fabric plane must be held horizontally relative to the slurry unlike the previously used method (see sections 4.4, 4.5, 4.6 and 4.7) where it had to be vertical. Therefore, a modification was necessary to the sample holder to allow such conditions. Tausif and Russell (2012) used a modified version of the standard test method BS ISO 15754 (ISO, 2009) to test the z-directional tensile strength (ZTS) using an aluminium platen sample holder with a square sample surface area of 625 mm<sup>2</sup>. A “410M double-sided tape (3M)” was used to fix the fabric sample to the sample holder. Using this sample holder with the tensiometer for the work discussed herein to test Z direction BM slurry absorption was not possible due to the sensitivity of the tensiometer load cell. Replacing the aluminium with a lighter PMMA-based material did not resolve the issue. An experiment was carried out nonetheless with the PMMA holder and it eventually resulted in an error message upon contact between the fabric and the BM slurry surface. Consequently, tensiometry could not be applied in this case and an alternative method was required.

### **4.8.2.2 Alternative Test Methods**

A number of published methods address the transplanar water transport through fibrous media, as reviewed by Fan and Qian, (2010), Manas et al., (2007), Miller and Tyomkin, (1984), Tang et al., (2015a), Tang et al., (2015b) and Tang et al., (2014), clothing materials as reviewed by Fan and Hunter, (2009) and Sinclair, (2014), or indeed wipes, such as in ITW Texwipe®, TM20 method (Texwipe, 2011). Additionally, the European Disposables and Nonwovens Association (EDANA) and the Association of the Nonwoven Fabrics Industry (INDA) have consolidated and standardised test methods known as nonwovens standard procedures (NWSP) of which the ones

addressing nonwovens' absorbency are NWSP 010.2.R1 (15) and NWSP 010.3.R0 (15) (EDANA and INDA, 2015).

Most of the existing experimental work using these methods have used water as the test liquid to compare the absorption behaviour of different fabrics whereas some have used saline water. BM slurry, however, differs from common aqueous liquids in its chemical composition and rheological properties as explained in section 4.4. Therefore, existing methods cannot be assumed to provide reliable results without modification. Furthermore, the short operational life of wipe fabrics means conventional methods may not provide a realistic assessment of performance as Tang et al. argue (Tang et al., 2014). Accordingly, methods that are not sensitive to the first few seconds of BM slurry absorption such as those in which the fabric sample is manually brought into contact with the test liquid or those where the liquid source is being moved towards the sample (Van Der Meeren et al., 2002, Tang et al., 2014) could not be considered. Some of the methods involved applying pressure on the fabric samples which leads to compression and a change in their structure which affects their absorption behaviour. Others researchers have considered the provision of a constant pressure head as absorption takes place, which is challenging (Tang et al., 2014).

#### **4.8.2.3 Requirements for a New Method**

The necessity to develop a new method to measure transplanar BM slurry absorption by nonwoven wipes stems from the following requirements:

- Real time measurements.
- Capability to measure the first 2 seconds with good resolution.
- Capability to simulate BM slurry absorption during wiping.
- Testing BM slurry retention which requires evaluating the amount of slurry that is picked up after the separation.
- Suitability to use BM slurry and a wide range of fabrics.

#### 4.8.2.4 *BM Slurry Absorption Assessment by Adaptation of a Tensile Tester*

Z-direction BM slurry absorption measurements were found to be possible by adapting a tensile testing instrument (Zwick®, Zwick Roell Z010 universal testing device). The load cell had a maximum capacity of 10 N and an error of 0.00005 g. The specimen grips used to hold the test platen were particularly suitable for absorption measurements, which involve very low forces (Zwick-GmbH, 2015). The test platen used is explained in section 4.8.2.1 and shown in Figure 4.57. The amount of 2 g of the test liquid (BM slurry) was placed on a plastic plate which was 3 mm thick. This in turn was placed on a compression test plate with a diameter of 120 mm. A schematic of the test setup is shown in Figure 4.57 and an image is given in Figure 4.58.

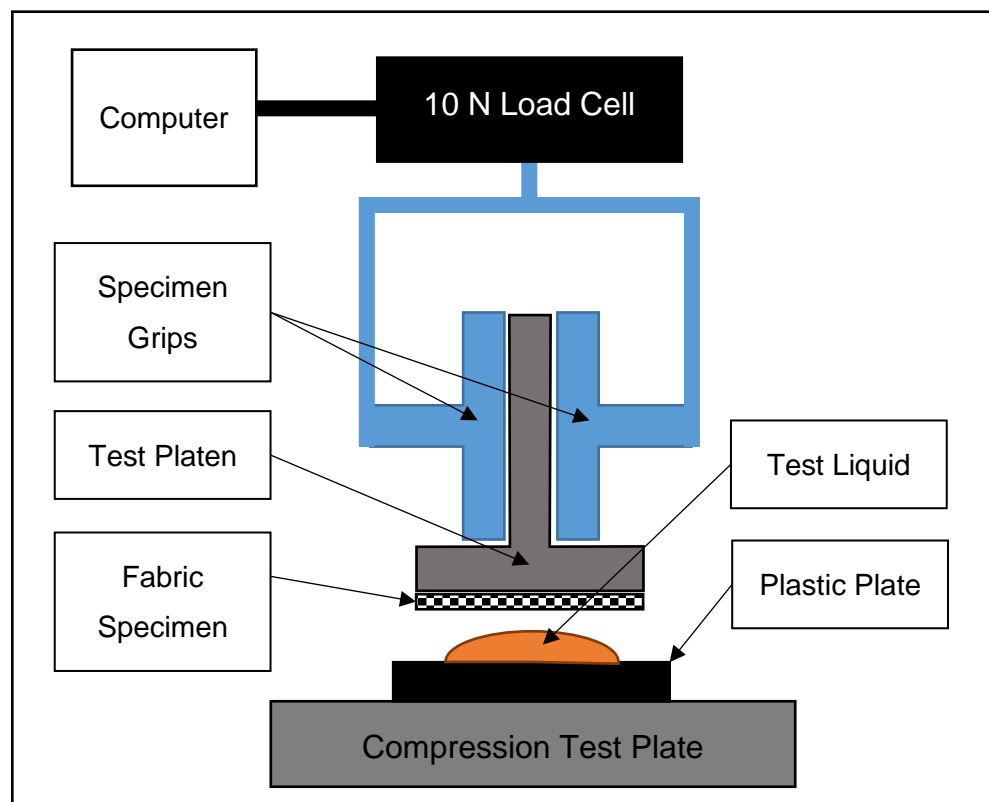
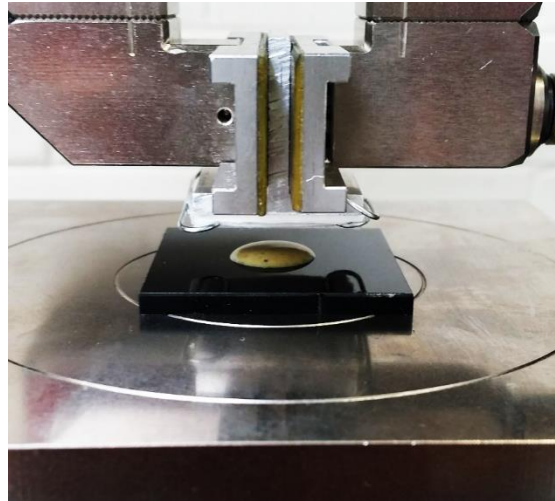


Figure 4.57: Schematic of the instrumental setup for Z-direction BM slurry absorption



*Figure 4.58: Test plate with BM slurry and fabric mounted on the platen prior to the Z-direction absorption measurement*

The use of Zwick equipment guaranteed a robust test method with high sensitivity. The test program was set to the compression method, this way the upper grips holding the fabric specimen could be programmed to approach the slurry specimen at a certain speed while recording the change of measured force with time. The approach speed was set to  $10 \text{ mm} \cdot \text{min}^{-1}$ . When the gauge length reached 4 mm, which was 1 mm above the plate bearing the slurry, the approach phase ended and the measurement continued until 60 seconds had passed since the start of the approach phase. That was when the measurement would stop and the upper grips would depart and move back to the start position to separate fabric from slurry.

When using a similar setup, Tausif and Russell (Tausif and Russell, 2012) measured the thickness of each fabric specimen to normalise their results. In this method, this step could be avoided because the upper and lower parts of the test setup, i.e. the fabric specimen and slurry, were separate. This meant that the zero-gauge length (zero position) could be set for each individual specimen regardless of their thicknesses. Additionally, this not only avoided having to change the program settings for samples of different thicknesses, but also it eliminated the variation in results that is produced by any change in fabric thickness between the specimens. The main steps in the procedure are now summarised.

1. Fabric samples were cut into square specimens of 25 mm side length and conditioned.
2. BM slurry was prepared as described in 2.5.3.
3. The equipment setup, i.e. the load cell, specimen grips and compression test plate, are prepared and mounted as shown in Figure 4.57 and Figure 4.58.
4. The tensile tester program was initiated.
5. The fabric specimen was then mounted on the test platen as described in section 4.8.2.1 and shown in Figure 4.57.
6. The test platen was carefully placed in the centre of the compression test plate facing down without applying pressure on the fabric specimen other than the weight of the test platen.
7. The upper part was then driven down manually until it the grips were in firm contact surface with the vertical part of the test platen.
8. The current position of the upper grips was then set as the zero position.
9. The grips were fastened and together with the test platen and fabric specimen, they were brought upwards to the start point, 10 mm from the zero position. This was done by the program once start position button was clicked.
10. At the start position, the force reading was set to zero.
11. The slurry specimen was then prepared. While the plastic plate was on the digital balance, 2 g of slurry was placed at its centre from a drop height of 10 mm using a plastic pipette. The exact weight of the BM slurry was recorded.
12. The plastic plate was then placed in the centre of the compression test plate below the test platen as shown in Figure 4.58. The program could then be started.
13. Upon running the program, the upper grips moved towards the slurry to a gauge length of 6 mm at a speed of 50 mm.min<sup>-1</sup>. Then the approach phase started and the computer began recording force measurements and time. During this phase, the grips move at a speed of 10 mm.min<sup>-1</sup>.

14. Upon reaching a gauge length of 4 mm, the upper grips stopped moving and were held in place until 60 s had elapsed since the beginning of the approach phase. Reading and recording force measurements continued throughout this phase.
15. After 60 s had passed, the force measurement recording stopped and the upper grips were moved away from the BM slurry to achieve separation.
16. Once the upper grips had retreated to their start position, the force reading was manually recorded.
17. Then the weight of BM slurry residing on the plastic plate was measured using the digital balance. See Figure 4.59.
18. The test platen and plastic plate were cleaned thoroughly after each experiment.



*Figure 4.59: An example of how the specimens appear after the z-direction BM slurry absorption experiment. Left: fabric specimen with a smudge of slurry picked up after contact. Right: plastic plate with residual slurry after contact.*

Good sensitivity was established using this method when the 10 N load cell was installed. Data readings were recorded in real time with a  $30 \text{ s}^{-1}$  frequency. This provided a good resolution for the duration of the test, including the first few seconds, which is of particular importance. The test setup therefore simulated to a satisfactory extent, the short duration contact conditions in which wipes are used, particularly when compared to other transplanar absorption test methods. This method also allows slurry retention to be determined by measuring the amount picked up after contact.

### **4.8.3 Transplanar BM Slurry Absorption with Local Porosity Variation in the Z Direction**

Changing the porosity profile through the fabric thickness is more complicated than through its plane. The simplest way is arguably by layering sheets of fabric of different global porosities over each other to ultimately make the required sample. However, this potentially produces gaps between the consecutive layers due to incomplete interfacial contact that will influence liquid absorption behaviour. This means that liquids will not readily transfer between adjacent layers that are simply laid over each other. The porous structure in the z-direction therefore has to be well integrated. One way of achieving good integration is to hydroentangle the layers to provide good mechanical connection and this step could be readily included during the manufacture of the fabric samples.

Several recent studies have addressed the influence of hydroentanglement settings on fabric structure (Mao and Russell, 2005, Ghassemieh et al., 2002, Venu et al., 2014, Tausif and Russell, 2012, Venu et al., 2017), some of which have suggested that exposing the web to the water jets on one side only, leads to patterning in the fibrous structure in the z-direction. It is well known that a difference in porosity through the fabric cross-section can be modulated by varying the water jet profile, i.e. the balance of specific energy and pressure applied to the face and back of the web during hydroentangling.

For consistency, the fibre blend used to make the sample fabrics was identical to that used throughout this Chapter and is as explained in section 3.1.1. The fabric sample made for this experiment had a nominal basis weight of  $75 \text{ g.m}^{-2}$ . It was hydroentangled using three manifolds, where all manifold pressures were 60 bar and directed towards the same (face) side of the fabric. This created a porosity gradient in the fabric's transplanar structure, but was successful in integrating the fabric such that it could be tested without delaminating.

#### 4.8.4 Materials and Methodology

The method for determining the z-direction BM slurry absorption explained in section 4.8.2.4 was used. The BM slurry used was prepared by mixing the lotion with BM (65% water content) at a weight ratio of 1:1. The fabric samples were made using the procedure explained in section 4.8.3. Both sides of the fabric were evaluated with three replicates in each case.

#### 4.8.5 Results and Discussion

Average BM slurry absorption curves were obtained from the replicate measurements and the resulting data for each side of the fabric are shown in Figure 4.60, where side B was directly impacted by the water jets (the face side) and side A was in contact with the conveyor belt during hydroentangling and was not directly impacted (back side).

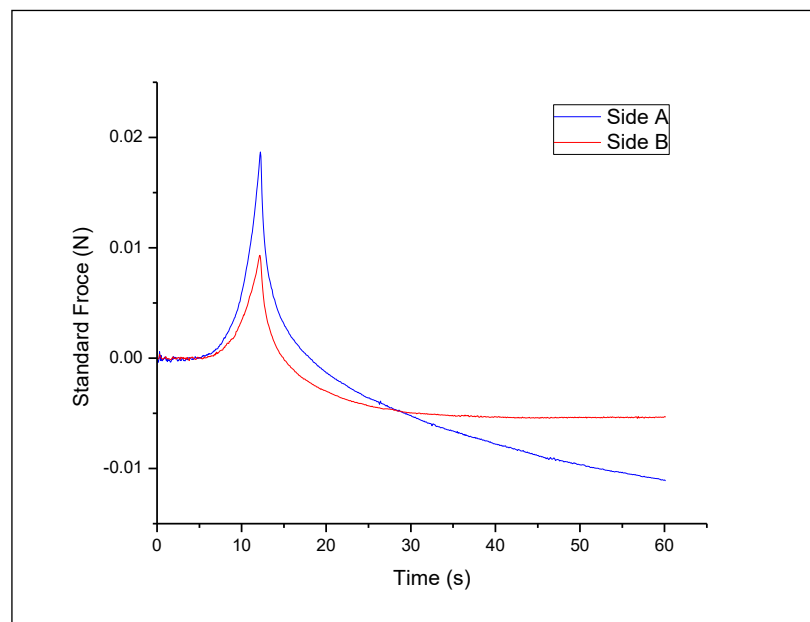


*Figure 4.60: Average BM slurry absorption force curves during the z-direction absorption experiments. Duration of 60 s. Side A: Conveyor side. Side B: Water jet side*

This absorption curve represents the changes in force that take place as the fabric sample interacts with the BM slurry in real time. As indicated in section 4.8.2.4, the force reading commences as soon as the gauge length reaches 6 mm and that is when  $t = 0$ . This represents the beginning of the approach phase at a speed of  $10 \text{ mm}\cdot\text{min}^{-1}$ , and as it approaches 4 mm, the force

measurement records the point at which the fabric sample makes contact with the BM slurry surface. This is shown in Figure 4.61 as phase 1. When the 4 mm gauge length is achieved, the sample stops moving because BM wetting commences (phase 2). Force reading continues until 60 s have elapsed and the time in which the grips are not in motion (phase 3) is when BM absorption is taking place. During phases 2 and 3, two main forces are applied on the sample which are then reflected in the force curve. The first is the wetting force caused by the surface tension of the BM slurry, which is detected as the fabric contacts the surface of the BM slurry droplet. This applies a tensile force on the sample. The second force is due to the resistance of the slurry to deformation, due to the small compressive force applied by the fabric specimen as it descends to its lower most position after contact with the BM slurry (Figure 4.62). Thus, the slurry's rheological properties are characterised by the compression force recorded by the curve.

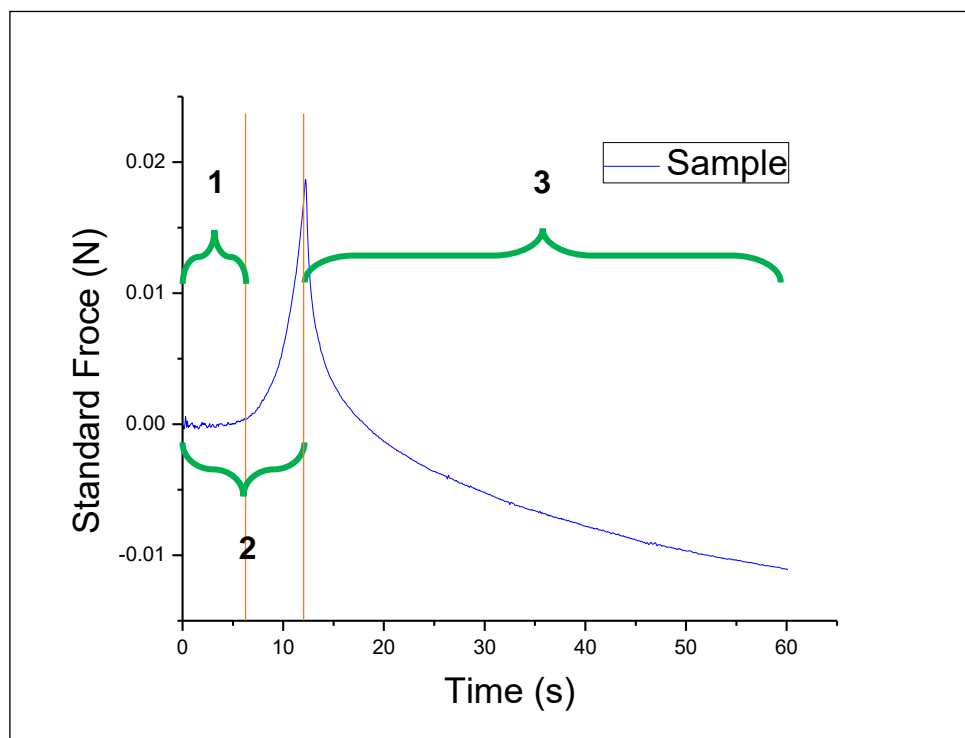


*Figure 4.61: The three phases of the BM slurry absorption force curve during z-direction measurements. 1: The approach phase as the fabric sample is moved towards the BM slurry droplet. 2: Total time of travel for the upper grips holding the fabric sample, which includes contact between the fabric sample and BM slurry droplet. 3: BM slurry absorption time*

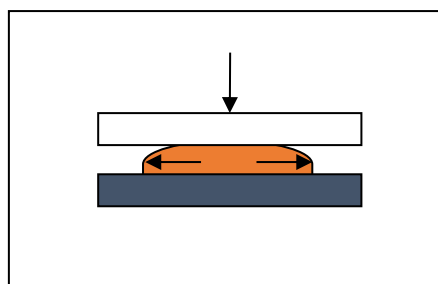


*Figure 4.62: BM slurry deformation at the end of the approach phase. Fabric specimen (white) applies pressure on the BM slurry (orange), which is deformed horizontally over the plastic plate (blue)*

Force readings markedly decrease at the beginning of phase three due to BM slurry absorption. The meniscus between the plastic plate and the fabric specimen at this stage is visible in Figure 4.63. The force reading decreases gradually with time as the sum of the forces approaches equilibrium. At this point, the distance between the fabric surface and the test plate is 4 mm and the thickness of the plastic plate is 3 mm, which means there is a 1 mm gap between the fabric surface and the plastic plate.

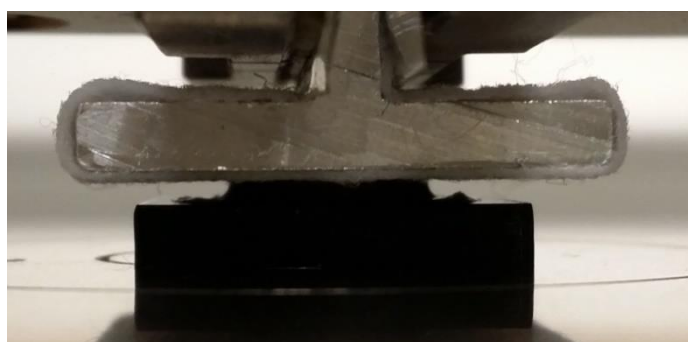


*Figure 4.63: Meniscus of the BM slurry formed between the plastic plate and the fabric surface during phase 3.*

#### 4.8.5.1 **Absorption Curve Parameters**

Several quantitative parameters can be defined from the BM slurry absorption force curve:

1. **Point of contact:** this is the point at which the fabric comes in to contact with the BM slurry droplet during phase 2. In these experiments, this was typically  $\sim t = 6$  s. This is the time it took the upper jaw to approach the slurry droplet.

2. **Peak force:** the force measured at the end of the approach phase as soon as the wipe specimen and the BM slurry are in closest contact, i.e. they are separated by 1 mm. This is the point at which the slurry is subjected to the highest level of deformation.
3. **Force change rate:** This can be expressed as  $\text{N}\cdot\text{s}^{-1}$ .
4. **Force at 60 seconds:** This is the force measured at the end of the measurement.
5. **Slurry pickup:** The weight of residual BM slurry on the plastic plate is measured before and after the experiment, and the difference is calculated to determine the magnitude of removal by the fabric sample.

#### 4.8.5.2 *The Point of Contact*

Typical force measurements at the point of contact between the fabric sample and BM slurry droplet are given in Figure 4.64.

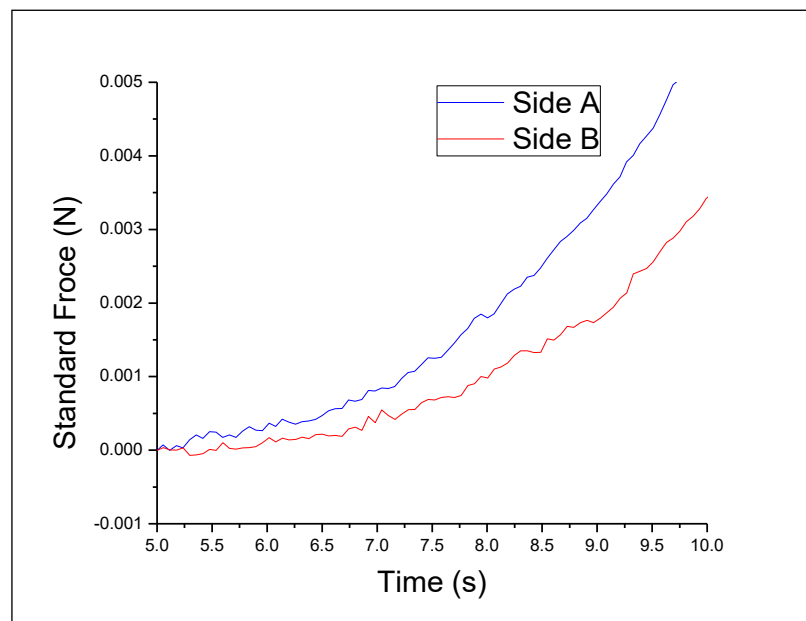


*Figure 4.64: Average curves showing the force measurements at the point of contact for each of the fabric sides. Side A: Conveyor side. Side B: Water jet side*

The graph shows an increase of force with time for both samples. The rate at which the force increases, however, varied. Side A shows a higher rate of increase than side B which can be explained by a relatively higher resistance to BM penetration (lower permeability) by sample A compared to sample B. This could be attributed to the difference in packing density of the two sides.

Side A is the conveyor side and is pressed against the fine conveyor mesh by the water jet stream. This meant side A had a relatively higher packing density which means side B has a relatively larger average pore size and consequently higher permeability than side A, which agrees with Mao's work (Mao, 2009a).

#### 4.8.5.3 **Peak Force**

A comparison of the mean peak force values for the two fabric samples, which were identical apart from their porosity, is shown in the form of a box chart in Figure 4.65. The statistical test revealed a significant difference ( $P=95\%$ ). Side A showed a higher peak force than side B which is consistent with the explanation in section 4.8.5.2 considering side A has a higher packing density than side B.

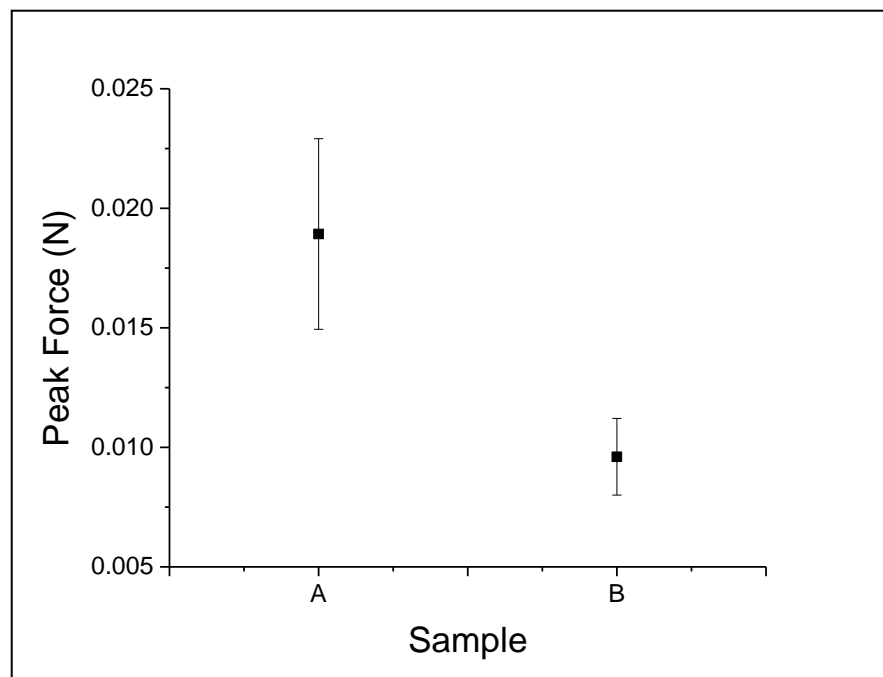


Figure 4.65: Comparison of mean peak force between the two samples. Sample A: Conveyor side. Sample B: Water jet side

#### 4.8.5.4 **Force Change with Time**

Upon reaching the end of phase 2 and at the beginning of phase 3, compression of the BM slurry droplet ceases and deformation due to compression is at its maximum level. The decrease in force at this point, is directly related to wetting and BM slurry absorption, which is detected as a

tensile force by the load cell. The rate at which the measured force is decreased can be calculated. Since this rate changes with time, comparison of the two fabric samples was based on the maximum recorded rate and the magnitude of the change in force during the first 2 seconds of phase 3. A higher average value was obtained for side A compared to side B and a comparison of the two mean values of the highest force change rate using the Tukey test showed a significant difference ( $P=95\%$ ) Figure 4.66. The results show a higher change for side A compared to side B. This is because of the higher capillary pressure on side A compared to side B. Side A had a relatively higher packing density which leads to a smaller equivalent capillary radius leading to a relatively high capillary pressure (see equation 4.4).

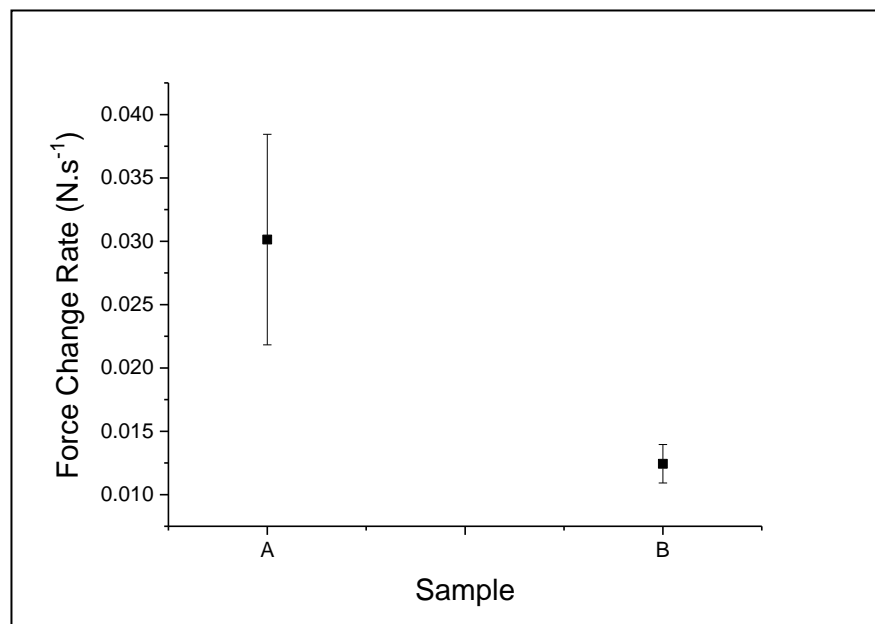


Figure 4.66: Comparison of the mean of highest recorded force change rate of the two samples. Sample A: Conveyor side. Sample B: Water jet side

#### 4.8.5.5 Absorption after 60 Seconds

The forces measured after 60 seconds for the two samples are plotted in Figure 4.67. Side B shows a higher average force measurement than side A. However, the statistical analysis is not significant at the 95% confidence level. This is because the two samples are taken from the same fabric and hence, they have the same global properties, particularly porosity. On the longer term, the two sides were not performing significantly different which is consistent with Washburn's equation. However, as mentioned in sections 4.5.1 and

4.8.1, the behaviour is significantly different at the short timescales. This is also consistent with the work of Gane et al. (2004) and Ridgway et al. (2006).

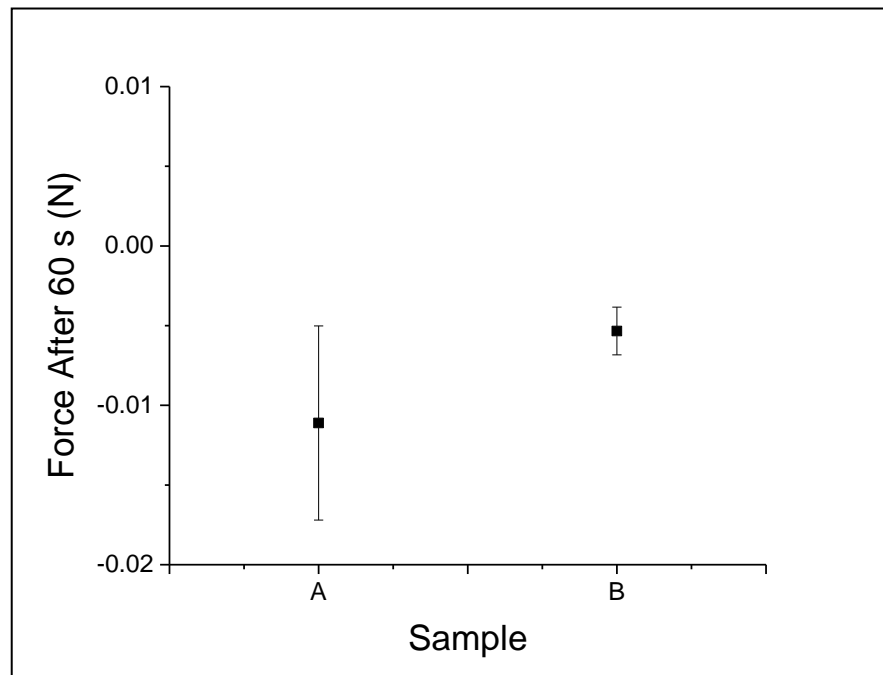
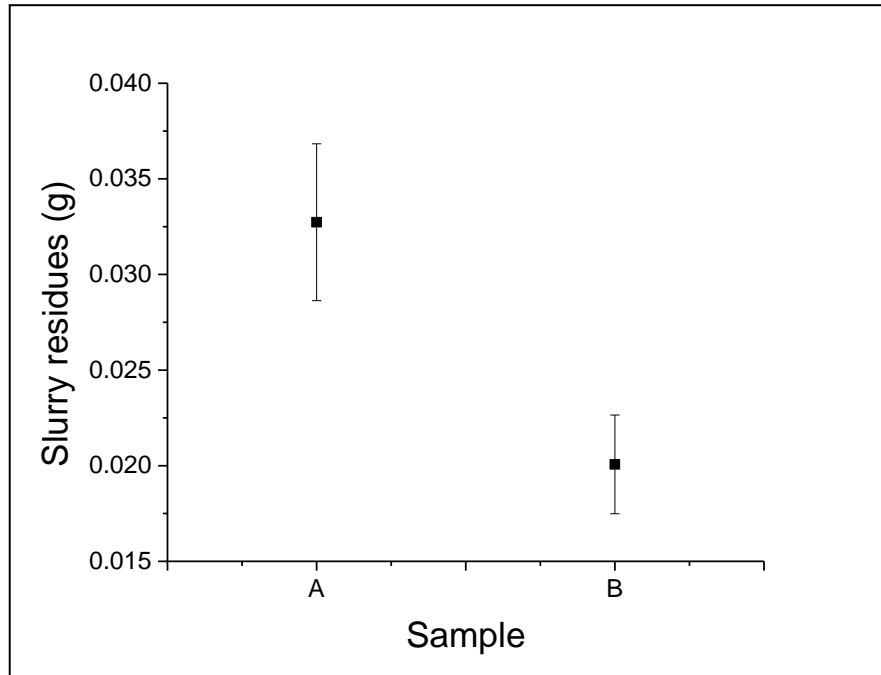


Figure 4.67: Comparison of the mean forces measured at  $t = 60$  s. Sample: Conveyor side. Sample B: Water jet side

#### 4.8.5.6 Slurry Pickup

The weight of the BM slurry droplet is recorded for each test run. At the end of each test, the computer stops reading force measurements and the upper jaw returns to its original position. The fabric specimen, therefore, is separated from the slurry droplet. Upon separation, a proportion of the slurry is retained in within the specimen's fibrous matrix. The amount of BM slurry left from the droplet on the plastic plate is the BM slurry residual. By weighing the plastic plate with the BM slurry residuals on it after the separation, the amount of slurry that's picked up by the fabric specimen can be calculated. This is by subtracting the weight of the residual BM slurry from the original weight of the slurry droplet. Figure 4.68 shows a comparison of the slurry residues for the two samples. It shows that side A left more slurry after separation compared to side B. The reason is that side A, having a relatively high packing density and a relatively low equivalent capillary radius, hence a relatively low porosity, has shown a higher resistance to BM slurry penetration which led to less retention of BM slurry within the fibrous matrix of the fabric. A significant

difference between the two sides (P= 95%) was found. The amount of slurry retained by each of the fabrics after testing are shown in Figure 4.69 where it shows that side B has picked up more BM slurry than side A and this was confirmed with the statistical analysis at (P=95%). This is consistent with the results of the slurry residues shown in Figure 4.68.



*Figure 4.68: Comparison of the mean weight of the slurry residues left by the two samples after separating the fabric from the slurry. Sample A: Conveyor side.  
Sample B: Water jet side*

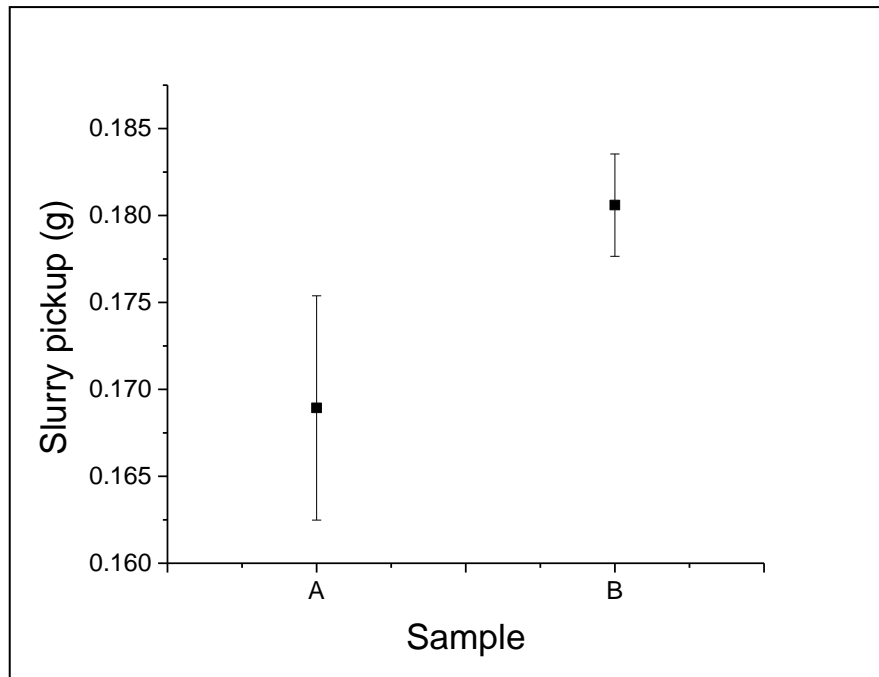


Figure 4.69: : Comparison of the mean weight of the slurry retained by the two samples after separation. Sample A: Conveyor side. Sample B: Water jet side

#### 4.8.6 Summary and conclusions

It is apparent from the experimental results presented herein that both the rate and volume of BM slurry absorption in hydroentangled fabrics is strongly influenced by both global porosity and local porosity. Interestingly, by modulating local porosity in the form of patterns within the fabric, it is possible to obtain improved BM slurry absorption behaviour, and the effects are detectable within the short, ~ 2 s, timeframe that is most relevant to baby wipe utilisation. Transplanar BM absorption is also influenced by fabric porosity, and to enable its investigation, a new instrumental absorption force measuring procedure was developed that provides a basis to study the interaction of the lotion with the fabric structure in real-time from the point of initial contact, to the end of the BM slurry absorption process. Not only does this provide a means to better understand how fabric structure and dimensions can be modulated to improve BM slurry absorption, but it also provides a means to determine how lotion loading and related parameters influence BM slurry removal and transfer to the fabric structure.

The results of the transplanar absorption investigation found significant differences in the absorption behaviour of fabric samples with opposing

porosity profile gradients. It was shown that the negative porosity profile sample performed relatively better. Based on that, it could be concluded that an enhancement in the transplanar BM slurry absorption can be achieved by introducing a negative porosity gradient to the fabrics Z direction structure. This is aligned with the theoretical modelling work discussed in section 4.8.1 and 4.7.1 and authored by Shou et al., (2014b).

The influence of the lotion will now be considered using the same instrumental measurement technique.

# **CHAPTER 5**

## **Influence of Lotion on Absorption Behaviour**

### **5.1 Introduction**

Lotion is added to wipes for several purposes, including to aid cleaning, skin care and to provide sensory signals such as perfumes for the consumer (Memari, 2011). While there is evidence of the positive influence of lotion loading on cleaning Koh (2009) and skin care Visscher et al. (2009), its influence on wiping efficiency, particularly BM slurry absorption is lacking. When used to pre-moisten the nonwoven wipe substrate, the lotion takes up a proportion of the available void volume and this raises questions about the resulting impact on the wipe's general BM absorption behaviour and whether or not it is influenced by the lotion loading. The influence of lotion on BM removal was therefore the focus of this chapter. Of particular interest was to investigate how the presence of lotion influences the planar and transplanar absorption of BM slurry into the fabric.

### **5.2 Effect of Lotion Loading on BM Slurry Absorption in the Machine Direction (MD)**

The use of tensiometry allows a comparison of BM slurry absorption behaviour in fabric samples regardless of their thickness because it measures the absolute forces involved as the specimen interacts with the BM slurry. This is particularly helpful in terms of minimising any external forces that could modify fabric thickness and therefore time-dependent absorption behaviour.

#### **5.2.1 Materials and Methodology**

The same hydroentangled fabric used in section 3.2 was studied with the same fibre blend and basis weight. They were premoistened with a lotion loading of 440% using the method explained in section 3.3. Specimens of the dry and wet samples were cut in to dimensions of 45 x 20 mm as described in

sections 4.4, as illustrated in Figure 5.1. The experimental procedure was identical to that presented in section 4.4.

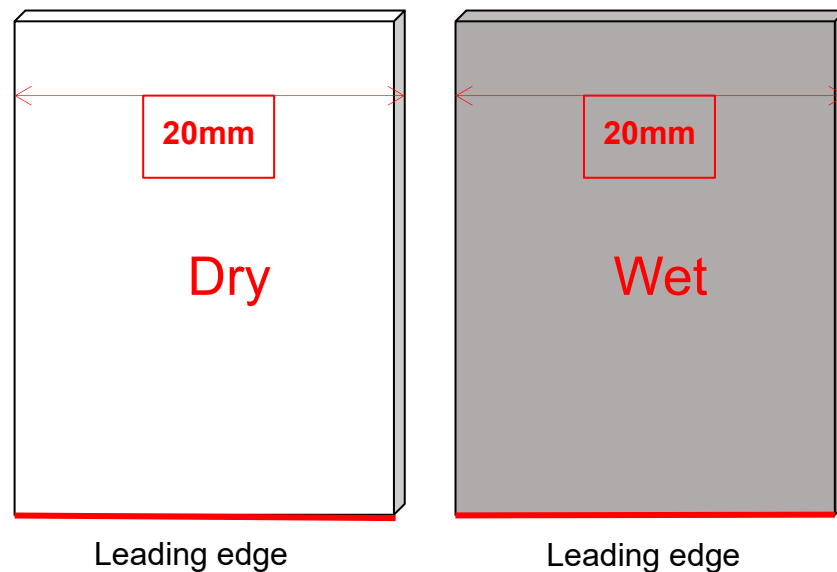


*Figure 5.1: Sample preparation. Specimens were cut in the dimensions 45 x 20 (mm) such that the MD was vertical. The leading edge was immersed in BM slurry at a depth of 0.5 mm*

## **5.2.2 Results and Discussion**

The results of this experiment are reported as absorbed BM slurry weight vs. time. The absorption rate can then be determined from either the slope of the tangent of the resulting curve at the desired time point, or by linear fitting the slope of the resulting BM slurry absorption curve between two time points. A plot showing the weight of BM slurry absorbed by the dry and wet samples during up to 60 s of contact with the slurry surface is presented in Figure 5.2. Mean BM slurry absorption rates were calculated for each sample based on the first two seconds response, which is shown in Figure 5.3, similar to previous experiments (see section 4.4).

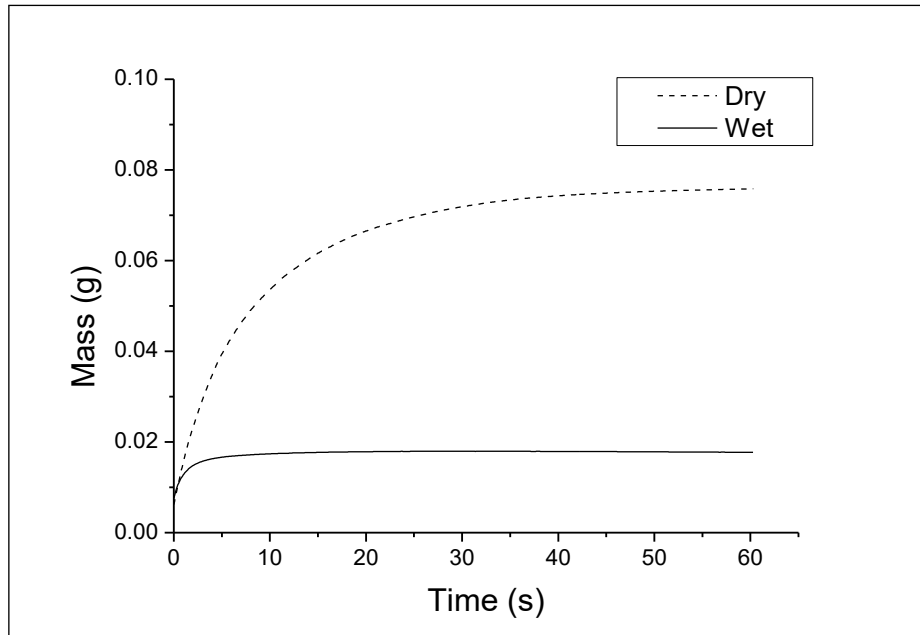


Figure 5.2: Tensiometry slurry absorption curves for the dry and wet hydroentangled samples

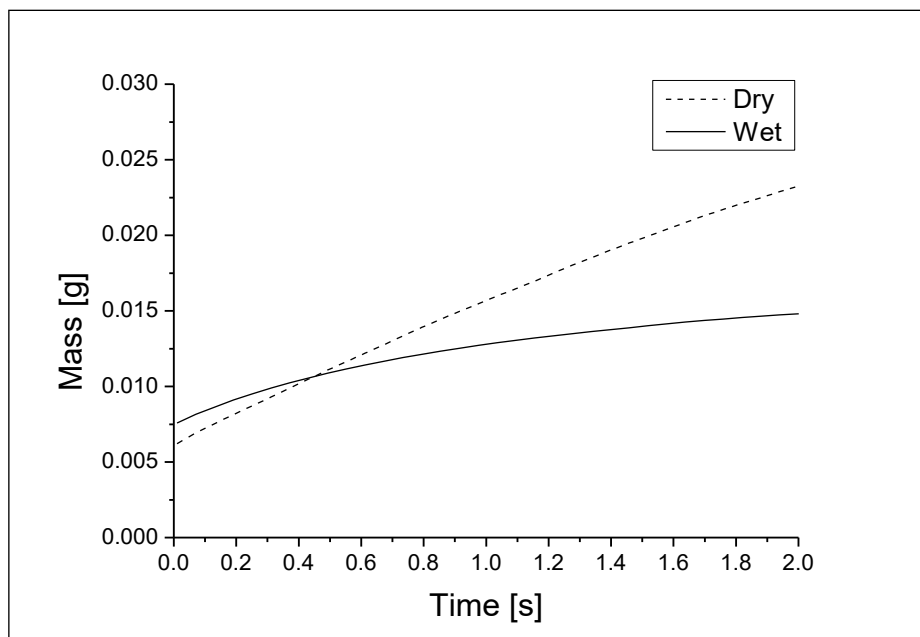


Figure 5.3: Plot of the tensiometer BM slurry absorption curves for dry and wet hydroentangled samples during the first two seconds of contact with the BM slurry surface.

A statistical analysis was carried out comparing the means of two second curve gradients for dry and wet fabric samples and a significant difference was found (P=95%). means were significantly different.

Since the weight of the BM slurry acts against absorption in this procedure, the results reflected those of test setup 2 in section 4.3.1.2. The same trends are not obvious in the present results as the dry fabric exhibited a faster absorption rate than the wet, lotion-loaded sample. In section 5.2, the advantage of the wet fabric when absorbing against gravity (demand absorption) was argued to be due to the faster wetting process as the specimens were pre-moistened with lotion. The same advantage could not be clearly observed in the results of this experiment. A potential explanation could be the difference between the two test methods. The tensiometer method involves immersion of the leading edge of the specimen. Over a short timescale, the process of immersion, even at a depth of 0.5 mm, could influence the results. This is particularly relevant since the tensiometer method is markedly more sensitive than the video capturing one. Furthermore, when examining Figure 5.3, note that the average curves for both samples start at different weight readings, before time  $t = 0$ . It is possible that the advantage of wetting was mostly favourable towards the wet sample during the immersion process and just after the readings began, the dry fabric took over. Further investigation is possible using the transplanar BM absorption method, which enables data to be recorded before the point of contact between the fabric specimen and the slurry surface. This is equivalent to the immersion time in the tensiometry method.

## **5.3 Effect of Lotion on Transplanar BM Slurry Absorption**

The Zwick absorption force test method introduced in section 4.8.2.4 is another way to assess the BM absorption behaviour based on bringing the fabric into contact with a droplet of slurry. Like the tensiometry method, this allows comparison between the dry and wet samples.

### **5.3.1 Materials and Methodology**

The hydroentangled fabrics used in this experiment were the same as used in section 5.3 and explained in section 3.1. Fabric pre-moistening was also carried out using the method explained in section 3.3, with a lotion loading of

440%. The same test conditions reported in section 4.8 were used to perform this experiment.

### 5.3.2 Results and Discussion

The resulting BM slurry absorption curves for the dry specimens and the wet specimens are plotted in Figure 5.4 and Figure 5.5 respectively. Average curves were then produced for each sample for comparison. The average curves are shown in Figure 5.6. An explanation of these absorption curves and how to interpret them is given in section 4.8.5.

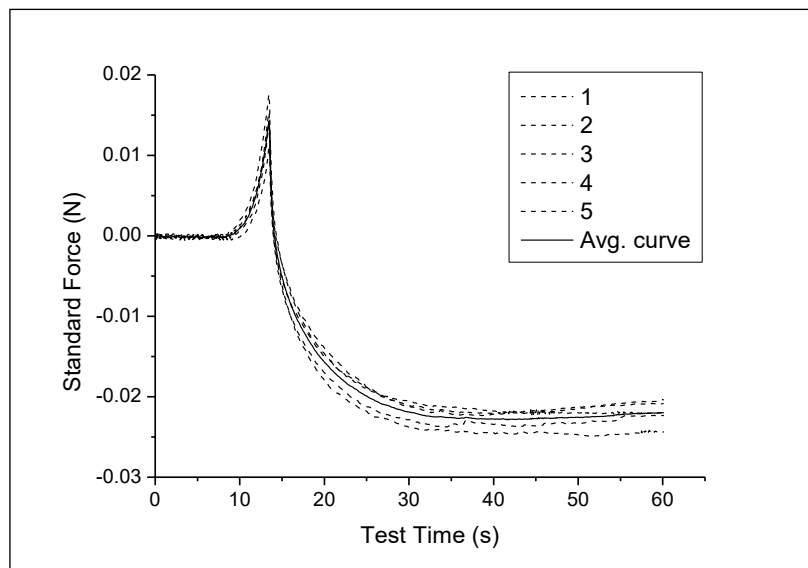


*Figure 5.4: Transplanar BM slurry absorption force curves showing the replicate results the dry fabric specimens measured over the duration of 60 s. The average curve is drawn as a continuous line.*

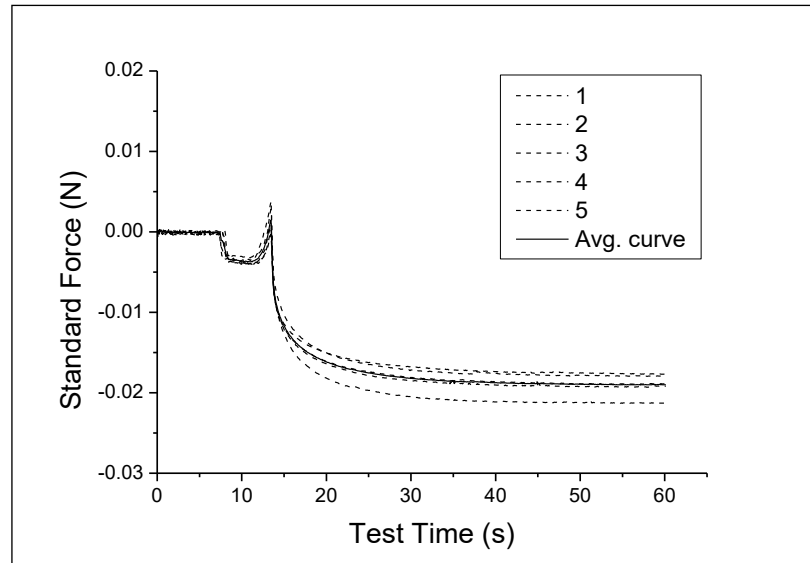


Figure 5.5: Transplanar BM slurry absorption force curves showing the replicate results the wet, lotion-loaded fabric specimens measured over the duration of 60 s. The average curve is drawn as a continuous line.

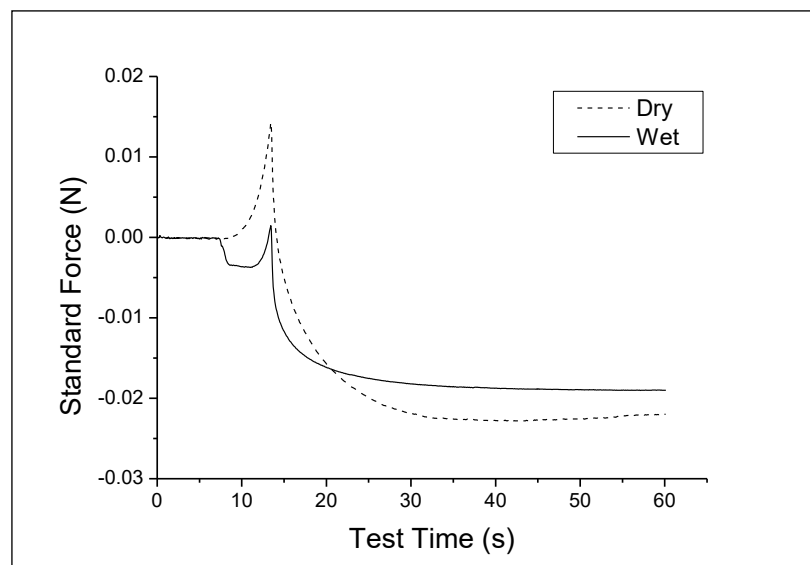
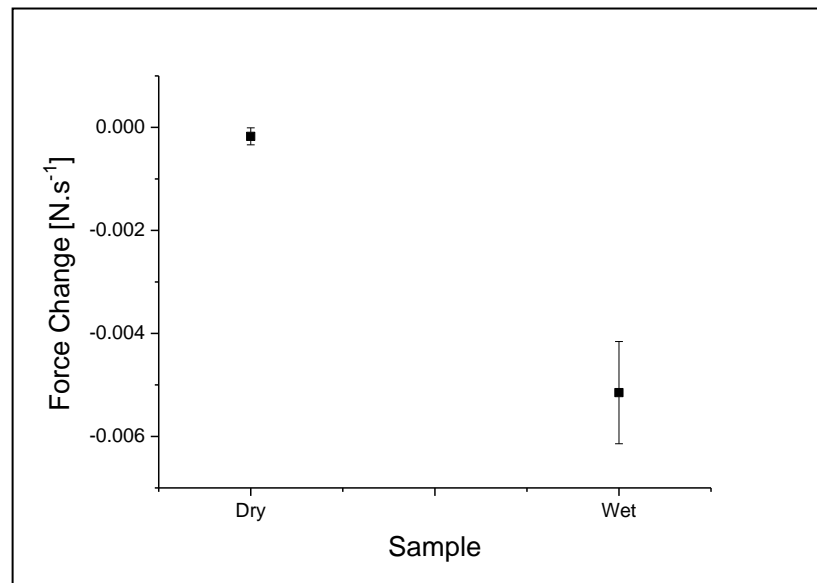


Figure 5.6: Comparison of the average transplanar BM slurry absorption force curves for the dry and wet samples for a duration of 60 s

At the point of contact the fabric interacts with the BM slurry, the absorption curve slopes for each of the dry and wet samples were calculated. As seen in Figure 5.6, the dry curve shows little or no change around the point of contact which leads to an average slope of near zero. The wet curve, on the other hand, shows a substantial change upon contact. The calculated slopes for all

specimens of the two samples were significantly different ( $P=95\%$ ). Figure 5.7 shows a comparison of the mean slopes at the point of contact.



*Figure 5.7: Comparison of the mean slopes of the absorption curves of the dry and wet fabric samples at the point of contact after transplanar BM slurry absorption*

In relation to the peak force, the average BM slurry absorption curves continue to show different behaviours between the dry and wet samples. Upon reaching the closest distance between the fabric specimen and the plastic plate, the force reading peaks in both samples. The peak force measurements, however, happen at different levels. The difference is statistically significant at the 95% confidence level. Figure 5.8 shows a comparisons of the mean peak force measurements for the dry and wet samples.

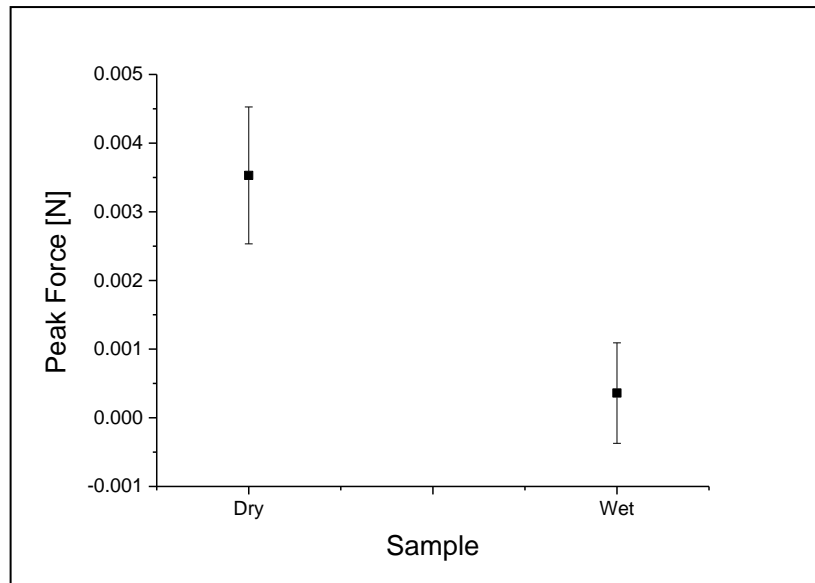


*Figure 5.8: Comparison between the mean peak force measurements of the dry and wet samples*

In relation to BM slurry absorption after 60 s, towards the end of the experiment, the absorption behaviour of the two samples was similar. The force readings at 60 seconds for the specimens of both samples were not significantly different ( $P=95\%$ ). A comparison is shown in Figure 5.9.

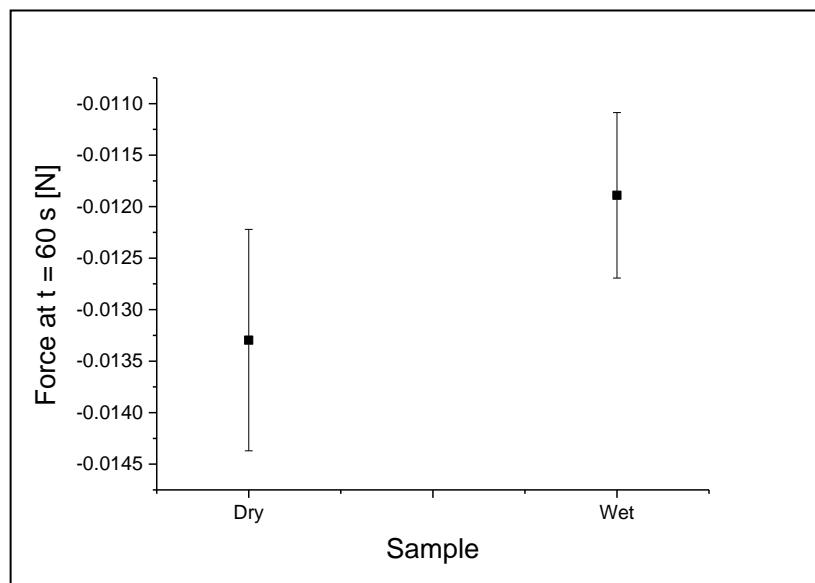


*Figure 5.9: Comparison between the mean force measurements of the dry and wet samples after 60 s*

A significant difference in BM slurry absorption behaviour was observed between the dry and wet samples using the transplanar method shortly after

contact occurs between the fabric sample and the surface of BM slurry. Over the long term, however, the difference in BM slurry absorption behaviour was insignificant ( $P=95\%$ ).

**Point of contact:** a marked change in the measured force was observed upon contact between the wet fabric specimens and BM slurry. Such force change was absent in the dry specimen absorption curves. As discussed in section 5.1, it is likely that the presence of lotion in the sample, increases the wetting capacity of the BM slurry when in contact with the fabric, and this is immediately evident in the recorded force data over a short timescale of just a few seconds.

**Peak force:** The difference in peak force data was also found to be statistically significant ( $p=95\%$ ). The peak in the dry fabrics could be explained by the lack of wetting. It is likely that BM slurry transport through the dry fabric is not as fast as in the lotion-loaded case. After the point of contact, the fabric specimen continues to approach the plastic plate until it reaches a defined distance (see section 4.8.2.4). The relatively slow absorption rate into the dry fabric, and the lack of rapid wetting led to greater deformation of the slurry pool and an increase in its area due to sideways displacement, Figure 5.10. On the other hand, a relatively fast penetration of the BM slurry into the wet sample takes place, which led to a greater weight of BM in the sample and therefore an increase in the tensile force reading. The peak force is still observed though a few seconds later as shown in Figure 5.6. This is because the lotion, at a load of 440%, takes up about one third of the available void volume in the fabric, reducing its effective porosity from 95% to 60%. This in turn produces resistance to BM slurry inlet into the interior of the fabric.

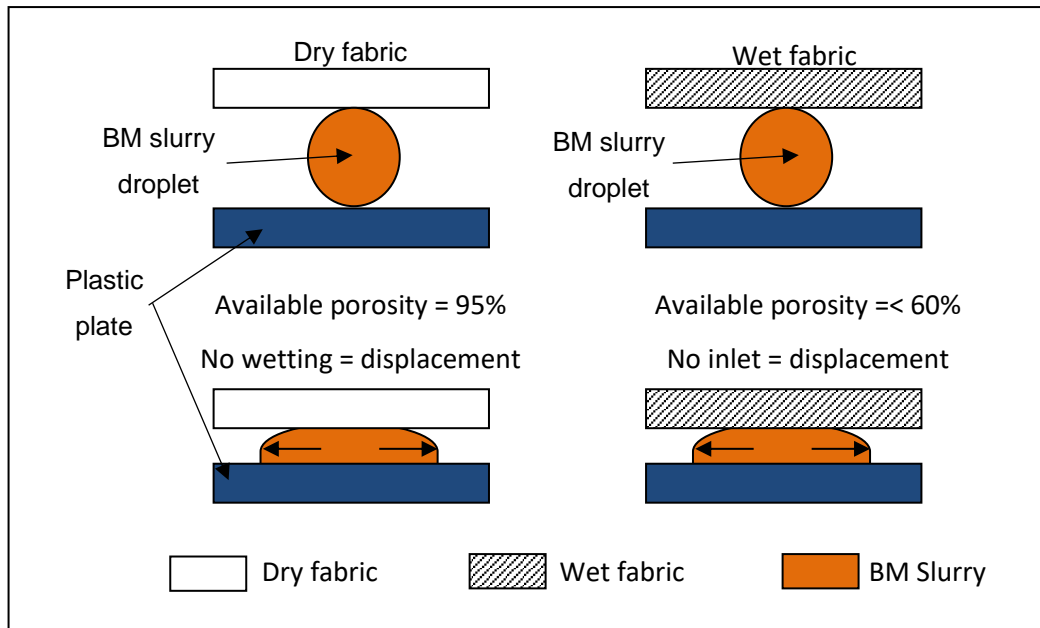


*Figure 5.10: Schematic illustrating BM slurry deformation as the fabric specimen approaches the plastic plate after contact occurs with the BM slurry surface.*

Looking at Figure 5.10, the case of dry fabric is on the left, the upper drawing shows the BM slurry droplet upon contact with the dry fabric. The dry fabric has void volume equal to 95% of its total volume (assuming a fabric sample with a porosity of 95%). The bottom drawing shows the BM slurry deformation as the fabric sample approaches. Despite the availability of void volume in the dry fabric, the lack of wetting leads to the displacement of the BM slurry during the approach phase.

The case of wet fabric is on the right, the upper drawing shows the BM slurry droplet upon contact with the wet fabric. The wet fabric has less void volume than the dry (assuming it is equal to 60% of its total volume). The bottom drawing shows the BM slurry deformation as the fabric sample approaches. Despite the good wetting properties of the lotion in the wet fabric, the lack of void volume leads to the displacement of the BM slurry during the approach phase.

Both the dry fabric and the wet fabric cause the displacement of BM slurry. It is logical that the increase in the lotion loading could improve the wetting properties of the fabric but it would reduce the available volume within its matrix. Vice versa, the decrease of lotion loading leaves more volume

available but reduces the wetting properties of the fabric. It is possible, therefore, to expect that there is an optimal level of lotion loading where wetting properties and void volume are maximised.

**Force at 60 seconds:** The force measurements at 60 seconds were not markedly different between the dry and wet samples. This is in alignment with the result discussion of the experimental data presented in section **Error! Reference source not found.**

Collectively, it is apparent that lotion loading, influences the BM slurry absorption behaviour of the fabric, and is particularly influential over a short term duration of ~2 s. A further question arises about the amount of lotion with which the nonwoven fabric is loaded. This is addressed in the next section.

## **5.4 Effect of Lotion Loading on Transplanar BM Slurry Absorption**

Theoretically, and based on the Lucas-Washburn equation (equation 4.64.2), absorption rate increases with the available volume within a porous medium (Washburn, 1921). However, earlier in this work (CHAPTER 4), evidence from the literature as well as from the presented experiments suggested that the Lucas-Washburn law does not describe absorption behaviour over short timescales of a few seconds. This was also highlighted by Wei in his work about absorption in porous media (Wei, 2003).

As argued in section 5.3.2, on the one hand, the presence of lotion promotes a faster wetting process, but on the other hand, it occupies a proportion of the available porous volume in the fabric, which subsequently resists liquid inlet compared to a dry fabric. Figure 5.11 shows the hypothetical influence of these two competing aspects on the measured peak force.

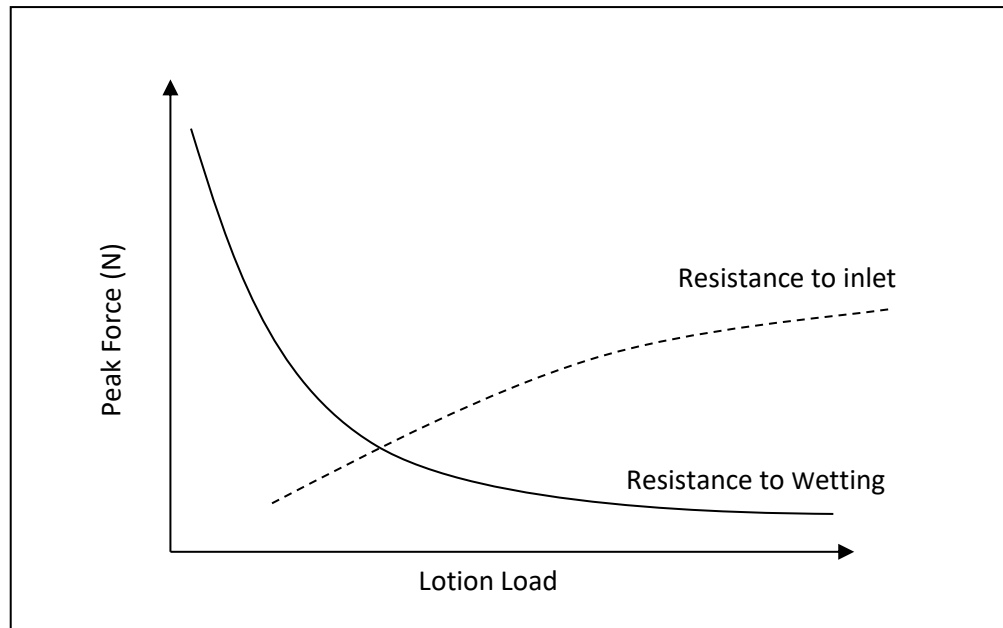


*Figure 5.11: The hypothetical influence of lotion loading on the peak force. The continuous line represents the resistance to wetting and the dashed line represents the resistance to inlet.*

This purpose of this experiment was to further investigate the influence of lotion loading on BM slurry absorption behaviour in the z-direction.

#### **5.4.1 Materials and Methodology**

The BM slurry absorption behaviours of four samples were compared in this experiment. The fabrics were the same as those described in previous experiments as explained in section 3.1. Three samples were loaded with the lotion used throughout this thesis, using the method explained in section 3.3 at varying lotion loadings of 100%, 200% and 440%. The transplanar BM slurry absorption curves for these three samples were compared together with that of the dry sample.

#### **5.4.2 Results and Discussion**

Figure 5.12 shows the average BM slurry absorption force curves for the samples with different lotion loadings.

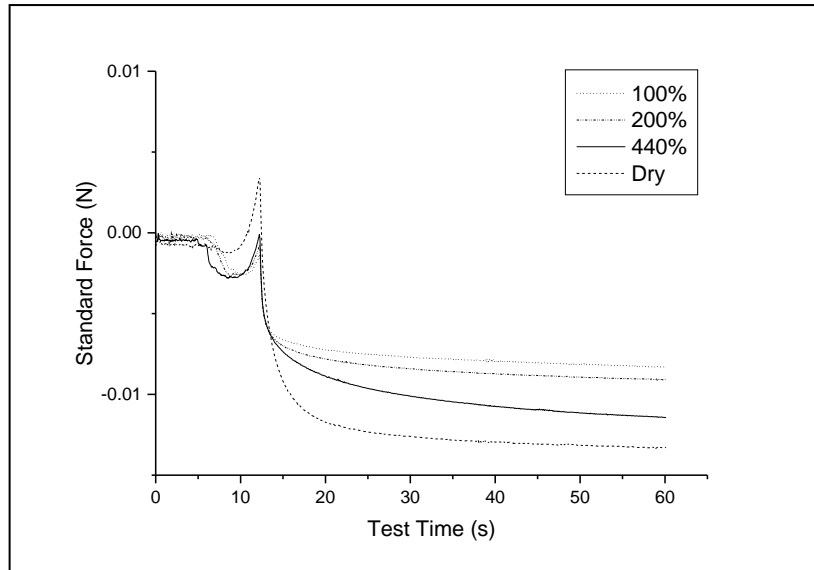


Figure 5.12: Average BM slurry absorption force curves for each of the lotion loaded samples

#### 5.4.2.1 At the Point of Contact

Figure 5.13 shows the box chart comparison of the absorption curves' slope at the point of contact for the four samples.

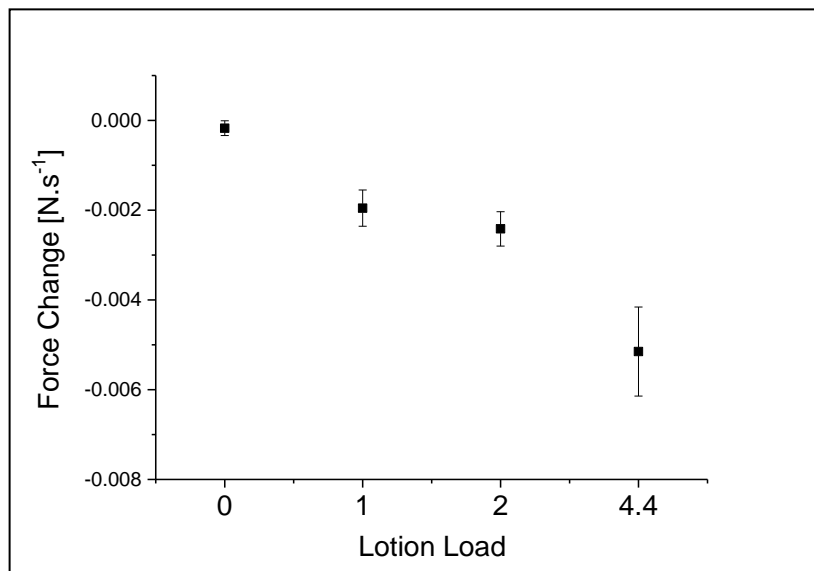


Figure 5.13: Comparison of the mean slopes of the absorption curves of the dry and different lotion load samples at the point of contact. Shown are lotion loads 0%, 100%, 200% and 440% respectively

The average force gradients (slopes) for each of the fabrics were statistically analysed (Figure 5.14).

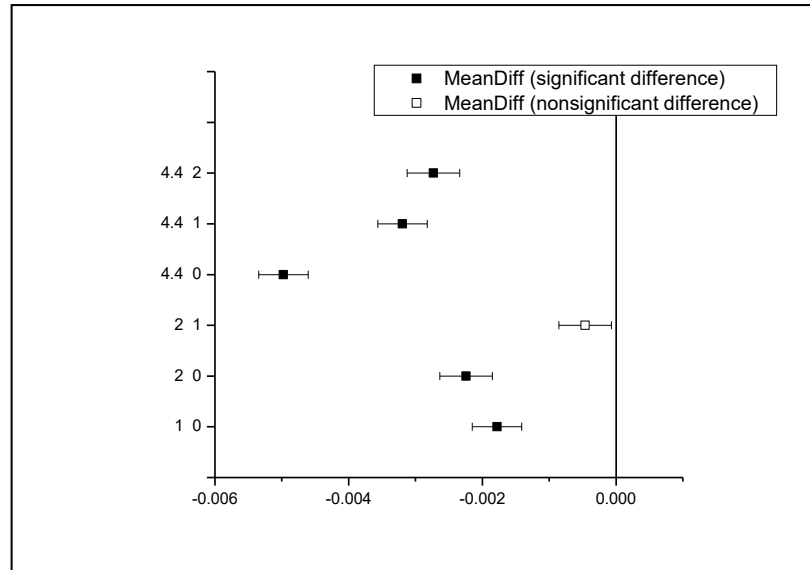


Figure 5.14: Tukey ANOVA for the slopes of the absorption force curves at the point of contact for samples with different lotion loadings. On the vertical axis, the pairs of samples are shown. 0 represents the dry sample, 1 represents the 100% lotion load, 2 for 200% and 4.4 for 440%.

Significant differences were observed between the samples, except between the 100% and 200% lotion loaded samples. Differences in the rates of BM slurry absorption (gradients at the point of contact) were not statistically significant at the 95% confidence level.

#### 5.4.2.2 **Peak Force**

Figure 5.15 shows the average peak force measurements for each of the samples and Figure 5.16 summarises the statistical analysis. Comparison of the peak force measurements for each pair of samples resulted in significant differences between the dry sample and all the wet (lotion-loaded) samples ( $P=95\%$ ). The differences between the peak force measurements and all other pairs were not statistically significant at the 95% confidence level. The dry sample showed a higher peak force than the wet samples. This agrees with the explanation in section 5.3.2, in the absence of lotion the fabric's wetting property is poor, therefore, as the dry sample approaches the BM slurry droplet and the plastic plate, BM slurry deforms into a flatter shape. This deformation explains the relatively higher peak in the measured force compared to the wet samples.

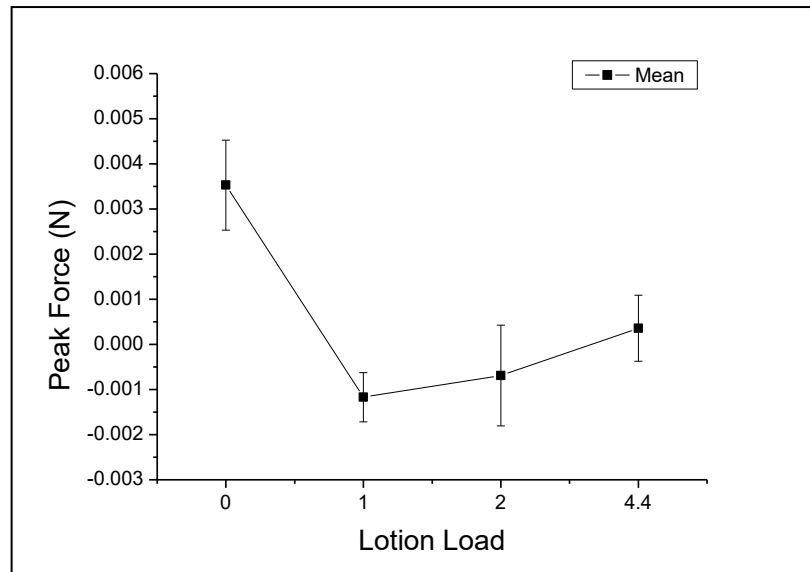


Figure 5.15: Average peak force measurements for the samples with different lotion loading. On the horizontal axis, the samples are represented by numbers. 0 represents the dry sample, 1 represents the 100% lotion load, 2 for 200% and 4.4 for 440%.

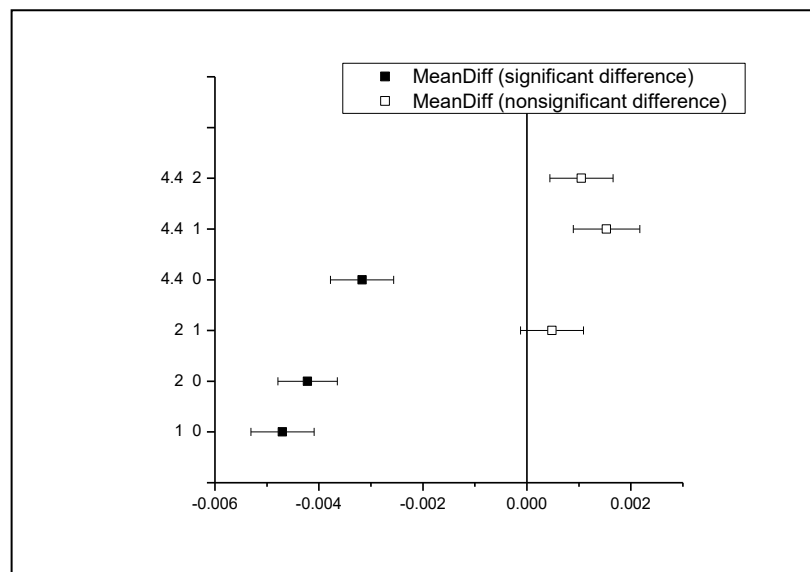


Figure 5.16: Tukey ANOVA for the peak force measurements for the samples with different lotion loadings. On the vertical axis, the pairs of samples are shown. 0 represents the dry sample, 1 represents the 100% lotion load, 2 for 200% and 4.4 for 440%.

#### 5.4.2.3 BM Slurry Absorption Force after 60 Seconds

Figure 5.17 shows the average force measurements at  $t = 60$  s for each of the samples and the statistical analysis is summarised in Figure 5.18.

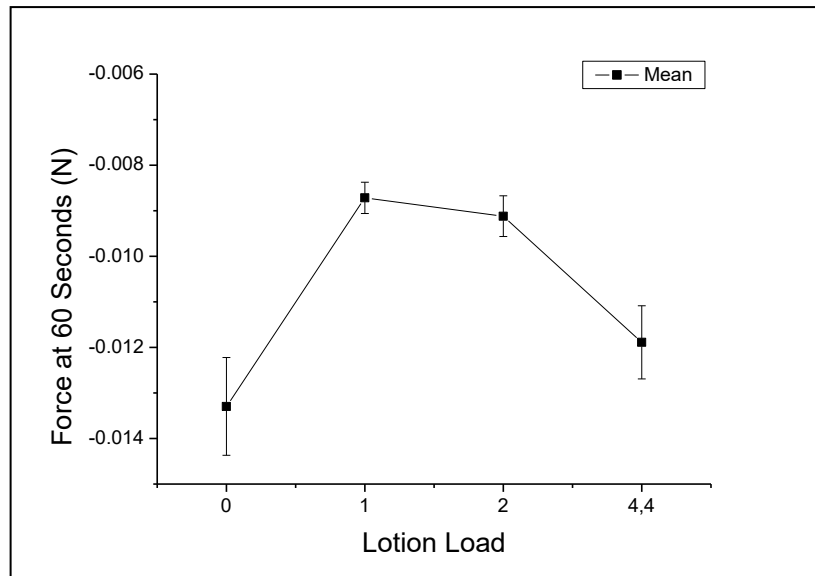


Figure 5.17: Average absorption force measurements at  $t = 60$  s for the samples with different lotion loadings. On the horizontal axis, the samples are represented by numbers. 0 represents the dry sample, 1 represents the 100% lotion load, 2 for 200% and 4.4 for 440%.

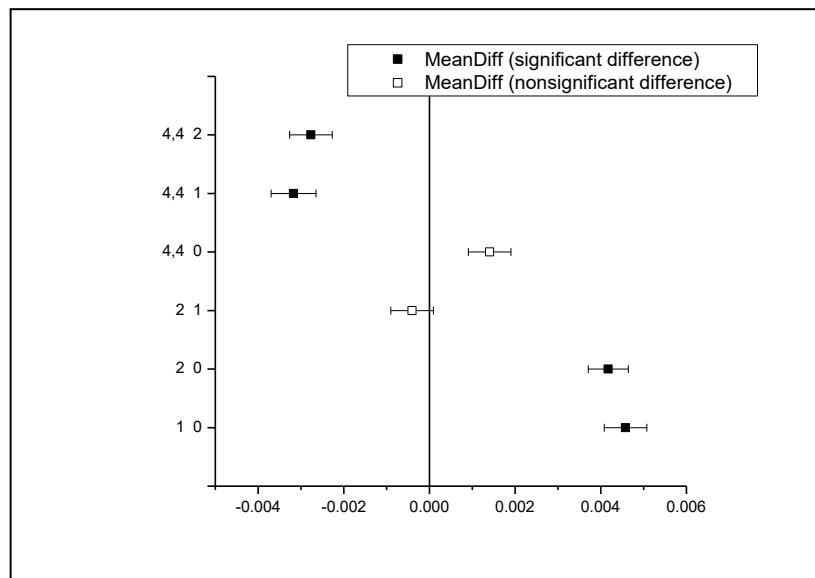


Figure 5.18: Tukey ANOVA for the force measurements at  $t = 60$  s for the samples with different lotion loadings. On the vertical axis, the pairs of samples are shown. 0 represents the dry sample, 1 represents the 100% lotion load, 2 for 200% and 4.4 for 440%.

Comparison of the force measurement at  $t = 60$  s for each pair of samples resulted in significant differences ( $P=95\%$ ) between the samples except between the dry and 440% lotion loaded samples as well as between the

100% and 200% lotion loaded samples. The differences between the two aforementioned pairs were not statistically significant at the 95% confidence level.

Collectively, it is apparent from these data that the presence of lotion in the fabric resulted in a significant increases in the rate of BM slurry absorption upon contact with the slurry as shown in Figure 5.13 and Figure 5.14. This is consistent with the explanation that the wetting process is improved by pre-moistening the fabric with lotion. The same is also evident in the peak force measurements, Figure 5.15 and Figure 5.16, where peak force measured with the dry fabric is significantly higher than that of the wet samples. The peak force measurement also shows a trend of increasing force with increasing lotion loading, which is consistent with the hypothesis that the presence of lotion initially resists BM slurry inlet. However, the statistical analysis did not confirm that this is a significant effect.

Over the longer term,  $t = 60 s$ , the force measurements decreased as the lotion load increased up to 200%. This could be explained by the lotion taking up a proportion of the pore volume, which increasingly resists the inlet of BM slurry. This is not the case at a lotion load of 440%, however. The difference in force measurements between the dry sample and the 440% lotion load sample is not significant, which confirms the earlier finding in section 0. A possible explanation is that the amount of lotion influences the rheology of the BM slurry as it mixes on contact, particularly its viscosity. Since the lotion's viscosity is much lower than the slurry's, the higher the lotion loading, the lower the resulting BM slurry viscosity is likely to be. By definition, this should allow for more slurry flow into the fabric under capillary forces, as viscosity is related to a fluid's resistance to flow (Barnes et al., 1989). Accordingly, the hypothetical influence of these two competing aspects i.e. the resistance to inlet and the resistance to flow on the measured force at  $t = 60 s$  can be illustrated in Figure 5.19.

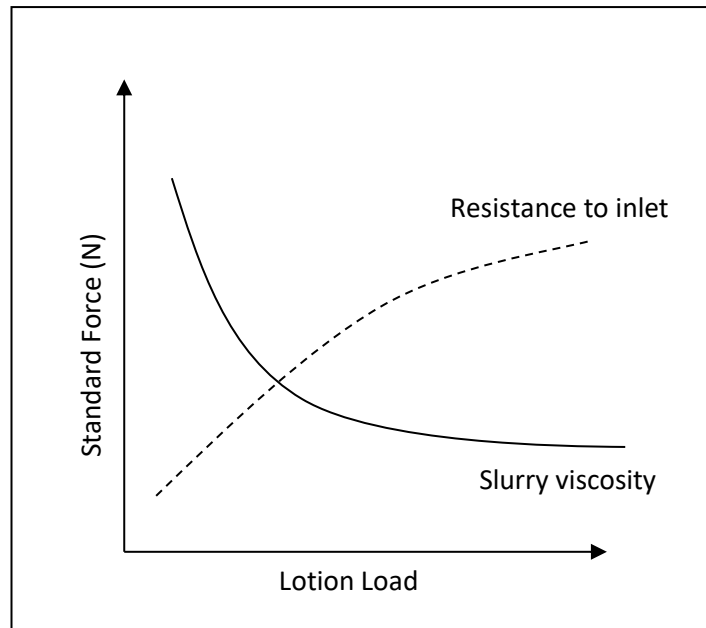


*Figure 5.19: The hypothetical influence of lotion load on the measured force at  $t = 60$  s. The continuous line represents the resistance due to slurry's viscosity and the dashed line represents the resistance to inlet.*

## 5.5 Summary

This chapter addressed the presence of lotion loading on the wipe substrates and how it influences their BM slurry absorption behaviour. In real wipes lotion loading is of the order of  $\sim 440\%$ , which means a large proportion of the available volume in the fabric for BM slurry absorption is already filled with fluid at the point of contact. However, over short wiping durations of just a few seconds, this was not found to impede the BM slurry absorption behaviour of the fabric. Additionally, the influence of the relative amount of lotion in the wipe on its absorption behaviour was investigated. It is evident from these experiments that the lotion plays a crucial role in assisting wetting at the point of contact between the fabric and BM slurry, promoting rapid BM slurry absorption, which is a critical requirement in real baby wipe usage.

There are two influences that the lotion has on the BM slurry absorption. The positive influence is improving wetting and allowing BM slurry to be absorbed faster. The negative influence is that lotion occupies a large proportion of the available volume in the fabric. These two conflicting influences suggest that there is an optimum level of lotion loading at which the negative influence is

minimised and the positive influence is maximised. Although the results suggested that the optimum lotion loading lies between 100 % and 200 %, more tests are required to achieve a statistical significance before this can be concluded.

# **CHAPTER 6**

## **Effect of Surface Features on BM Slurry Removal**

### **6.1 Materials and Methodology**

The Dynamic Cleaning method (DCM) was originally designed to simulate wiping by consumers using baby wipe products and was utilised in these experiments to determine wiping performance. The design and operation of the DCM instrument, including the experimental procedure used herein, was explained in section 2.4.2. To utilise this method it is necessary to apply a known volume of BM slurry on a support surface known as a skin mimic that simulates aspects of human skin. Details of this skin mimic surface are given in section 2.6. As in the wiping of normal skin, when the fabric is moved over the slurry a separation process takes place, wherein a proportion of the BM slurry is lifted from the surface. However, this may not necessarily equate to all of the slurry, but rather it may be just a proportion.

To better understand the cleaning process and dirt removal mechanisms in this work, the scale of dirt removal was classified into three categories, Figure 6.1. These categories are the bulk scale, the film scale and the sub-cellular scale.

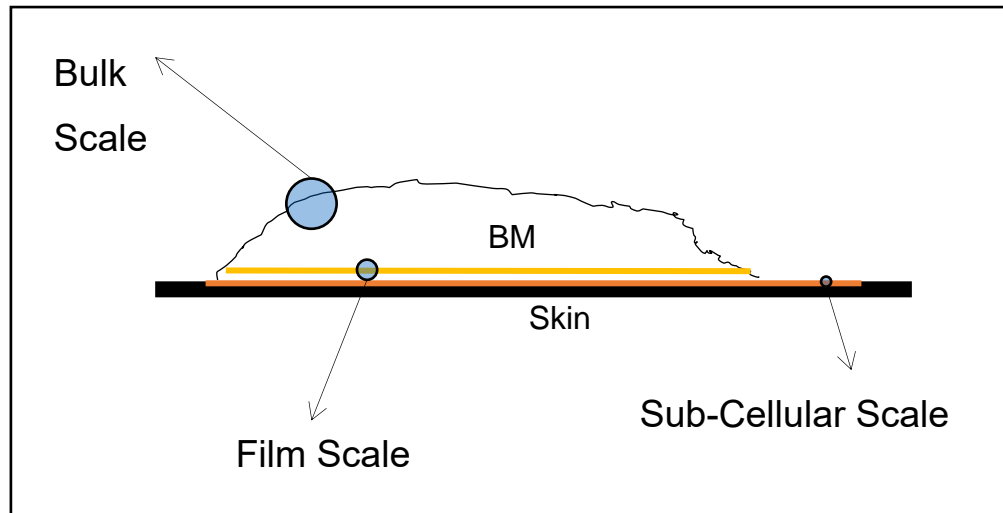


*Figure 6.1: Classification of the scales of BM removal from the skin surface*

Herein, bulk removal is defined as that part of the BM slurry that can be mechanically removed by the fabric. The bulk component is mainly attached to the film by cohesive forces and is not in direct contact with the skin.

The film is defined as the layer of BM slurry, which is attached to the skin by either mechanical or adhesive forces that are greater than the cohesive forces of the BM. Generally this layer has stronger attachment to the skin than to the bulk of BM above it.

The sub-cellular scale is defined as the very thin layer of cells or molecules that are in direct contact with the skin cells, bearing in mind the composition of bowel movement, explained in section 2.5. This layer can consist of bacteria, dead skin cells, mucus or sebum molecules or undigested baby food like cellulose. The thickness of this layer is dependent on the dimensions of its composition.

This scale classification is important because of its relevance to understanding the fundamental the role of lotion in baby wipe cleaning efficiency. In the presence of lotion, the contact area of a pre-moistened wet wipe with the skin will be larger than that of a solid-solid system, such as would exist between a dry fabric and the skin. This might suggest that a fabric-lotion system will clean more efficiently at the scale where dirt is in direct contact with the skin, namely the film scale.

To elucidate the extent to which structural features effect the cleaning at various scales, specifically the bulk and film layers, experimental work was conducted.

### **6.1.1 Area and Shape of the BM Slurry Smudge**

In previous experiments the removal of a discrete droplet of BM slurry has been considered, however, in reality, the BM slurry may be spread over the skin surface to form what can be referred to as a 'smudge'. This is typically characterised as a relatively thin layer of contamination that extends over a relatively large area. This smudge can be replicated on the test surface of the DCM instrument by coating a known volume of BM slurry over a fixed area.

To define the area and shape of the BM smudge several aspects were considered. The area must be large enough to cover the topographic and geometric features of the artificial skin surface and be within the dimensions of the contacting wipe sample. It must also conform, size wise, with the real wiping process so that it is relevant in size. The average hand width is known to be ~ 74 mm for females and ~ 84 mm for males, with lengths of ~ 172 mm and ~189 mm respectively (TheAverageBody.com, 2012).

The shape of the smudge was selected by considering the wiping motion of the DCM and the homogeneity of the applied BM. The design of the DCM with a cylinder that rotates around an axis perpendicular to its linear movement suggested that the BM smudge should be in the form of a right-angle quadrilateral. Given that wiping can in practice take place in all direction, an equilateral smudge area may be considered most appropriate. The selected shape for the BM smudge is chosen to be a five-centimetre-sided quadrant.

### **6.1.2 Formation of the BM Slurry Smudge for DCM Measurements**

In the normal operation of the DCM method, the BM slurry is usually applied to the skin substitute surface, manually using a syringe. However a reproducible method was needed to form a BM slurry smudge on the surface prior to DCM measurements. To this end, a K Control Coater (Figure 6.2) was employed to produce BM smudges in a variety of thicknesses and evaluate

the degree of variation in the resulting coating layer. This device uses pre-cut k-bars of known depth dimensions or a continuous blade to spread the coating formulation, in this case BM slurry, over the required contact surface to make a thin film of predictable dimensions.



*Figure 6.2: K Control Coater device. Courtesy of RK PrintCoat Instruments Ltd.*

The rectangular shape of the BM smudge was achieved by cutting stencils made of polyester films provided by HiFi Industrial Film Ltd. These films also contributed to determining the smudge thickness, as sample films provided had defined thicknesses of 23  $\mu\text{m}$ , 100  $\mu\text{m}$  and 350  $\mu\text{m}$ . By cutting rectangular shapes in them, gaps of the aforementioned thicknesses were formed. Additional thickness of 100  $\mu\text{m}$  was often added to the gap by adjusting the blade height on the coater to avoid obstruction when its blade passed over the stencil edges. The setup before loading the BM slurry is shown in Figure 6.3.

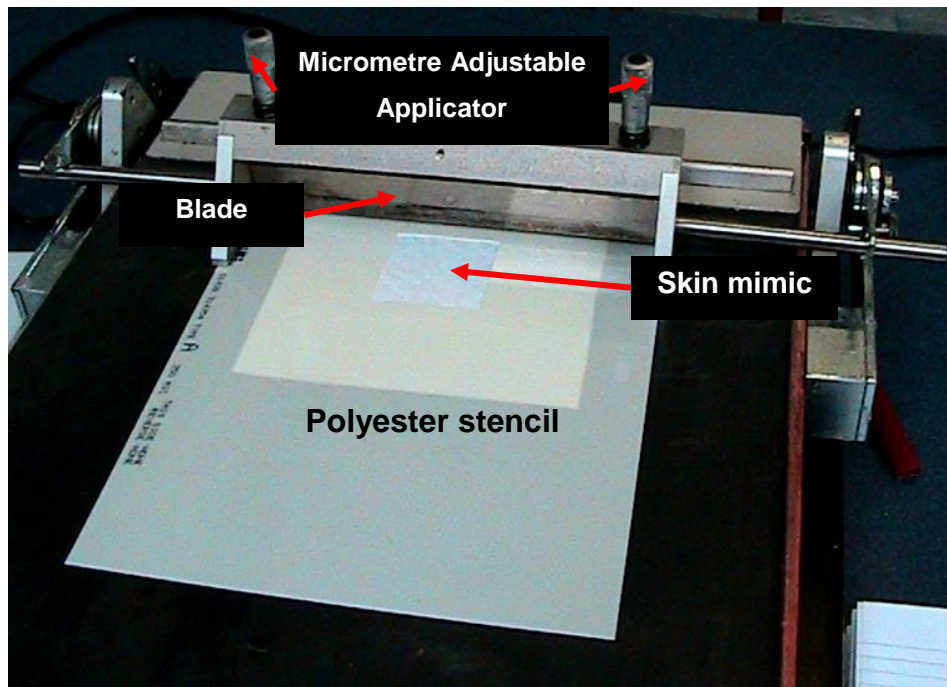


*Figure 6.3: BM smudge formation apparatus*

Samples were loaded with a fixed volume of BM slurry using this method for each of the gap settings on the apparatus of 123  $\mu\text{m}$ , 200  $\mu\text{m}$  and 450  $\mu\text{m}$ , Figure 6.4 shows a snapshot of the BM apparatus in operation. Ten replicates were made and the weight of the artificial skin surface (the skin mimic) sample was measured before and after the BM slurry application to assess the smudge weight variation.

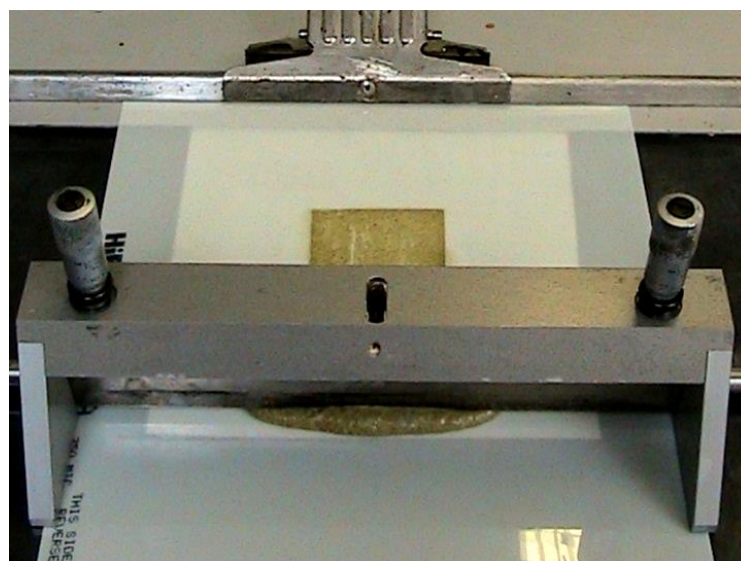


*Figure 6.4: BM application apparatus in action*

### 6.1.2.1 *Results and Discussion*

The BM slurry laydown weights corresponded to the nominal gap settings of 123  $\mu\text{m}$ , 200  $\mu\text{m}$  and 450  $\mu\text{m}$ . Figure 6.5 shows optical microscope images of the resulting BM slurry smudges on the skin mimic surface for each of the nominal gap settings applied. Figure 6.6 shows overview images of the same smudges.

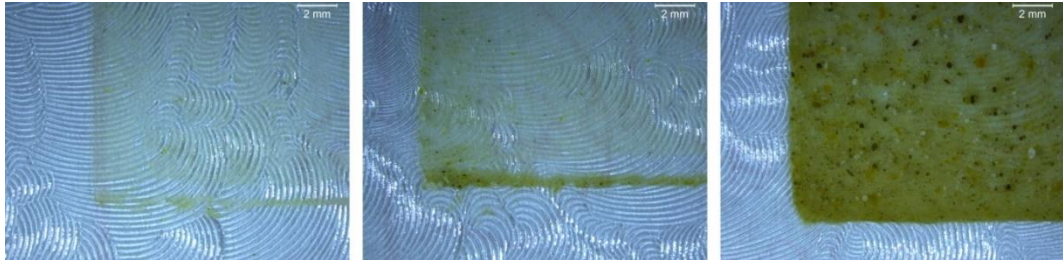


*Figure 6.5: Microscopic images of the BM smudge lower left corner for the nominal thicknesses of 123  $\mu\text{m}$  (left), 200  $\mu\text{m}$  (middle) and 450  $\mu\text{m}$  (right). (reflected light, bright field)*



*Figure 6.6: Macroscopic images of the BM smudge for the nominal thicknesses of 123  $\mu\text{m}$  (left), 200  $\mu\text{m}$  (middle) and 450  $\mu\text{m}$  (right)*

The BM slurry smudges produced with gap settings of 123  $\mu\text{m}$ , 200  $\mu\text{m}$  and 450  $\mu\text{m}$  during k-bar coating produced coating weights proportional to the gap setting. Theoretically the correlation between the BM slurry smudge thickness and its weight can be expected to be linear, as represented in equation 6.1.

$$w = g \cdot \rho \cdot A \cdot h \quad 6.1$$

Where,

$w$ : BM weight

$g$ : gravity acceleration constant

$\rho$ : BM density  
A: BM smudge area  
h: BM smudge thickness

Equation 6.1 expresses the BM smudge weight as a function of the BM smudge thickness. When considering the acceleration of gravity, the BM smudge area and its density as constants, the relation between the weight and the thickness becomes linear.

A linear fit between BM thickness versus weight was observed ( $R^2 = 0.828$ ) as shown in Figure 6.7. The deviation from a linear fit, may be explained by a change in the BM slurry density as the smudge thickness decreases because of agglomeration of the solid particles in the slurry. Referring to equation 6.1, the BM weight (w) is a function of two variables, the BM thickness (h) and its density ( $\rho$ ), and therefore, the relationship between (w) and (h) would differ. Despite the slight variation, the smudge weights were all statistically significant different (P=95%), with a coefficient of variation ranging between 7-10%. Thus, this approach was pursued in the formation of BM slurry smudges for DCM measurements.

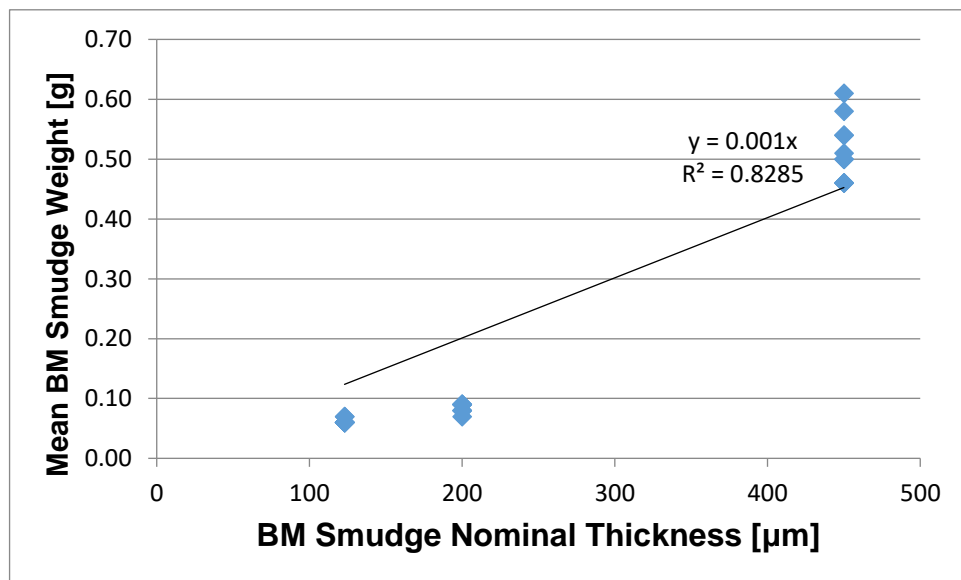


Figure 6.7: Linear fit of data points for BM smudge nominal thickness versus mean BM slurry smudge weight

### **6.1.3 BM Smudge Thickness for the Film Removal Scale**

It may be expected that lotion-loaded wipe substrates could be more effective at removing both the bulk and the film layer BM slurry contamination. A comparison of the cleaning efficiency of lotion-loaded and dry wipe substrates was therefore conducted using the skin mimic surface on the DCM instrument.

#### **6.1.3.1 *Materials and Methods***

A 5 cm square BM slurry smudge was applied to the skin mimic for each sample. Particles used to make the BM powder were pre-sieved to ensure the maximum particle diameter did not exceed 300  $\mu\text{m}$ , this ensured that thin films could be cast without disrupting the basic composition of the BM slurry during the smudge casting process. The gap setting on the k-bar knife coating apparatus was set to 350  $\mu\text{m}$ . The dry wipes samples were cut from the hydroentangled substrate described in section 3.1, with a basis weight of (56  $\text{g}\cdot\text{m}^{-2}$ ). The lotion composition and method of preparation and the lotion loading are summarised in section 3.3. Ten replicates were made for each sample, and measurements were made for both dry and lotion loaded samples. The settings used on the DCM and the procedure for loading the fabric samples and performing the wipe cycle are fully reported in section 2.4.2. After the wiping cycle on the DCM that BM slurry residues on the skin mimic surface were weighed and examined using optical microscopy to determine the approximate BM slurry film thickness.

#### **6.1.3.2 *Results and Discussion***

The results of the BM thickness optimisation experiments are given in the form of macro- and microscopic images of the BM residue on the skin mimic sample after wiping, in addition to the images of the contaminated wipes (both dry and with lotion-loading). Figure 6.8 shows the dry wipe and wet (lotion-loaded) wipe after wiping using the DCM, and Figure 6.9 shows the corresponding skin mimic samples with BM residues.

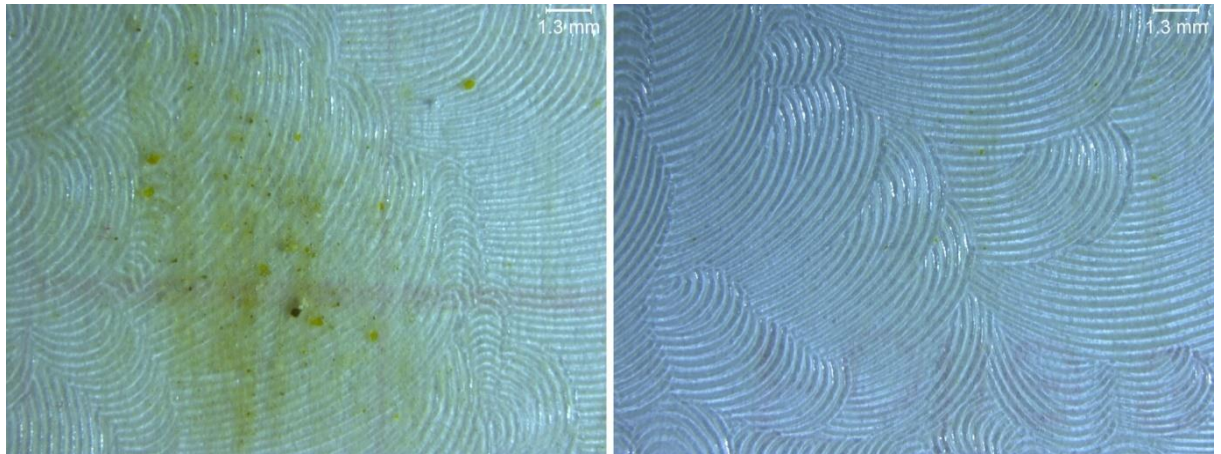


*Figure 6.8: Macroscopic images of the contaminated dry wipe surface (left) and the contaminated wet wipe surface (lotion loading 440%) (right).*



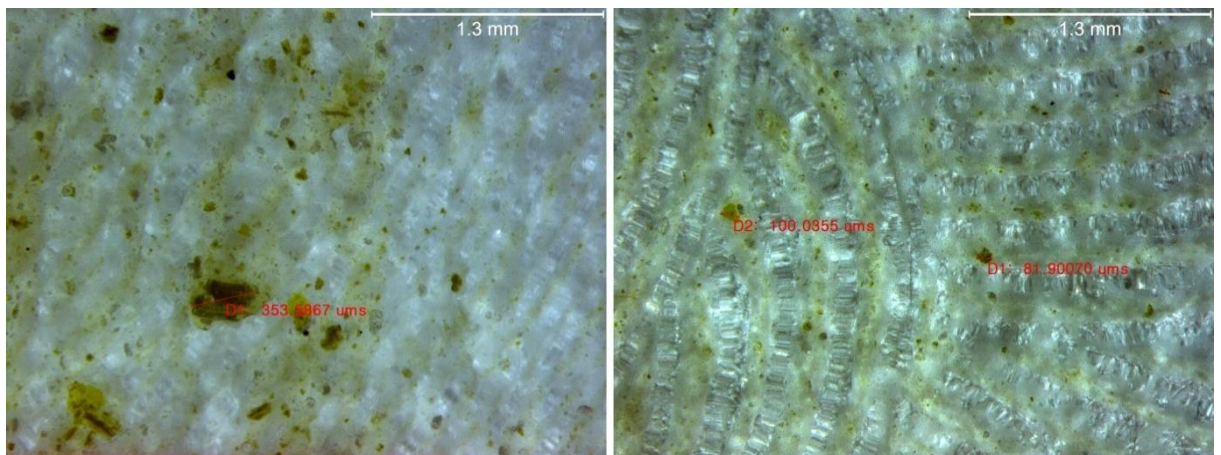
*Figure 6.9: Macroscopic images of the dry-wiped skin mimic surface (left) and the wet-wiped skin mimic surfac (lotion loading 440%) (right)*

Figure 6.10 shows microscopic images of a the skin mimic surface after being wiped with a dry wipe and a skin mimic sample after being wiped with an identical fabric loaded with 440% of lotion.



*Figure 6.10: Microscopic images of the dry-wiped skin mimic sample (left) and wet-wiped skin mimic sample (lotion loading 440%) (right) (reflected light, bright field)*

Figure 6.11 shows measured diameters of large particles left on the wiped skin mimic surface after wiping with dry and wet wipes respectively. For dry wiping conditions particles were  $\sim 354 \mu\text{m}$  in diameter, but in wet wiping conditions, this decreased to  $82 \mu\text{m}$ - $100 \mu\text{m}$ .



*Figure 6.11: Microscopic images of the wiped skin mimic samples (left: dry, right: wet 440%) showing dimension measurements of contaminant particles (reflected light, bright field)*

It is apparent from the microscopic images of the dry- and wet-wiped samples that there is a difference in the wiping efficiency, and for wet wiping conditions there is greater evidence of that the film layer is disrupted and separated, as compared to dry wiping. One indication is the area covered by the BM residues, where under sufficient magnification (Figure 6.11) it can be

observed that on the wet-wiped sample the BM resides almost entirely within the grooves of the skin mimic surface. By comparison, in dry wiping conditions, BM residue is present both within and above the grooves, such that the skin mimic texture is more difficult to discern. In short, less BM is removed during dry wiping and a thicker layer resides on the skin mimic surface after wiping. The greater residual particle size in the BM (Figure 6.11) after dry wiping on the skin mimic surface is a further indication of poorer wiping efficiency.

These findings are supported by the gravimetric assessment of the fabric samples after wiping. The weight of the skin mimic sample after being wiped with the dry sample is of relevance here as it is assumed that BM film (definition of BM film in section 6.1.3 is left on the skin mimic after wiping with a dry wipe. To calculate the film thickness, the weight measurement of the remaining BM on the dry-wiped sample was plotted along with the data points shown in Figure 6.7 and the linear fit function was then extrapolated. Using the linear fit function formula also shown in Figure 6.7, this thickness can be also calculated (equation 6.2):

$$y = 0.001x \quad 6.2$$

Where (y) represents the weight of BM in grams and (x) represents the BM layer thickness in micrometres. Putting the observed weight of the BM remains after dry-wiping, which is roughly 0.03 g, in the equation calculates a thickness of 30  $\mu\text{m}$ . This thickness obviously does not correspond with the BM particle size measured on dry-wiped samples. Figure 6.9 shows that BM residues are not homogeneously distributed on the sample area. The two indications of particle size and BM distribution suggest that this approach might be of less accuracy for the purpose of identifying the BM film removal scale. Consequently, the BM smudge thickness of 350  $\mu\text{m}$  is adopted which fulfils the third objective of the dynamic cleaning method development as mentioned in 6.1.3.

## 6.2 Influence of Fabric Surface Texture on Dynamic Wiping Efficiency

This section considers the influence of fabric structure on the removal efficiency of BM slurry using the DCM method, wherein the hydroentangled fabric structure was modified during manufacture.

### 6.2.1 Fabric Manufacture

For the experimental work presented in this section, the fabrics used were made as explained in section 3.1, with differences in their texture being introduced in-line during the hydroentangling process by modifying the design of the conveyor belt. This method was chosen for two reasons. Firstly, the resulting fabrics were compositionally and dimensionally identical to those previously discussed, as well as the control sample.

#### 6.2.1.1 *Results and Discussion*

The resulting fabrics had different topographical features as shown in Figure 6.12, Figure 6.13 and Figure 6.14.



*Figure 6.12: Plain prototype fabric (Control)*

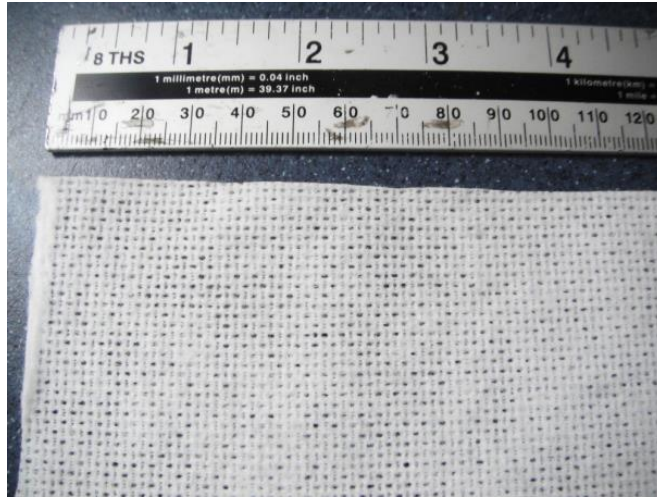


Figure 6.13: Prototype fabric with apertures



Figure 6.14: Prototype fabric with corrugation

After weighing the fabric sheets and measuring their dimensions, the resulting basis weight was calculated and the results are shown in Table 9.

	Length [m]	Width [m]	Area [m <sup>2</sup> ]	Weight [g]	Basis Weight [g.m <sup>-2</sup> ]	Average BW
Aperture	0.30	0.22	0.07	3.60	54.55	49.63
	0.30	0.22	0.07	3.31	50.15	
	0.30	0.22	0.07	3.16	47.88	
	0.30	0.23	0.07	3.17	45.94	
Corr.	0.23	0.23	0.05	2.15	40.64	44.13
	0.31	0.23	0.07	3.33	46.70	
	0.30	0.26	0.08	3.52	45.13	
	0.30	0.23	0.07	3.04	44.06	

Table 9: Basis weights of the experimental fabrics

The fabrics had distinctly different structures but were compositionally identical. The resulting basis weights were slightly lower than the desired value of  $56 \text{ g.m}^{-2}$ , but this was an expected consequence of the hydroentanglement process.

The amount of fabrics produced for this experiment was limited by the availability of raw material. Therefore, 7 repetitions of each sample were tested.

### **6.2.2 Assessment of Wiping Efficiency using the DCM**

To determine the extent to which the structural differences introduced in the four fabric samples (including the unstructured control) affected the dynamic wiping efficiency, DCM testing was carried out, using the BM slurry smudge and the skin mimic surface.

In the DCM test, a single wipe cycle was employed for each BM slurry sample. Each test was replicated seven times for each sample. The wiping linear velocity was  $10 \text{ cm.s}^{-1}$  and the wiping rotational velocity was  $10 \text{ cm.s}^{-1}$ , with a wiping pressure of 13.8 kPa. The wiping parameters were chosen according to the method explained in sections 2.4.1 and 6.1.

A batch of 65% water content BM was used. BM slurry was prepared using the method described in section 2.5.3. A square of  $25 \text{ cm}^2$  of BM slurry was applied to the skin mimic with a nominal thickness of  $350 \mu\text{m}$  using the coating method developed in section 6.1. This thickness was chosen because it was concluded in section 6.1.3 that it is the thickness of the film of BM that needs to be cleaned.

Wiping efficiency assessment involved analysing the post-wiping image of the residual BM on the skin mimic and wipe surfaces. This subtraction method is explained in section 3.4. Integrated density values (IDVs) were obtained from the fluorescence images of the wiped skin mimics and the wipe surfaces and the three fabric samples were compared.

Fluorescence images were taken for each specimen of the skin mimic wiped by the wipe specimens for each of the fabrics. The images were produced in greyscale, and an example is shown in Figure 6.15.

To identify the BM distribution pattern, a detailed analysis of the surfaces of the wipes and the skin mimics was carried out. The area of interest on each of the wipe and the skin mimic specimens was divided into 24 areas aligned in the wiping direction. These areas were rectangular and identical in size. Each of them covered the whole area of interest and was 5 mm wide as illustrated in Figure 6.16 for the skin mimic and Figure 6.17 for the wipe surface.

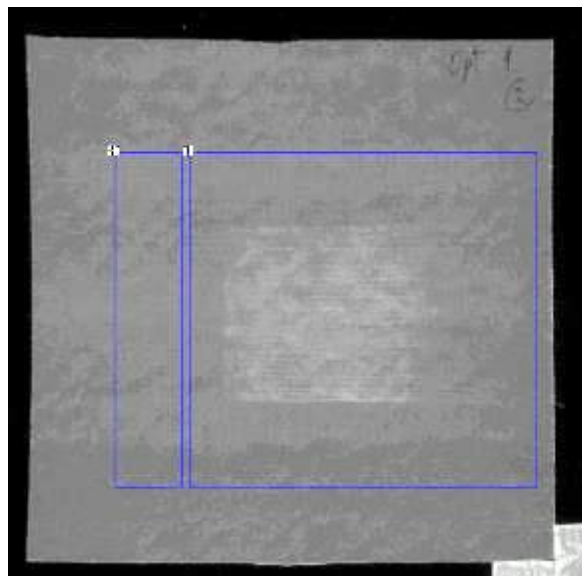


*Figure 6.15: Example of a greyscale image of a skin mimic with BM residues obtained using fluorescence imaging. The blue frames represent the areas of interest for IDV readings (left frame: background, right frame: object)*

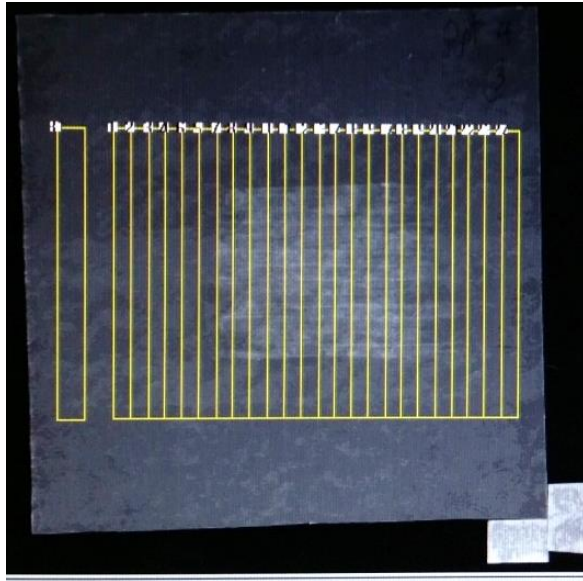


*Figure 6.16: Composite image layout of a skin mimic specimen using fluorescence imaging. 24 areas of interest and one background area*

The areas were defined by frames, which can be drawn using the image analysis tool “SpotDenso”. These frames were saved as a template and used to obtain IDVs for the images of the used wipes as well as the skin mimic samples for each of the three structured fabrics.

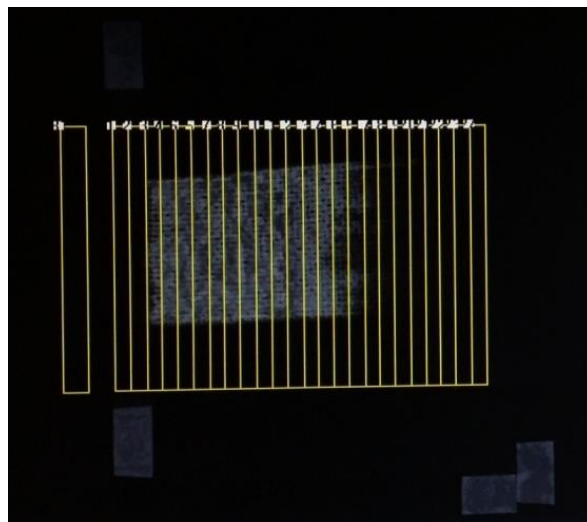


*Figure 6.17: Composite image layout of a used wipe sample. 24 areas of interest and one separate background area*

The BM slurry distribution on the wipe surfaces was found to be heterogeneous. Some areas of BM accumulation on the wipe were too thick to allow transmission of the fluorescent light. This prevented a representative

IDV reading with fluorescence imaging of such areas. To obtain more representative IDV readings, white light images of the wipes were taken using the same imaging system to be analysed in the same way. For the analysis, therefore, the same set of frames was used, this is shown in Figure 6.18. These images were in greyscale as well and thus the obtained IDVs from each of the constituent frames would express the intensity of white light in the areas surrounded by them. These IDVs represented the area covered with BM for each constituent frame.

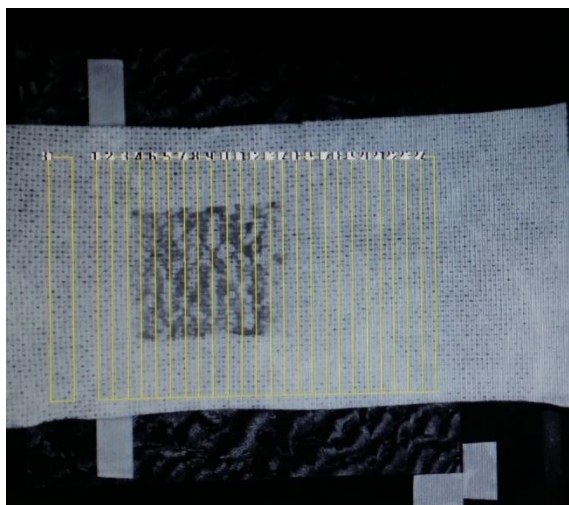


*Figure 6.18: Composite image layout of a wipe specimen using white light. 24 areas of interest and one background area*

To obtain more accurate data to characterise the area of BM slurry coverage, colour images of the same used wipes were taken. A light microscope was used for this purpose. The microscopic images were then transferred back to the imaging system to analyse for BM coverage based on colour contrast.

A new set of frames was made to analyse these images because they were obtained by a different imaging system, Figure 6.19. The new set of frames suited the dimensions and scale of these microscopic images better. The width of each of the constituent frames was kept at 5 mm.

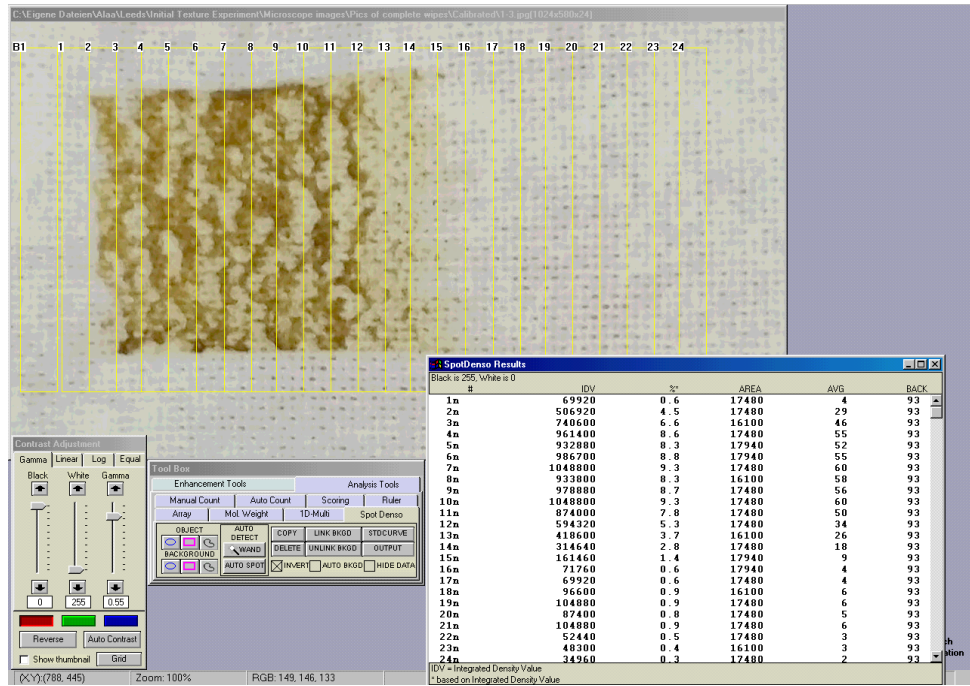


Figure 6.19: Composite image layout of a wipe specimen using light microscopy. 24 areas of interest and one background area

The IDVs obtained from each of the constituent areas in the composite images were plotted against the distance from where the measurement was taken<sup>1</sup>. This produced a curve that starts with the IDV reading at the leading edge and ends with the IDV reading at the trailing edge. This curve is referred to as the “cleaning profile curve”. For each fabric sample, eight samples were tested and similar curves were produced. Ultimately, the average curves were plotted for comparison.

In addition to the detailed quantitative evaluation of wiping efficiency using image processing, the used wipes were also examined under an optical microscope for qualitative evaluation. Evidence of structure-related wiping behaviour and distribution patterns of residual BM on both the skin mimic and the wipe were investigated.

<sup>1</sup> The point (0) on the distance axis was defined as the point of the start of the smudge of BM residing on the skin mimic or being picked up on the wipe. Two additional areas were set to measure IDVs before this point, therefore, the readings start from the point (-10) on the distance axis.

### 6.2.2.1 Results and Discussion

In relation to the quantitative assessment of wiping efficiency, the resulting IDVs for the complete area of interest are shown in Table 10.

Skin Mimic Sample	Integrated Density Values ( $\times 10^{-6}$ )		
	Aperture	Corrugation	Plain (control)
1	333.91	327.80	437.24
2	257.14	337.63	260.59
3	375.88	231.90	382.79
4	263.51	357.02	397.93
5	311.06	347.46	-
6	352.50	368.44	277.86
7	411.21	319.03	264.58
8	529.42	-	416.79
9	-	-	354.36
Mean	354.33	327.04	349.02
Standard Deviation	88.11	45.20	71.66
CV%	25%	14%	21%

*Table 10: IDV results of the processing of the fluorescence images of the skin mimic specimens for the three fabric samples. The missing data in the table are due to a fault in the test such as the slip of wipe on the cylinder which produced no results or unrealistic results*

A statistical analysis of variance (ANOVA) was performed to compare the means of the resulting IDVs. At a confidence level of 95%, the data did not show any significant differences between the three means, as shown in Figure 6.20 and Figure 6.21.

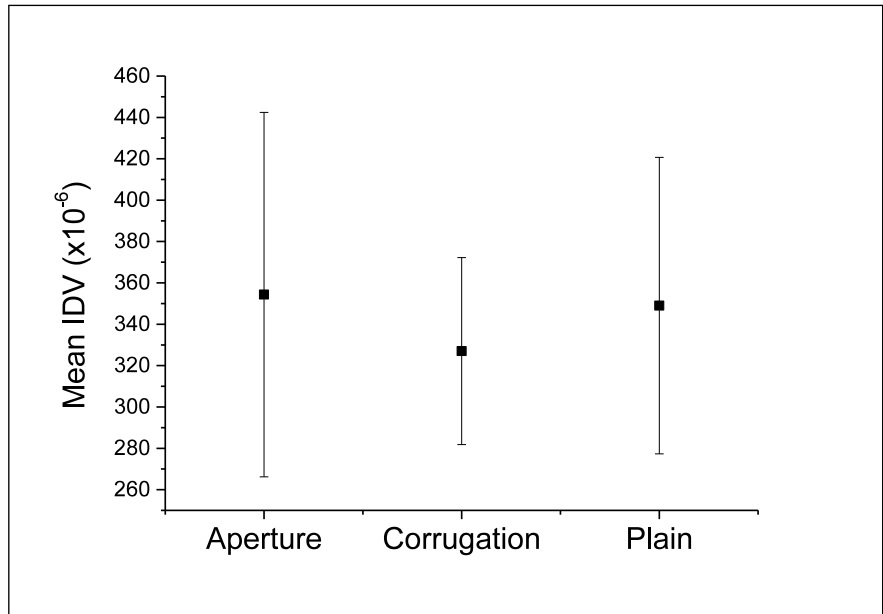


Figure 6.20: A graph of the mean IDVs for each of the three tested options

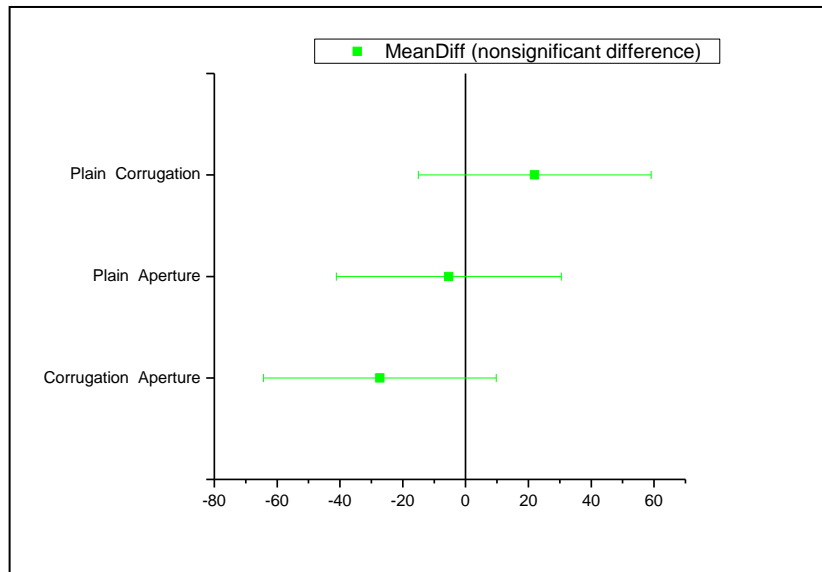


Figure 6.21: Statistical means comparison of the average IDVs of the three options

Fluorescence images of the skin mimic specimens were processed to read the IDV measurements. Average cleaning profile curves resulting from the skin mimic images for the three fabric types (aperture, corrugation and plain) are shown in Figure 6.22.

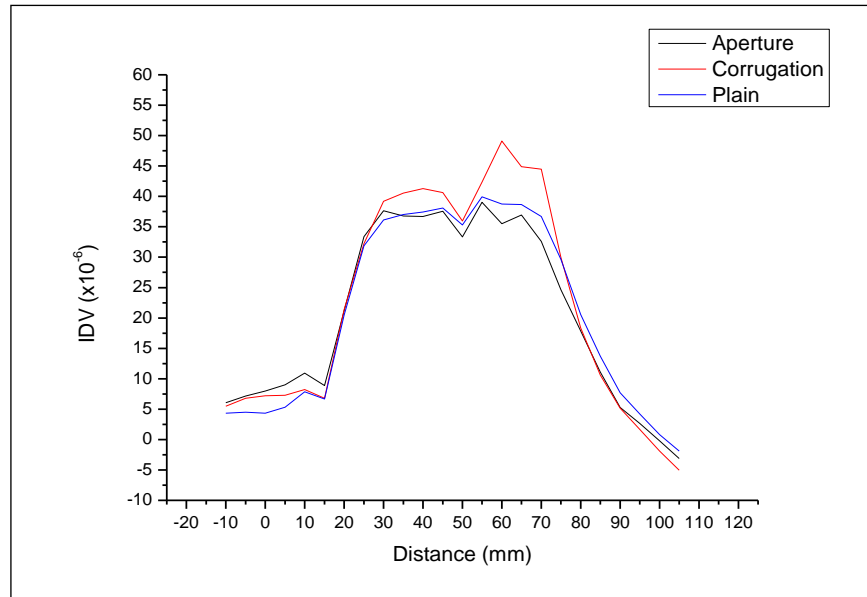


Figure 6.22: Average cleaning profile curves for the skin mimic samples wiped by the three texture options (fluorescence imaging)

Average cleaning profile curves resulting from the wipes fluorescence images for each of the fabrics are shown in Figure 6.23.

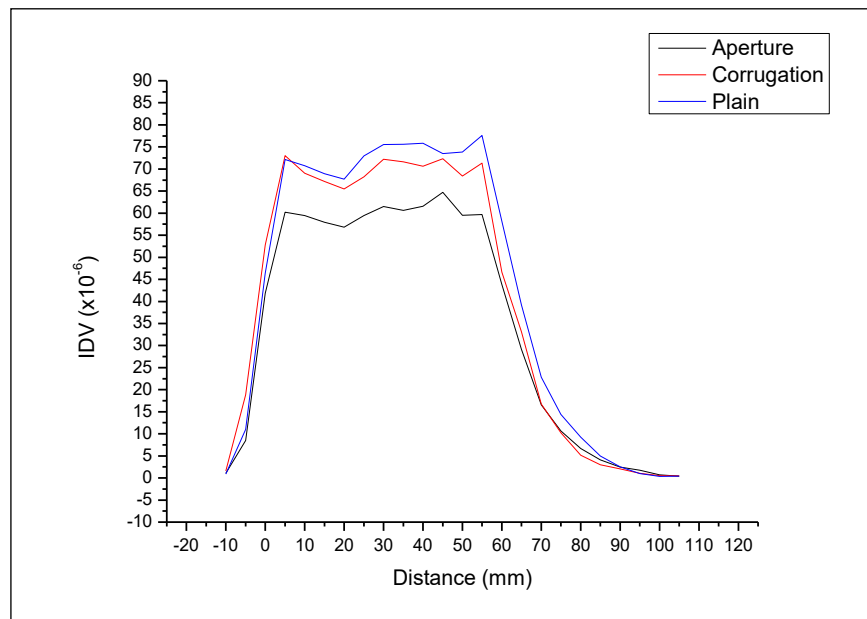


Figure 6.23: Average cleaning profile curves for the wipes samples for the three texture options (fluorescence imaging)

The resulting average cleaning profile curves of white light images for the three fabric samples are shown in Figure 6.24.

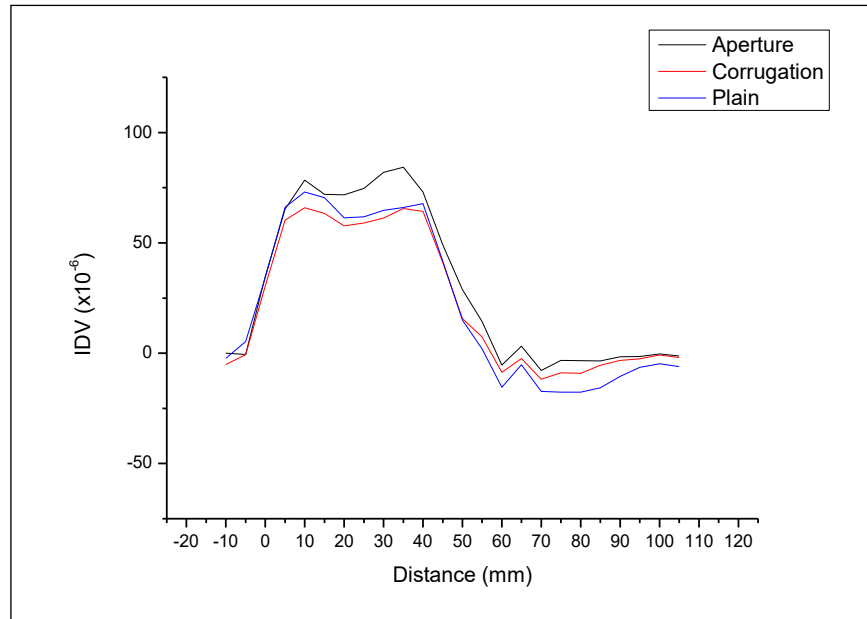


Figure 6.24: Average cleaning profile curves for the three fabric samples produced from images of the wipes samples taken under white light

Figure 6.25 shows the average cleaning profile curves resulting from analysing the microscopic images for each of the different fabric structures.

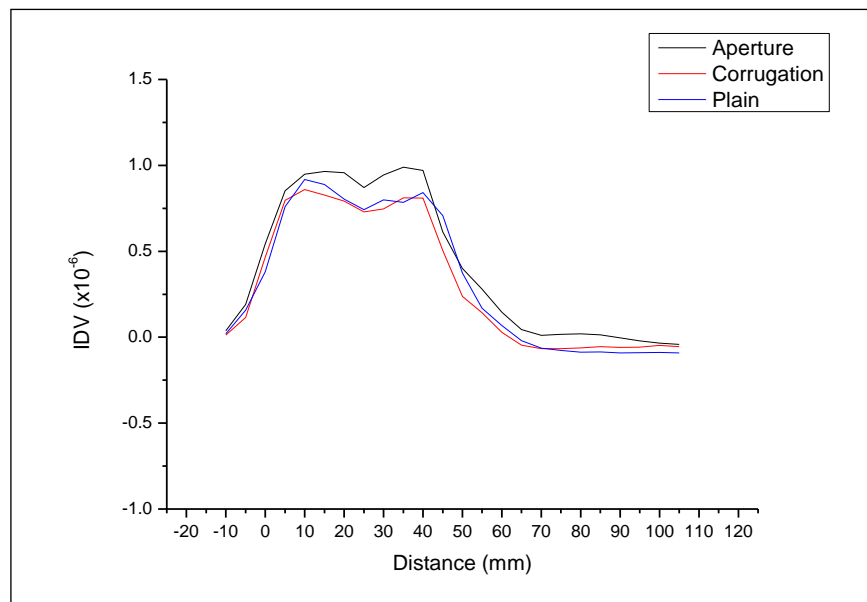
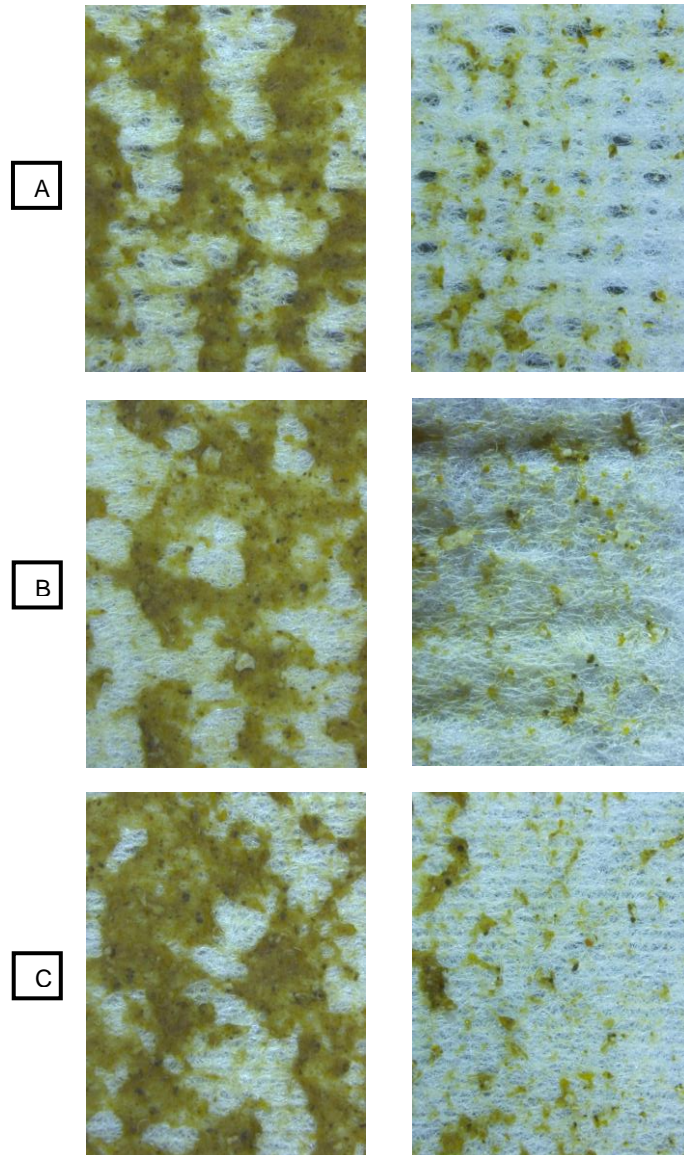


Figure 6.25: Average cleaning profile curves for the three fabric samples produced from coloured images of the wipes

### 6.2.2.1.1 Qualitative Evaluation of Wiping Efficiency

The BM slurry distribution on the wipe surface was not continuous. There were signs of BM smearing towards the trailing edge, Figure 6.26. The front line of

BM (at the leading edge) was not always completely covered with BM and did not start the same distance from the leading edge. The density of the BM slurry coverage of the wipe area increased gradually from the leading edge and then decreased towards the trailing edge.



*Figure 6.26: Coloured images of the wiper's surface after the DCM wipe cycle. The images on the left are areas of the wiper which fall at distances from the leading edge where the BM slurry distribution is homogeneous. The images on the right are areas of the wiper near the trailing edge where smearing occurs. A: apertured sample, B: corrugated sample, C: plain sample*

On the surface of the apertured fabric, some evidence of BM slurry penetration through the apertures was observed. The optical microscope images showed BM slurry penetration through low density surface features e.g. through the

apertures, Figure 6.27. BM slurry penetration through the fabric structure may be important for retaining the BM after its initial removal from the skin surface. The size, shape and arrangement of the apertures (or any other surface features) may therefore be expected to influence BM slurry penetration and are therefore factors to be considered in further investigation.

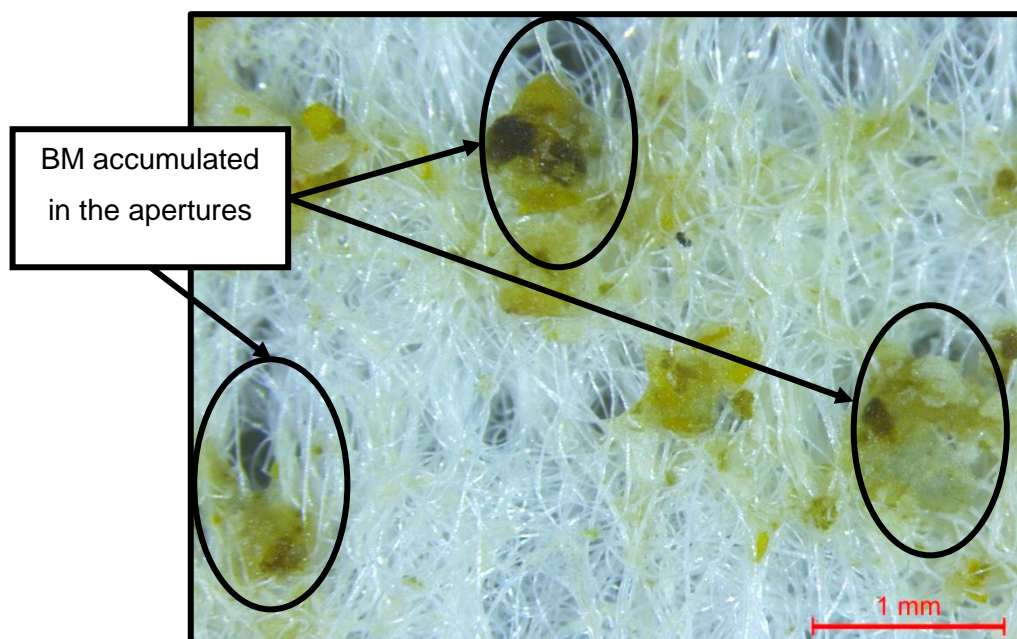


*Figure 6.27: BM accumulation in the apertures on the wipe's surface*

An examination of the overall shape and distribution of BM slurry on the wipe's surface demonstrated that the area covered by BM slurry was not continuous. A pattern in the BM distribution throughout the contact area of the wipe and a difference in the level of contamination, in the wiping direction, from the leading edge to the trailing edge was observed.

Based on an overall assessment of the fluorescence imaging data, as shown in Figure 6.15, a single dimensional value can be provided to characterise the general wiping efficiency. Composite fluorescence imaging evaluation gives a two-dimensional value which could be interpreted to understand BM distribution.

Due to the relatively thin film of BM residue on the skin mimic, this method could be used to give an approximate estimation of its quantity. However, quantifying BM pick up by the image processing of wipes might not be as

reliable compared to the skin mimics. This is due to the thickness of BM accumulated on the wipes surface or penetrated with their fibrous structure.

The overall evaluation of cleaning efficiency indicated by IDVs for the three fabric samples showed no significant differences at this scale.

In the composite image analysis, the IDV curves in the area between the leading and the trailing edges are relatively flat and this indicates a homogeneous BM distribution. Near the leading edge, the IDVs rise steeply. This point marks the distance at which the wipe meets the BM smudge. As the cleaning profile curves progress towards the trailing edge, the IDVs descend gradually, which suggests that BM was being removed gradually, which in turn suggests chances of smearing. The areas beyond 50 mm are areas which were clean before wiping. Therefore, any reading of IDVs would be due to smearing. The cleaning profile curves of the white light and coloured images of the wipes' surface, shown in Figure 6.24 and Figure 6.25, seemed to start the gradual descend before the end of the BM smudge, i.e. before the distance of 50 mm. This could be explained by the slight stretching and changing in wipes dimensions during wiping. When adopting this explanation, the cleaning profile curves of fluorescence images of wipes do not conform. This could be explained by the nature of the light used for detection of BM. It is suggested that amounts of BM at certain concentrations could only be visible via fluorescence imaging and not by visible light. This hypothesis could be investigated in future work.

The average cleaning profile curve produced from the fluorescence images of the wipes of the aperture fabric showed lower IDV at the curve's flat part than the plain fabric as shown in Figure 6.23. This suggests that the fluorescence is relatively lower in this area. Since the corresponding skin mimic results were not significant, the explanation could possibly be that more BM is penetrating the fabric through the structural features (apertures). Amounts of accumulated BM could become too thick for their fluorescence to penetrate through and reach the UV camera and therefore they become unquantifiable using this imaging technique.

The same effect is not apparent in the case of the corrugated fabric however. Structural features, such as apertures, tend to have sharper angles compared to corrugation. It is suggested that the sharper the surface features the greater their influence on BM distribution and subsequently on BM scooping and removal. This conclusion is in alignment with the theory explained in section 2.3.1. Two clues supporting this conclusion are the examination of BM distribution on the aperture wipes' surface, shown in Figure 6.27, and the statistical analysis comparing the cleaning profile curves which showed significance. The result an ANOVA at the 95% confidence level for each of the twenty-four constituent areas of interest for all specimens of the aperture option with their respective constituent areas of interest for the corrugated and plain fabrics showed that the IDV data of the aperture options differ significantly from the other two fabrics in the distance range 10-60 mm. This range is where BM distribution was considered homogeneous for all fabrics and appears on the cleaning profile curves as the flat part in Figure 6.23. This encouraged further research into the influence of the geometrical characteristics of structural features and their arrangements on the wiping efficiency. It must be noted that the IDV measurement was preferred over the gravimetric method because of the presence of liquids which would evaporate and cause inaccuracies in the measurements.

Under the conditions in which the fabrics were manufactured and the materials used, in addition to the testing conditions and methods used in this experiment, it could be concluded that the surface topography which was produced in the fabrics wipes did not influence the overall wiping performance. However, fabric structural features do appear to influence the distribution of BM on the wipe as well as the level of BM penetration through the fabric, and thus the fabric architecture and fibre arrangement are strongly suggested to be important factors. It is believed that introducing an arrangement of carefully designed structural features on the fabric surface could therefore influence the overall wiping performance.

The next section presents a fundamental approach to study the influence of structural features which have a specific geometrical design on the wiping efficiency.

## 6.3 Influence of Structural Geometric Surface Features on Wiping Efficiency

In the previous section, it was found that prominent structural features in the hydroentangled fabrics could influence wiping efficiency. This section considers how introducing specific structural features can influence wiping efficiency compared to a plain hydroentangled fabric.

### 6.3.1 Fabric Prototyping

The available technologies in nonwoven fabric manufacture are becoming increasingly capable of providing customised fibre arrangement and surface texture. The manufacturing technologies nowadays enable the production of fabrics with geometrical features that can be controlled to a certain accuracy. This experiment aims to explore the possibilities of manufacturing nonwoven fabrics with the structural features, illustrated in section 2.3.4, to investigate their influence on wiping efficiency.

The most convenient and available method of rapid prototyping was 3D printing. The array of shearing elements was given a thick body to support them, this formed the male plate of the mould. A female plate was then created using the same software. A rendered image of the female plate is shown in Figure 6.28.

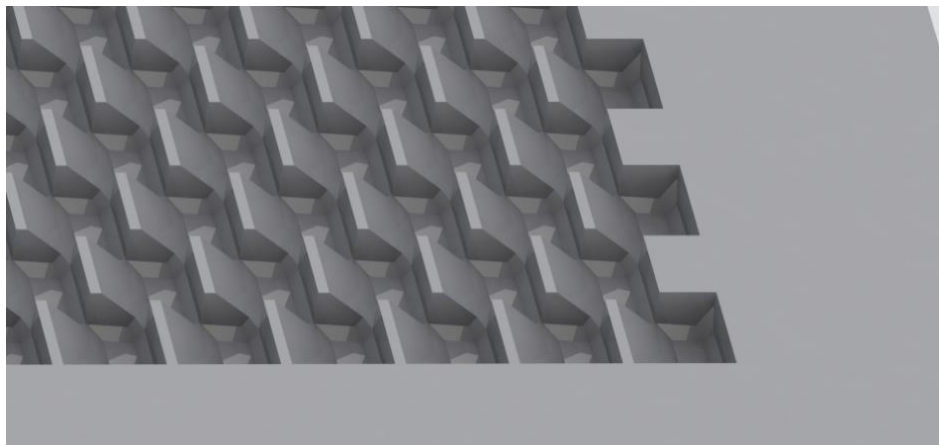


*Figure 6.28: 3D rendered image of the female mould plate*

The mould plates were then 3D printed and ready to be used to make fabric prototypes. The mould was used to compress the same hydroentangled fabrics prepared using the procedure in section 6.2.1.1 for the plain fabric. Pattern application used the equipment explained in section 4.5.2.2 and is illustrated in Figure 4.27. Suitable pressing and time parameters were then considered:

At a pressure of 12 tons for a duration of 30 min, the fabric was difficult to separate from the female part and contained holes. Also, it was hard to separate the mould pieces. The resulting fabric is shown in Figure 6.29.



*Figure 6.29: Resulting fabric from compression at 12 tons for the duration of 30 min*

Compression at 5 tons for a duration of 30 min made separation easier for the mould pieces and fabric. After mould separation, the fabric was left on the female part for 20 min and then peeled off. The resulting fabric was less damaged and the texture definition was excellent, Figure 6.30.



*Figure 6.30: Resulting fabric from compression at 5 tons for the duration of 30 min*

Compression at  $50 \text{ kg/cm}^2$  for a duration of 30 min: manual separation of mould pieces is possible and damage to fabric is minimised upon immediate separation from the female piece. Texture seems in good condition; however, it may be weaker than the other two compression settings, Figure 6.31.



*Figure 6.31: Resulting fabric from compression at  $50 \text{ kg/cm}^2$  for the duration of 30 min*

### 6.3.2 Assessment of Wiping Efficiency

The fabric prepared according to the design explained in section 2.3.4 had structural features that resembled shearing elements designed specifically for efficient removal of BM slurry and leaving a clean surface behind. The fabric was tested using the DCM and compared with the plain fabric of identical composition. The test parameters were: three swipes for each BM sample, 3 repetitions for each sample, wiping linear velocity: 10 cm.s<sup>-1</sup>, wiping rotational velocity: 10 cm.s<sup>-1</sup> and wiping pressure: 2 psi which is equal to 13.7895 kPa. The wiping parameters were chosen according to the method explained in section 6.1.

A batch of 65% water content BM was used, The BM slurry preparation procedure was the same as reported in section 2.5.3. A square of 25cm<sup>2</sup> of BM was applied to the skin mimic with a nominal thickness of 350µm.

The wiping efficiency assessment method involved post-wiping image processing of the images the skin mimic surfaces containing BM slurry. The method is explained in section 3.4. Integrated density values (IDVs) were obtained from the fluorescence images of the wiped skin mimics and the new fabric and the plain control fabric were compared.

#### 6.3.2.1 Results and Discussion

The resulting IDVs for the complete area of interest after three wipes are shown in Table 11.

Skin Mimic Surface	Integrated Density Values (x10 <sup>-6</sup> )	
	New Structure	Plain (control)
1	1.77486	3.34442
2	1.7588	3.19886
3	1.90618	3.25645
Mean	1.81328	3.26658
Standard Deviation	0.08085	0.07331
CV%	4.5%	2.2%

*Table 11: IDV results of the processing of the fluorescence images of the skin mimic specimens for the two fabric options, new structure and plain*

A statistical analysis of variance (ANOVA) was performed to compare the means of the resulting IDVs. At a confidence level of 95%, the difference between the two means was significant, as shown in Figure 6.32. Images of the skin mimic for the plain and new structured fabric sample are shown in Figure 6.33. Images of the three wipes from each sample after use are shown in Figure 6.34, Figure 6.35 and Figure 6.36.

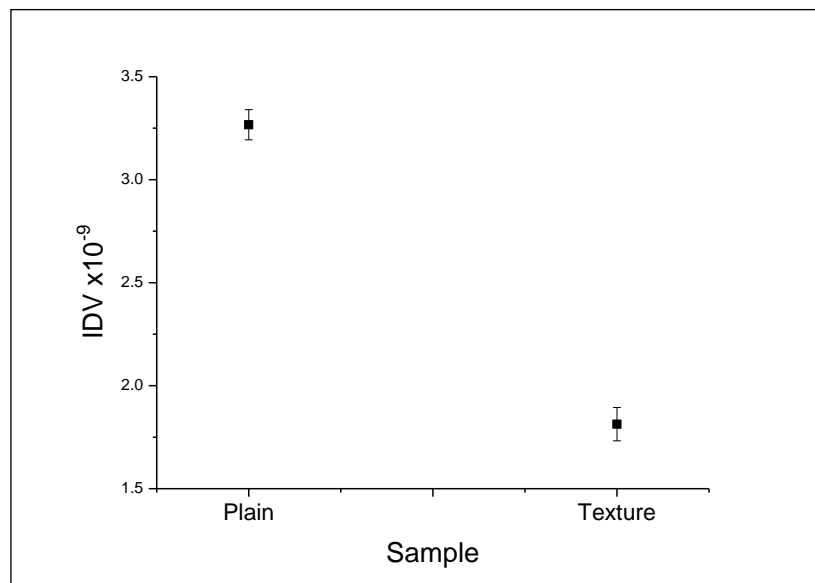


*Figure 6.32: A graph of the average IDVs for each of the tested options, the plain and the new structured fabric*

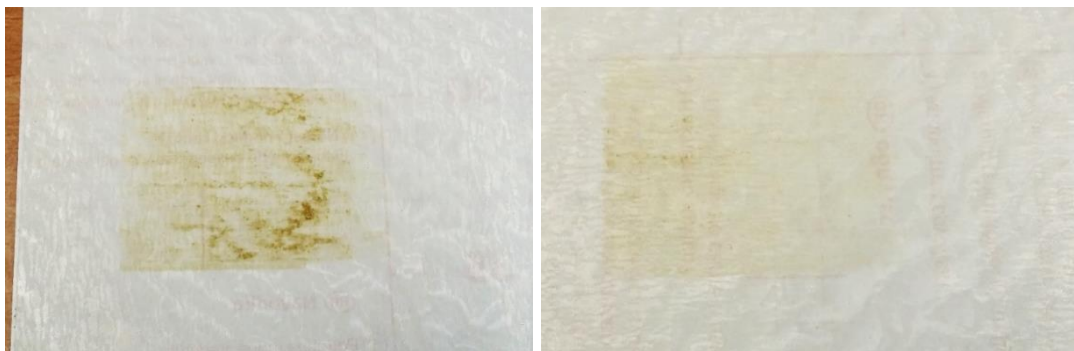


*Figure 6.33: On the left, BM residues on a skin mimic after 3 wipes with plain hydroentangled fabric. On the right, BM residues on a skin mimic after 3 wipes with the new structured hydroentangled fabric*



*Figure 6.34: On the left, first wipe of the plain plain hydroentangled fabric. On the right, first wipe of the new structured hydroentangled fabric*



*Figure 6.35: On the left, second wipe of the plain plain hydroentangled fabric. On the right, second wipe of the new structured hydroentangled fabric*



*Figure 6.36: On the left, third wipe of the plain plain hydroentangled fabric. On the right, third wipe of the new structured hydroentangled fabric*

# CHAPTER 7

## Conclusions

The research presented herein has focused on establishing an improved understanding the mechanisms of wiping process and the influencing factors in relation to hydroentangled wipe substrates parameters. BM is a more complex material than water alone, and therefore, it could not be assumed that its absorption behaviour would entirely mirror that of water. By obtaining an improved understanding of how the structure of the nonwoven wiping substrate influences BM wiping efficiency, the aim for this work has been achieved.

The principal mechanisms of BM removal and retention have been discussed thoroughly in 2.3. In a systematic approach, experimental work was planned and carried out addressing these mechanisms. The design of the experimental work was presented in Figure 3.8 in section 3.6. Thus the first objective of this research has been achieved.

Several experiments were designed and carried out addressing the influence of fabric structure properties such as porosity and porosity distribution on the mechanisms of BM capture and retention. This was achieved by studying the absorption behaviour of nonwoven fabrics which was presented in chapters 4 and 5. Findings about the adherence of BM slurry absorption to conventional absorption laws under certain conditions and the unconventional behaviour under others has added to the understanding of wiping mechanisms and how fabric structure influences them. The influence of fabrics' surface features on the dynamic BM removal, as presented in chapter 6, was also studied and in conclusion it was found that engineered geometrical surface patterns can positively influence the wiping fabric's performance. This investigation of how fabric structural properties influence BM removal, capture and retention satisfies the second objective of this project.

Throughout this document, the development of new characterisation techniques for the dynamic wiping performance of nonwoven fabrics and how they interact with BM is presented. This was shown as the development of

methods to characterise BM absorption behaviour under different user relevant conditions, chapter 4. And the development of the dynamic cleaning method which is shown in chapter 6. These methods have proven to be robust and have therefore fulfilled their objective as well as the third objective of this research.

The findings of the experimental part of this document helped identify certain parameters related to the nonwoven fabric's structure, which are capable of positively influencing the wiping performance compared to existing industry benchmark. Such parameters are porosity and porosity gradients, lotion loading and surface geometry and pattern. This fulfils the 4 and final objective of this research.

## **7.1 Contributions**

There has been no similar studies in the public domain contributing to the knowledge of how BM fluids behave when interacting with a porous medium like the nonwoven fabric. The findings of the experiments studying BM slurry absorption through local porosity profiles have proven that the absorption behaviour does not follow the conventional laws of absorption. Some theoretical and experimental work have been done in this regard, but none addressed that of the absorption behaviour of BM slurry by fibrous media.

The design and implementation of shearing elements have not been explored in regards to nonwovens when used as wiping material. Particularly when removing human waste such as BM. This work has made a first step in this direction and the results were positive. This encourages further work in this direction.

Several characterisation methods for the performance of wiping and the interaction of nonwoven fabrics with BM have been discussed and new methods have been developed. The developed method used in this work are novel and contribute to the list of already existing ones in characterising the interaction between fibrous media and contaminants.

## **7.2 Limitations**

While this work presents new findings on many fronts, the experimental work has been carried out under particular circumstances. The work had to be relevant to the application of baby wipes, this induced certain boundary conditions to which the findings are limited. Such conditions are the materials used, the wiping parameters e.g. speed and pressure and others.

## **7.3 Recommendations for Future Work**

Based on the experimental results obtained during this study, a number of areas can be identified for further study in relation to the removal of BM slurry.

During this work, the base fibre composition of the wipe was not altered from that is current industrial use. The extent to which changes in fibre composition could aid BM slurry absorption, and particularly the absorption rate would be interesting to determine, using for example fibres that are inherently more hygroscopic.

Based on the findings relating to local porosity, there is also substantial scope to develop more complex porosity profile patterns both in terms of planar arrangement and transplanar gradients. By pursuing this approach, it is likely that improvements in BM slurry absorption rates can be achieved without substantially compromising absorptive capacity over relevant timescales of use.

Similarly, the concept of introducing patterns in the surface of the wipe that have been rationally designed to aid BM slurry removal during dynamic wiping has significant potential to improve wiping efficiency. At present, such surface features, whether they take the form of embossed or apertured patterns, are provided more for visual appearance than for functional benefit in many industrial wipe substrates.

# CHAPTER 8

## References

- AGACHE, P. G., MONNEUR, C., LEVEQUE, J. L. & RIGAL, J. 1980. Mechanical properties and Young's modulus of human skin in vivo. *Archives of Dermatological Research*, 269, 221-232.
- ATTERBURY, O., BHATTACHARJEE, H. R., COOPER, D. W. & PALEY, S. J. 1997. Comparing cleanroom wipers with a dry abrasion resistance test. *Micro*, 15, 83-+.
- BADER, D. L. & BOWKER, P. 1983. Mechanical characteristics of skin and underlying tissues in vivo. *Biomaterials*, 4, 305-308.
- BAHNERS, T., OPWIS, K., TEXTOR, T., LABUDA, W. & SCHOLLMEYER, E. 2006. *The effect of laser-induced micro-roughness of textile fibers on adhesion and capture of micrometer-sized particles*, Leiden, Vsp Bv-C/O Brill Acad Publ.
- BAL, K., FAN, J., SARKAR, M. K. & YE, L. 2011. Differential spontaneous capillary flow through heterogeneous porous media. *International Journal of Heat and Mass Transfer*, 54, 3096-3099.
- BANSAL, S., VON ARNIM, V., STEGMAIER, T. & PLANCK, H. 2011. Effect of fibrous filter properties on the oil-in-water-emulsion separation and filtration performance. *Journal of Hazardous Materials*, 190, 45-50.
- BARDINA, J. 1988. Methods for surface particle removal: A comparative study. *Particulate Science and Technology*, 6, 121-131.
- BARNES, H. A., HUTTON, J. F. & WALTERS, K. 1989. Chapter 1 - Introduction. In: H.A. BARNES, J. F. H. & WALTERS, K. (eds.) *Rheology Series*. Elsevier.
- BERARDESCA, E. E. P. W. K. P. 2001. *Bioengineering of the skin : skin biomechanics*, Boca Raton, Fla.; London, CRC ; Chapman & Hall.
- BHATTACHARJEE, H. R. & PALEY, S. J. 1997. Evaluating sample preparation techniques for cleanroom wiper testing. *Micro*, 15, 39-45.
- BHATTACHARJEE, H. R. & PALEY, S. J. 1998. Comprehensive particle and fiber testing for cleanroom wipers. *Journal of the IEST*, 41, 19-25.
- BHATTACHARJEE, H. R., PALEY, S. J., PAVLIK, T. J. & ATTERBURY, O. 1993. THE USE OF SCANNING ELECTRON-MICROSCOPY TO QUANTIFY THE BURDEN OF PARTICLES RELEASED FROM CLEAN-ROOM WIPING MATERIALS. *Scanning*, 15, 301-308.
- BOSANQUET, C. H. 1923. LV. On the flow of liquids into capillary tubes. *Philosophical Magazine Series 6*, 45, 525-531.
- BOURNE, M. C. 1968. Texture Profile of Ripening Pears. *Journal of Food Science*, 33, 223-226.
- BURDICK, G., EICHENLAUB, S., BERMAN, N. & BEAUDOIN, S. 2003a. A comprehensive model for cleaning semiconductor wafers.
- BURDICK, G. M., BERMAN, N. S. & BEAUDOIN, S. P. 2001. Describing Hydrodynamic Particle Removal from Surfaces Using the Particle Reynolds Number. *Journal of Nanoparticle Research*, 3, 453-465.

- BURDICK, G. M., BERMAN, N. S. & BEAUDOIN, S. P. 2003b. A Theoretical Analysis of Brush Scrubbing Following Chemical Mechanical Polishing. *Journal of The Electrochemical Society*, 150, G140-G147.
- BURDICK, G. M., BERMAN, N. S. & BEAUDOIN, S. P. 2003c. A Theoretical Evaluation of Hydrodynamic and Brush Contact Effects on Particle Removal during Brush Scrubbing. *Journal of The Electrochemical Society*, 150, G658-G665.
- BURDICK, G. M., BERMAN, N. S. & BEAUDOIN, S. P. 2005. Hydrodynamic particle removal from surfaces. *Thin Solid Films*, 488, 116-123.
- BUTLER-SMITH, P. W., AXINTE, D. A. & DAINE, M. 2011. Ordered diamond micro-arrays for ultra-precision grinding—An evaluation in Ti–6Al–4V. *International Journal of Machine Tools and Manufacture*, 51, 54-66.
- CELEN, L. Procter & Gamble Internal Communications.
- CHATTERJEE, P. K. 1985. *Absorbency*, Amsterdam; New York; New York, NY, Elsevier Scientific Pub.
- CHATTERJEE, P. K. & GUPTA, B. S. 2002a. *Absorbent Technology*, Elsevier Science.
- CHATTERJEE, P. K. & GUPTA, B. S. 2002b. Chapter I Porous structure and liquid flow models.
- CHATTERJEE, P. K. G. B. S. 2002. *Absorbent technology* [Online]. Amsterdam; Oxford: Elsevier Science. Available: <http://www.sciencedirect.com/science/book/9780444500007>.
- ČIEGIS, R. & ZEMITIS, A. 1997. The mathematical simulation of the liquid transport in a multilayered nonwoven. *Mathematical Modelling and Analysis*, 2, 9-34.
- CIESLICKI, K. 1988. APPLICATION OF THE STRAINING CAPTURE MECHANISM IN GAPS TO THE MEASUREMENT OF PARTICLE CONCENTRATION AND SIZE DISTRIBUTION. *Particle & Particle Systems Characterization*, 5, 94-99.
- DAS, D., PRADHAN, A. K. & POURDEYHIMI, B. 2012. Dependence of the liquid absorption behavior of nonwovens on their material and structural characteristics: Modeling and experiments. *Journal of Applied Polymer Science*, 126, 1053-1060.
- DAWBER, R. P. R., MARKS, R. & SWIFT, J. A. 1972. SCANNING ELECTRON MICROSCOPY OF THE STRATUM CORNEUM. *British Journal of Dermatology*, 86, 272-281.
- DERMATOLOGY.ABOUT.COM. 2013. *Stratum Corneum Anatomy - The Key to Healthy, Attractive Skin* [Online]. Available: [http://dermatology.about.com/od/anatomy/ss/sc\\_anatomy.htm](http://dermatology.about.com/od/anatomy/ss/sc_anatomy.htm) 2013].
- DESTEPHEN, J. A. & CHOI, K. J. 1996. Modelling of filtration processes of fibrous filter media. *Separations Technology*, 6, 55-67.
- DHANIYALA, S. & LIU, B. Y. H. 1997. Theory and experiments on commercial fibrous filters. *Advances in Filtration and Separation Technology, Vol 11 1997*, 145-152.
- DHANIYALA, S. & LIU, B. Y. H. 2001. Experimental investigation of local efficiency variation in fibrous filters. *Aerosol Science and Technology*, 34, 161-169.
- DIAB-ELSCHAHAWI, M., ASSADIAN, O., BLACKY, A., STADLER, M., PERNICKA, E., BERGER, J., RESCH, H. & KOLLER, W. 2010. Evaluation of the decontamination efficacy of new and reprocessed microfiber cleaning cloth

compared with other commonly used cleaning cloths in the hospital. *American Journal of Infection Control*, 38, 289-292.

- DULLIEN, F. A. L. 1992a. 1 - Pore Structure. *Porous Media (Second Edition)*. San Diego: Academic Press.
- DULLIEN, F. A. L. 1992b. 2 - Capillarity in Porous Media. *Porous Media (Second Edition)*. San Diego: Academic Press.
- EDANA. 2013. *Quality of Life and Absorbent Hygiene Products* [Online]. EDANA. Available: <http://www.edana.org/docs/default-source/default-document-library/quality-of-life-and-absorbent-hygiene-products---1.pdf?sfvrsn=2> [Accessed June 28th 2013].
- EDANA & INDA. 2015. *Nonwovens Standard Procedures* [Online]. Available: <http://www.edana.org/docs/default-source/default-document-library/toc-cover-preamble.pdf?sfvrsn=1> 2016].
- ESCOFFIER, C., DE RIGAL, J., ROCHEFORT, A., VASSELET, R., LEVEQUE, J.-L. & AGACHE, P. G. 1989. Age-Related Mechanical Properties of Human Skin: An In Vivo Study. *J Investig Dermatol*, 93, 353-357.
- FAN, J. & HUNTER, L. 2009. *Engineering Apparel Fabrics and Garments*, Elsevier Science.
- FAN, J. & QIAN, X. 2010. Characterization of liquid, water and/or moisture transport properties of fabrics. Google Patents.
- FAN, J. T., SARKAR, M. K., SZETO, Y. C. & TAO, X. M. 2007. Plant structured textile fabrics. *Materials Letters*, 61, 561-565.
- FRIEDMAN, H. H., WHITNEY, J. E. & SZCZESNIAK, A. S. 1963. The Texturometer—A New Instrument for Objective Texture Measurement. *Journal of Food Science*, 28, 390-396.
- GANE, P., SCHOELKOPF, J., SPIELMANN, D., MATTHEWS, G. & RIDGWAY, C. 1999. Observing fluid transport into porous coating structures: some novel findings. *Tappi J*, 83, 77.
- GANE, P. A. C., RIDGWAY, C. J. & SCHOELKOPF, J. 2004. Absorption Rate and Volume Dependency on the Complexity of Porous Network Structures. *Transport in Porous Media*, 54, 79-106.
- GERKE, H. H. & VAN GENUCHTEN, M. T. 1993. Evaluation of a first-order water transfer term for variably saturated dual-porosity flow models. *Water Resources Research*, 29, 1225-1238.
- GERKE, H. H. & VAN GENUCHTEN, M. T. 1996. Macroscopic representation of structural geometry for simulating water and solute movement in dual-porosity media. *Advances in Water Resources*, 19, 343-357.
- GHASSEMIEH, E., ACAR, M. & VERSTEEG, H. 2002. Microstructural analysis of non-woven fabrics using scanning electron microscopy and image processing. Part 1: Development and verification of the methods. *Proceedings of the Institution of Mechanical Engineers, Part L: Journal of Materials: Design and Applications*, 216, 199-207.
- GKD. 2017. *Process Belts* [Online]. Available: <https://gkd.uk.com/> 2017].
- GRANT, D. C., LIU, B. Y. H., FISHER, W. G. & BOWLING, R. A. 1989. PARTICLE CAPTURE MECHANISMS IN GASES AND LIQUIDS - AN ANALYSIS OF OPERATIVE MECHANISMS IN MEMBRANE FIBROUS FILTERS. *Journal of Environmental Sciences*, 32, 43-51.

- HALL, C., GREEN, K., HOFF, W. D. & WILSON, M. A. 1996. A sharp wet front analysis of capillary absorption into n-layer composite. *Journal of Physics D-Applied Physics*, 29, 2947-2950.
- HENDRIKS, F. 2005. *Mechanical behaviour of human epidermal and dermal layers in vivo*. Technische Universiteit Eindhoven.
- HERMAN, B. F., VICTORIA E. CENTONZE; LAKOWICZ, JOSEPH R.; MURPHY, DOUGLAS B.; SPRING, KENNETH R.; DAVIDSON, MICHAEL W. 2015. *Fluorescence Microscopy* [Online]. Michael W. Davidson, The Florida State University. Available: <http://micro.magnet.fsu.edu/primer/techniques/fluorescence/fluorointrohome.html> 2017].
- HOHENDORFF, B., WEIDERMANN, C., BURKHART, K. J., ROMMENS, P. M., PROMMERSBERGER, K. J. & KONERDING, M. A. 2010. Lengths, girths, and diameters of children's fingers from 3 to 10 years of age. *Ann Anat*, 192, 156-61.
- HOLMES, S. 1986. The Digestive-System, 2nd Edition - Ryall, Rj. *International Journal of Nursing Studies*, 23, 89-90.
- HOLZMELSTER, A., RUDISILE, M., GREINER, A. & WENDORFF, J. H. 2007. Structurally and chemically heterogeneous nanofibrous nonwovens via electrospinning. *European Polymer Journal*, 43, 4859-4867.
- HUANG, Y., GUO, D., LU, X. & LUO, J. 2011a. A lubrication model between the soft porous brush and rigid flat substrate for post-CMP cleaning. *Microelectronic Engineering*, 88, 2862-2870.
- HUANG, Y., GUO, D., LU, X. & LUO, J. 2011b. Modeling of particle removal processes in brush scrubber cleaning. *Wear*, 273, 105-110.
- ISO, B. 2009. Paper and Board – Determination of z-directional Tensile Strength.
- KALPAKJIAN, S. & SCHMID, S. R. 2008. *Manufacturing processes for engineering materials*, Upper Saddle River, N.J., Pearson Hall.
- KEMMER, N. 1977. *Vector Analysis: A Physicist's Guide to the Mathematics of Fields in Three Dimensions*, Cambridge University Press.
- KIM, H., KIM, H. J., HUH, H. K., HWANG, H. J. & LEE, S. J. 2015. Structural design of a double-layered porous hydrogel for effective mass transport. *Biomicrofluidics*, 9, 024104.
- KIM, J. & KIM, H.-Y. 2012. On the dynamics of capillary imbibition. *Journal of Mechanical Science and Technology*, 26, 3795-3801.
- KOENIG, D. W., DVORACEK, B. & VONGSA, R. 2013. In vitro prediction of in vivo skin damage associated with the wiping of dry tissue against skin. *Skin Research and Technology*, 19, e453-e458.
- KOH, E. 2009. *Influence of hydroentangled fabric structure on wiping performance*. PhD, University of Leeds.
- KOLARSICK, P. A. J., KOLARSICK, M. A. & GOODWIN, C. 2011. Anatomy and Physiology of the Skin. *Journal of the Dermatology Nurses' Association*, 3, 203-213.
- KRUSS-GMBH. *Kruss Tensiometer* [Online]. Available: <https://www.kruss.de/services/education-theory/glossary/tensiometer/> 2016].
- LANDERYOU, M., EAMES, I. & COTTENDEN, A. 2005. Infiltration into inclined fibrous sheets. *Journal of Fluid Mechanics*, 529, 173-193.

- LANDERYOU, M. A., YERWORTH, R. J. & COTTENDEN, A. M. 2003. Mapping liquid distribution in absorbent incontinence products. *Proc Inst Mech Eng H*, 217, 253-61.
- LENTNER, C. & PHARMACEUTICALS, G. 1981. *Geigy scientific tables: Units of measurement, body fluids, composition of the body, nutrition*, Ciba-Geigy.
- LEVI, K. 2009. *Biomechanics of human stratum corneum: dry skin conditions, tissue damage and alleviation*. PhD, Stanford University.
- LI, C., SHEN, Y., GE, H., SU, S. & YANG, Z. 2016. ANALYSIS OF SPONTANEOUS IMBIBITION IN FRACTAL TREE-LIKE NETWORK SYSTEM. *Fractals*, 24, 1650035.
- MAKHSOUS, M. & LIN, F. 2009. A Finite-Element Biomechanical Model for Evaluating Buttock Tissue Loads in Seated Individuals with Spinal Cord Injury. In: GEFEN, A. (ed.) *Bioengineering Research of Chronic Wounds: A Multidisciplinary Study Approach*. New York: Springer.
- MANAS, S., JINTU, F. & XIAOMING, Q. 2007. Transplanar water transport tester for fabrics. *Measurement Science and Technology*, 18, 1465.
- MAO, N. 2000. *Effect of fabric structure on the liquid transport characteristics of nonwoven wound dressings*. University of Leeds.
- MAO, N. 2009a. Permeability in Engineered Non-woven Fabrics Having Patterned Structure. *Textile Research Journal*, 79, 1348-1357.
- MAO, N. 2009b. Unsteady-state Liquid Transport in Engineered Nonwoven Fabrics having Patterned Structure. *Textile Research Journal*, 79, 1358-1363.
- MAO, N. 2016. 6 - Methods for characterisation of nonwoven structure, property, and performance A2 - Kellie, George. *Advances in Technical Nonwovens*. Woodhead Publishing.
- MAO, N. & RUSSELL, S. 2005. STRUCTURE-PROCESS-PROPERTY RELATIONSHIPS OF HYDROENTANGLED FABRICS.
- MAO, N. & RUSSELL, S. J. 2000a. Directional Permeability in Homogeneous Nonwoven Structures Part I: The Relationship between Directional Permeability and Fibre Orientation. *The Journal of The Textile Institute*, 91, 235-243.
- MAO, N. & RUSSELL, S. J. 2000b. Directional Permeability in Homogeneous Nonwoven Structures Part II: Permeability in Idealised Structures. *The Journal of The Textile Institute*, 91, 244-258.
- MAO, N. & RUSSELL, S. J. 2003a. Anisotropic liquid absorption in homogeneous two-dimensional nonwoven structures. *Journal of Applied Physics*, 94, 4135-4138.
- MAO, N. & RUSSELL, S. J. 2003b. Modeling Permeability in Homogeneous Three-Dimensional Nonwoven Fabrics. *Textile Research Journal*, 73, 939-944.
- MAO, N. & RUSSELL, S. J. 2008. Capillary pressure and liquid wicking in three-dimensional nonwoven materials. *Journal of Applied Physics*, 104, 034911.
- MAO, N. & RUSSELL, S. J. 2010. 5 - Modelling of nonwoven materials A2 - Chen, X. *Modelling and Predicting Textile Behaviour*. Woodhead Publishing.
- MASON, O. Procter & Gamble Internal Communications. Basic Cleaning Model.
- MASOODI, R. & PILLAI, K. 2012. Single-Phase Flow (Sharp-Interface) Models for Wicking. *Wicking in Porous Materials*. CRC Press.

- MASOODI, R., PILLAI, K. M. & VARANASI, P. P. 2007. Darcy's law-based models for liquid absorption in polymer wicks. *AIChE Journal*, 53, 2769-2782.
- MCNAUGHT, A. D. & WILKINSON, A. I{UPAC}. *Compendium of Chemical Terminology, 2nd ed. (the "Gold Book")*, WileyBlackwell; 2nd Revised edition edition.
- MEEKER, S. P., BONNECAZE, R. T. & CLOITRE, M. 2004. Slip and flow in pastes of soft particles: Direct observation and rheology. *Journal of Rheology*, 48, 1295-1320.
- MEMARI, A. 2011. *Development of Cleaning and Dispensing Test Methods for Wet Wipes*. Master's, HTW-Aalen.
- MILLER, B. & TYOMKIN, I. 1984. Spontaneous Transplanar Uptake of Liquids by Fabrics. *Textile Research Journal*, 54, 706-712.
- MITTAL, K. L. 2006. Contact Angle, Wettability and Adhesion, Volume 4. VSP - An imprint of BRILL.
- NG, C. K., MELKOTE, S. N., RAHMAN, M. & SENTHIL KUMAR, A. 2006. Experimental study of micro- and nano-scale cutting of aluminum 7075-T6. *International Journal of Machine Tools and Manufacture*, 46, 929-936.
- OATHOUT, J. M. 1999. Determining the dynamic efficiency of cleanroom wipers for removal of liquids and particles from surfaces. *Journal of the IEST*, 42, 17-26.
- OATHOUT, J. M. 2000. Determining the dynamic efficiency with which wiping materials remove liquids from surfaces. *International Nonwovens Journal*, 9, 30-34.
- OATHOUT, J. M. & MATTINA, C. F. 1998. Quantifying fibrous debris released by and generated from wiping materials. *Textile Research Journal*, 68, 756-763.
- OH, J. H. L. S. H. K. K. W. 2006. Image Analysis: A Novel Technique to Determine the Efficiency of Wiping Cloths. *Fibers and Polymers*, 7, 73-78.
- PAN, N. & GIBSON, P. 2006. *Thermal and Moisture Transport in Fibrous Materials*, Elsevier Science.
- PAN, N. & ZHONG, W. 2006. Fluid Transport Phenomena in Fibrous Materials. *Textile Progress*, 38, 1-93.
- PATNAIK, A., RENGASAMY, R. S., KOTHARI, V. K. & GHOSH, A. 2006. Wetting and Wicking in Fibrous Materials. *Textile Progress*, 38, 1-105.
- QIN, W. Procter & Gamble Internal Communications. Development of Artificial Bowel Movement.
- REIGER, M. M. 2000. *Harry's Cosmeticology, Volumes I-II (8th Edition)*. Chemical Publishing Company Inc.
- RIDGWAY, C. J. & GANE, P. A. C. 2002. Dynamic absorption into simulated porous structures. *Colloids and Surfaces A: Physicochemical and Engineering Aspects*, 206, 217-239.
- RIDGWAY, C. J., GANE, P. A. C. & SCHOELKOPF, J. 2002. Effect of Capillary Element Aspect Ratio on the Dynamic Imbibition within Porous Networks. *Journal of Colloid and Interface Science*, 252, 373-382.
- RIDGWAY, C. J., GANE, P. A. C. & SCHOELKOPF, J. 2006. Achieving Rapid Absorption and Extensive Liquid Uptake Capacity in Porous Structures by Decoupling Capillarity and Permeability: Nanoporous Modified Calcium Carbonate. *Transport in Porous Media*, 63, 239-259.

- RIDGWAY, C. J., SCHOELKOPF, J., MATTHEWS, G. P., GANE, P. A. C. & JAMES, P. W. 2001. The Effects of Void Geometry and Contact Angle on the Absorption of Liquids into Porous Calcium Carbonate Structures. *Journal of Colloid and Interface Science*, 239, 417-431.
- RIOUX, R. W. 2003. *The Rate of Fluid Absorption in Porous Media*. Master, The University of Maine.
- RODMAN, C. A. Fibers for nonwovens with emphasis on filtration theory and applications. In: ANON, ed., 1990 Boston, MA, USA. Publ by American Assoc of Textile Chemists & Colorists, 233-246.
- ROE, D. C. Procter & Gamble Internal Communications. Fecal Ingredients.
- ROE, D. C., MASON, O. E. C. & SOMMER, R. J. Procter & Gamble Internal Communications. Analysis of BM Samples.
- ROSENTHAL, A. J. 2010. TEXTURE PROFILE ANALYSIS – HOW IMPORTANT ARE THE PARAMETERS? *Journal of Texture Studies*, 41, 672-684.
- RUSSELL, S. J. 2007. *Handbook of Nonwovens*, CRC Press.
- SANDFORD, E., CHEN, Y., HUNTER, I., HILLEBRAND, G. & JONES, L. 2013. Capturing skin properties from dynamic mechanical analyses. *Skin Research and Technology*, 19, e339-e348.
- SAUERESSIG. 2017. *Saueressig FLEXOembossing®* [Online]. Available: <http://saueressig.com/en/werkzeuge/portfolio-werkzeuge/pragen/pragezylinder/> 2017].
- SHIMETA, J. & JUMARS, P. A. 1991. Physical-Mechanisms and Rates of Particle Capture by Suspension-Feeders. *Oceanography and Marine Biology*, 29, 191-257.
- SHIUE, A., HU, S. C., LIN, C. H. & LIN, S. I. 2011. Quantitative Techniques for Measuring Cleanroom Wipers with Respect to Airborne Molecular Contamination. *Aerosol and Air Quality Research*, 11, 460-465.
- SHOU, D. & FAN, J. 2015. Structural optimization of porous media for fast and controlled capillary flows. *Physical Review E*, 91, 053021.
- SHOU, D., YE, L., FAN, J., FU, K., MEI, M., WANG, H. & CHEN, Q. 2014a. Geometry-Induced Asymmetric Capillary Flow. *Langmuir*, 30, 5448-5454.
- SHOU, D. H., YE, L., FAN, J. T. & FU, K. K. 2014b. Optimal Design of Porous Structures for the Fastest Liquid Absorption. *Langmuir*, 30, 149-155.
- SINCLAIR, R. 2014. *Textiles and Fashion: Materials, Design and Technology*, Elsevier Science.
- SMITH, J. H. 1971. *Embossed Nonwoven Wiping and Cleaning Materials*. 848,502.
- SUN, Y., KHARAGHANI, A. & TSOTSAS, E. 2016. Micro-model experiments and pore network simulations of liquid imbibition in porous media. *Chemical Engineering Science*, 150, 41-53.
- TANG, K.-P. M., KAN, C.-W. & FAN, J.-T. 2014. Evaluation of water absorption and transport property of fabrics. *Textile Progress*, 46, 1-132.
- TANG, K. P. M., CHAU, K. H., KAN, C. W. & FAN, J. T. 2015a. Characterizing the transplanar and in-plane water transport properties of fabrics under different sweat rate: Forced Flow Water Transport Tester. *Scientific Reports*, 5, 17012.
- TANG, K. P. M., WU, Y. S., CHAU, K. H., KAN, C. W. & FAN, J. T. 2015b. Characterizing the transplanar and in-plane water transport of textiles with

gravimetric and image analysis technique: Spontaneous Uptake Water Transport Tester. *Scientific Reports*, 5, 9689.

- TAUSIF, M. & RUSSELL, S. J. 2012. Characterisation of the z-directional tensile strength of composite hydroentangled nonwovens. *Polymer Testing*, 31, 944-952.
- TEXWIPE. 2011. *Determination of Basis Weight, Absorbency - Texwipe Method 20* [Online]. Available: <https://www.texwipe.com/technical-data/test-methods/tm20.pdf> 2017].
- THEAVERAGEBODY.COM. 2012. *Average Hand* [Online]. Available: [http://www.theaveragebody.com/average\\_hand\\_size.php](http://www.theaveragebody.com/average_hand_size.php) [Accessed 15/10/2013 2013].
- VAN DER MEEREN, P., COCQUYT, J., FLORES, S., DEMEYERE, H. & DECLERCQ, M. 2002. Quantifying Wetting and Wicking Phenomena in Cotton Terry as Affected by Fabric Conditioner Treatment. *Textile Research Journal*, 72, 423-428.
- VENU, L. B. S., SHIM, E., ANANTHARAMAIAH, N. & POURDEYHIMI, B. 2014. Impacts of high-speed waterjets on web structures. *The Journal of The Textile Institute*, 105, 430-443.
- VENU, L. B. S., SHIM, E., ANANTHARAMAIAH, N. & POURDEYHIMI, B. 2017. Structures and properties of hydroentangled nonwovens: effect of number of manifolds. *The Journal of The Textile Institute*, 108, 301-313.
- VERKOUTEREN, J. R., COLEMAN, J. L., FLETCHER, R. A., SMITH, W. J., KLOUDA, G. A. & GILLEN, G. 2008. A method to determine collection efficiency of particles by swipe sampling. *Measurement Science & Technology*, 19.
- VISSCHER, M., ODIO, M., TAYLOR, T., WHITE, T., SARGENT, S., SLUDER, L., SMITH, L., FLOWER, T., MASON, B., RIDER, M., HUEBNER, A. & BONDURANT, P. 2009. Skin Care in the NICU Patient: Effects of Wipes versus Cloth and Water on Stratum Corneum Integrity. *Neonatology*, 96, 226-234.
- WALTON, R. C., SMITH, P. R. & HORN, D. 2010. *Non-woven Wet Wiping*. 11/688,853.
- WANG, Y. C., CHEN, C. H. & LEE, B. Y. 2012. THE DESIGN MODEL OF MICRO END-MILLS MADE BY USING THE FINITE ELEMENT METHOD. *Transactions of Famena*, 36, 41-50.
- WASHBURN, E. W. 1921. The Dynamics of Capillary Flow. *Physical Review*, 17, 273-283.
- WEI, R. 2003. *The Rate of Fluid Absorption in Porous Media*.
- XU, K., VOS, R., VEREECKE, G., DOUMEN, G., FYEN, W., MERTENS, P. W., HEYNS, M. M., VINCKIER, C. & FRANSAER, J. 2004. Particle adhesion and removal mechanisms during brush scrubber cleaning. *Journal of Vacuum Science & Technology B: Microelectronics and Nanometer Structures*, 22, 2844-2852.
- XU, K., VOS, R., VEREECKE, G., DOUMEN, G., FYEN, W., MERTENS, P. W., HEYNS, M. M., VINCKIER, C., FRANSAER, J. & KOVACS, F. 2005. Fundamental study of the removal mechanisms of nano-sized particles using brush scrubber cleaning. *Journal of Vacuum Science & Technology B: Microelectronics and Nanometer Structures*, 23, 2160-2175.

- YAMAMOTO, N., KUMAGAI, K., FUJII, M., SHENDELL, D. G., ENDO, O. & YANAGISAWA, Y. 2005. Size-dependent collection of micrometer-sized particles using nylon mesh. *Atmospheric Environment*, 39, 3675-3685.
- ZWICK-GMBH. 2015. *Specimen grips and test fixtures > Screw grips* [Online]. Available: <http://www.zwick.co.uk/en/products/specimen-grips-and-test-fixtures/screw-grips.html> [2017].

# CHAPTER 9 Appendices

## 9.1 Appendix 1

Pressure (kPa)	Dry weight (g)	Wet weight (g)	Lotion Load (%)
62	1.89	9.51	403
	1.95	9.45	385
	1.9	8.64	355
	1.92	8.89	363
	1.92	8.92	365
	1.96	8.97	358
	1.9	9.08	378
	1.91	8.7	355
	1.93	8.74	353
	1.94	8.86	357
	1.95	9.25	374
	2	9.09	355
	1.91	8.58	349
	1.93	9.14	374
	1.99	9.44	374
	1.96	8.95	357
	1.93	8.67	349
	1.93	8.78	355
	1.99	9.2	362
Average	1.89	8.52	351
	1.935	8.969	364
69	1.99	8.49	327
	1.91	8.08	323
	1.9	8.16	329
	1.93	8.24	327
Average	1.9325	8.2425	327
76	1.94	7.85	305
	1.96	7.99	308
	1.9	7.64	302
Average	1.93	7.82	305
83	1.93	7.49	288
	1.96	7.62	289
	1.92	7.49	290
	1.88	7.29	288
Average	1.9225	7.4725	289
90	1.9	7.19	278
	1.9	7.39	289
	1.86	6.98	275
Average	1.886667	7.186667	281

Table 12: Lotion loading results using the pad mangle method

## 9.2 Appendix 2

Wipe no.	Dry weight [g]	Wet weight [g]	Lotion weight [g]	Lotion load [%]
1	2.04	10.97	8.93	438
2	1.97	10.52	8.55	434
3	2.04	10.74	8.70	426
4	1.99	11.30	9.31	468
5	2.04	10.99	8.95	439
6	2.04	10.89	8.85	434
7	2.06	11.36	9.30	451
8	2.00	10.93	8.93	447
9	2.03	10.95	8.92	439
10	1.99	10.79	8.80	442
11	2.04	11.24	9.20	451
12	2.03	11.10	9.07	447
13	2.08	11.16	9.08	437
14	2.01	10.64	8.63	429
15	2.04	10.77	8.73	428
16	2.08	11.91	9.83	473
17	2.02	10.42	8.40	416
18	2.03	10.63	8.60	424
19	2.06	10.86	8.80	427
20	2.00	10.61	8.61	431
Average	2.03	10.94	8.91	439
Stdev	0.03	0.34	0.33	14
CV%	1.5%	3.2%	3.7%	3.2%

*Table 13: Lotion loading results variation using the hand mangle method*